Structural and Material Instability

Cifuentes, Gustavo Cifuentes

Publication date:
2005

Document Version
Publisher's PDF, also known as Version of record

Aalborg **UNIVERSITY**

Structural

Structural and Material Instability

Gustavo Cifuentes Cifuentes

ISSN 1395-7953 R0509

Ph.D. Thesis defended publicly at Aalborg University on October 3, 2005

Structural and Material Instability

Gustavo Cifuentes Cifuentes

Submitted to the Department of Building Technology
and Structural Engineering
Aalborg University, in partial fulfillment
of the requirements for the degree of
PhD.
Defended publicly on October 3, 2005

Preface

The present report is submitted in partial fulfillment of the requirements for obtaining the degree of Ph.D. The research is carried out at the Department of Building Technology and Structural Engineering, Aalborg University, under the supervision of Professor Dr. Techn. Esben Byskov.

First of all, I wish to express my gratitude to Esben Byskov for always taking the time to give inspiring advice and encouragement. I also want to thank Jes Christoffersen for his advice and critical contributions during the first and second years of this project.

During my stay at Brown University in the fall of 2003, I had many inspiring discussions and received useful advice from professor Alan Needleman to whom I am grateful. He made my stay at Brown an unforgettable experience.

Finally, I want to thank my wife for her support and help correcting my written language during these years.

Abstract

This work is a small contribution to the general problem of structural and material instability. In this work, the main subject is the analysis of cracking and failure of structural elements made from quasi-brittle materials like concrete. The analysis is made using the finite element method.

Three approaches are considered to solve the problem: First by using interface elements to model the discontinuities, second by using elements with embedded cracks based on the extended finite element method, and finally an alternative approach to embed the discontinuities in the elements.

The first approach (the use of interface elements) is used successfully to model cases where the path of the discontinuity is known in advance, this is the case of the analysis of pull-out of fibers embedded in a concrete matrix. This method is applied to the case of non-straight fibers, and fibers with forces that have components on the plane of the discontinuity. A rate and state dependent friction law is used to model the friction, and a cohesive model is also considered, both of those as constitutive models for the interface elements. Additionally, a simple procedure to handle large slip of the fiber is considered.

Numerical problems associated with the use of elements with embedded cracks based on the extended finite element method are presented in the next part of this work. And an alternative procedure is used in order to successfully remove these numerical problems.

In the final part of this work, a computer program based on the finite element method for the analysis of cracks in structural elements is presented; in this program the interface and elements with embedded discontinuities are implemented.

In order to provide support to the thesis, some appendices are included. In particular, appendix A is included to present the notation. Appendix B gives an overview of various solution schemes for non-linear finite element analysis; this is motivated by the need for a more pedagogic presentation of that subject. Appendix C and D mainly serve as background material for the historical review in chapter 2. Finally, appendix E is the users' manual for the computer program in chapter 7.

Resumé

Denne afhandling er et lille bidrag til den generelle probematik vedrørende ustabilitet i struktur og materiale. Afhandlingens vigtigste tema er analyse af revner og sammenbrud i strukturelle elementer i kvasi-skrøbelige materialer som beton. Analysen er udført ved brug af den finitte elementmetode.

Tre forskellige fremgangsmåder tages i betragtning for at løse problemet: Først ved at bruge berøringsflade-elementer til at modellere diskontinuiteterne, derefter ved at bruge elementer med indstøbte revner baserede på den udvidede finitte elementmetode, og til sidst en alternativ fremgangsmåde med at indkorporere diskontinuiteterne i elementerne.

Den første metode (brugen af berøringsflade-elementer) er vellykket gennemført til at modellere tilfælde hvor diskontinuitetens bane er kendt på forhånd, dette er tilfældet ved analyse af udtrækning af fibre indstøbt i en betonmatrix. Denne metode er anvendt i tilfælde af ulige fibre, samt fibre med kræfter der har komponenter på diskontinuitetsplanet. En tilstands- og fartafhængig friktionsmodel er brugt til at modellere friktionen, en sammenhængende model tages også i betragtning, begge som konstitutive modeller for berøringsflade-elementerne. Derudover tages en simpel procedure til behandling af større fiberforskydninger i betragtning.

Næste del af afhandlingen præsenterer numeriske problemer forbundet med brugen af elementer med indstøbte revner baserede på den udvidede finitte elementmetode. Og en alternativ fremgangsmåde anvendes til at fjerne disse numeriske problemer på en vellykket måde.

I den sidste del af afhandlingen præsenteres et computerprogram, baseret på den finitte elementmetode, til at analysere revner i strukturelementer; i dette program implementeres berøringsfladen og elementerne med indstøbte diskontinuiteter.

For at understøtte afhandlingen indbefattes nogle appendikser. Appendiks A er inkluderet for at præsentere notationen. Appendiks B giver et overblik over flere forskellige løsningsmodeller til ikke-lineær finit elementanalyse: dette er for at præsentere emnet på en mere pædagogisk måde. Appendiks C og D fungerer hovedsageligt som baggrundsmateriale for den historiske redegørelse i kapitel 2.

Afslutningsvis består Appendiks E af brugervejledningen til computerprogrammet i kapitel 7.

Resumen

El presente trabajo es una pequena contribucion al problema de la estabilidad de estructuras. El trabajo se enfoca en el analisis del agrietamiento y la falla de sistemas estructurales fabricados utilizando materiales con comportamiento fragil, tales como el concreto. El analisis se lleva a cabo utilizando el metodo de los elementos finitos.

Se presentan tres maneras de resolver el problema: La primera forma consiste en la utilizacion de elementos interfaciales para modelar las discontinuidades. La segunda forma consiste en la utilizacion de elementos finitos con la discontinuidad incluida, estos elementos son construidos con base en el metodo extendido de los elementos finitos. Finalmente es presentada una nueva alternativa para incluir la discontinuidad dentro del elemento finito.

El primer metodo (uso de elemetos interfaciales) se usa con exito para modelar casos en los que se conoce de antemano la posicion de la discontinuidad, este es el caso del analisis de pruebas de extraccion de fibras embebidas en una matriz de concreto. El metodo es aplicado al caso de fibras no rectas y fibras con fuerzas que tienen componentes en el pano de la discontinuidad. Con el objeto de modelar la friccion en la discontinuidad se utiliza un modelo dependiente del estado y la velocidad de carga. Un modelo cohesivo tambien es considerado. Ambos modelos se utilizan como modelos constitutivos para los elementos interfaciales. Se estudia un procedimiento simple para manejar el caso de grandes deslizamientos de la fibra.

En la siguiente parte de este trabajo se encuentra que el uso de elemetos finitos con discontinuidades internas basado en el metodo extendido de los elementos finitos, puede dar lugar a errores numericos, asi que un procedimiento alternativo es requerido para incluir dentro del elemento la discontinuidad, una alternativa exitosa es presentada.

En la parte final de este trabajo, se presenta un programa de computador basado en el metodo de los elementos finitos para el analisis de grietas en elementos estructurales. En dicho programa se implementaron los elementos interfaciales y los elementos con discontinuidades internas.

Con el proposito de tener una presentacion completa de algunos temas se incluyen algunos apendices. En particular el apendice A se incluyo para presentar la notacion incluida en el texto. El apendice B presenta diferentes soluciones al problema del analisis no lienal con elementos finitos. Dicho apendice esta motivado parcialmente en la necesidad de tener una presentacion del tema mas completa y pedagogica de lo que existe actualmente. Los apendices C y D dan soporte a la revision historica presentada en el capitulo 2. Finalmente el manual del usuario para el programa de computador presentado en el capitulo 7 se incluye en el apendice E.

Contents

List of Figures

List of Tables

Chapter 1

Introduction

A definition of stability is provided by Belytschko, Liu & Moran (2000), this definition was originally used by Liapunov. Consider a process governed by an evolution equation, and let the solution for the initial conditions $\mathbf{d}_A(0)$ be denoted by $\mathbf{d}(t)$. Now consider solutions for initial conditions $\mathbf{d}_B(0)$ where $\mathbf{d}_B(0)$ are small perturbations of $\mathbf{d}_A(0)$. This means that the vector $\mathbf{d}_B(0)$ is close to $\mathbf{d}_A(0)$ in some norm:

$$\|\mathbf{d}_A(0) - \mathbf{d}_B(0)\| \leq \epsilon \tag{1.1}$$

A solution is stable if for all initial conditions that satisfy (1.1) the solution satisfies

$$\|\mathbf{d}_A(t) - \mathbf{d}_B(t)\| \leq C\epsilon \tag{1.2}$$

That means that the solution is stable if small perturbations of the initial configuration result in small changes in the solution. Classical solutions and implications of instability can be found e.g. in Budiansky (1974), Hutchinson (1974), Cedolin & Bažant (1991).

In the case of material instability, the growth of the perturbation is taken as an indicator of instability, in the same way as it is used in the general problem of structural instability. Material instabilities are usually associated with localized growth of deformation.

The problem of material instability is a problem of material failure and it is manifested as strain localization, damage and fracture. The problem can be studied at different scales, for example at a micro-scale using micro-mechanical models.

In classical instability theory, the problem always involves a length scale factor, for instance the radius of gyration in the case of buckling of a rod. In classical material instability the lack of the length scale is notorious. This has been manifested as a mesh dependence of the solution in finite element analysis, also in the lack of convergence of solutions. One or several length scales can be introduced into the solution by means of the use of higher order theories.

If Finite Element Analysis is used with models including these length scales, then it is required to use finite elements that have sizes comparable to the size of the length scale, which is impossible in the case of large structural elements.

Here possibilities are investigated to solve problems including fracture without taking care of the scale factor: this is done by modeling cracking at a scale larger than the thickness of the localization zone. Two approaches are presented in detail, the first one is the use of interface elements, and the second approach consists in the use of elements with embedded cracks modeling the cracks as strong discontinuities.

The first approach, namely the use of interface elements, is practical and relatively easy to implement using the finite element method, but it does not remove the fundamental problem and can produce ill-posed solutions. However, as used here, the discrete method using interface elements produces reliable results. It is not necessary to use re-meshing if the discontinuity path is known in advance as in the problem of pull-out of fibers embedded in a concrete matrix.

The second approach consists in introducing the discontinuity into the finite element, a version of this approach based on (Moës, Dolbow & Belitschko 1999) and (Wells & Sluys 2001) is intended, but in examples shown here, this approach fails due to numerical problems. A more robust approach to embed cracks is presented based on (Alfaiate, Simone & Sluys 2003). The elements based on the alternative approach are able to solve the numerical difficulties.

In chapter 2 of this report, a historical review of the problem of analysis of cracking in quasi-brittle materials is presented.

Chapter 3 consists in a paper about the use of interface elements to model the pull-out test in fiber reinforced concrete. The theory used in this paper is presented in detail in chapter 4. Chapter 4 includes new results not reported in the paper and also includes the implementation of a cohesive model.

Chapter 5 presents the strong discontinuity approach using the extended finite element method (X-FEM), it is concluded that a numerical problem exists using this method and subsequently an alternative approach to solve the problem is presented in chapter 6.

Finally, a computer program implementing the interface elements and elements with embedded discontinuities is presented in chapter 7. The user manual for the program is presented in appendix E, the program itself is provided as a CD-ROM in the same appendix.

Several other appendices are provided: appendix A consists in some notes in tensor analysis, this appendix provides the theoretical background and notation used throughout the text. The numerical solution schemes presented throughout the report are based on the arc-length control strategy for solving non-linear problems with finite elements; appendix B explains the theoretical framework for this solution.

Higher order theories are presented as a solution to the problem of localization and as a means of introducing length scale parameters into classical theories of mechanics. In appendix C some of these theories are reviewed, and simple elastic problems are solved by using these theories in appendix D.

Every chapter or appendix is a separate entity, the nomenclature is kept as constant as possible, the names of variables however, are explained in each chapter.

Bibliography

Alfaiate, J., Simone, A. & Sluys, L. J. (2003), 'Non-homogeneous displacement jumps in strong embedded discontinuities', *International Journal of Solids and Structures* **40**, 5799–5817.

Belytschko, T., Liu, w. K. & Moran, B. (2000), *Nonlinear finite elements for continua and structures*, John Wiley, New York.

Budiansky, B. (1974), Theory of buckling and post-buckling behavior of elastic structures, *in* 'Advances In Applied Mechanics', Vol. 14, Academic Press, Inc., pp. 1–65.

Cedolin, x. & Bažant, Z. P. (1991), *Theory of stability*, Engineering Mechanics Series, Mc.Graw-Hill Book Company, Singapore.

Hutchinson, J. W. (1974), Plastic buckling, *in* 'Advances In Applied Mechanics', Vol. 14, Academic Press, Inc., pp. 1 65.

Moës, N., Dolbow, J. & Belitschko, T. (1999), 'A finite element method for crack growth without remeshing', *Int. J. Numer. Meth. Engng.* **46**, 131–150.

Wells, G. N. & Sluys, L. J. (2001), 'A new method for modelling cohesive cracks using finite elements', *Int. J. Numer. Meth. Engng.* **50**, 2667–2682.

Chapter 2

Historical review

Contents

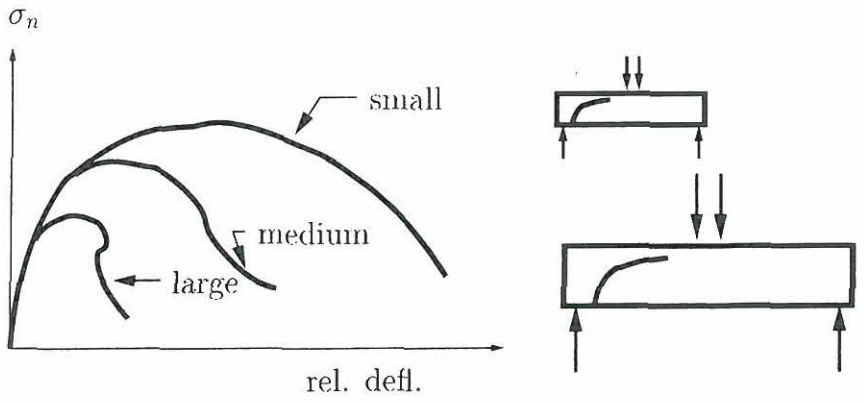

Figure 2.1: Load deflection diagrams of geometrically similar structures of different sizes

2.1 Introduction

Modeling the fracture and damage phenomena in quasi-brittle materials like concrete has proven to be a difficult task. Material failure processes manifest themselves as fracture process zones, shear (localization) bands, or discrete crack discontinuities. In the failure process of most materials, two phases can be identified: first, the localization of strains in small zones; later, during the loading process, integrity is completely lost and displacement discontinuities develop across planes in a material. All approaches to the problem have to take into account the following three characteristics that have been difficult to fulfill.

1. First, crack initiation depends on stresses, but the actual formation of cracks requires a certain energy, that means that energy criteria must be used.

2. Second, the calculations need to be objective. The results must not depend on subjective aspects such as the choice of coordinates, the choice of mesh, etc.

3. Third, the results must reflect the size effects. The size effect is defined through a comparison of geometrically similar structures of different sizes, and is normally characterized in terms of the nominal stress σ_n at maximum load. When the σ_n values of geometrically similar structures of different sizes are the same, we say that there is no size effect. A dependence of σ_n on the structure size (dimension) is called the size effect (ACI Committee 446 Fracture Mechanics 1992). The real case that exists is illustrated in figure 2.1. According to Carpinteri, Chiaia & Ferro (1997), the scaling properties of the concrete are due to their heterogeneous and disordered micro-structure, together with the competition between energy release due to micro-cracking and stress redistribution due, in turn, to progressive damage.

The analysis must also take into account the problem of localization. Strain localization is a notion describing a deformation mode in which the whole deformation of a specimen occurs in one or more narrow bands, while the rest of the

specimen usually exhibits unloading. Localization is a frequently encountered failure phenomenon in different materials and is considered as a precursor to discrete fracture. Localization is produced by material heterogeneity, which introduces local weakness and strong non-linear behavior, which is an instability triggering strain localization. As a result of the inhomogeneous deformation, a softening response at the structural level is observed (Pamin 1994).

Three main approaches exist for modeling cracking in quasi-brittle materials: the discrete crack model Ngo & Scordelis (1967), the smeared crack model Rashid (1968) and micro-mechanical models (Vonk, Rutten, van Mier & Fijneman 1991), (Van Mier, Vervuurt & Schlagen 1994). In the discrete model, when cracking is to be formed, new degrees of freedom are created and geometrical discontinuities are assumed to occur. In the smeared crack model, the crack process is lumped in the element considered. In micro-mechanical models, the continuum is replaced a priori by lattices of truss or beam elements, or alternatively, constitutive materials and interfaces between them are modeled separately.

In this document, focus is directed to a hybrid approach between the discrete and the continuum approach, the so-called strong discontinuity approach (Larsson, Runesson & Ottosen 1993) (Simo, Oliver & Armero 1993). The strong discontinuity approach will be compared to the classical discrete approach using interface elements. The strong discontinuities will be explored in the context of the extended finite element method (X-FEM) in the form described first by Belitschko & Black (1999) and used with cohesive models by Wells & Sluys (2001).

In the following parts of this review, the classical approaches to fracture will be considered until finally the strong discontinuity emerges.

2.2 Micro-mechanical models

In the micro-mechanical models, the constituents of the material are modeled separately and constitutive relations are formulated for the interface between them (Vonk et al. 1991), alternatively lattice models are employed

Lattice models for concrete were created by Van Mier et al. (1994) based on models originally created by physicists (Herrmann, Hansen & Roux 1989), (Hrennikoff 1941).

In this approach, the micro-structure of the material is mapped in a lattice of truss or beam elements by assigning them different properties in the case of concrete representing the grains and mortar.

The constitutive models used for modeling the mechanical behavior of materials have traditionally been derived following a phenomenological approach, without explicit considerations of the micro-structure of the material. Micro-structural mechanics approaches assuming the material to have an underlying micro-structure of lattice type have resulted in constitutive models of micro-polar type, see e.g. (Chang, Wang, Sluys & van Mier 2002*a*) and (Chang, Wang, Sluys & van Mier 2002*b*).

The micro-mechanical models can provide valuable insight into the failure mechanism at the micro-scale and their qualitative effect on macroscopic fracture. However, the large computational costs which result from the high level of detail render them less suitable for large-scale simulations.

2.3 Discrete models

In these models, material damage is represented by a macroscopic dominant crack.

The first discrete models for concrete are introduced by Clough (1962) and Ngo & Scordelis (1967). In this method, the cracking is assumed to occur as soon as the nodal force, (that is) normal to the element boundaries, exceeds the maximum tensile force that can be sustained. New degrees of freedom at that node location are created and a geometrical discontinuity is assumed to occur between the old node and the newly created node. In this form, the contribution of cracking to inelastic deformation is lumped into a discontinuity.

The discrete models have been improved by using re-meshing techniques (Ingraffea & Saouma 1985), (Carter, Ingraffea & Bittencourt 1995), (Camacho & Ortiz 1996) and the use of interface elements as predefined cracks.

First, linear elastic fracture mechanics is used to decide where and in which direction a crack will propagate, then a new mesh is formed in which the crack can propagate a certain distance. Linear elastic fracture mechanics analyses are carried out in this geometrically changed structure, and new propagation directions are decided. The process is repeated until complete failure occurs.

A major advance in concrete fracture was made in 1976 by Hillerborg, Modeer & Peterson (1976) who improved and adapted to concrete the cohesive zone model. They were inspired by the softening and plastic models of fracture process zone initiated in the works by Barenblatt (1959), Barenblatt (1962), and Dugdale (1960) and developed earlier for materials other than concrete by Rice (1968), Smith (1974), Knauss (1974) and Kfouri & Rice (1977).

The finite element analysis of concrete incorporating the cohesive zone model (also called the fictitious crack model) predicts a deterministic size effect. This conclusion was strengthened and the model further refined by Petersson (1981).

An alternative approach is the cohesive surface formulation of Xu & Needleman (1994) which has been used to model damage in brittle materials (Camacho & Ortiz 1996). The basic assumption of the cohesive surface framework is that the separation process is confined to a set of discrete planes. A constitutive model is then specified for each cohesive surface that allows separation to occur.

In a cohesive surface formulation, constitutive relations are specified independently for the bulk material and for one or more cohesive surfaces (usually in the form of a relation between surface tractions and displacement jumps across the cohesive surface), (Needleman 1987), (Xu & Needleman 1994). The bulk and cohesive constitutive relations together with appropriate balance laws and boundary conditions completely specify the problem. Fracture emerges as a natural outcome of the deformation process without introducing any additional failure criterion.

In the approach by (Rots 1988), interface elements of zero thickness are inserted into the finite element mesh at locations where a crack is expected to propagate. The non-linearity of the response is incorporated by the use of the fictitious crack concept, the process zone is concentrated in a fictitious extension of the actual physical crack. This fictitious crack can then transfer tractions with a magnitude related to the crack opening.

The discrete models are well suited for highly localized deformations, but not

so well suited for more distributed inelastic deformations which may take place in the early stages of failure. An additional problem arises if the cohesive surfaces are taken to have a non-zero initial compliance, the presence of the cohesive surfaces contributes to the overall compliance of the body. Then, if cohesive surfaces are added between all elements as the computational mesh is refined, the overall compliance depends on the mesh, and an ill-posed problem results. Introducing initially rigid surfaces like in (Camacho & Ortiz 1996) introduces other difficulties (Falk, Needleman & Rice 2001).

2.4 Continuum approaches

Rashid (1968) introduced the concept of smeared cracking.

In the smeared model, the contribution by cracking to the inelastic deformation is represented by cracking strain distributed over a finite volume. The material is then modeled as a continuum. Final fracture is represented by a zone in which the load-bearing capacity is completely lost.

After Rashid (1968), two major modifications to the smeared model were introduced: first, the shear retention factor introduced by Suidan & Schnobrich (1973); second, the replacement of the sudden stress drop upon crack initiation by a descending branch in the tensile stress-strain relation. By use of the descending branch the contribution of the stiffness of the concrete between the cracks in reinforced applications (tension-stiffening) is represented. Plain concrete also has some residual load-carrying capacity after reaching the tensile strength. It is concluded that the brittle models in concrete were then replaced by tension softening models.

With the softening models, better results could be obtained, however, when this softening is implemented using classical (local) constitutive models, the results are not objective.

Problems associated with the shear retention factor were discovered first by Cope, Rao, Clark & Norris (1980): the problem is that the principal stresses in a cracked integration point can rotate upon further loading due to the introduction of the shear retention factor. This rotation in the descending branch of the stress-strain curve can lead the strength in another direction than the one normal to the crack to exceed the tensile strength of the material if the crack is fixed. To avoid this problem, the rotating crack model was introduced by Cope et al. (1980).

The rotating and fixed crack models were redefined in the framework of continuum damage mechanics, these models were considered as special cases of anisotropic damage models (Mazars & Pijaudier-Cabot 1989), (Mazars & Pijaudier-Cabot 1996). A more comprehensive review of the continuum damage-based approaches is found in (De Borst 2002).

A new problem is addressed: finite element solutions to standard damage problems often do not seem to converge upon mesh refinement. They do converge to a solution, but this solution is physically meaningless. This is because continuum damage models presume a certain local homogeneity of the micro-structural damage distribution. The development of damage in these models is localized in a surface while the surrounding material is unaffected. This localization of damage is in contradiction with the supposed homogeneity of the damage field.

The use of tension softening models was accompanied by unphysical mesh sensitivity (Bažant 1976), (Crisfield 1982). Adapting the concept of the Fictitious Crack Model, (Bažant & Oh 1983) introduced the crack band model, in which the fracture energy introduced by Hillerborg was smeared out over the area in which the crack localizes (the width of one element). In one-dimensional finite elements, the inclusion of the Fictitious Crack Model becomes the global behavior insensitive to the mesh size. In two and three-dimensional cases, the response is not completely insensitive to the mesh size, this is because it is very difficult to estimate the value of the band width.

The Crack Band Model can yield reasonable solutions, but it does not resolve the fundamental difficulty resulting from the stress softening: when the classical (local) constitutive models are used to analyze problems in which localization occurs, it results in mesh dependent solutions. This is due to the lack of an internal length scale in the model. The mesh dependence is just a reflection of the real problem which is that beyond a certain level of damage accumulation, the governing set of partial differential equations locally changes type: in the static case there is loss of ellipticity, in the dynamic case the change is from hyperbolic to elliptic. The result is that the boundary value problem becomes ill-posed.

The reason of the change in type of equations comes from the fact that the force displacement relations measured in testing devices are simply mapped onto stress-strain curves by dividing the force and the elongation by the original load-carrying area and the original length of the specimen, respectively. This mapping is done without taking into account the changes in the micro-structure that occur when the material is so heavily damaged. Therefore, the mathematical description ceases to be a meaningful representation of the physical reality (De Borst 1997).

To overcome this deficiency, it is necessary to introduce a regularization technique, for example: introduction in the smeared model of additional terms in the continuum description which reflect the changes in the micro-structure that occur during fracture (enrichment of the continuum by higher-order terms), or, alternatively, taking into account the viscosity of the material. A few methods introducing higher-order theories are briefly discussed in the appendix C and some simple elastic problems are solved using higher-order theories in the appendix D.

The following regularization techniques have been proposed: use of non-local models (Bažant, Belytschko & Chang 1984), (Pijaudier-Cabot & Bažant 1987); use of gradient approaches (Aifantis 1984), (Schreyer & Chen 1986), (Lasry & Belytschko 1988), (Mühlhaus & Aifantis 1991), (De Borst & Muhlhaus 1992), (Pamin 1994), (Gutierrez & De Borst 1999); Cosserat models (Mühlhaus & Vardoulakis 1987), (De Borst 1991), (De Borst 1993); and rate-dependent models (Sluys 1992). Fundamental questions still remain unsolved for these models, for example: the role of the enhancement in crack modeling and the treatment of boundaries are not yet clarified (Peerlings, De Borst, Brekelmans & Geers 2002). All these models (i) introduce a length scale parameter, (ii) keep the mathematical problem well posed and (iii) remove mesh size and mesh-orientation dependence.

The size of the mesh needed, when regulariztion techniques are used, is defined by the length scale parameter (size of the localization zone), the constitutive equation for softening (shape of the localization zone), and the type of element (order of

interpolation) that is used.

The major disadvantage of these strategies is that the localization zone must be analyzed with a very fine mesh, which is impossible for the analyses of large structures. Another drawback is that at the later stages of failure, the continuum models are not able to reflect the development of discrete surfaces. Where a discrete surface should develop, the strain and strain rate approach to infinitum, leading to spurious spreading of inelastic deformations.

2.5 Embedded discontinuities

Embedded discontinuity models overcome the limitations of smeared and discrete crack models. By capturing a crack within an element it is effectively possible to model a discrete (or highly localized) phenomenon within a continuum framework.

Embedded discontinuities offer a hybrid approach between smeared and discrete modeling.

In the case of the discrete modeling, the need for re-meshing is a big disadvantage and mesh realignment procedures are difficult to implement (Larsson 1990). The re-meshing is not necessary when the discontinuity that represents the crack or the shear band is already incorporated in the shape functions of the finite element.

The weakness of the smeared models is their inherent dependency on element size and alignment when applied to softening materials. This deficiency can be solved by regularization techniques. The inclusion of a length scale sets the width of a localization band, making it independent of the mesh. The inclusion of a length scale also implies a level of observation at which the length scale is significant. The displacement field must be sufficiently well resolved to adequately represent variations in deformation at the level of the internal length scale. Then it is required to have a fine mesh within the localization zone in order to capture the high strain gradients.

With embedded discontinuities, the width of the failure zone is less than the width of a single element.

There are two classical versions of the embedded discontinuity model, the weak discontinuity approach (Ortiz, Leroy & Needleman 1987),
(Belytschko, Fish & Engelman 1988), (Sluys & Berends 1998), and the strong discontinuity approach (Simo et al. 1993), (Armero & Garikiparti 1995), (Lofti & Sheng 1995), (Larsson & Runesson 1996).

In the weak approach, a band is defined within the element where the strains are different (in magnitude) from the strains in the remainder of the element, the band is incorporated using a multi-field variational principle. Figure 2.2 illustrates a finite element with a weak discontinuity.

In the weak discontinuity approach, the displacement is continuous along the element. In the limiting case when the band width w approach for $w \rightarrow 0$, the strains locally attain the form of a Dirac function and the displacements become discontinuous over a single discrete plane, thus producing the strong discontinuity.

The weak discontinuity approach avoids the need to deal with unbounded strains as a result of the displacement jump, but the ability of such an element to overcome

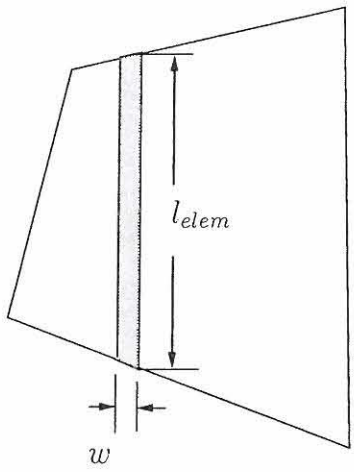

Figure 2.2: Embedded discontinuity in a finite element.

mesh alignment dependence (Sluys 1997) and to reproduce full crack separation in mode I type problems is questionable (Jirásek 1998).

In the strong discontinuity approach, additional discontinuous shape functions are added to an element in order to represent the deformations in conjunction with a specially constructed interpolation function that is used in calculating the internal force vector.

Dvorkin, Cutino & Gioia (1990) considered strong discontinuities by modifying the principle of virtual work. The kinematical concept of strong discontinuities has been proposed for the computational description of localization bands in terms of an interface discretization by Larsson et al. (1993). Lofti & Sheng (1995) extended the three-field Hu-Washizu variational statement for bodies with internal discontinuities. The displacement jump is incorporated into a finite element as an incompatible mode in the strain field (Dvorkin et al. 1990), (Klisinski, Runesson & Sture 1991), (Simo et al. 1993). Finally, a unified framework for analyzing strong discontinuities was put forth by Simo et al. (1993) based on the enrichment strain concept (Simo & Rifai 1990). A variational inconsistent formulation is used (which results in non-symmetric matrices irrespectively of the material model used), this approach leads to a variational formulation that is based on constant strain elements (Wells & Sluys 2001*c*).

Simo et al. (1993), Larsson & Runesson (1996), Armero & Garikipati (1996), (Wells & Sluys 2001*c*), Oliver (1996) and Oliver (1996) directly embedded strong discontinuities into the domain of a finite element based on the enhanced strain concept (Simo & Rifai 1990). These strategies were also applied to geometrically linear fluid saturated porous media by Larsson, Runesson & Sture (1996) and Steinmann & Betsch (2000). Borja (2000) presented a standard Galerkin formulation of the strong discontinuity approach and has shown its equivalence to assumed enhanced strain approximations. A comprehensive review and comparison of various embedded discontinuity approaches is provided by Jirásek (2000).

The element for strong discontinuities is then based on the fact that under certain conditions, continuum constitutive laws and unbounded strains are compatible

(Simo et al. 1993). This then allows strong discontinuities to be treated within a continuum framework. Through the use of regularized discontinuity jumps, conventional continuum relationships can be applied, avoiding the need to formulate discrete traction-displacement relationships. However, the application of a regularized displacement jump can lead to spurious behavior unique to embedded discontinuities, namely stress locking in the absence of significant rotation of the stress field (Wells & Sluys 2000).

The elements with strong discontinuities created in this way can easily be implemented into existing finite element codes, the additional modes can be statically condensed, providing the magnitude of the displacement jump.

The application of continuum constitutive laws in strong discontinuity analysis is based on the regularization of the displacement jump, resulting in a bounded, although fictional, strain field. In this respect, embedded models are lacking when compared to higher-order models where the strain field in the localized zone is an objective measure of deformation. However, the application of embedded discontinuities is intended for cases where the typical element size is significantly larger than the identifiable length scale of the material.

Wells & Sluys (2001*a*) found that as part of the formulation, it is required to have interpolations representing the bounded part of the enhanced strains, exact representation is required to avoid locking and to trigger the correct failure mode, this is practically impossible to achieve in the tree-dimensional case. In that form, the strong discontinuity is not effective in three dimensions for problems involving kinematic constraints. In three-dimensional analysis the crack pattern obtained is very diffuse, the sign of the loading function tends to oscillate during iterative processes, and the problem becomes more severe upon mesh refinement (Wells & Sluys 2001*c*).

2.6 Strong discontinuities in the context of X-FEM

Recently the Element Free Galerkin Method, a mesh-free method, has been successful in modeling static and dynamic fracture in two dimensions (Belytschko, Lu & Gu 1994), (Fleming, Chu, Moran & Belytschko 1997), and three dimensions (Sukumar, Moran, Black & Belytschko 1997). This approach is fundamentally different from previously proposed models based on incompatible strain modes.

The meshless methods are robust in solving crack tip problems, and this characteristic has attracted many researches (Belytschko, Krongauz, Organ, Fleming & Krysl 1996), (Strouboulis, Copps & Babuška 2001). However, meshless methods have the problem that imposing the boundary condition is difficult (Belytschko et al. 1996).

The idea of the partition of unity (Melenk & Babuška 1996) in the context of finite element analysis to embedded local solutions of boundary value problems was first exploited by Oden, Duarte & Zienkiewicz (1998) for problems with internal boundaries. The technique was called the 'Generalized Finite Element Method'.

The partition of unity via the Finite Element Method (FEM) makes use of the shape functions in the finite element method; it loses the benefit of meshlessness,

but it gains in robustness and versatility, because, it is easy to impose the boundary conditions.

The partition of unity finite element method is denominated extended finite element method (X-FEM) (Daux, Moës, Dolbow, Sukumar & Belytschko 2000). The approximation function in X-FEM is node based (nodal-cover-domain-based interpolation), while in FEM it is element based. Moës et al. (1999) and Belitschko & Black (1999) developed special X-FEM formulations that allow the user to construct enrichment functions which are independent of the geometry of the mesh. In X-FEM, element mesh is constructed in the usual way as in FEM, but individual cover domain comprises a patch of elements connected to nodes. The node base approximation function is then defined over its cover domain. In other words, each node has its influence domain extended over a patch of elements. Nodal-cover domains overlap each other. At an arbitrary location, the representative value is the sum of the influences from the overlapping cover domains.

A notable improvement and progress in discrete crack growth modeling without the need for re-meshing was conceived by Moës et al. (1999). The generalized Heaviside function was proposed as a means to model the crack away from the crack tip, with rules for the introduction of the discontinuities and crack-tip enrichments. The method has been used incorporating a cohesive model by Wells & Sluys (2001). Remmers, de Borst & Needleman (2003) extended the method to include continuous crack growth involving crack initiation at multiple locations and the subsequent growth and coalescence of the nucleated cracks. Fan, Liu & Lee (2004) embedded an analytical solution exactly describing the stress field around the crack tip in the element shape functions.

There are no restrictions on allowable element types and displacement jumps are continuous across element boundaries. The displacement jump is added by extending the basis of the underlying finite element interpolation. Functions with displacement jumps are added selectively to the support of individual nodes in order to model a propagation discontinuity. A single field (displacement) variational principle is used to obtain the discrete equations.

Resuming: The extended finite element method alleviates shortcomings associated with meshing of the crack surfaces in existing methods. The finite element method is used as the building block in the extended finite element method. The finite element approximation is enriched by additional functions through the notion of partition of unity (Melenk & Babuška 1996). For crack modeling, a discontinuous function (Generalized Heaviside step function) and the two-dimensional linear elastic asymptotic crack tip displacements fields are used to account for the crack.

In X-FEM, the additional functions are used to model the presence of cracks (also voids and inhomogeneities), as well as to improve accuracy in problems where some aspects of functional behavior of the solution field is known a priori. For crack modeling, a discontinuous function and the two-dimensional asymptotic crack-tip displacement fields are added to the displacement-based finite element approximation.

Compared with the enhanced modes method, this method is variationally consistent. The displacement jumps are continuous across element boundaries and the interpolation of the jump can be of any polynomial order. The symmetry of the tan-

gent stiffness matrix is conserved if the material tangent matrix is symmetric. The method can be implemented with any underlying base element. It is also possible to extend cohesive cracks in arbitrary directions independently of the structure of the finite element mesh. When cohesive surfaces are added during calculation, there is no need for a high initial stiffness to minimize the effect of increasing the initial compliance of the medium due to the presence of cohesive surface elements.

The extended finite element method alleviates much of the burden associated with mesh generation by not requiring the finite element mesh to conform to cracks. The essence of the X-FEM lies in subdividing a model problem into two distinct parts: mesh generation for the geometric domain (cracks not included), and enrichment of the finite element approximation by additional functions that model the flaws and other geometrical entities.

The crack is modeled by enriching the nodes whose nodal shape function supports intersect the interior of the crack by a discontinuous function, and enriching the nodes whose nodal shapes function supports intersect the crack front (crack tip) by the two-dimensional asymptotic crack tip fields.

It has been found that it is, however, essential to use a fine mesh in regions where stress gradients are high in order to accurately calculate the normal vector to the discontinuity path (Wells & Sluys 2001).

The advantages in this method come at the cost of increased complexity in implementation since extra global degrees of freedom are required during the calculation and the integration scheme must be adapted in the elements.

The procedure is computationally efficient, since only a relatively small number of the total number of nodes need to be enhanced. A crucial advantage over interface elements is that deformations at the discontinuity are purely inelastic.

In chapter 5 numerical problems that arise with the use of the formulation based on X-FEM are reported. These problems can be avoided by using an alternative approach to embed the strong discontinuities; this new approach is based on the work presented by Alfaiate et al. (2003) and here it is derived in chapter 6. The alternative formulation is based on the principle of virtual work considering the kinematics of the strong discontinuity.

2.7 Concluding remarks

Different approaches to model the fracture and damage of quasi-brittle materials were presented. This historical review is not complete, however, only the main models that have been used in connection with finite element analysis are presented.

The approaches considered here were: the micro-mechanical model, the discrete model, the continuum approach, and, finally, the embedded discontinuity approach. In relation to embedded discontinuities, only the embedded strong discontinuities were considered in this document.

The micro-mechanical models were not considered in detail here, they are suitable to model the behavior at the micron-scale, but, unfortunately, they have a large computational cost, which made them impractical for studying large structural components.

The discrete analysis is probably the best choice if the path of the macroscopic dominant crack is known in advance; in that case, this method has proved to be efficient and reliable. The discrete model loses part of its efficiency if re-meshing is required. The method is used in combination with cohesive models e.g. (Needleman 1987).

The continuum approach or smeared crack model based on classical (local) theories of mechanics produces results that are not objective and have a lack of convergence. In order to solve the problem of using smeared models, introduction of length scale parameters into the formulation is required. This is done by use of regularization techniques, for example by using higher-order theories. A drawback of these methods is that a fine mesh is required. The size of the elements must be chosen in order to adequately represent variations in deformation at the level of the internal length scale.

The embedded discontinuities approach is a hybrid between the continuum and the discrete approaches. A framework for this method is based on the enrichment strain concept (Simo et al. 1993), where a variational inconsistent formulation is used. The method has been used successfully, but problems related with stress locking and difficulties to obtain the crack path in three-dimensional analysis are reported (Wells & Sluys 2000), (Wells & Sluys 2001*a*).

Based on a completely different theory -the property of the partition of unity of the finite elements (Babuška & Melenk 1997)- Moës et al. (1999) embeds discontinuities into finite elements. This method can solve the problem without the stress locking observed in the incompatible mode approach at the cost, however, of increasing the complexity of the implementation.

The observation of numerical problems in the embedded cracks using the X-FEM method justifies the use of alternative procedures like the one presented by Alfaiate et al. (2003).

Bibliography

ACI Committee 446 Fracture Mechanics (1992), Fracture mechanics of concrete: Concepts, models and determination of material properties, *in* Z. P. Bažant, ed., 'Fracture mechanics of concrete structures', pp. 3 140.

Aifantis, E. C. (1984), 'On the microstructural origin of certain inelastic models', *J. Eng. Mater. Technol.* **106**, 326–330.

Alfaiate, J., Simone, A. & Sluys, L. J. (2003), 'Non-homogeneous displacement jumps in strong embedded discontinuities', *International Journal of Solids and Structures* **40**, 5799–5817.

Armero, F. & Garikiparti, K. (1995), Recent advances in the analysis and numerical simulation of strain localization in elastic solids, Pineridge Press, Barcelona, Spain, pp. 547–561.

Armero, F. & Garikipati, K. (1996), 'An analysis of strong discontinuities in multiplicative finite strain plasticity and their relation with the numerical simulation of strain localization in solids', *Int. J. Solids Structures* **33**(20–22), 2863–2885.

Babuška, I. & Melenk, J. M. (1997), 'The partition of unit method', *Int. J. Numer. Meth. Engng.* **40**, 727 758.

Barenblatt, G. I. (1959), 'The formation of equilibrium cracks in brittle fracture. general ideas and hypothesis, axially symmetric cracks', *Prikl Mat Mekh* **23**(3), 434 444.

Barenblatt, G. I. (1962), 'The mathematical theory of equilibrium cracks in brittle fracture', *Adv Appl Mech* **7**, 55–129.

Bažant, Z. P. (1976), 'Instability, ductility and size effect in strain softening concrete', *ASCE J. Engng. Mech.* **102**, 144 331.

Bažant, Z. P., Belytschko, T. B. & Chang, T. (1984), 'Continuum model for strain softening', *ASCE J. Engng Mechanics Division* **110**, 1666–1692.

Bažant, Z. P. & Oh, B. (1983), 'Crack band theory for fracture of concrete', *RILEM Materials and structures* **16**, 155 177.

Belitschko, T. & Black, T. (1999), 'Elastic growth in finite elements with minimal remeshing', *Int. J. Numer. Meth. Engng.* **45**, 601–620.

Belytschko, T., Fish, J. & Engelman, B. E. (1988), 'A finite element with embedded localization zones', *Comput. Methods Appl. Mech. Engrg.* **70**, 59 89.

Belytschko, T., Krongauz, Y., Organ, D., Fleming, M. & Krysl, P. (1996), 'Meshless methods: An overview and recent developments', *Comput. Methods Appl. Mech. Engrg.* **139**, 3–47.

Belytschko, T., Lu, Y. Y. & Gu, L. (1994), 'Element-free galerkin methods', *International Journal for Numerical Methods in Engineering* **37**, 229 256.

Borja, R. I. (2000), 'A finite element model for strain localization analysis of strongly discontinuous fields based on standard galerkin approximation', *Comput. Methods Appl. Mech. Engng.* **190**, 1529–1549.

Camacho, G. T. & Ortiz, M. (1996), 'Computational modeling of impact damage in brittle materials', *Internat. J. Solids Structures* **33**, 2899 2938.

Carpinteri, A., Chiaia, B. & Ferro, G. (1997), 'A new explanation for size effects on the flexural strength of concrete', *Magazine of Concrete Research* **49**(178), 45 53.

Carter, B., Ingraffea, A. & Bittencourt, T. N. (1995), Topology-controlled modelling of linear and nonlinear 3d crack propagation in geomaterials, *in* 'Fracture of Brittle, Disordered Material', E and FN Spon, London, pp. 301 318.

Chang, C. S., Wang, T. K., Sluys, L. J. & van Mier, J. G. M. (2002*a*), 'Fracture modelling using a micro-structural mechanics approach-i. theory and formulation', *Engineering Fracture Mechanics* **69**, 1941–1958.

Chang, C. S., Wang, T. K., Sluys, L. J. & van Mier, J. G. M. (2002*b*), 'Fracture modelling using a micro-structural mechanics approach-ii. finite element analysis', *Engineering Fracture Mechanics* **69**, 1959–1976.

Clough, R. W. (1962), Stress distribution of norfolk dam, Technical report, Department of Civil Engineering, University of California, Berkeley.

Cope, R. J., Rao, P. V., Clark, L. A. & Norris, P. (1980), Modelling of reinforced concrete behavior for finite element analysis of bridge slabs, *in* C. Taylor, E. Hinton & D. Owen, eds, 'Numerical methods for nonlinear problems', Swansea: Pineridge Press, pp. 457–470.

Crisfield, M. A. (1982), 'Local instabilities in the non-linear analysis of of reinforced concrete beams and slabs', *Proc. Instn. Civ. Engnrs. Part 2* **73**, 135–145.

Daux, C., Moës, N., Dolbow, J., Sukumar, N. & Belytschko, T. (2000), 'Arbitrary cracks and holes with the extended finite element method', *International Journal for Numerical Methods in Engineering* **48**(12), 1741–1760.

De Borst, R. (1991), 'Simulation of strain localization:a repraisal of the cosserat continuum', *Engineering Computations* **8**, 317–332.

De Borst, R. (1993), 'A generalisation of j2-flow theory for polar continua', *Computer Methods in Applied Mechanics and Engineering* **103**, 347 362.

De Borst, R. (1997), 'Some recent developments in computational modelling of concrete fracture', *Int. J. Fracture* **86**, 5 36.

De Borst, R. (2002), 'Fracture in quasi-brittle materials: a review of continuum damage-based approaches', *Engineering Fracture Mechanics* **69**, 95–112.

De Borst, R. & Muhlhaus, H. B. (1992), 'Gradient dependent plasticity: Formulation and algorithmic aspects', *Int. J. Num. Meth. Eng.* **35**, 521 539.

Dugdale, D. S. (1960), 'Yielding of steel sheets containing slits', *J. Mech. Phys. Solids* **8**, 100–108.

Dvorkin, E. N., Cutino, A. M. & Gioia, J. (1990), 'Finite-elements with displacement interpolated embbeded localization lines insensitive to mesh size and distortions', *International Journal for Numerical methods in Engineering* **3**(3), 541–564.

Falk, M. L., Needleman, A. & Rice, J. (2001), 'A critical evaluation of cohesive zone models of dynamic fracture', *Journal de Physique IV* **11 Pr5**, 43 50.

Fan, S. C., Liu, X. & Lee, C. K. (2004), 'Enriched partition-of-unity finite element method for stress intensity factors at crack tips', *Computers and structures* **82**, 445 461.

Fleming, M., Chu, Y., Moran, B. & Belytschko, T. (1997), 'Enriched element free galerkin methods for crack tip fields', *International Journal for numerical methods in engineering* **40**, 1483 1504.

Gutierrez, M. A. & De Borst, R. (1999), 'Deterministic and stochastic analysis of size effects and damage evolution in quasi-brittle materials', *Archive of Applied Mechanics* **69**, 665 676.

Herrmann, H. J., Hansen, H. & Roux, S. (1989), 'Fracture of disordered, elastic lattices in two dimensions', *Physical review B* **39**, 637–648.

Hillerborg, A., Modeer, M. & Peterson, P. E. (1976), 'Analysis of crack propagation and crack growth initiation in brittle solids', *Cement and Concrete Research* **6**, 773–782.

Hrennikoff, A. (1941), 'Solution problems of elasticity by the framework method', *J. of applied mechanics* **12**, 169–175.

Ingraffea, A. R. & Saouma, V. (1985), Numerical modelling of discrete crack propagation in reinforced and plain concrete, *in* 'Fracture mechanics of concrete', Martinus Nijhoff Publishers, Dordrecht, pp. 171–225.

Jirásek, M. (1998), Finite elements with embedded cracks, technical report lsc, Technical Report Internal report 98/01, Ecole Polytechnique Fedderale de Lausanne, Switzerland.

Jirásek, M. (2000), 'Comparative study on finite elements with embedded discontinuities', *Comput. Methods Appl. Mech. Engrg.* **188**, 307 330.

Kfouri, A. P. & Rice, J. R. (1977), Elastic-plastic separation energy rate for crack advance in finite growth steps, *in* D. Taplin, ed., 'Fracture 1977 (Proceedings, 4th International conference on fracture, ICF4, Waterloo)', Vol. 1, University of Waterloo, Ontario, Canada, pp. 43–59.

Klisinski, M., Runesson, K. & Sture, S. (1991), 'Finite elements with inner softening band', *ASCE Journal of Engineering Mechanics* **117**(3), 575–587.

Knauss, W. C. (1974), 'On the steady propagation of a crack in a viscoelastic plastic solid', *J.Appl. Mech. ASME* **41**(1), 234–248.

Larsson, R. (1990), Numerical simulation of plastic localization, PhD thesis, Chalmers University of Technology, Götcborg.

Larsson, R. & Runesson, K. (1996), 'Element-embedded localization band based on regularized strong discontinuity', *J. Engnr. Mech. ASCE* **122**, 402–411.

Larsson, R., Runesson, K. & Ottosen, N. S. (1993), 'Discontinuous displacement aproximations for capture plastic localization', *Int. J. Num. Meth. Engnr.* **36**, 2087 2105.

Larsson, R., Runesson, K. & Sture, S. (1996), 'Embedded localization band in undrained soil based on regularized strong discontinuity-theory and fe-analysis', *Int. J. Solids Structures* **33**(20–22), 3081–3101.

Lasry, D. & Belytschko, T. B. (1988), 'Localization limiters in transient problems', *Int. J. Solids and Structures* **24**, 581–597.

Lofti, H. & Sheng, P. B. (1995), 'Embedded representation of fracture in concrete with mixed finite elements', *Int. J. for Numerical Methods in Engineering* **38**, 1307–1325.

Mazars, J. & Pijaudier-Cabot, G. (1989), 'Continuum damage theory-aplication to concrete', *ASCE J. Engng Mech* **115**, 345–365.

Mazars, J. & Pijaudier-Cabot, G. (1996), 'From damage to fracture mechanics and conversely: a combined approach', *Int. J. Solids Structures* **33**(20–22), 3327–3342.

Melenk, J. M. & Babuška, I. (1996), 'The partition of unity finite element method: Basic theory and applications', *Comput. Methods Appl. Mech. Engrg.* **139**, 289 314.

Moës, N., Dolbow, J. & Belitschko, T. (1999), 'A finite element method for crack growth without remeshing', *Int. J. Numer. Meth. Engng.* **46**, 131–150.

Mühlhaus, H. B. & Aifantis, E. C. (1991), 'A variational principle for strain gradient plasticity', *Internat. J. solids structures* **28**(7), 845–857.

Mühlhaus, H. B. & Vardoulakis, I. (1987), 'The thickness of shear bands in granular materials', *Geotechnique* **37**, 271 283.

Needleman, A. (1987), 'A continuum model for void nucleation by inclusion debonding', *Journal of Applied Mechanics* .

Ngo, D. & Scordelis, A. C. (1967), 'Finite element analysis of reinforced concrete beams', *Journal of the American Concrete Institute* **64**, 152–163.

Oden, J. T., Duarte, C. A. & Zienkiewicz, O. C. (1998), 'A new cloud-based hp finite element method', *Computer methods in applied mechanics and Engineering* **153**(1–22), 117–126.

Oliver, J. (1996*a*), 'Modelling strong discontinuities in solid mechanics via strain softening constitutive equations. part 1: Fundamentals', *International Journal for Numerical Methods in Engineering* .

Oliver, J. (1996*b*), 'Modelling strong discontinuities in solid mechanics via strain softening constitutive equations. part 2: Numerical simulation', *International Journal for Numerical Methods in Engineering* .

Ortiz, M., Leroy, Y. & Needleman, A. (1987), 'A finite element method for localized failure analysis', *Comp. Meth. Appl. Mech. Eng.* **61**, 189 214.

Pamin, J. K. (1994), Gradient dependent plasticity in numerical simulation of localization phenomena, PhD thesis, Technische Universiteit Delft.

Peerlings, R. H. J., De Borst, R., Brekelmans, W. A. M. & Geers, M. G. D. (2002), 'Localization issues in local and nonlocal continuum approaches to fracture', *European Journal of Mechanics A/Solids* **21**, 175–189.

Petersson, P. (1981), Crack growth and development of fracture zones in plain concrete and similar materials, Technical Report TVBM-1006, Division of building materials, Lund Institute of Technology, Lund, Sweden.

Pijaudier-Cabot, G. & Bažant, Z. P. (1987), 'Non-local damage theory', *Journal of Engineering Mechanics* **113**(10), 1512 1533.

Rashid, Y. R. (1968), 'Analysis of prestressed concrete pressure vessels', *Nuclear Engineering and Design* **7**(4), 334–355.

Remmers, J. J. C., de Borst, R. & Needleman, A. (2003), 'A cohesive segments method for the simulation of crack growth', *Computational mechanics* **31**(1 2), 69–77.

Rice, J. (1968), Mathematical analysis in the mechanics of fracture, *in* H. Liebowitz, ed., 'Fracture an advanced treatise', Vol. 2, Academic Press, pp. 191 308.

Rots, J. G. (1988), Computational modelling of concrete fracture, PhD thesis, Delft University of Technology, Delft.

Schreyer, H. L. & Chen, Z. (1986), 'One-dimensional softening with localization', *J. Appl. Mech.* **53**, 791 797.

Simo, J. C., Oliver, J. & Armero, F. (1993), 'An analysis of strong discontinuities induced by strain-softening in rate-independent inelastic solids', *Comp. Mech.* **12**, 277–296.

Simo, J. c. & Rifai, M. S. (1990), 'A class of mixed assumed strain methods and the method of incompatible modes', *International Journal for Numerical Methods in Engineering* **29**, 1595–1638.

Sluys, L. J. (1992), Wave propagation, Localization and Dispersion in Softening Solids, PhD thesis, Deltf University of Technology, Deltf.

Sluys, L. J. (1997), Discontinuous modelling of shear banding, *in* D. Owen, E. Onate & E. Hinton, eds, 'Computaional plasticity, fundamentals and applications', CIMNE, Barcelona, Spain, pp. 735–744.

Sluys, L. J. & Berends, A. H. (1998), 'Discontinuous failure analysis for mode-i and mode-ii localization problems', *Int. J. Solids Structures* **35**, 4257–4274.

Smith, E. (1974), 'The structure in the vicinity of a crack tip: a general theory based on the cohesive crack model', *Engng Fract Mech* **6**, 213 222.

Steinmann, P. & Betsch, P. (2000), 'A localization capturing fe-interface based on regularized strong discontinuities at large inelastic strains', *nternational Journal of Solids and Structures* **37**, 4061 4082.

Strouboulis, T., Copps, K. & Babuška, I. (2001), 'The generalized finite element method', *Comput. Methods appl. Mech. Engrg.* **190**, 4081 4193.

Suidan, M. & Schnobrich, W. C. (1973), 'Finite element analysis of reinforced concrete', *ASCE J. Struct. Div.* **99**, 2109–2122.

Sukumar, N., Moran, B., Black, T. & Belytschko, T. (1997), 'An element-free galerkin method for three-dimensional fracture mechanics', *Computational Mechanics* **20**, 170 175.

Van Mier, J. G. M., Vervuurt, A. & Schlagen, E. (1994), Boundary and size effects in uniaxial tensile tests: a numerical and experimental study, *in* 'Fracture and damage in quasibrittle structures', E and F Spon, London, pp. 289 302.

Vonk, R. A., Rutten, H. S., van Mier, J. G. M. & Fijneman, H. J. (1991), Micromechanical simulation of concrete softening, *in* J. G. van Mier, J. G. M. Rots & A. Bakker, eds, 'Fracture processes in concrete, rock and ceramics, Proc. Int. RILEM-ESIS conf.', Champan and Hall, London, pp. 129–138.

Wells, G. N. & Sluys, L. J. (2000), 'Application of embedded discontinuities for softening solids', *Engineering Fracture Mechanics* **65**, 263–281.

Wells, G. N. & Sluys, L. J. (2001*a*), 'Analysis of slip planes in three-dimensional solids', *Comput. Methods Appl. Mech. Engrg.* **190**, 3591 3606.

Wells, G. N. & Sluys, L. J. (2001*b*), 'A new method for modelling cohesive cracks using finite elements', *Int. J. Numer. Meth. Engng.* **50**, 2667–2682.

Wells, G. N. & Sluys, L. J. (2001*c*), 'Three-dimensional embedded discontinuity model for brittle fracture', *International Journal of Solids and Structures* **38**, 897–913.

Xu, X. & Needleman, A. (1994), 'Numerical simulations of fast crack growth in brittle solids', *Journal of the Mechanics and Physics of Solids* **42**, 1397–1434.

Chapter 3

An analysis of Fiber Pull-Out in Fiber Reinforced Concrete

Contents

Cifuentes, G., Needleman, A. and Byskov, E.

An Analysis of Fiber Pull-Out in Fiber Reinforced Concrete

G. Cifuentes[1], A. Needleman[2] and E. Byskov[1]
[1]**Department of Building Technology and Structural Engineering, University of Aalborg, DK-9000 Aalborg, Denmark**
[2]***Division of Engineering, Brown University, Providence, RI***

Abstract

Pull-out of a fiber from a concrete matrix is analyzed numerically. The concrete matrix and the steel fiber are modeled as linear elastic materials while the frictional resistance between the fiber and the matrix is characterized by a rate- and state-dependent frictional constitutive relation. The calculations are carried out within a two-dimensional plane strain framework and are restricted to small amounts of sliding. The fiber geometry and material and frictional properties are chosen to model the configurations studied experimentally by Weiler & Grosse (1996). A particular focus is set upon the difference in response between straight and hooked fibers. Parameter studies are then undertaken to investigate the effects of clamping pressure, inclination of the pull-out force and the fiber hook.

Keywords: C: Pull-Out Strength
C: Finite Element Analysis
E: Fiber Reinforcement
E: Modeling
C: Fracture Toughness

3.1 Introduction

In Fiber Reinforced Concrete (FRC) fibers are added to the cementitious matrix. The role of these fibers consists in providing bridging forces across crack faces, increasing the energy required for crack propagation, thus enhancing toughness. Indeed, because of the significance of fiber pull-out in a wide variety of fiber reinforced materials, there is a large amount of literature on the subject involving both experimental and modeling studies, e.g. McCartney (1987), Budiansky, Hutchinson & Evans (1986), Hutchinson & Jensen (1990), Cox (1993), Freund (1992), Povirk & Needleman (1993), Chanvillard & Aitcin (1996), Cox, Sridhar & Beyerlin (2001), Sridhar, Yang & Cox (2003) and several others.

Analyses of fiber pull-out have generally considered straight fibers with the pull-out force applied parallel to the fiber axis. In order to increase the pull-out resistance and dissipation, fibers with shapes deviating from the common straight shape have been developed. In particular, here we focus attention on hooked fibers. In addition, in a concrete matrix the fibers are randomly oriented. As a result of that, the pull-out force has a component oblique to the fiber axis.

Friction between the fiber and the matrix is generally characterized in terms of Coulomb friction, e.g Ballarini, Ahmed & Mullen (1990), Mital & Chamis (1991), Kumar & Reddy (1996), Li & Mobasher (1998). However, there are significant limitations in the Coulomb characterization of friction. The analyses of Renardy (1992) and Adams (1995) show that sliding along interfaces between elastic solids is unstable to periodic perturbations for a wide range of friction coefficients and material properties. As a consequence, such problems are ill-posed, leading to a lack of convergence in numerical computations. In addition, rate dependent features seen in some fiber pull-out experiments are not captured by the rate independent Coulomb description but can be so by a rate- and state-dependent frictional law (Povirk & Needleman 1993).

Here, analyses of a two-dimensional plane strain fiber pull-out test are carried out with the fiber-matrix interface characterized by a a modified Dieterich-Ruina friction law, see (Dieterich 1979) , (Rice & Ruina 1983) and Povirk & Needleman (1993).

In the study carried out here, the matrix as well as the fiber are considered as elastic bodies in plane strain allowing for the study of non-straight fibers and loads with components in the crack plane.

In the first part of the paper, the frictional models are introduced. In the second part, the finite element implementation is presented. In the third part, results of analyses of pull-out tests are discussed.

3.2 Problem Formulation

The boundary value problem analyzed is a two-dimensional plane strain model of the pull-out of a steel fiber from a concrete matrix. As sketched in figure. 3.1, a single steel fiber embedded in a concrete matrix is considered. Both the steel fiber and the concrete matrix are taken to be isotropic linear elastic materials. The interface between the fiber and the surrounding matrix is characterized by a rate

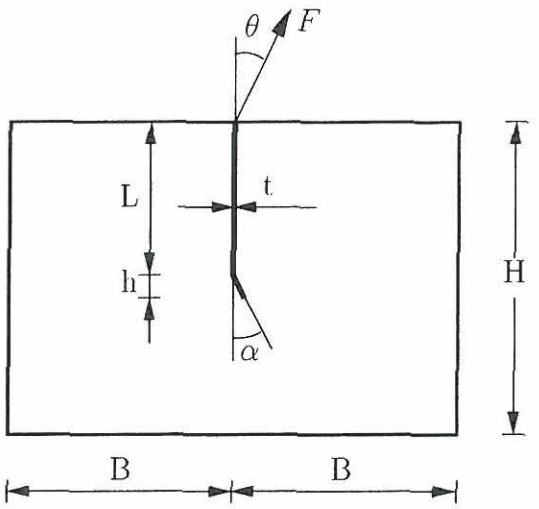

Figure 3.1: Single fiber embedded in a concrete matrix.

and state friction law as specified subsequently in Section 3.3. Geometry changes are neglected. In addition to restricting attention to small displacement gradients, in the present context, neglecting geometry changes also restricts the analyses to small amounts of sliding. The analyses are carried out incrementally and the rate principle of virtual work is written as:

$$\int_V \dot{\delta} dV + \int_{S_i} \dot{\mathbf{t}} \delta \dot{\mathbf{u}} dS = \int_{S_e} \dot{\mathbf{t}} \delta \dot{\mathbf{u}} dS \tag{3.1}$$

where denotes the stress tensor, denotes the strain tensor, $\mathbf{t} = \cdot\mathbf{n}$ is the traction vector, with $\mathbf{n}$ the normal surface, and an overdot ($\dot{}$) signifies rates. Furthermore, V is the volume of the body, S_e is the external surface of the body and S_i the interface surface.

The boundary conditions used in the finite element analysis on the region analyzed are shown in figure 3.2. For the symmetric case $u_1 = 0$ for $x_1 = 0$ and $u_2 = 0$ for $x_2 = 0$. In the non-symmetric case: $u_1 = 0$ only in the node located at the origin and $u_2 = 0$ for $x_2 = 0$. Where x_1 and x_2 define a Cartesian system of coordinates with the associated displacements u_1 and u_2.

The load is applied as nodal loading in the nodes corresponding to the top of the fiber.

3.3 Friction Law

The frictional constitutive relation used is the same one as that in Povirk & Needleman (1993), which is based on the work by Ruina (1981) and Rice & Ruina (1983). The constitutive relations for the friction have the following features: (i) an instantaneous increase in the coefficient of friction in response to a step increase in the rate of sliding; (ii) a subsequent decrease to a steady state value of the coefficient of friction, which is a decreasing function of the rate of sliding; and (iii) the approach to the steady state occurs over a characteristic distance that is independent of the rate of sliding.

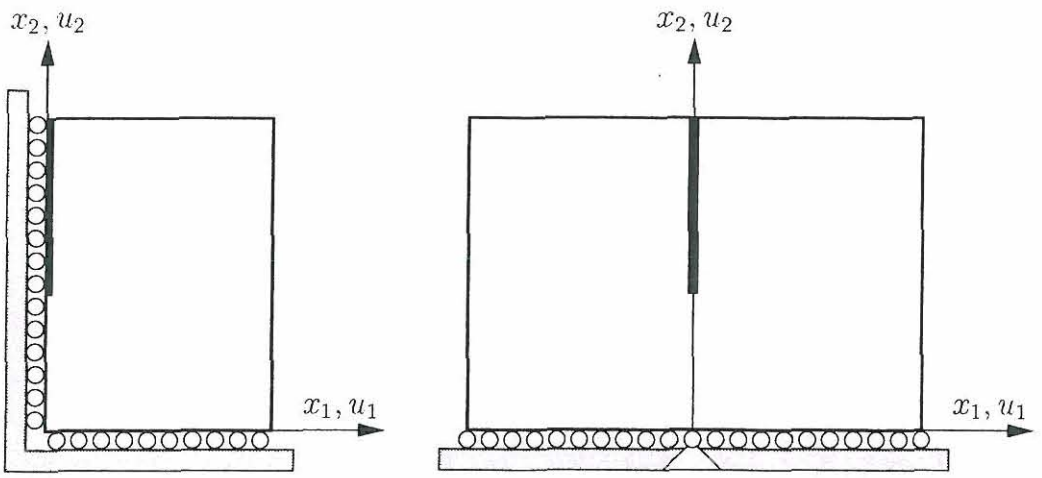

Figure 3.2: Boundary conditions for (a) symmetric and (b) non-symmetric cases.

The coefficient of friction μ is defined as $-|t_s|/t_n$ for $t_n < 0$, where t_s and t_n are the shear and normal tractions, respectively. It is assumed that μ can be written as:

$$\mu = g(\theta) f(\dot{q}) \tag{3.2}$$

where $\dot{q}$ is the rate of sliding, and θ is an internal variable that characterizes the state of contact between the two surfaces, $\theta = \infty$ represents the highest contact quality and $\theta = 0$ represents the lowest contact quality.

The functions f and g are:

$$f(\dot{q}) = \left(\frac{\dot{q}}{\dot{q}_0} + 1 \right)^{1/m} \tag{3.3}$$

$$g(\theta) = \left(\mu_d + (\mu_s - \mu_d) \exp\left[- (d_c/\theta \dot{q}_1)^p \right] \right) (d_c/\theta \dot{q}_0 + 1)^{-1/m} \tag{3.4}$$

where μ_s, μ_d, m, p, $\dot{q}_0$, $\dot{q}_1$, d_c and $\dot{\theta}_0$ are constants.

The evolution equation for the internal variable θ is chosen as:

$$\dot{\theta} = \dot{\theta}_0 \left(1 - \frac{\theta \dot{q}}{d_c} \right) \tag{3.5}$$

The following definitions of normal $\dot{q}_n$ and tangential rate sliding $\dot{q}_s$, rate normal traction $\dot{t}_n$, and rate of tangential traction $\dot{t}_s$ are used:

$$\begin{aligned} \dot{q}_n &= \mathbf{n} \cdot \dot{\mathbf{u}}, \quad \dot{q}_s = \mathbf{s} \cdot \dot{\mathbf{u}} \\ \dot{t}_n &= \mathbf{n} \cdot \dot{\mathbf{t}}, \quad \dot{t}_s = \mathbf{s} \cdot \dot{\mathbf{t}} \end{aligned} \tag{3.6}$$

where $\mathbf{n}$ is the outward pointing unit normal of the interface, $\mathbf{s}$ is the corresponding tangential unit vector, $\dot{\mathbf{u}}$ is the vector of velocity and $\dot{\mathbf{t}}$ is the vector of rate tractions. The sliding rate is written as the sum of an elastic part and an inelastic part in a manner similar to the decomposition of strain rates in small-strain plasticity. An elastic stiffness is also assumed in the normal direction when the surfaces are in

contact, and finally it is assumed that the rate forces are zero if no contact exists. The traction rates are then:

$$\dot{t}_n = \begin{cases} C_n \dot{q}_n & \text{for } t_n < 0 \\ 0 & \text{for } t_n \geq 0 \end{cases} \tag{3.7}$$

$$\dot{t}_s = \begin{cases} C_s(\dot{q}_s - \text{sgn}(t_s))\dot{q} & \text{for } t_n < 0 \\ 0 & \text{for } t_n \geq 0 \end{cases} \tag{3.8}$$

where C_n and C_s are the normal and tangential elastic stiffnesses associated with the interface, respectively.

Solving for $\dot{q}$ the relations (3.2), (3.3) and (3.4) gives:

$$\dot{q} = \begin{cases} \dot{q}_0 \left[(|t_s| - t_n g(\theta))^m - 1 \right] & \text{for } (|t_s| - t_n g(\theta)) > 1 \\ 0 & \text{for } (|t_s| - t_n g(\theta)) \leq 1 \end{cases} \tag{3.9}$$

3.4 Finite Element Implementation

The rate contribution of an interface element to the virtual work relation (3.1) is given by

$$\int_{S_i} \dot{\mathbf{t}} \delta \dot{\mathbf{u}} \, dS = \delta \dot{\mathbf{v}}^T \int_{S_i}^T \mathbf{D}\mathbf{B} \, dS \dot{\mathbf{v}} + \delta \dot{\mathbf{v}}^T \int_{S_i}^T \dot{\mathbf{R}} \, dS \tag{3.10}$$

where $\mathbf{v}$ is the displacement vector, $\mathbf{D}$ is the material tangent matrix, $\mathbf{R}$ is the vector of nodal forces produced by the friction, and is the matrix relating the displacement jump across the matrix-fiber interface to the nodal displacements via

$$\mathbf{q} = \begin{bmatrix} q_n \\ q_s \end{bmatrix} = \begin{bmatrix} u_n^u - u_n^l \\ u_s^u - u_s^l \end{bmatrix} = \mathbf{B}\mathbf{u} \tag{3.11}$$

where the super-indexes u or l in the displacements refer to the upper or lower sides of the interface element.

As described in Povirk & Needleman (1993) a rate time tangent modulus method, Peirce, Shih & Needleman (1984), is used to integrate the friction law. Between time increment m and $(m+1)$ $\dot{q}^{slip}$ is written as

$$\dot{q} = (1 - \gamma)\dot{q}_m + \gamma \dot{q}_{m+1} \tag{3.12}$$

where γ is an integration parameter.

Then, the contribution of an interface element to the tangent stiffness matrix $\mathbf{K}_t$ is:

$$_t = \int_{S_i}^T \mathbf{D}\mathbf{B} \, dS \tag{3.13}$$

and the contribution to the incremental nodal forces $\dot{\mathbf{f}}$ is:

$$\dot{} = - \int_{S_i}^T \dot{\mathbf{R}} \, dS \tag{3.14}$$

After the integration of the friction law, it is found that:

$$\mathbf{D} = \begin{bmatrix} C_n & 0 \\ -C_s^{tan}\mathrm{sgn}(t_s)\gamma\Delta t\partial\dot{q}\partial t_n C_n & C_s^{tan} \end{bmatrix} \tag{3.15}$$

and

$$\dot{\mathbf{R}} = \begin{bmatrix} 0 \\ -C_s^{tan}\mathrm{sgn}(t_s)\left[\dot{q}_m + \gamma\Delta t\partial\dot{q}\partial\theta\dot{\theta}\right] \end{bmatrix} \tag{3.16}$$

From (3.7), (3.8), (3.9) and (3.12) in matrix form, the traction rates are given by

$$\begin{aligned} \dot{\mathbf{t}} = & \begin{bmatrix} C_n & 0 \\ -C_s^{tan}\mathrm{sgn}(t_s)\gamma\Delta t\partial\dot{q}\partial t_n C_n & C_s^{tan} \end{bmatrix} \begin{bmatrix} \dot{q}_n \\ \dot{q}_s \end{bmatrix} \\ & + \begin{bmatrix} 0 \\ -C_s^{tan}\mathrm{sgn}(t_s)\left[\dot{q}_m + \gamma\Delta t\partial\dot{q}\partial\theta\dot{\theta}\right] \end{bmatrix} \end{aligned} \tag{3.17}$$

3.4.1 Solution Procedure

Four node isoparametric quadrilateral elements are used for the concrete matrix and the steel fiber with 2×2 point Gaussian integration in each element. Along the fiber-matrix interface four node interface elements are used with four point Gaussian integration. Various finite element meshes are used. Figure 3.3 shows the finite element mesh used for the calculation with a fiber having a 45° hook. The thickness of the fiber is 0.8mm, and it is embedded 30mm in a block of concrete with $H = 55$mm and $B = 40$mm. The mesh consists of 1215 quadrilateral elements, 64 interface elements 1354 nodes and 2679 degrees of freedom. The discretization is refined around the fiber end with the smallest element being 0.45 mm by 0.54 mm.

The deformation history is obtained using the arc-length control strategy, see e.g. (Crisfield 1981) and (Crisfield 1991), including two simple modifications of the standard algorithm, which are due to the inclusion of rate forces that are dependent on displacements and time, and due to the explicit inclusion of time in the frictional constitutive law.

In the implementation, a linear relation between the load level λ and time is assumed. The increment in time is always taken as a positive number, corresponding to the slope of the curve λ vs. t in the value of λ considered.

The increment in load level is defined as $\Delta\lambda = \dot{\lambda}\Delta t$ and the corresponding increment in nodal displacements is $\Delta = \dot{\Delta}t$. The shape of the total external nodal forces are represented by the vector $\mathbf{q}_0$ and proportional loading is supposed such that:

$$\mathbf{q} = \lambda\mathbf{q}_0 \qquad \text{and} \qquad \frac{\partial\mathbf{q}}{\partial\lambda} = \mathbf{q}_0 \tag{3.18}$$

where $\mathbf{q}$ is the external load corresponding to the load level λ.

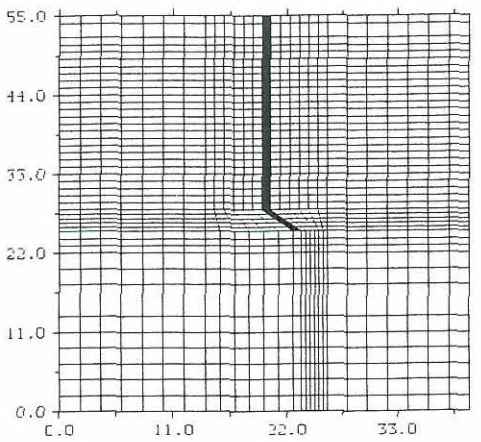

Figure 3.3: Finite elements used for a case with hooked ends.

The tangential displacement $\boldsymbol{\delta}_T$ is defined in the form:

$$\Delta = \Delta\lambda\boldsymbol{\delta}_T \tag{3.19}$$

Then it is required for (3.19) that:

$$\boldsymbol{\delta}_T = ^* \tag{3.20}$$

where is the tangent stiffness matrix, and the load * is defined as:

$$^* = \mathbf{q}_0 + \frac{\Delta t}{\Delta\lambda}. \tag{3.21}$$

The solution, disregarding the iterative part, proceeds in the following sequence for step i:

1. Compute $\Delta t = \Delta\lambda^{(i-1)}/\dot{\lambda}$ where $\dot{\lambda}$ is the slope of the curve load level vs. time.
2. Compute $\dot{\mathbf{R}}$, , and * using the values of variables resulting from step $(i-1)$.
3. Compute the tangential displacement resulting from (3.20).
4. Compute $\Delta\lambda$ by using:

$$\Delta\lambda = \pm\frac{\Delta l}{\sqrt{\boldsymbol{\delta}_T^T\boldsymbol{\delta}_T + \psi^{2*T*}}} \tag{3.22}$$

where the sign depends on the traced branch of the loading path, Δl is the radius of the spherical hyper-surface in the space $(\lambda, \mathbf{u})$, and ψ is a scalar factor which takes into account that λ and $\mathbf{u}$ have different scales.

5. Compute Δ using (3.19)

6. Update the results using:

$$_i = _{i-1} + \Delta \tag{3.23}$$
$$\lambda_i = \lambda_{i-1} + \Delta\lambda \tag{3.24}$$
$$\theta_i = \theta_{i-1} + \dot{\theta}\Delta t \tag{3.25}$$
$$q_i = q_{i-1} + \dot{q}\Delta t \tag{3.26}$$
$$_i = _{i-1} + \Delta \tag{3.27}$$

Additionally, the variable $\dot{q}^{slip}$ is updated using the equation (3.9).

The procedure described is repeated until a maximum displacement or a maximum load level is reached.

3.5 Numerical Results

The analyses are done to simulate the pull-out of a hooked fiber, with hooks changed from $\alpha = 0°, 5°, 10°, 15°, 30°$ and $45°$, under a vertical pull-out force ($\theta = 0°$), where α and θ are the angle between the axis of the fiber and the hook and between the axis of the fiber and the applied force, respectively, as can be seen in figure 3.1. The analyses were also done in straight fibers for forces with components in the plane of the crack, such that $\theta = 0°, 5°$ and $10°$. In all cases, the calculations supposed a fiber thickness of 0.8 mm, embedded 30 mm. With a hooked end of 3 mm, calculations are carried out for a reference set of parameters chosen to simulate the test carried out in (Weiler & Grosse 1996) using a cold-drawn steel wire fiber, with a diameter of $t = 0.8$ mm, embedded $L + h = 30$mm in a concrete matrix with and without hooked ends where in all cases $h = 3$mm. The range of values for the friction coefficients and the elastic properties used for the concrete and steel are based on values in Li & Stang (1997). The range of values of the clamping pressure is based on (Stang 1996). In table 3.1, the range of values used in the analysis of different properties is presented, different values of the parameters were used in analyses in order to find the best values in order to reproduce the experimental results. In table 3.1 a reference value is also indicated, this corresponds to the value that best fit the experimental results. The range of values of C_n and C_s were chosen for stability reasons, values out of this range have produced unstable results. The values of the constants δ_c, $\dot{q}_1$, $\dot{q}_0$, p, m and θ_0 were taken from (Povirk & Needleman 1993).

3.5.1 Comparison with Experiment

A plot comparing the slip displacement for the analysis using the reference values of parameters from table 3.1 and the experimental results by Weiler & Grosse (1996) is to be found in figure 3.4. Due to the fact that the analyses were made considering the problem as plane strain cases, a thickness of 1mm was considered; in order to compare these quantities with the experimental result, a factor of 0.8 was applied to the analytical results.

Property	Range investigated	Reference value
C_n	$0.3 - 30$ GPa/mm	3GPa/mm
C_s	$0.1 - 10$ GPa/mm	1GPa/mm
ϕ_n	1×10^{-5}	1×10^{-5}
σ_{max}		30Mpa
τ_{max}	$1.6 - 5$ MPa	2Mpa
μ_s	$1.0 - 0.25$	0.5
μ_d	$0.25 - 0.05$	0.15
δ_c		4mm
$\dot{q}_1$		10mm/s
$\dot{q}_0$		100mm/s
p		0.5
m		5
θ_0		4.6052
E_f		210GPa
E_c		30GPa
ν_f		0.3
ν_c		0.2
p_0	$2 - 10$ MPa	5Mpa

Table 3.1: Properties used in the analysis. E_f and E_c correspond to elastic moduli of the fiber and concrete. ν_f and ν_c correspond to Poisson ratio of the fiber and concrete matrix.

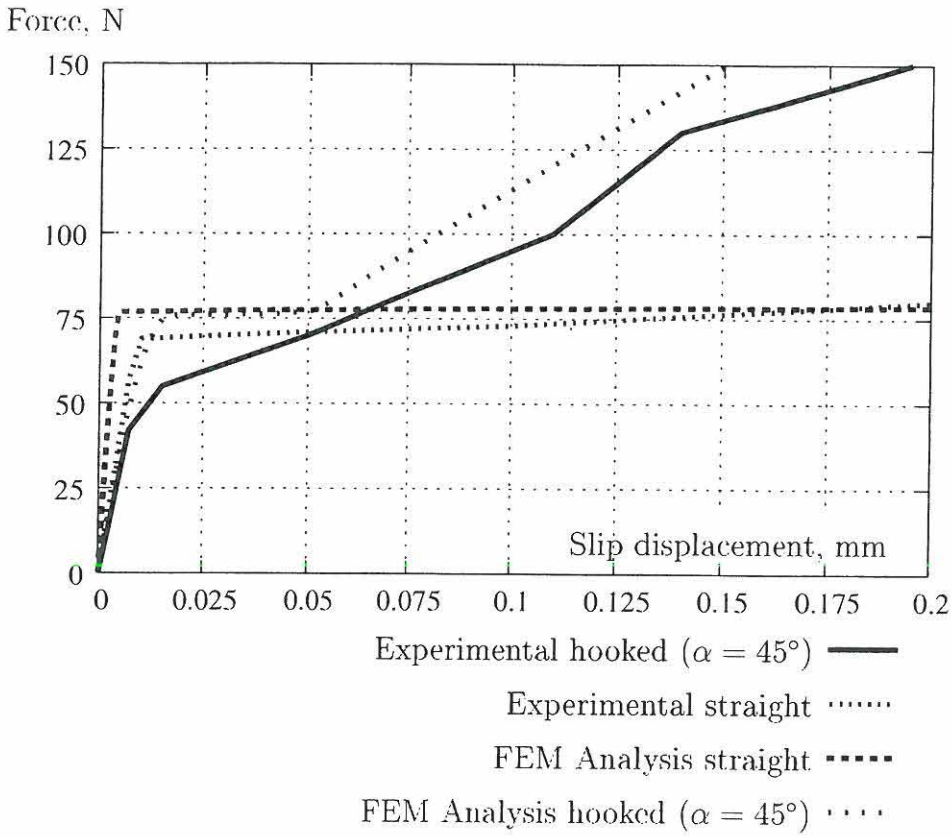

Figure 3.4: Slip displacement experimental and numerical results, using the reference values for the parameters according to table 3.1.

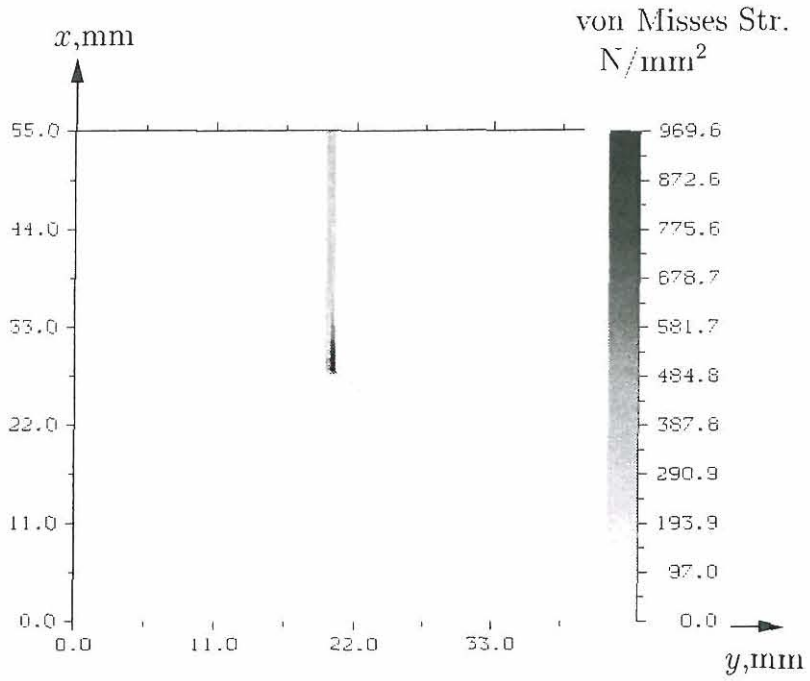

Figure 3.5: Contour plot of Misses stresses, for the hooked ($\alpha = 45°$) fiber.

Values of Misses stress for the hooked fiber are shown as contour plots in figure 3.5. According to the values of stresses, yielding of the steel fiber is expected, this was not considered in these analyses, but it is known to occur during the tests.

3.5.2 Parameter Studies

The effect of considering different values for parameters, between the ranges in table 3.1 was investigated using the straight fiber. The values indicated as reference values were used in the analysis in order to reproduce the experimental results for the straight fiber. Several analyses were carried out using different values of variables; first the influence of the elastic stiffness is investigated, results including variations in the elastic stiffness (C_n and C_s) are shown in figure 3.6. In this figure it can be observed that this parameter have effect only on the initial slope of the curve Force vs Displacement, the amount of force is not affected in a significant form. Larger values of the elastic constants usually result in instability of the model; smaller values were not used, because they fail to adequately represent the initial slope of the curve force vs slip displacement.

The effect of variations on the value considered for the static friction coefficient can be seen in figure 3.7. Changes in this coefficient produce important changes in the resisted force and also have effect on the slope of the initial part of the slip displacement vs force diagram. A value of $\mu_s = 0.5$ results in good agreement with the force expected for the range of values of slip displacement considered.

The effect of the clamping pressure is shown in figure 3.8. As expected, the clamping pressure was an important factor in the pull-out test. Failures in the estimation of this force can produce meaningless results. Even if the friction model supposes a non-constant friction coefficient, the shear tractions depend directly on

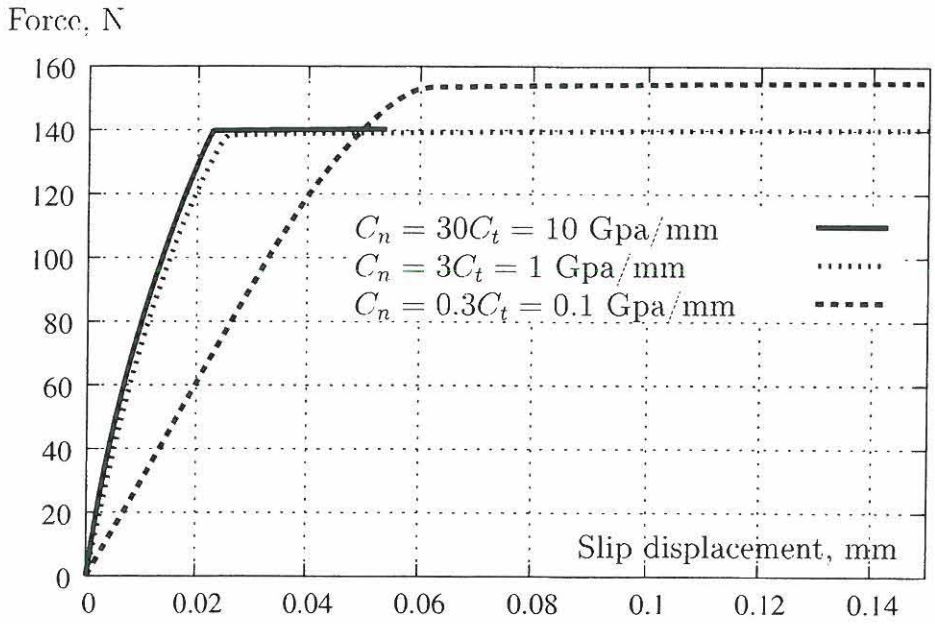

Figure 3.6: Effect of variations in elastic stiffness.

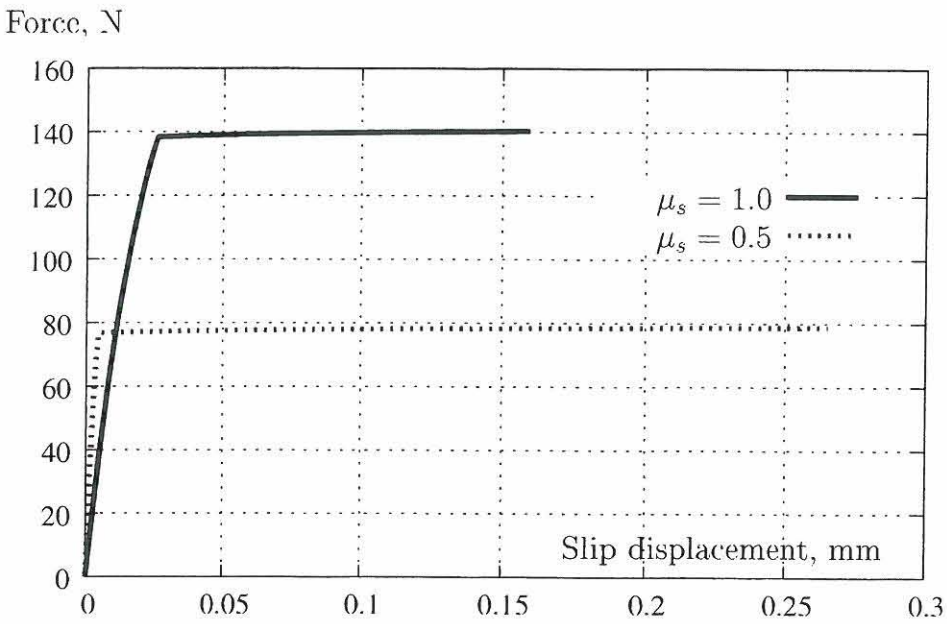

Figure 3.7: Effect of variation of the static friction coefficient.

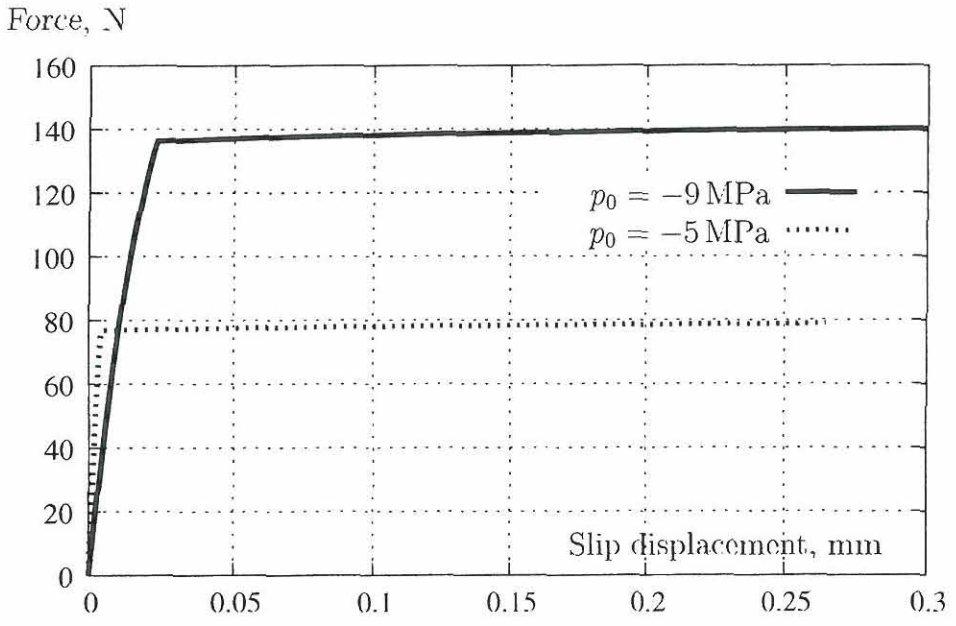

Figure 3.8: Effect of the clamping pressure.

the values of the normal traction. It can be observed that the clamping pressure also has a minor effect on the initial stiffness, measured as the slope in the force-displacement curve.

The effect of the component of the force in the plane of the crack is presented in graphic 3.9. In this figure it can be observed that the inclination of the force has a null effect initially, but in this case after a slip greater than 0.05mm for $\theta \geq 10°$ an increment in the force is required in order to extract the fiber.

The effect of hooked ends in the slip is shown in figure 3.11, figure 3.10 shows the first 0.1mm of slip displacement while figure 3.11 shows the first 0.6mm. In figure 3.10 the effect of the hook over the initial stiffness of the system can be seen, the presence of the hook increases the initial stiffness. However, the yielding value of the curve (slip displacement increasing without increasing the magnitude of the force) remains constant. In figure 3.11, it is shown that further increments in the force are required in order to increase the slip; the starting point for these increments, and the slope of the second ascending part of the curve slip-vs force, depends on the angle of the hook.

It is also interesting to compare the shear tractions along the fiber for different cases. The case of a straight fiber with the pull-out force applied normal to the plane of the discontinuity can be seen in figure 3.12. The shear traction shown in figure 3.12 can be related with the variation of the normal traction along the fiber, for this case, factors affecting the magnitude of the frictional coefficient have a small effect on the shear tractions. The smaller values at the tip of the fiber (near position 30mm) can be attributed to the fact that the normal tractions are smaller in that part of the fiber, more than to variations in the friction coefficient.

The shear tractions on the lower side of the fiber, for the case when the force has a component corresponding to $\theta = 5°$, in different steps for this case, are shown in figure 3.13.

From figure 3.13 it is evident that for small components of the force in the plane

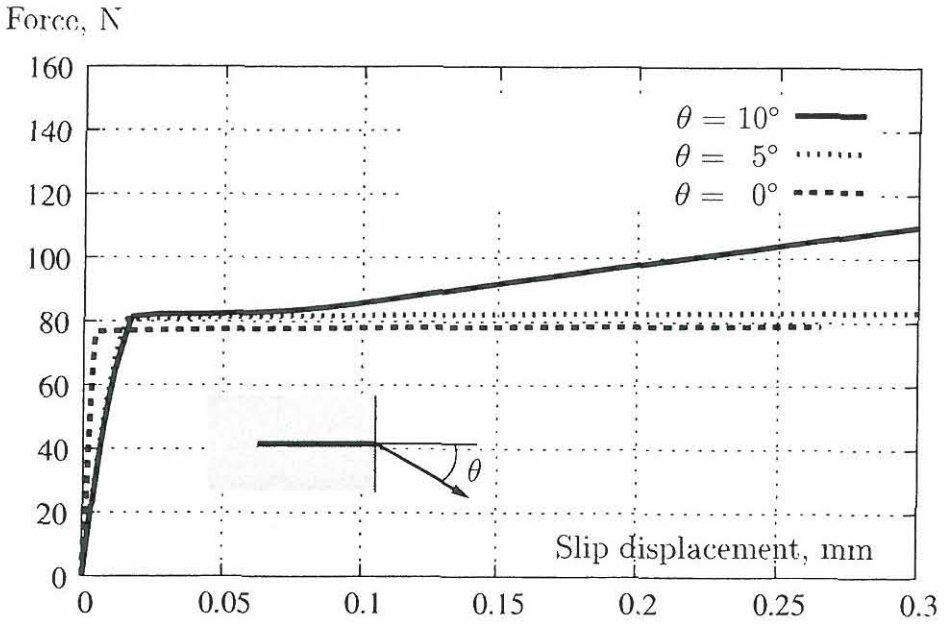

Figure 3.9: Effect of components of the force in the plane of the crack for varying values of the inclination θ of the applied load.

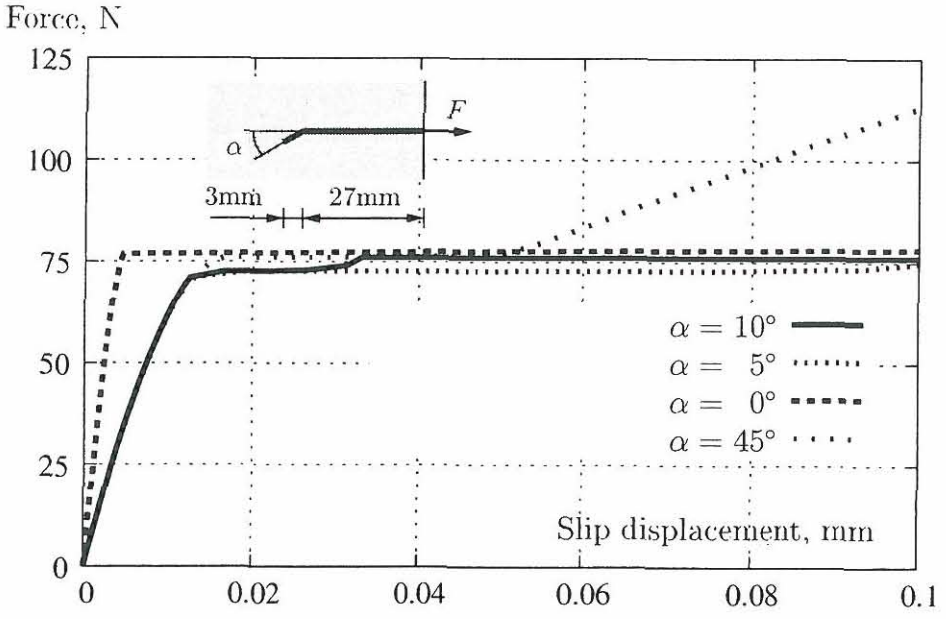

Figure 3.10: Slip displacement, comparing three cases including hooked ends.

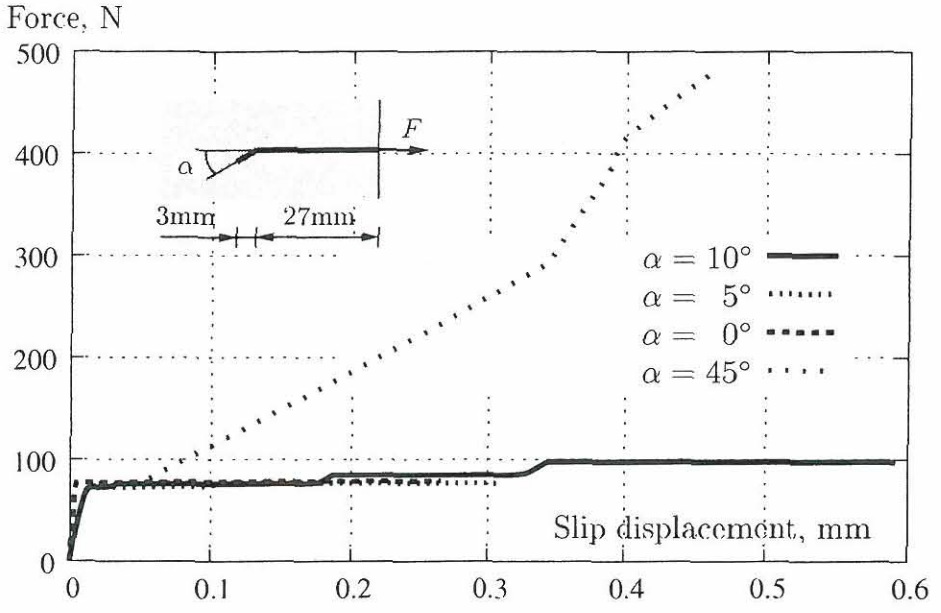

Figure 3.11: Slip displacement, comparing three cases including hooked ends.

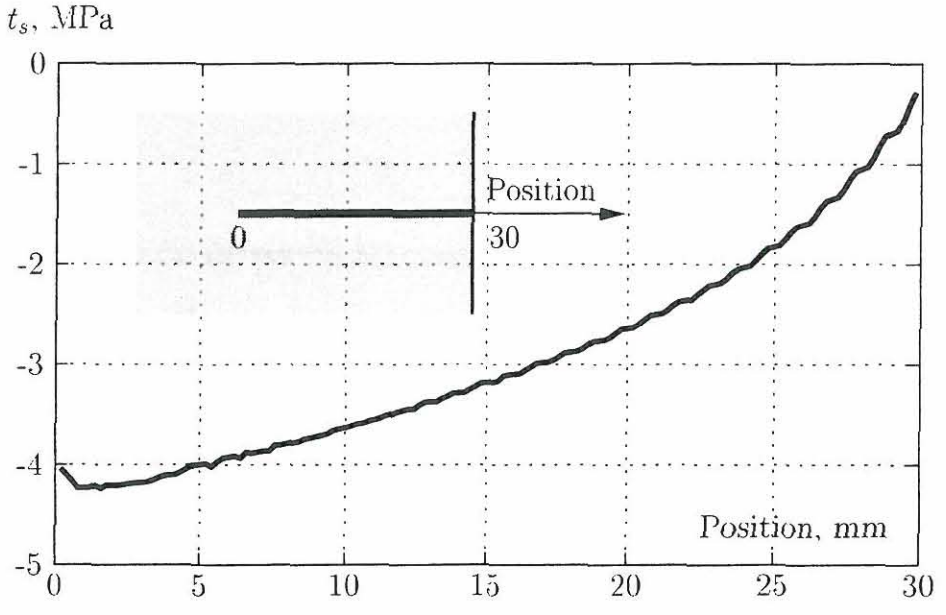

Figure 3.12: Shear tractions along the fiber.

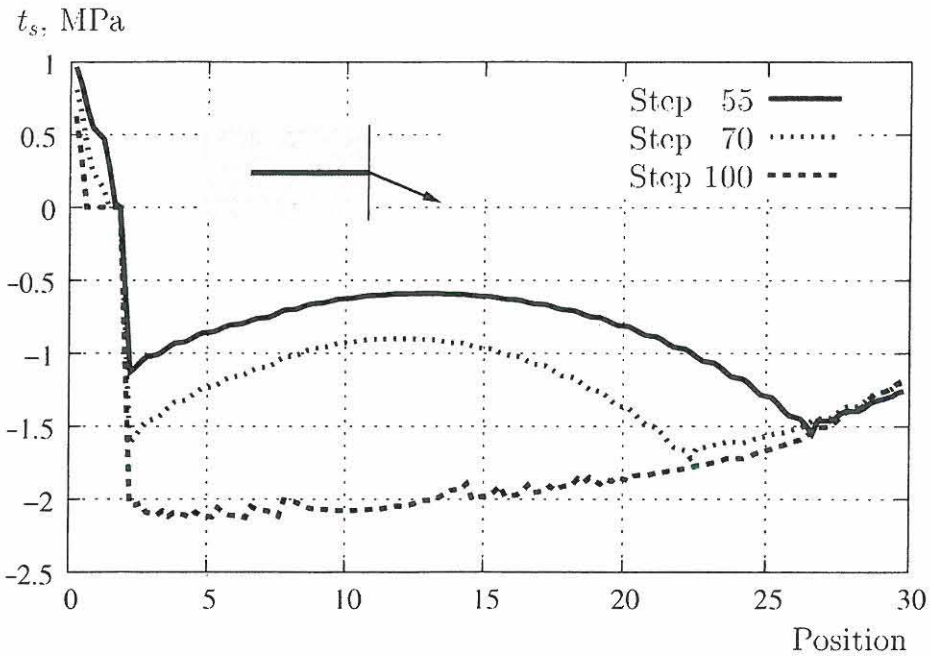

Figure 3.13: Shear tractions along the lower side of the fiber at different steps for $\theta = 5°$.

of the crack a bending effect exist, the bending effects are more important at the beginning of the pull-out. The tractions along the fiber are reaching a maximum value starting from the pulled end and then this is kept with small variations.

The shear tractions for the lower side of the fiber when a hook is considered are shown in figure 3.14, when the hook has an angle of 5°. From this figure, the existence of stress concentrations around the starting point of the hook is evident. Again, a detailed observation of this graphic shows a bending effect as in the case of components of the force in the plane of the discontinuity. However, the plastic effects that exist around the beginning of the hook in this case are not considered in the analysis, and unrealistic values of shear tractions are produced in a small zone of the fiber.

3.6 Conclusions

The results presented here show that it is possible to model the behavior of a pull-out test for fiber reinforced concrete using interface finite elements for friction. The model shows that the modified Dieterich-Ruina model, presented in Section 3.3 and used here, produces reliable results.

The results provide clear proof that the elastic constants affect the initial slope of the curve relating slip-displacement to force, but have little effect on the strength. The factors that really affect the strength are the static friction coefficient and the clamping pressure.

Once yielding in the slip-force diagram is reached, factors like the direction of the force or the existence of hooked ends become important and affect the ultimate strength of the fiber to pull-out.

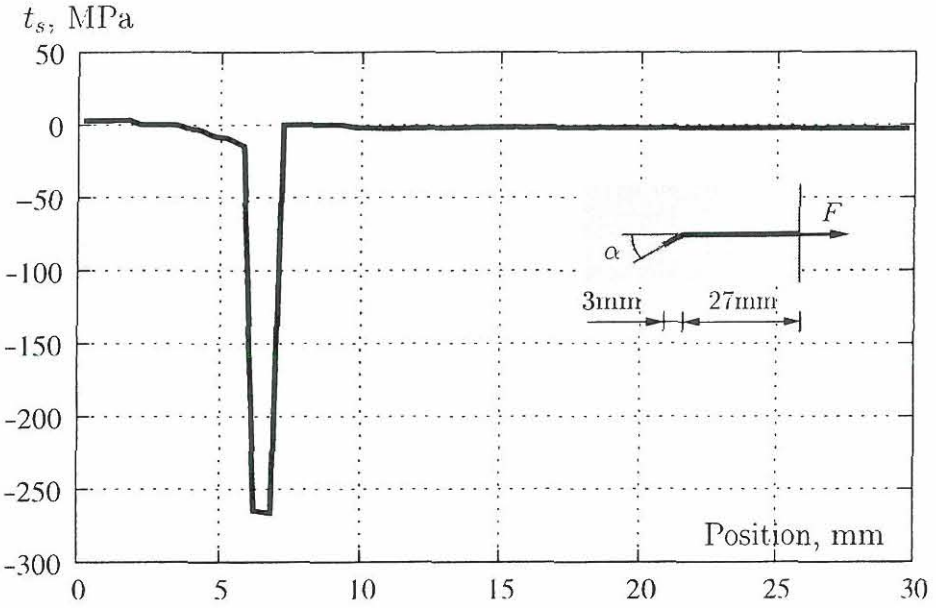

Figure 3.14: Shear tractions in the final step (1000) for the fiber, lower side of fiber. Hook angle 5°.

The analysis carried out shows the relative importance of different factors affecting the pull-out of a fiber, in particular three external factors are very important: first, the clamping pressure; second, the shape of the fiber; and third, the direction of the pull-out force.

Other factors affecting the pull-out are the length of the fiber and the interface characteristics of the fiber. These aspects were not included in this research, but they can easily be studied using the same kind of frictional finite elements.

The analyses were performed supposing small displacements, results of pull-out tests can correspond to slip distances of several mm. The analyses carried out here were performed on slip displacements of a maximum value of 0.2mm. In order to extend analysis to a wider range of slips, large displacements must be considered. The contact zone between the two materials has to be updated, and the normal traction in the position after displacement of the element should be used to estimate the shear traction in the element.

In the case of hooked ends, plastic effects in the fibers made from elastic-plastic materials are important, this is due to the stress concentration at the beginning of the hook.

Bibliography

Adams, G. G. (1995), 'Self-excited oscillations of two elastic half-spaces sliding with a constant coefficient of friction', *Journal of applied mechanics - Transactions of the ASME* **62**, 867–872.

Ballarini, R., Ahmed, S. & Mullen, R. L. (1990), *in* 'Proceedings of the international conference on interfaces in metal ceramics composites, February 19 22; 1990', pp. 349–388.

Budiansky, B., Hutchinson, J. W. & Evans, A. G. (1986), 'Matrix fracture in fiber-reinforced ceramics', *Journal of the mechanics and physics of solids* **34**, 167–189.

Chanvillard, G. & Aitcin, P. (1996), 'Pull-out behavior of corrugated steel fibers', *Advanced cement based materials* **4**, 28–41.

Cox, B. N. (1993), 'Scaling for bridged cracks', *Mechanics of materials* **15**, 87–98.

Cox, B. N., Sridhar, N. & Beyerlin, I. J. (2001), 'Inertial effects in the pull-out mechanism during dynamic loading of a bridged crack', *acta mater.* **49**, 3863–3877.

Crisfield, M. A. (1981), 'A fast incremental-iterative solution procedure that handles "snap-through"', *Computers and Structures* **13**, 55–62.

Crisfield, M. A. (1991), *Non-linear Finite Element analysis of Solids and Structures*, Vol. Volume 1: essentials, John Wiley and Sons, Chichester.

Dieterich, J. H. (1979), 'Modelling of rock friction 1. experimental results and constitutive equations', *J. Geophys. Res.* **84**(B5), 2161–2168.

Freund, L. B. (1992), 'The axial force needed to slide a circular fiber along a hole in an elastic-material and implications for fiber pull-out', *European Journal of Mechanics, A-Solids* **11**, 1 19.

Hutchinson, J. W. & Jensen, H. M. (1990), 'Models of fiber debonding and pullout in brittle composites with friction', *Mechanics of materials* **9**, 139–163.

Kumar, R. K. & Reddy, J. N. (1996), 'Stress distributions during fiber pull-out', *Journal of applied mechanics-Transactions of the ASME* **63**, 301–306.

Li, C. Y. & Mobasher, B. (1998), 'Finite element simulations of fiber pullout toughening in fiber reinforced cement based composites', *Advanced cement based materials* **7**, 123–132.

Li, V. C. & Stang, H. (1997), 'Interface property characterization and strengthening mechanism in fiber reinforced cement based composites', *Advanced cement based materials* **6**, 1–20.

McCartney, L. N. (1987), 'Mechanics of matrix cracking in brittle-matrix fiber-reinforced composites', *Proc. Roy. Soc. London* **A409**, 329–350.

Mital, S. K. & Chamis, C. (1991), 'Fiber pushout test - a 3-dimensional finite element computational simulation', *J. Compos. Technol. Res.* **13**, 14–21.

Peirce, D., Shih, C. F. & Needleman, A. (1984), 'A tangent modulus method for rate dependent solids', *Comp. Struct.* **18**, 857–887.

Povirk, G. L. & Needleman, A. (1993), 'Finite elements simulations of fiber pull-out', *Journal of Engineering Materials and Technology* **115**, 286–291.

Renardy, M. (1992), 'Ill-posedness at the boundary for elastic solids sliding under coulomb-friction', *Journal of elasticity* **27**(3), 281–287.

Rice, J. & Ruina, A. L. (1983), 'Stability of steady frictional slipping', *Journal of Applied Mechanics, ASME* **50**, 343–349.

Ruina, A. (1981), Friction laws and instabilities: A quasi-static analysis of some dry frictional behavior, PhD thesis, Brown University.

Sridhar, N., Yang, Q. D. & Cox, B. N. (2003), 'Slip, stick, and reverse slip characteristics during dynamic fibre pullout', *Journal of the Mechanics and Physics of Solids* **51**, 1215 1241.

Stang, H. (1996), 'Significance of shrinkage-induced clamping pressure in fiber-matrix bonding in cementitious composite materials', *Advanced cement based materials* **4**, 106–115.

Weiler, B. & Grosse, C. (1996), 'Pullout behaviour of fibers in steel fiber reinforced concrete', *FMPA Journal* pp. 116–127.

Chapter 4

Interface elements

Contents

4.1 Introduction

In order to model the behavior of quasi-brittle materials like concrete, different approaches are considered; generally these approaches can be divided into continuum and discrete approaches. The first discrete approaches were introduced in concrete by Clough (1962) and Ngo & Scordelis (1967).

The discrete approach originally consisted in creating new degrees of freedom at node locations where a discontinuity was expected to occur, this way the contribution of cracking to inelastic deformation was lumped in a discontinuity. The process of creating the discontinuity can be improved by using re-meshing techniques (Ingraffea & Saouma 1985), (Camacho & Ortiz 1996).

Another improvement to the discrete method has been the use of interface elements as predefined cracks. The cohesive surface formulation of Xu & Needleman (1994) has been used to model damage in brittle materials (Camacho & Ortiz 1996). The basic assumption of the cohesive surface framework is that the separation process is confined to a set of discrete planes. A constitutive model is then specified for each cohesive surface that allows separation.

In a cohesive surface formulation, constitutive relations are specified independently for the bulk material and for one or more cohesive surfaces (usually in the form of a relation between surface tractions and displacement jumps across the cohesive surface), (Needleman 1987), (Xu & Needleman 1994). The bulk and cohesive constitutive relations together with appropriate balance laws and boundary conditions completely specify the problem. Fracture emerges as a natural outcome of the deformation process without introducing any additional failure criterion.

In the approach by (Rots 1988), interface elements of zero thickness are inserted into the finite element mesh at locations where a crack is expected to propagate. The non-linearity of the response is incorporated by the use of the fictitious crack concept, the process zone is concentrated in a fictitious extension of the actual physical crack. This fictitious crack can then transfer tractions with a magnitude related to the crack opening.

In Povirk & Needleman (1993) and in Cifuentes, Needleman & Byskov (2005) the interface elements with zero thickness were equipped with frictional models in order to analyze pull-out tests. In this case the re-meshing is not required because the discontinuity path is known in advance.

In this document the interface elements make use of cohesive and frictional models, the background explaining how to create the elements and the solution are indicated. The frictional and cohesive models are presented in detail. The interface elements created are applied to the case of fiber pull-out in fiber reinforced concrete extending the analysis in Cifuentes et al. (2005) by considering cracking of the concrete matrix and updating the contact surface in order to include large slips in the analysis.

It is concluded that the discrete approach can be used successfully in cases like the pull-out test where the discontinuity path is known in advance. In that case the rate and state frictional models used here produce good results and some of the most important parameters affecting the pull-out test are identified.

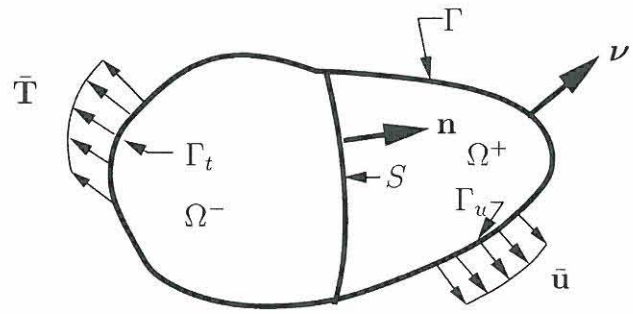

Figure 4.1: The domain Ω crossed by a discontinuity.

4.2 Problem formulation

Considering the domain Ω with boundary Γ shown in figure 4.1. It contains the discontinuity (S) which splits the domain into two parts denoted Ω^+ and Ω^-. The prescribed tractions on Γ_t are denoted $\overline{\mathbf{T}}$ and the prescribed displacements on Γ_u are denoted $\bar{\mathbf{u}}$, where Γ_u and Γ_t are in the external boundary. $\boldsymbol{\nu}$ is a unit normal to the external boundary Γ.

The field equations governing the boundary value problem can be written as (Oliver 1996):

$$\nabla\boldsymbol{\sigma} + \mathbf{f} = \mathbf{0} \qquad \text{in } \Omega \setminus S \tag{4.1}$$

$$\boldsymbol{\varepsilon} = (\nabla\mathbf{u})^S \qquad \text{in } \Omega \setminus S \tag{4.2}$$

$$\mathbf{u} = \bar{\mathbf{u}} \qquad \text{in } \Gamma_u \tag{4.3}$$

$$\boldsymbol{\sigma}\cdot\boldsymbol{\nu} = \bar{\mathbf{T}} \qquad \text{in } \Gamma_t \tag{4.4}$$

$$\boldsymbol{\sigma}^+\cdot\mathbf{n} = \boldsymbol{\sigma}^-\cdot\mathbf{n} \qquad \text{in } S \tag{4.5}$$

$$\mathbf{T}_S = \mathbf{T}^+ = \boldsymbol{\sigma}^+\cdot\mathbf{n} \qquad \text{in } S \tag{4.6}$$

$$\mathbf{T}_S = \mathbf{T}^+ = -\mathbf{T}^- \qquad \text{in } S \tag{4.7}$$

where $\boldsymbol{\sigma}$ is the stress tensor, $\boldsymbol{\varepsilon}$ is the strain tensor, $\mathbf{f}$ are the body forces, $\mathbf{u}$ is the displacement vector, $\mathbf{n}$ is the unitary vector normal to the interface, and $\mathbf{T}_S$ are the tractions across the discontinuity. $(\cdot)^S$ stands for the symmetric part of $(\cdot)^S$.

Equation (4.1) is the classical equilibrium equation. Equation (4.2) is the strain-displacement relation. Equations (4.3) and (4.4) are the essential and natural boundary conditions, respectively. Equations (4.5) and (4.6) state the continuity of the traction vector across the discontinuity S.

The constitutive relations are stated in the form

$$\boldsymbol{\sigma} = \boldsymbol{\sigma}(\boldsymbol{\varepsilon}) \qquad \text{in } \Omega \setminus S \tag{4.8}$$

$$\mathbf{T}_S = \mathbf{T}_S(\mathbf{q}) \qquad \text{in } S \tag{4.9}$$

where $\mathbf{q} = \mathbf{u}^+ - \mathbf{u}^-$ is the interface sliding.

Equations (4.1)-(4.9) provide a sufficient and well posed set of equations to solve the problem.

4.3 Weak formulation

Considering the virtual work principle:

$$-\int_{\Omega\setminus S}\boldsymbol{\sigma}\colon(\nabla\delta\mathbf{u})^S d\Omega+\int_S \mathbf{T}_S\cdot\delta\mathbf{q}d\Gamma+\int_{\Gamma_t\setminus S}\bar{\mathbf{T}}\cdot\delta\mathbf{u}d\Gamma+\int_{\Omega\setminus S}\mathbf{f}\cdot\delta\mathbf{u}d\Omega=0 \quad (4.10)$$

Considering that:

$$\int_{\Omega\setminus S}\boldsymbol{\sigma}\colon(\nabla\delta\mathbf{u})^S d\Omega=\int_{\Omega^+}\boldsymbol{\sigma}\colon(\nabla\delta\mathbf{u})^S d\Omega+\int_{\Omega^-}\boldsymbol{\sigma}\colon(\nabla\delta\mathbf{u})^S d\Omega \quad (4.11)$$

Using the divergence theorem:

$$-\int_{\Omega^-}\boldsymbol{\sigma}\colon(\nabla\delta\mathbf{u})^S d\Omega=\int_{\Omega^-}\nabla\cdot\boldsymbol{\sigma}\delta\mathbf{u}d\Omega-\int_{\Gamma_t^-}\boldsymbol{\nu}\cdot\boldsymbol{\sigma}\delta\mathbf{u}d\Gamma-\int_S\mathbf{n}^-\cdot\boldsymbol{\sigma}^-\cdot\delta\mathbf{u}^-d\Gamma \quad (4.12)$$

$$-\int_{\Omega^+}\boldsymbol{\sigma}\colon(\nabla\delta\mathbf{u})^S d\Omega=\int_{\Omega^+}\nabla\cdot\boldsymbol{\sigma}\delta\mathbf{u}d\Omega-\int_{\Gamma_t^+}\boldsymbol{\nu}\cdot\boldsymbol{\sigma}\delta\mathbf{u}d\Gamma-\int_S\mathbf{n}^+\cdot\boldsymbol{\sigma}^+\cdot\delta\mathbf{u}^+d\Gamma \quad (4.13)$$

where $\Gamma_t^+=\Gamma_t\cap\Omega^+$ and $\Gamma_t^-=\Gamma_t\cap\Omega^-$. Considering:

$$\int_S\mathbf{T}_S\cdot\delta\mathbf{q}d\Gamma=\int_S\mathbf{T}^+\cdot\delta\mathbf{u}^+d\Gamma+\int_S\mathbf{T}^-\cdot\delta\mathbf{u}^-d\Gamma \quad (4.14)$$

The result is:

$$\begin{aligned}&\int_{\Omega^+}\nabla\cdot\boldsymbol{\sigma}\delta\mathbf{u}d\Omega+\int_{\Omega^+}\nabla\cdot\boldsymbol{\sigma}\delta\mathbf{u}d\Omega+\int_{\Omega\setminus S}\mathbf{f}\cdot\delta\mathbf{u}d\Omega+\int_{\Gamma_t}\bar{\mathbf{T}}\delta\mathbf{u}d\Gamma\\&-\int_{\Gamma_t^+}\boldsymbol{\nu}\cdot\boldsymbol{\sigma}\cdot\delta\mathbf{u}d\Gamma-\int_{\Gamma_t^-}\boldsymbol{\nu}\cdot\boldsymbol{\sigma}\cdot\delta\mathbf{u}d\Gamma+\int_S\mathbf{T}^+\cdot\delta\mathbf{u}^+d\Gamma+\int_S\mathbf{T}^-\cdot\delta\mathbf{u}^-d\Gamma\\&-\int_S\mathbf{n}^+\cdot\boldsymbol{\sigma}^+\cdot\delta\mathbf{u}^+d\Gamma-\int_S\mathbf{n}^-\cdot\boldsymbol{\sigma}^-\cdot\delta\mathbf{u}^-d\Gamma=0\end{aligned} \quad (4.15)$$

Finally

$$\begin{aligned}&\int_{\Omega^-}(\nabla\cdot\boldsymbol{\sigma}+\mathbf{f})\cdot\delta\mathbf{u}d\Omega+\int_{\Omega^+}(\nabla\cdot\boldsymbol{\sigma}+\mathbf{f})\cdot\delta\mathbf{u}d\Omega\\&+\int_{\Gamma_t^+}(\bar{\mathbf{T}}-\boldsymbol{\nu}\cdot\boldsymbol{\sigma})\cdot\delta\mathbf{u}d\Gamma+\int_{\Gamma_t^-}(\bar{\mathbf{T}}-\boldsymbol{\nu}\cdot\boldsymbol{\sigma})\cdot\delta\mathbf{u}d\Gamma\\&+\int_S(\mathbf{T}^+-\mathbf{n}^+\cdot\boldsymbol{\sigma}^+)\cdot\delta\mathbf{u}d\Gamma+\int_S(\mathbf{T}^--\mathbf{n}^-\cdot\boldsymbol{\sigma}^-)\cdot\delta\mathbf{u}d\Gamma=0\end{aligned} \quad (4.16)$$

From (4.16) it is recovered the equations (4.1) -(4.6) :

4.4 Constitutive relations

4.4.1 The cohesive model

This constitutive model is defined in (Xu & Needleman 1993). In this model, the tractions are described as functions of the displacement jump across the interface. The condition that work cannot be extracted from the interface, in a closed cycle for an elastic interface, leads to the existence of a potential ϕ, for which

$$\mathbf{T} = \frac{\partial \phi}{\partial \mathbf{q}} \tag{4.17}$$

The potential used here allows for a shear failure mode in the interface region.

The following definitions of normal q_n and tangential sliding q_s, normal traction T_n, and tangential traction T_s are used:

$$\begin{aligned} q_n &= \mathbf{n}\cdot\mathbf{q}, \quad q_s = \mathbf{s}\cdot\mathbf{q} \\ T_n &= \mathbf{n}\cdot\mathbf{T}, \quad T_s = \mathbf{s}\cdot\mathbf{T} \end{aligned} \tag{4.18}$$

where $\mathbf{n}$ and $\mathbf{s}$ are unit vectors pointing in normal and tangential directions, respectively to the interface.

The dependence on the displacements is given in terms of the normal and tangential slidings. In particular ϕ, has the form

$$\phi(\mathbf{q}) = \phi_n + \phi_n \exp\left(-\frac{q_n}{\delta_n}\right)\left\{\left(1 - r + \frac{q_n}{\delta_n}\right)\frac{(1-c)}{(r-1)} - \left(c + \frac{(r-c)}{(r-1)}\frac{q_n}{\delta_n}\right)\exp\left(-\frac{q_s^2}{\delta_s^2}\right)\right\} \tag{4.19}$$

with

$$c = \frac{\phi_s}{\phi_n} \qquad \text{and} \qquad r = \frac{q_n^*}{\delta_n} \tag{4.20}$$

where ϕ_n is the work of normal separation, ϕ_s is the work of tangential separation, δ_n and δ_s are the interface characteristic length parameters, and q_n^* is the value of q_n after complete shear separation under the condition of zero normal tension, $T_n = 0$.

The interface tractions are obtained according to equation (4.17), by differentiation of (4.19):

$$T_n = \frac{\phi_n}{\delta_n}\exp\left(-\frac{q_n}{\delta_n}\right)\left\{\frac{q_n}{\delta_n}\exp\left(-\frac{q_s^2}{\delta_s^2}\right) + \frac{(1-c)}{(r-1)}\left[1 - \exp\left(-\frac{q_s^2}{\delta_s^2}\right)\right]\left(r - \frac{q_n}{\delta_n}\right)\right\} \tag{4.21}$$

$$T_s = \frac{\phi_n}{\delta_n}\left(2\frac{\delta_n}{\delta_s}\right)\frac{q_s}{\delta_s}\left\{c + \frac{(r-c)}{(r-1)}\frac{q_n}{\delta_n}\right\}\exp\left(-\frac{q_n}{\delta_n}\right)\exp\left(-\frac{q_s^2}{\delta_s^2}\right) \tag{4.22}$$

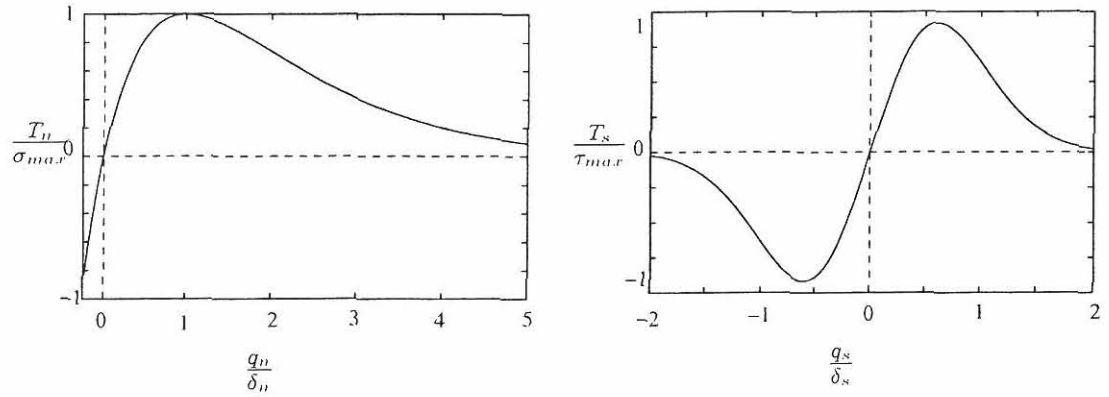

Figure 4.2: The tractions when (a) $q_s = 0$ or (b) $q_n = 0$

The maximum value of $|T_s| = \tau_{\max}$ occurs when $|q_s| = \sqrt{2}\delta_s/2$. The normal and shear work of separation are related to $\sigma_{\max}$ and $\tau_{\max}$, respectively, by

$$\phi_n = \sigma_{\max} e \delta_n \qquad \phi_s = \sqrt{\frac{e}{2}} \tau_{\max} \delta_s \tag{4.23}$$

where $e = \exp(1)$. For the case $\phi_n = \phi_s$, the tractions are shown in figure 4.2 when only q_n or q_s is different from zero. If it is assumed that $\phi_n = \phi_s$ then $c = 1$. The equations are reduced to:

$$\phi(\mathbf{q}) = \phi_n - \phi_n \exp\left(-\frac{q_n}{\delta_n}\right)\left(1 + \frac{q_n}{\delta_n}\right)\exp\left(-\frac{q_s^2}{\delta_s^2}\right) \tag{4.24}$$

$$T_n = \frac{\phi_n}{\delta_n}\frac{q_n}{\delta_n}\exp\left(-\frac{q_n}{\delta_n}\right)\exp\left(-\frac{q_s^2}{\delta_s^2}\right) \tag{4.25}$$

$$T_s = \left(\frac{\phi_n}{\delta_n}\right)\left(\frac{q_n}{\delta_n} + 1\right)\left(2\frac{\delta_n}{\delta_s}\right)\frac{q_s}{\delta_s}\exp\left(-\frac{q_n}{\delta_n}\right)\exp\left(-\frac{q_s^2}{\delta_s^2}\right) \tag{4.26}$$

4.4.2 The Friction Model

Introduction

Frictional sliding is a major failure mode at the interfaces in engineering materials and structures composed of two constituents. Frictional sliding also plays a major role in fiber bridging during failure of fiber reinforced composite materials (including fiber reinforced concrete). For these materials the fracture toughness is governed by the debonding and frictional sliding of the fibers.

The Coulomb law of friction was published in 1781 by the french engineer C.A.Coulomb. The classical Coulomb law asserts that relative sliding between two bodies in contact along plane surfaces will occur when the net shear force parallel to the plane reaches a critical value proportional to the net normal force pressing

the two bodies together. The constant of proportionality is the coefficient of friction. Only the total contact force and total friction force are considered without considering how these forces are distributed on the contact surface.

Duvaut & Lions (1976) and Duvaud (1980) showed that if Coulomb's law is applied pointwise in contact problems involving linear elastic bodies, then the contact stress developed normal to the contact surface is ill defined, except for some very special cases. There are several aspects of actual friction phenomena that suggest alternative friction laws (limiting the use of Coulomb law to total global contact forces).

The major source of friction modeling has been carried out in the field of earthquake physics. In geophysics, friction models have a major component of earthquake source modeling since Brace & Byerlee (1966) and Byerlee (1970) hypothesized earthquakes to be stick-slip frictional sliding of slabs. Stick-slip displacement means that under a constant relative displacement rate, a non-constant slip motion is observed. More recently, rate- and state-dependent friction models were applied to nucleation of earthquakes and creep behavior of faults (Dieterich 1992).

Heaton (1990) argued that the mode of rupture in large earthquakes, is such that the duration of slip is short compared to the overall duration of the rupture. This, he said, is due to the self-healing nature of rupture, in the form of pulse.

State and rate friction generates stable pulse-like rupture where anything else than state and rate friction leads to ill-posedness and stabilities that manifest themselves in the form of mesh dependence in numerical simulations.

The rate- and state-dependent constitutive relations for frictional sliding assume the dependence of the shear traction at the interface on the slip velocity at the interface $\dot{q}^{slip}$ and internal variables θ_i, through the relationship:

$$T_s = \mu(\theta_i, \dot{q}^{slip})\sigma_0 \tag{4.27}$$

where $\mu(\theta_i, \dot{q}^{slip})$ is the coefficient of friction at constant normal load, σ_0 is the constant normal traction at the interface and an overdot means rates $\dot{(\,)} = \partial()/\partial t$. The internal state variables are the macroscopic continuum parameters that account for the change of contact quality between the surfaces over time.

The rate- and state-friction models address the following fundamental observations on friction (Dieterich 1979), (Rice & Ruina 1983):

1. There is an instantaneous increase in the coefficient of friction in response to a step increase in the rate of sliding, (called the direct effect).

2. There is a subsequent decrease to a steady state value of the coefficient of friction, which is a decreasing function of the rate of sliding.

3. The approach to the steady state occurs over a characteristic distance that is independent of the rate of sliding.

In the Dieterich-Ruina friction laws whit one state variable, the coefficient of friction has a logarithmic dependence on both the state variable and slip velocity represented by the expression

$$\mu = \mu_0 + a \ln\left(\frac{\dot{q}^{slip}}{\dot{q}_0}\right) + b \ln\left(\frac{\dot{q}_0 \theta}{d_c}\right) \tag{4.28}$$

where d_c is the characteristic slip distance, and a and b are constants representing the degree of velocity weakening and the direct effect. The constant μ_0 corresponds to the coefficient of friction when the steady-state sliding velocity is equal to the normalizing velocity $\dot{q}_0$.

There are two types of evolution equations for the state variable that are used in the literature. In the so-called Ruina-Dieterich slip friction law, the state can evolve only during slip, and hence, there is no re-strengthening during truly stationary contact. The evolution equation is:

$$\dot{\theta} = -\left(\frac{\dot{q}^{slip}\theta}{d_c}\right) \ln\left(\frac{\dot{q}^{slip}\theta}{d_c}\right) \tag{4.29}$$

In the Dieterich-Ruina slowness friction law there is re-strengthening in truly stationary contact and the state variable evolves at zero slip velocity. The evolution equation is:

$$\dot{\theta} = 1 - \frac{\dot{q}^{slip}\theta}{d_c} \tag{4.30}$$

Equation (4.28) is not defined for $\dot{q}^{slip} = 0$ producing problems in numerical simulations. To solve the problem, a regularization has been proposed by Rice & Ben-Zion (1996) producing:

$$\mu = a \times \operatorname{arcsinh}\left[\frac{\dot{q}^{slip}}{2\dot{q}_0} \exp\left(\frac{\mu_0 + b \ln\left(\frac{\dot{q}_0\theta}{d_c}\right)}{a}\right)\right] \tag{4.31}$$

$$\dot{\theta} = 1 - \frac{\left|\dot{q}^{slip}\right| \theta}{d_c} \tag{4.32}$$

The above formulation behaves very close to the Dieterich-Ruina law, except for infinitesimally small slip velocities.

Another way of regularizing the Dieterich-Ruina friction law is given by Povirk & Needleman (1993), and is analyzed in detail below on page 55.

The Prakash-Clifton formulation allows for the evolutionary effects of normal stress variations on the friction stress. The fundamental expression (4.27) is replaced by:

$$T_s = f(\psi, \dot{q}^{slip})(\theta_1 + \theta_2) \tag{4.33}$$

in which

$$f(\psi, \dot{q}^{slip}) = \mu_0 + a \ln\left(\frac{\dot{q}^{slip}}{\dot{q}_0}\right) + \psi(\dot{q}^{slip}) \tag{4.34}$$

represents the rate- and state-dependence of the Rice-Dieterich slip law. The evolutionary effects of normal stress variation is represented by the state variables $\theta_i = \theta_i(\theta_j, \sigma)$. The evolution equations are:

$$\dot{\psi} = -\frac{\dot{q}^{slip}}{d_\psi}\left[\psi + b \ln\left(\frac{\dot{q}^{slip}}{\dot{q}_0}\right)\right] \tag{4.35}$$

$$\dot{\theta}_1 = -\frac{\dot{q}^{slip}}{d_1}\left[\theta_1 - c\sigma\right] \tag{4.36}$$

$$\dot{\theta}_2 = -\frac{\dot{q}^{slip}}{d_2}\left[\theta_2 - d\sigma\right] \tag{4.37}$$

The values of c and d are constrained by the equation $c + d = 1$ which ensures that the steady-state coefficient of friction is independent of normal pressure. The numerical problems at $\dot{q}^{slip} = 0$ still exist because the friction stress is not defined at that point. A regularization to the Prakash-Clifton law based on (Povirk & Needleman 1993) is proposed by (Coker, Rosakis & Needleman 2003).

Modified Dieterich-Ruina friction law

The friction model used here follows the model used in Povirk & Needleman (1993), which is based on the work by Ruina (1981) and Rice & Ruina (1983).

The coefficient of friction μ is defined as $-|T_s|/T_n$ for $T_n < 0$, where T_s and T_n are the shear and normal tractions, respectively. It is assumed that μ can be written as:

$$\mu = g(\theta) f(\dot{q}^{slip}) \tag{4.38}$$

where $\dot{q}^{slip}$ is the slip rate, and θ is an internal variable that characterizes the state of contact between the two surfaces, $\theta = \infty$ represents the highest contact quality and $\theta = 0$ represents the lowest contact quality.

The functions f and g are:

$$f(\dot{q}^{slip}) = \left(\frac{\dot{q}^{slip}}{\dot{q}_0} + 1\right)^{1/m} \tag{4.39}$$

$$g(\theta) = \left(\mu_d + (\mu_s - \mu_d) \exp\left[-\left(\frac{d_c/\theta}{\dot{q}_1}\right)^p\right]\right)\left(\frac{d_c/\theta}{\dot{q}_0} + 1\right)^{-1/m} \tag{4.40}$$

where μ_s, μ_d, m, p, $\dot{q}_0$, $\dot{q}_1$, d_c and $\dot{\theta}_0$ are constants.

The evolution equation for the internal variable θ is chosen as:

$$\dot{\theta} = \dot{\theta}_0\left(1 - \frac{\theta \dot{q}^{slip}}{d_c}\right) \tag{4.41}$$

The slip rate is written as the sum of an elastic part and an inelastic part in a manner similar to the decomposition of strain rates in small-strain plasticity. An elastic stiffness is also assumed in the normal direction when the surfaces are in contact, and finally it is assumed that the rate forces are zero if no contact exists. The traction rates are then:

$$\dot{t}_n = \begin{cases} C_n \dot{q}_n & \text{for } T_n < 0 \\ 0 & \text{for } T_n \geq 0 \end{cases} \tag{4.42}$$

$$\dot{t}_s = \begin{cases} C_s(\dot{q}_s - \text{sgn}(T_s))\dot{q}^{slip} & \text{for } T_n < 0 \\ 0 & \text{for } T_n \geq 0 \end{cases} \tag{4.43}$$

where C_n and C_s are the normal and tangential elastic stiffnesses respectively associated with the interface.

Solving for $\dot{q}^{slip}$ the relations (4.38), (4.39) and (4.40) gives:

$$\dot{q}^{slip} = \begin{cases} \dot{q}_0 \left[\left(\dfrac{|T_s|}{-T_n g(\theta)} \right)^m - 1 \right] & \text{for } \left(\dfrac{|T_s|}{-T_n g(\theta)} \right) > 1 \\ 0 & \text{for } \left(\dfrac{|T_s|}{-T_n g(\theta)} \right) \leq 1 \end{cases} \tag{4.44}$$

These equations have been integrated by Povirk & Needleman (1993) using a rate time tangent modulus method developed for metal plasticity by Peirce et al. (1984). From increment m to increment $(m+1)$ it is assumed that:

$$\dot{q}^{slip} = (1-\gamma)\dot{q}^{slip}_m + \gamma \dot{q}^{slip}_{m+1} \tag{4.45}$$

where γ is an integration parameter that can range in value from 0 to 1. In the cases studied here, $\gamma = 1$ furnished the numerically most stable results. The sliding rate at increment $(m+1)$ is approximated by a first order expansion in T_s, T_n and θ:

$$\dot{q}^{slip}_{m+1} = \dot{q}^{slip}_m + \Delta t \left(\frac{\partial \dot{q}^{slip}}{\partial |T_s|} \text{sgn}(T_s)\dot{t}_s + \frac{\partial \dot{q}^{slip}}{\partial T_n}\dot{t}_n + \frac{\partial \dot{q}^{slip}}{\partial \theta}\dot{\theta} \right) \tag{4.46}$$

Combining (4.43), (4.45) and (4.46) gives:

$$\dot{t}_s = C_s^{\text{tan}} \dot{q}_s - \dot{R} \quad \text{for} \quad T_n < 0 \tag{4.47}$$

where

$$C_s^{tan} = \frac{C_s}{1 + \gamma \Delta t \dfrac{\partial \dot{q}^{slip}}{\partial |T_s|} C_s} \tag{4.48}$$

$$\dot{R} = C_s^{tan} \text{sgn}(T_s) \left[\dot{q}^{slip}_m + \gamma \Delta t \left(\frac{\partial \dot{q}^{slip}}{\partial T_n} C_n \dot{q}_n + \frac{\partial \dot{q}^{slip}}{\partial \theta}\dot{\theta} \right) \right] \tag{4.49}$$

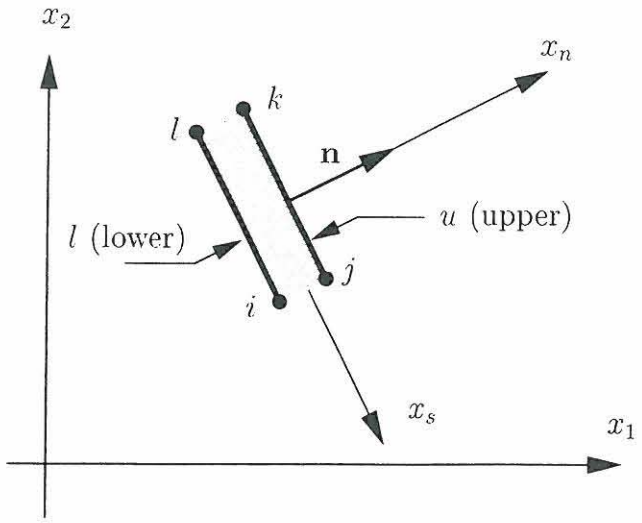

Figure 4.3: Interface two-dimensional element with 4 nodes.

4.5 Finite Element Implementation

4.5.1 Interface Elements

Consider the element shown in figure 4.3 where two coordinate systems are shown: the local system aligned with the vectors **s-n**, and the global (x_1, x_2)-system. The displacement vector is denoted $\mathbf{u}_l$ in the local coordinate system and $\mathbf{u}$ in the global system. Their components are:

$$\begin{aligned} \mathbf{u}_l^T &= \begin{bmatrix} u_s^l & u_n^l & u_s^u & u_n^u \end{bmatrix} \\ \mathbf{u}^T &= \begin{bmatrix} u_1^l & u_2^l & u_1^u & u_2^u \end{bmatrix} \end{aligned} \tag{4.50}$$

where $()^T$ indicates the matrix transpose. The displacements in the systems are interrelated through the rotation matrix $\mathbf{R}_2$:

$$\begin{bmatrix} u_1 \\ u_2 \end{bmatrix} = \begin{bmatrix} \cos\alpha & -\sin\alpha \\ \sin\alpha & \cos\alpha \end{bmatrix} \begin{bmatrix} u_s \\ u_n \end{bmatrix} = \mathbf{R}_2 \begin{bmatrix} u_s \\ u_n \end{bmatrix} \tag{4.51}$$

and

$$\begin{bmatrix} u_s \\ u_n \end{bmatrix} = \mathbf{R}_2^T \begin{bmatrix} u_1 \\ u_2 \end{bmatrix} \tag{4.52}$$

where α is the angle between the local and the global coordinate systems.

For a general two-dimensional interface element the nodal displacement vector is denoted $\mathbf{v}_l$ in the local coordinate system and $\mathbf{v}$ in the global coordinate system, respectively. Their components are given by:

$$\begin{aligned} \mathbf{v}_l^T &= \begin{bmatrix} u_s^1 & u_n^1 & u_s^2 & u_n^2 & u_s^3 & u_n^3 & \cdots \end{bmatrix} \\ \mathbf{v}^T &= \begin{bmatrix} u_1^1 & u_2^1 & u_1^2 & u_2^2 & u_1^3 & u_2^3 & \cdots \end{bmatrix} \end{aligned} \tag{4.53}$$

where $\mathbf{v}_l$ and $\mathbf{v}$ are related by:

$$\mathbf{v}_l = \mathbf{R}^T \mathbf{v} \tag{4.54}$$

with

$$\mathbf{R}^T = \begin{bmatrix} \mathbf{R}_2^T & \mathbf{0} & \mathbf{0} & \cdots \\ \mathbf{0} & \mathbf{R}_2^T & \mathbf{0} & \cdots \\ \mathbf{0} & \mathbf{0} & \mathbf{R}_2^T & \cdots \\ \vdots & \vdots & \vdots & \ddots \end{bmatrix} \tag{4.55}$$

where $\mathbf{R}$ is a rotational matrix relating both systems of coordinates.

In the local coordinate system, the displacements are interpolated between the nodes using the shape function matrix $\mathbf{N}_l$, such that:

$$\mathbf{u}_l = \mathbf{N}_l \mathbf{v}_l \tag{4.56}$$

In particular, for the two-dimensional element shown in figure 4.3:

$$\mathbf{N}_l = \begin{bmatrix} N_1 & 0 & 0 & 0 & 0 & 0 & N_2 & 0 \\ 0 & N_1 & 0 & 0 & 0 & 0 & 0 & N_2 \\ 0 & 0 & N_1 & 0 & N_2 & 0 & 0 & 0 \\ 0 & 0 & 0 & N_1 & 0 & N_2 & 0 & 0 \end{bmatrix} \tag{4.57}$$

Then from (4.56) and (4.54):

$$\mathbf{u}_l = \mathbf{N}\mathbf{v} \tag{4.58}$$

where

$$\mathbf{N} = \mathbf{N}_l \mathbf{R}^T \tag{4.59}$$

The relative displacements $\mathbf{q}_l$ in the local system between two points in the upper and lower part of the element are:

$$\mathbf{q}_l = \begin{bmatrix} q_s \\ q_n \end{bmatrix} = \begin{bmatrix} u_s^u - u_s^l \\ u_n^u - u_n^l \end{bmatrix} = \mathbf{L}\mathbf{u}_l \tag{4.60}$$

where

$$\mathbf{L} = \begin{bmatrix} -1 & 0 & 1 & 0 \\ 0 & -1 & 0 & 1 \end{bmatrix} \tag{4.61}$$

The relative displacements in the local system can be expressed in terms of the nodal displacements in the global system as:

$$\mathbf{q}_l = \mathbf{B}\mathbf{v} \tag{4.62}$$

where

$$\mathbf{B} = \mathbf{L}\mathbf{N} \tag{4.63}$$

Finally, the incremental form of the tractions is given by:

$$\dot{\mathbf{T}}_l = \begin{bmatrix} \dot{T}_s \\ \dot{T}_n \end{bmatrix} = \mathbf{D}\dot{\mathbf{q}}_l + \dot{\mathbf{Q}} \tag{4.64}$$

where for the cohesive model:

$$\mathbf{D} = \begin{bmatrix} \frac{\partial T_s}{\partial q_s} & \frac{\partial T_s}{\partial q_n} \\ \frac{\partial T_n}{\partial q_s} & \frac{\partial T_n}{\partial q_n} \end{bmatrix} \tag{4.65}$$

and $\dot{\mathbf{Q}}$ is the null matrix. In the friction case we may get:

$$\mathbf{D} = \begin{bmatrix} C_s^{tan} & -C_s^{tan}\mathrm{sgn}(T_s)\gamma\Delta t\frac{\partial \dot{q}^{slip}}{\partial T_n}C_n \\ 0 & C_n \end{bmatrix} \tag{4.66}$$

and

$$\dot{\mathbf{Q}} = \begin{bmatrix} -C_s^{tan}\mathrm{sgn}(T_s)\left[\dot{q}_m^{slip} + \gamma\Delta t\frac{\partial \dot{q}^{slip}}{\partial \theta}\dot{\theta}\right] \\ 0 \end{bmatrix} \tag{4.67}$$

4.5.2 The large slip friction problem

A problem occurs if conventional interface elements are used to model the frictional laws when the displacements have the same order of magnitude as the size of the element. As illustrated in figure 4.4, for two points which are initially adjacent, one in the upper surface and the other in the lower surface, after the displacement, the tractions at these points occur on two different locations and can therefore be completely different at the two points. The same problem arises for the internal parameter θ.

The problem is worse if the magnitude of the slip displacement q_s is greater than the size of the element. In that case, not only the magnitude of θ and $\mathbf{T}$ is different, but the element is also reproducing a non-physical contact between surfaces, the lower surface and the upper surface are not in contact at all.

In order to solve this problem, here it is supposed that the tractions $\mathbf{T}$ and θ are functions that depend on the position on the lower contact surface. It will be supposed that $\mathbf{T}$ and θ are smooth functions and that the values can be interpolated between known points. The values of $\mathbf{T}$ and θ are computed and stored in every step of the analysis in several points along the axis s defined in figure 4.5.

If the tangential slip displacement q_s exceeds the size of the element, the connectivities of the interface elements are updated. This is only possible if all interface elements have the same length.

4.5.3 Numerical Solution to the Nonlinear Problem

The problem is solved using the arc-length control strategy, see e.g. (Crisfield 1981) and (Crisfield 1991), including two simple modifications of the standard algorithm,

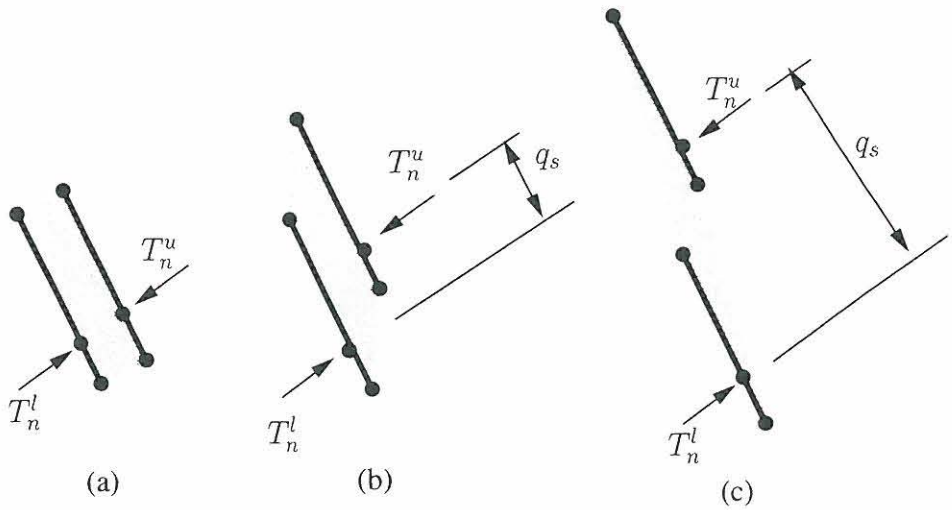

Figure 4.4: Large slip displacements in a conventional interface finite element (a) before displacement, (b) slip is less than the size of the element, and (c) slip greater than the size of the element.

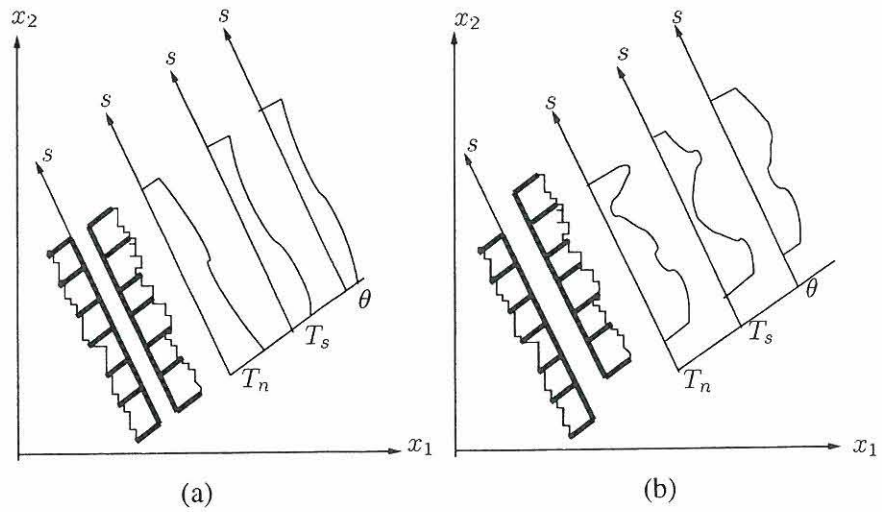

Figure 4.5: The state variable θ and the tractions are functions of the position along the axis 's'. (a) the initial situation, (b) after some slip has occurred.

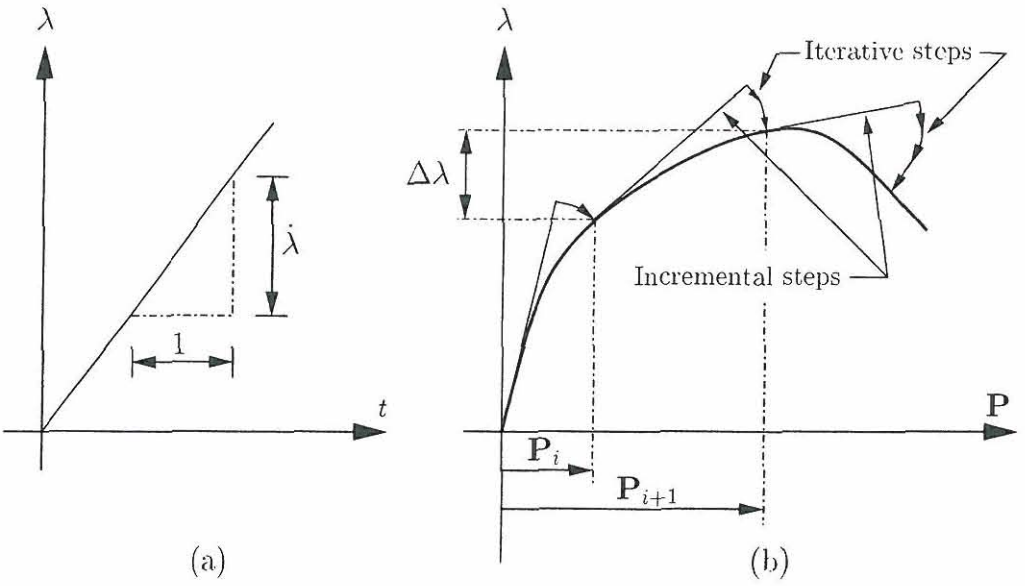

Figure 4.6: (a) Load level vs time, (b) Solution sequence.

which are due to the inclusion of rate forces that are dependent on displacements and time, and due to the explicit inclusion of time in the constitutive friction law.

In the implementation, a curve relating the load level λ with time is defined. In the present contribution it is assumed as the linear relation shown in figure 4.6(a). The increment in time is always taken as a positive number, corresponding to the slope of the curve λ vs. t in the value of λ considered.

The increment in load level is defined as $\Delta\lambda = \dot{\lambda}\Delta t$ and the corresponding increment in nodal displacements is $\Delta\mathbf{P} = \dot{\mathbf{P}}\Delta t$. The shape of the total external nodal forces is represented by the vector $\mathbf{q}_0$ and proportional loading is supposed such that:

$$\mathbf{q} = \lambda\mathbf{q}_0 \qquad \text{and} \qquad \frac{\partial \mathbf{q}}{\partial \lambda} = \mathbf{q}_0 \tag{4.68}$$

where $\mathbf{q}$ is the external load corresponding to the load level λ.

The tangential displacement $\boldsymbol{\delta}_T$ is defined in the form:

$$\Delta\mathbf{P} = \Delta\lambda\boldsymbol{\delta}_T \tag{4.69}$$

Then it is required for (4.69) that:

$$\mathbf{K}\boldsymbol{\delta}_T = \mathbf{f}^* \tag{4.70}$$

where $\mathbf{K}$ is the tangent stiffness matrix, and the load $\mathbf{f}^*$ is defined as:

$$\mathbf{f}^* = \mathbf{q}_0 + \frac{\Delta t}{\Delta\lambda}\dot{\mathbf{f}} \tag{4.71}$$

The solution, disregarding the iterative part, proceeds in the following sequence for step i:

1. Compute $\Delta t = \Delta\lambda^{(i-1)}/\dot{\lambda}$ where $\dot{\lambda}$ is the slope of the curve load level vs. time.

2. Compute $\dot{\mathbf{R}}$, $\mathbf{K}$, and $\mathbf{f}^*$ using the values of variables resulting from step $(i-1)$.

3. Compute the tangential displacement resulting from (4.70).

4. Compute $\Delta\lambda$ by using:

$$\Delta\lambda = \pm \frac{\Delta l}{\sqrt{\boldsymbol{\delta}_T^T \boldsymbol{\delta}_T + \psi^2 \mathbf{f}^{*T} \mathbf{f}^*}} \tag{4.72}$$

where the sign depends on the traced branch of the loading path, Δl is the radius of the spherical hyper-surface in the space $(\lambda, \mathbf{u})$, and ψ is a scalar factor which takes into account that λ and $\mathbf{u}$ have different scales.

5. Compute $\Delta\mathbf{P}$ using (4.69).

6. Update the results using:

$$\mathbf{P}_i = \mathbf{P}_{i-1} + \Delta\mathbf{P} \tag{4.73}$$
$$\lambda_i = \lambda_{i-1} + \Delta\lambda \tag{4.74}$$
$$\theta_i = \theta_{i-1} + \dot{\theta}\Delta t \tag{4.75}$$
$$q_i = q_{i-1} + \dot{q}\Delta t \tag{4.76}$$
$$\boldsymbol{\sigma}_i = \boldsymbol{\sigma}_{i-1} + \Delta\boldsymbol{\sigma} \tag{4.77}$$

The procedure described is repeated until a *maximum* displacement or a maximum load level is reached.

4.6 Numerical examples

4.6.1 Introduction

In Fiber Reinforced Concrete (FRC) fibers are added to the cementitious matrix. The role of these fibers consists in bridging forces between cracks, where the fibers can act as ligaments. In this form, it is possible to have a reduced crack propagation compared with conventional concrete.

The crack bridging force can be characterized by a fiber pull-out test performed on a single fiber. The results of the test give a good indication of the behavior of the fiber in the structure.

The pull-out test itself under uniform friction and when the slip extends over distances that are large compared to the fiber diameter has been investigated by Marshall, Cox & Evans (1985), McCartney (1989), Hutchinson & Jensen (1990), Freund (1992), more recently including high loading rates by Cox et al. (2001) and Sridhar et al. (2003).

There are important differences between the pull-out test and the behavior in situ, the most notable difference being that the fibers in the concrete matrix are randomly oriented. Therefore, the forces have two components and the fiber is bent in the crack plane, sometimes developing plastic deformation (Chanvillard & Aitcin 1996).

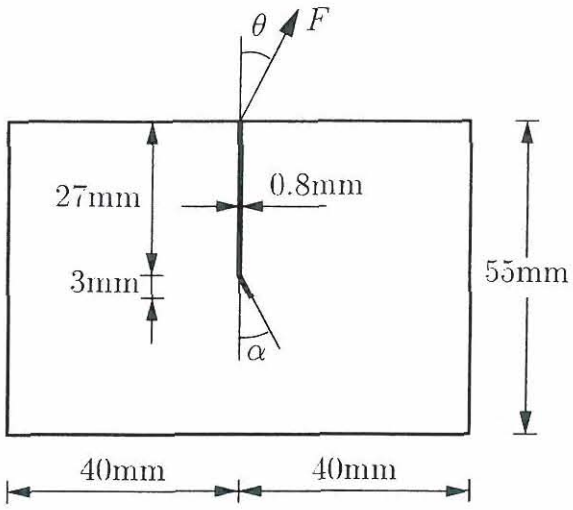

Figure 4.7: Single fiber embedded in a concrete matrix.

Modeling of fiber pull-out in FRC has been performed using interface elements including Coulomb friction models (Ballarini et al. 1990), (Mital & Chamis 1991), (Li & Mobasher 1998). An analysis using interface elements equipped with a rate- and state-dependent friction law has been done by Cifuentes et al. (2005). The analysis by Cifuentes et al. (2005) considers the fiber and the concrete matrix as elastic bodies in plane strain, thus allowing the study of hooked ends in the fibers and non-symmetric load condition. The study is extended here in order to include large slip displacements and cohesive forces.

All the numerical examples presented here assume a modified Ruina-Dieterich model for the friction and a Xu-Needleman cohesive model for the cohesive part, in both cases supposing plane strain conditions.

The elements used here are quadrilateral isoparametric with four nodes. These elements are used for the concrete matrix and the fiber. The interface between the concrete and the fiber uses four node interface elements. The interface between the fiber and the concrete matrix is modeled using the elements developed in section 4.5, and the integration is performed numerically using four Gauss integration points and the cohesive and friction models.

4.6.2 A hooked fiber pull-out test

The first examples correspond to pull-out test carried out in (Weiler & Grosse 1996) over a cold-drawn steel wire fiber produced by a Belgian manufacturer, with a diameter of 0.8 mm, embedded 30 mm with and without hooked ends. As sketched in figure 4.7, a single fiber embedded in a concrete matrix is considered. Both the fiber and the concrete matrix are taken to be isotropic linear elastic materials. The interface between the fiber and the surrounding matrix is characterized by a rate and state friction law as specified in Section 4.4.2. Geometry changes are neglected. In addition to restricting attention to small displacement gradients, in the present context, neglecting geometry changes also restricts the analysis to small amounts of sliding.

Property	Range investigated	Value most used here
C_n	$0.3 - 30$ GPa/mm	3 GPa/mm
C_s	$0.1 - 10$ GPa/mm	1 GPa/mm
ϕ_n	$1x10^{-5}$	$1x10^{-5}$
σ_{max}		30 Mpa
τ_{max}	$1.6 - 5$ MPa	2 Mpa
μ_s	$1 - 025$	0.5
μ_d	$0.25 - 0.05$	0.15
δ_c		4 mm
$\dot{q}_1$		10 mm/s
$\dot{q}_0$		100 mm/s
p		0.5
m		5
θ_0		4.6052
E_f		210 GPa
E_c		30 GPa
ν_f		0.3
ν_c		0.2
p_0	$2 - 10$ MPa	5 Mpa

Table 4.1: Properties used in the analysis. E_f and E_c correspond to elastic moduli of the fiber and concrete. ν_f and ν_c correspond to Poisson ratio of the fiber and concrete matrix.

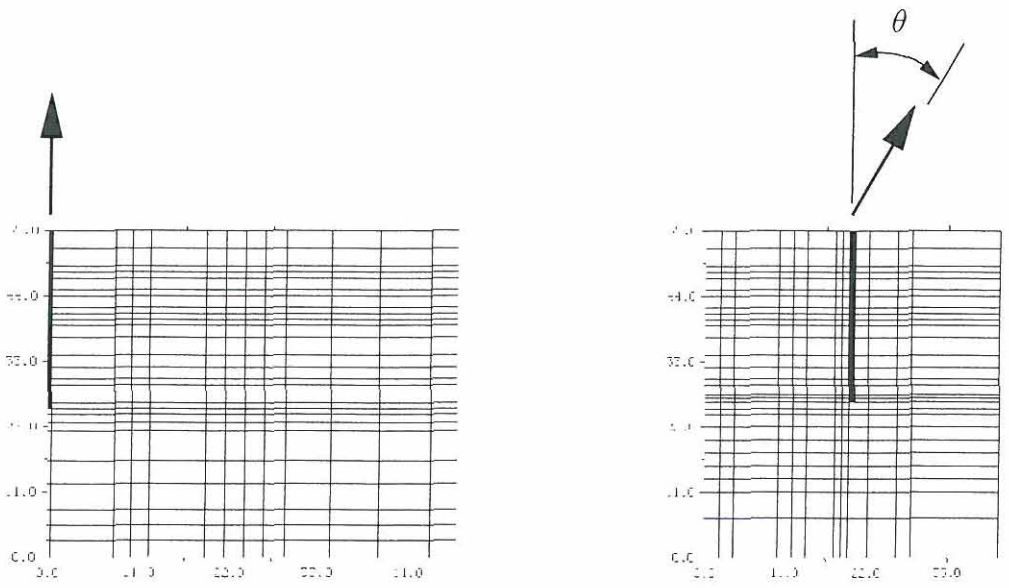

(a) (b)

Figure 4.8: Finite elements used for (a) symmetric cases and (b) non-symmetric cases.

The properties used for the interface were based on the values presented by Li & Stang (1997). A clamping pressure was introduced into the analysis. For this, a range of values based on (Stang 1996) has been used. In table 4.1 the range of values for different parameters used in the analysis is presented.

The finite element mesh shown in figure 4.8 was used. The boundary conditions are shown in figure 4.9. A hook at the end of the fiber was studied using the mesh shown in figure 4.10.

Several graphics of force vs slip displacement are used to illustrate the effect of the different parameters in the friction law. First the influence of the elastic stiffness is investigated, and the results including variations in the elastic stiffness (C_n and C_s) are shown in figure 4.11. Larger values of the elastic constants usually result in instability of the model; smaller values were not used, because they fail to represent adequately the initial slope of the curve force vs slip displacement.

The effect of the static coefficient of friction can be seen in figure 4.12. Changes in this coefficient produces important changes in the resisted force and in the slope of the initial part of the slip displacement vs force diagram. A value of $\mu_s = 0.5$ results in good agreement with the force expected for the range of values of the slip displacement considered.

The effect of the clamping pressure is shown in figure 4.13. As expected, the clamping pressure was an important factor in the pull-out test. Failures in the estimation of this force can produce meaningless results. Even if the friction model supposes a non-constant coefficient of friction, the shear tractions depend directly on the values of the normal traction.

The effect of the component of the force in the plane of the crack is presented in figure 4.14.

Finally the effect of the hooked ends in the slip is shown in figure 4.15. The

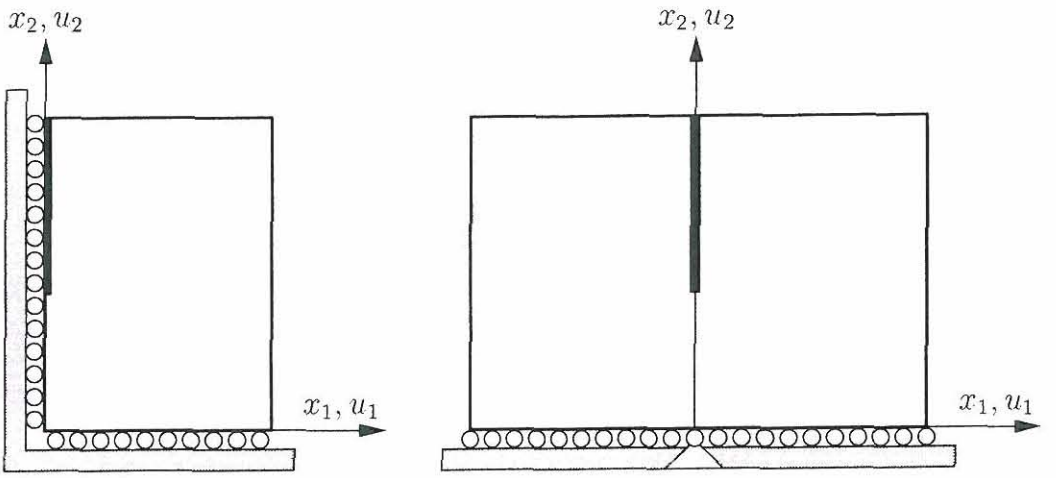

Figure 4.9: Boundary conditions for (a) symmetric and (b) non-symmetric cases.

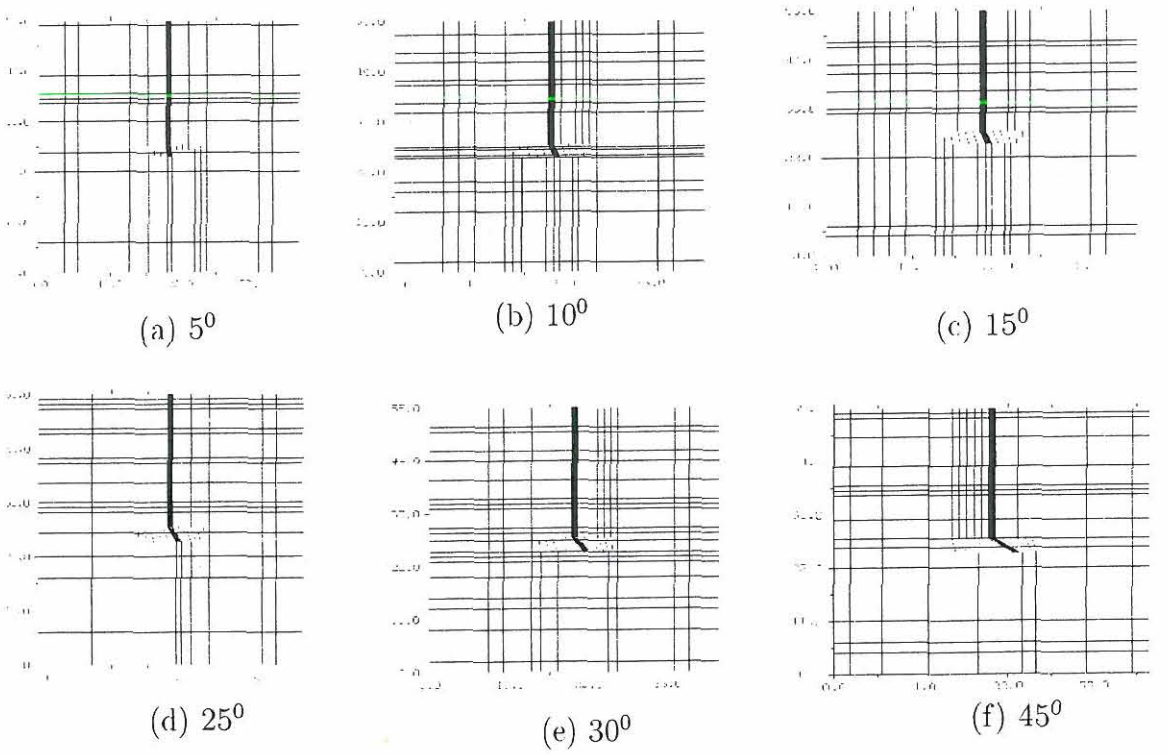

Figure 4.10: Finite elements used for fibers with hooked ends.

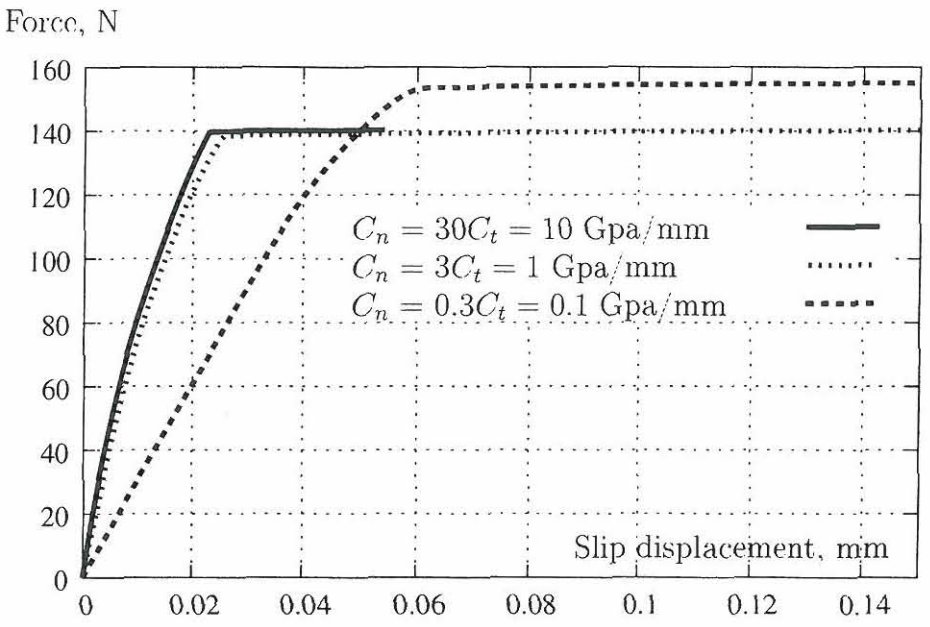

Figure 4.11: Effect of variations in elastic stiffness.

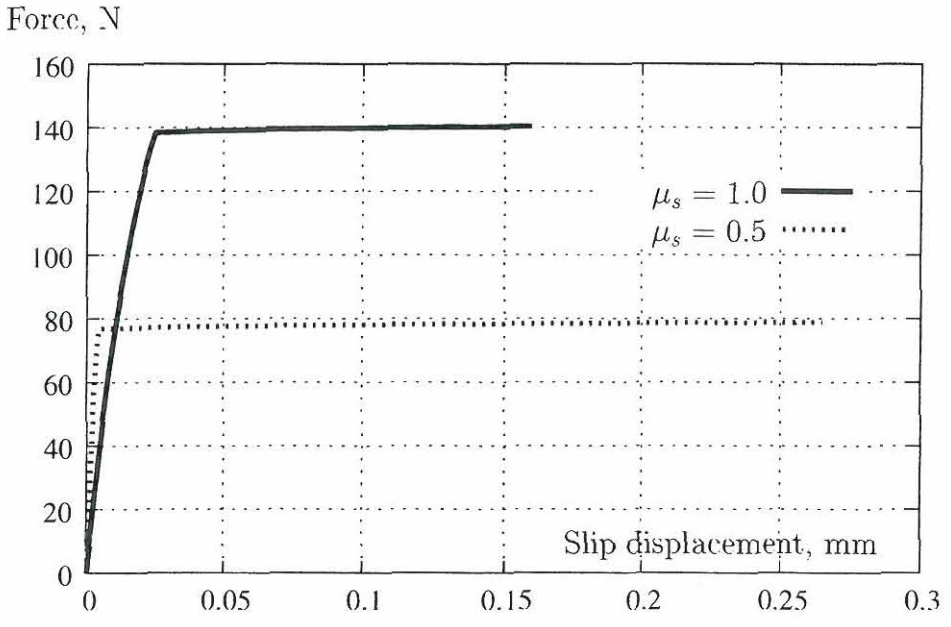

Figure 4.12: Effect of variation of the static coefficient of friction.

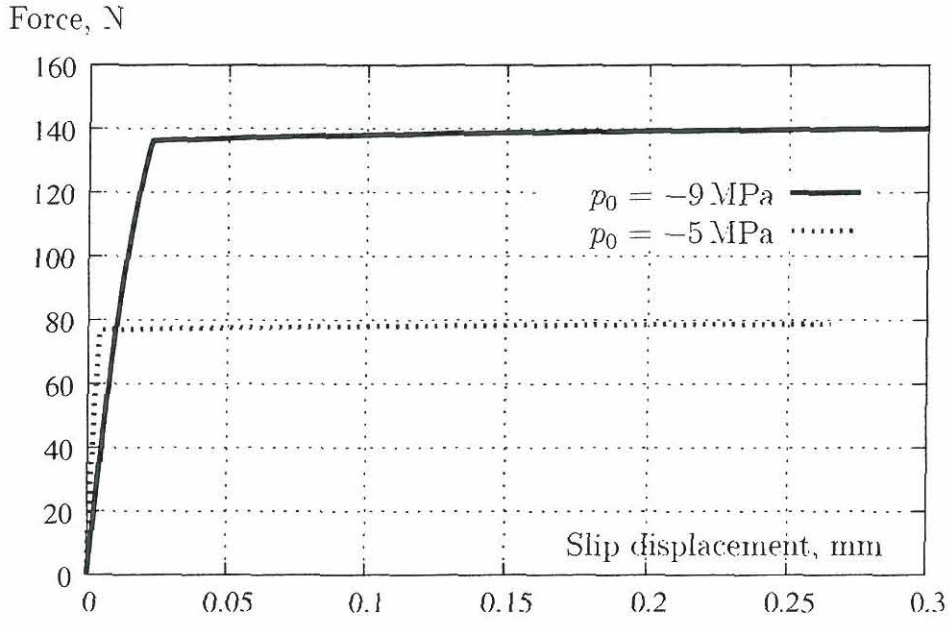

Figure 4.13: Effect of the clamping pressure.

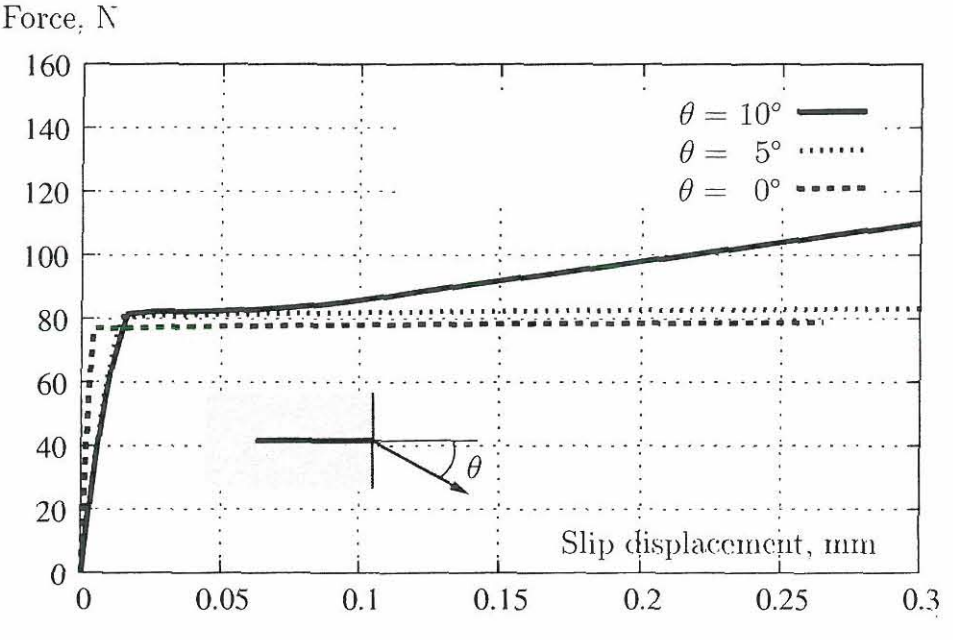

Figure 4.14: Effect of components of the force in the plane of the crack for varying values of the inclination θ of the applied load.

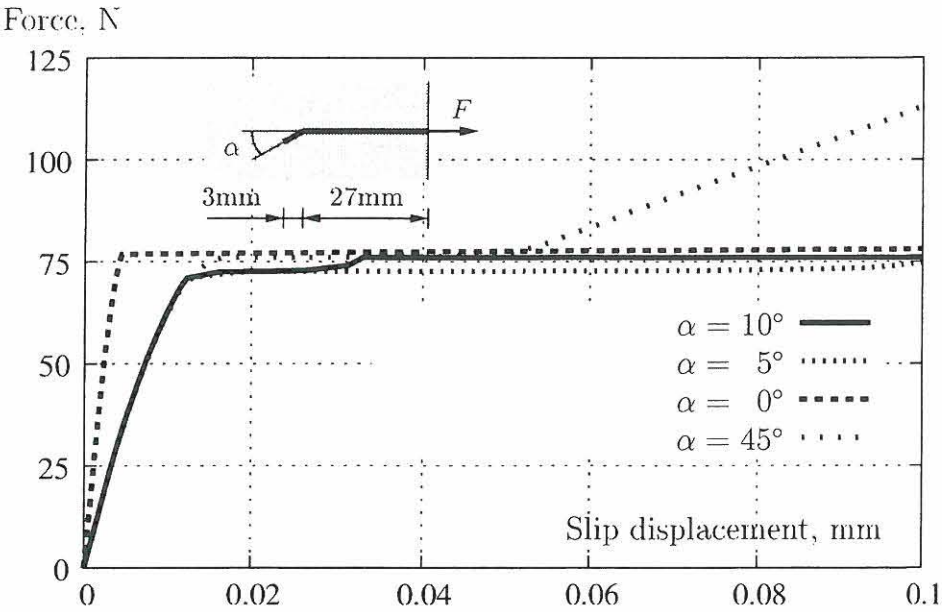

Figure 4.15: Slip displacement, comparing three cases including hooked ends.

effect of hook, as is observed, has a bigger influence after a slip displacement of 0.05mm. The net effect of the hook is the increment in the force required to produce a displacement after some initial displacement has ocurred.

Results including the large slip analysis were carried out until a displacement of 4 mm is reached. It is possible to observe in figure 4.16 that the force required to slip the fiber is increasing in magnitude until a large displacement (1.5 mm) is reached. In the case presented in figure 4.16 for displacements greater than 1.5 mm, the load level remains constant.

The effect of the component of the force in the plane of cracking is also illustrated in figure 4.17, showing that for small components of the force in the plane of the crack, the bending effects are more important than at the beginning of the pull-out. The tractions at both sides of the fiber are reaching a maximum value starting from the pulled end and then this is kept with small variations.

4.6.3 Analysis including cracking of concrete

A new series of analyses were carried out for a system composed of two straight fibers parallel one to another as shown in figure 4.18. A complete list of parameters used is presented in table 4.2.

As in section 4.6.2 the properties used for the materials and interfaces were based on the values presented by Li & Stang (1997) and Zhang & Li (2002), and a clamping pressure of 5Mpa was introduced into the analysis based on (Stang 1996).

To simulate the cracking of the concrete matrix, only cohesive interface elements using the cohesive model defined in section 4.4.1 were used between the quadrilateral elastic elements representing the concrete matrix. In figure 4.19 all the elements are shown by shrinking the mesh. Observe that the symmetry of the problem has been used.

Three finally deformed shapes are shown in figure 4.20. In this figure it is possible

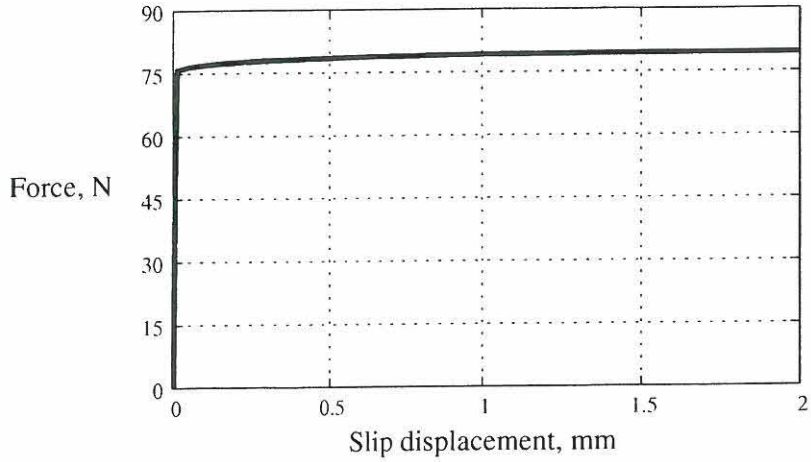

Figure 4.16: Force vs slip displacement in a pull-out test of a single steel fiber with $t = 0.8$ mm

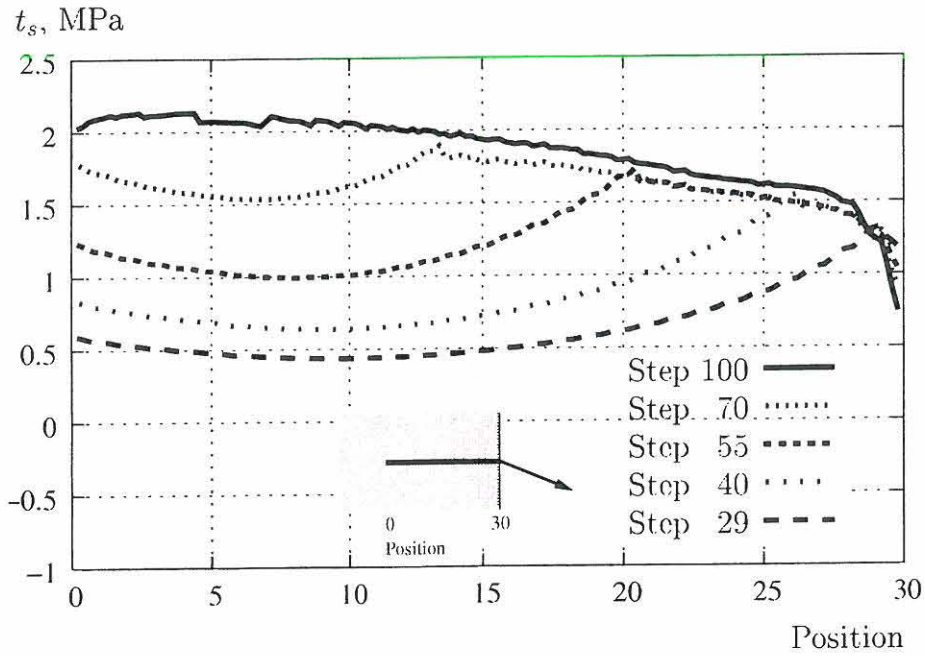

Figure 4.17: Shear tractions along the upper side of the fiber at different steps for $\theta = 5°$.

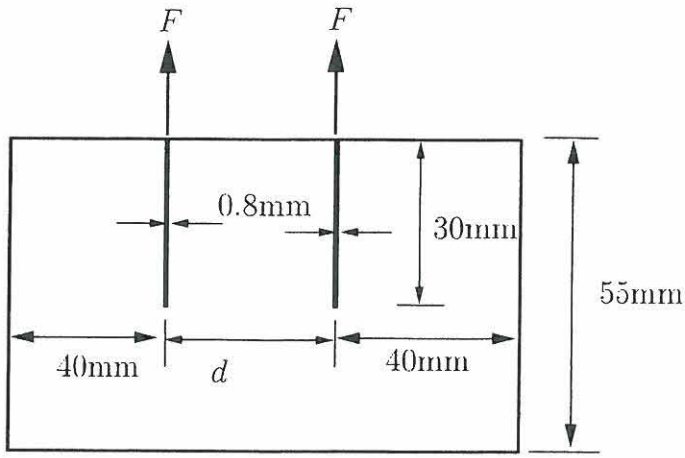

Figure 4.18: Two fibers embedded in a concrete matrix

Prop.	Concrete matrix	Steel fiber	interface Steel-Conc.	interface Conc.-Conc.
E	30 GPa	210 GPa		
ν	0.2	0.3		
C_n			3 GPa/mm	30 GPa/mm
C_s			1 GPa/mm	10 GPa/mm
ϕ_n			$1x10^{-5}$	0.1
σ_u	2.8 Mpa	30 Mpa		
τ_u	2.8 MPa	10 Mpa		
μ_s			0.5	
μ_d			0.15	
δ_c			4 mm	
$\dot{q}_1$			10 mm/s	
$\dot{q}_0$			100 mm/s	
p			0.5	
m			5	
θ_0			4.6052	

Table 4.2: Properties used in the analysis. E and ν are the elastic modulus and Poisson ratio, respectively.

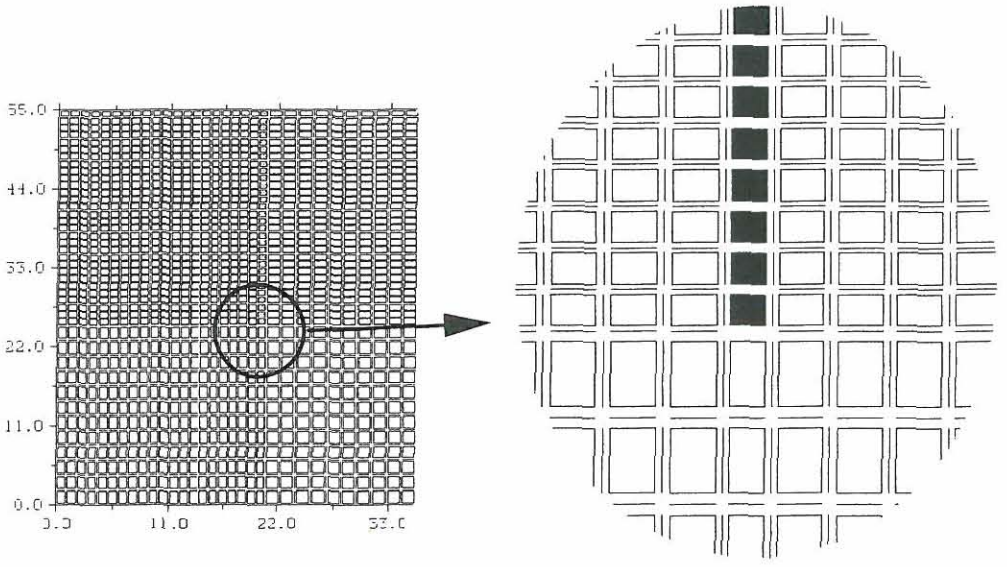

Figure 4.19: A typical mesh showing shrinked elements. The lines between quadrilateral elements are the interface elements.

to observe that during the pull-out, a block of concrete between the fibers is pulled, this effect is reduced with the increment of the distance between fibers.

The effect of the group of fibers can be observed in figure 4.21 where the force required to pull out the fibers is compared with the case of an isolated fiber. When the distance is small, the magnitude of the total force required to extract the two fibers is the same as in the case of a single fiber. This is probably due to the fact that in this plane strain analysis, the contribution to the pull-out force is due to a single side of the fiber. At the other side, the concrete is moving with the fiber, and the friction force is then zero. This effect is reduced when the distance between fibers increases.

4.7 Conclusions

In this document the implementation of interface elements has been presented. The constitutive models corresponding to a cohesive surface and to a friction surface have been explained. This method and a solution scheme based on the arc-length control strategy have been applied to model the pull-out test of fibers embedded in a concrete matrix, extending the results presented in Cifuentes et al. (2005).

A simple procedure, just updating the contact surfaces, is proposed to model large slip between the concrete and the fiber. This approach is valid if the strains are small and if the tractions and state variables do not have large variations over small distances.

It is concluded that the rate- and state dependent friction model is able to adequately represent the behavior observed in fiber pull-out tests. It is also concluded that it is possible to model the pull-out test including concrete cracking. In order to do this, modeling of the concrete using a cohesive model and the use of a friction

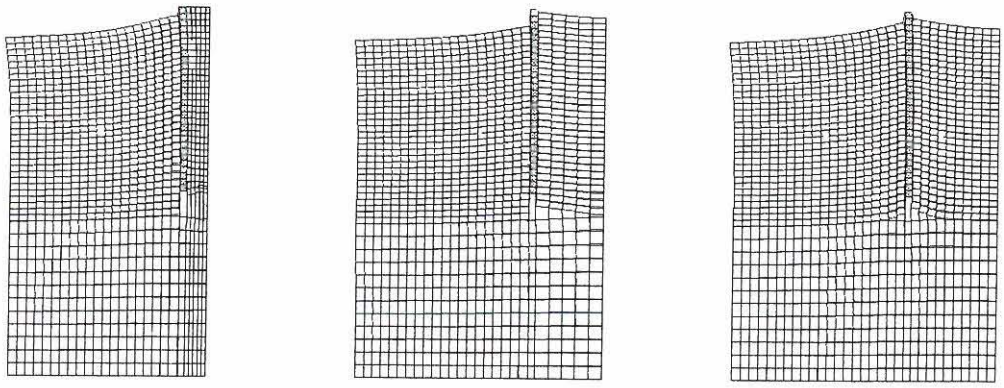

Figure 4.20: Three deformed shapes for different distances between fibers.

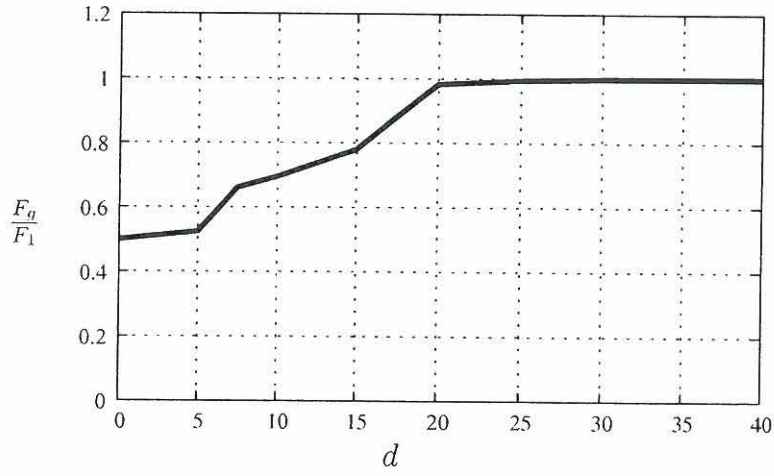

Figure 4.21: Forces required to pull out a single fiber as a function of the distance between fibers. F_1 is the force required to pull out a single fiber, F_g is the force required for every fiber, d is the distance between fibers. The fibers are made in steel, embedded 30 mm in the concrete matrix with a thickness of 0.8 mm.

model are required for the interface fiber-concrete.

From the numerical examples it is concluded that factors like the shape of the fiber, the clamping pressure in the system, and the direction of the pull-out force are important. However, it is clearly evident from the analysis that the presence of other fibers can dramatically affect the pull-out force, diminishing the capacity of every single fiber.

In the future, different fiber arrangements must be studied using the same kind of models. Ideally the analysis must be extended to the third dimension using the same theory as the one presented here.

Modeling of new pull-out tests is required in order to test the accuracy of the large slip analysis presented here. The results obtained here are similar to the results in Cifuentes et al. (2005) for small slip distances, but the author, using the present approach, was unable to model the descending branch of the curve slip vs force. Modeling of more cases is required to know the limits to the validity of the results.

Bibliography

Ballarini, R., Ahmed, S. & Mullen, R. L. (1990), *in* 'Proceedings of the international conference on interfaces in metal ceramics composites, February 19–22; 1990', pp. 349 388.

Brace, W. F. & Byerlee, J. P. (1966), 'Stick-slip as a mechanism for earthquakes', *Science* **153**(3739).

Byerlee, J. D. (1970), 'Mechanics of stick-slip', *Tectonophysics* **9**(5).

Camacho, G. T. & Ortiz, M. (1996), 'Computational modeling of impact damage in brittle materials', *Internat. J. Solids Structures* **33**, 2899–2938.

Chanvillard, G. & Aitcin, P. (1996), 'Pull-out behavior of corrugated steel fibers', *Advanced cement based materials* **4**, 28–41.

Cifuentes, G. C., Needleman, A. & Byskov, E. (2005), 'An analysis of fiber pull-out in steel fiber reinforced concrete', *In preparation* **1**(1), 1 20.

Clough, R. W. (1962), Stress distribution of norfolk dam, Technical report, Department of Civil Engineering, University of California, Berkeley.

Coker, D., Rosakis, A. J. & Needleman, A. (2003), 'Dybamic crack growth along a polymer composity-homalite interface', *J. Mech. Phys. Solids* **51**, 425–460.

Cox, B. N., Sridhar, N. & Beyerlin, I. J. (2001), 'Inertial effects in the pull-out mechanism during dynamic loading of a bridged crack', *acta mater.* **49**, 3863 3877.

Crisfield, M. A. (1981), 'A fast incremental-iterative solution procedure that handles "snap-through"', *Computers and Structures* **13**, 55 62.

Crisfield, M. A. (1991), *Non-linear Finite Element analysis of Solids and Structures*, Vol. Volume 1: essentials, John Wiley and Sons, Chichester.

Dieterich, J. H. (1979), 'Modelling of rock friction 1. experimental results and constitutive equations', *J. Geophys. Res.* **84**(B5), 2161 2168.

Dieterich, J. H. (1992), 'Earthquake nucleation on faults with rate-dependent and state-dependent strenght', *Tectonophysics* **211**(1–4), 115–134.

Duvaud, G. (1980), 'Problemes mathematiques de la mecanique-equilibre d'an solide elastique avec contact unilateral et frottement de coulomb', *C.R. Acad. Sci. Paris* **290 (Serie A)**, 263–265.

Duvaut, G. & Lions, J. L. (1976), *Inequalities in mechanis and physics*, Springer Verlag, Berlin.

Freund, L. B. (1992), 'The axial force needed to slide a circular fiber along a hole in an elastic-material and implications for fiber pull-out', *European Journal of Mechanics, A-Solids* **11**, 1–19.

Heaton, T. H. (1990), 'Evidence for and implication of self-healing pulses of slip in earthquake rupture', *Physics of the earth and planetary interiors* **64**(1), 1–20.

Hutchinson, J. W. & Jensen, H. M. (1990), 'Models of fiber debonding and pullout in brittle composites with friction', *Mechanics of materials* **9**, 139–163.

Ingraffea, A. R. & Sauoma, V. (1985), Numerical modelling of discrete crack propagation in reinforced and plain concrete, *in* 'Fracture mechanics of concrete', Martinus Nijhoff Publishers, Dordrecht, pp. 171 225.

Li, C. Y. & Mobasher, B. (1998), 'Finite element simulations of fiber pullout toughening in fiber reinforced cement based composites', *Advanced cement based materials* **7**, 123–132.

Li, V. C. & Stang, H. (1997), 'Interface property characterization and strengthening mechanism in fiber reinforced cement based composites', *Advanced cement based materials* **6**, 1 20.

Marshall, D. B., Cox, B. N. & Evans, A. G. (1985), 'The mechanics of matrix cracking in brittle-matrix fiber composite', *Acta Metall* **33**, 2013 2021.

McCartney, L. N. (1989), 'New theoretical model of stress transfer between fibre and matrix in a uniaxially fibre-reinforced composite', *Proc. Roy. Soc. London* pp. 215–244.

Mital, S. K. & Chamis, C. (1991), 'Fiber pushout test - a 3-dimensional finite element computational simulation', *J. Compos. Technol. Res.* **13**, 14 21.

Needleman, A. (1987), 'A continuum model for void nucleation by inclusion debonding', *Journal of Applied Mechanics* .

Ngo, D. & Scordelis, A. C. (1967), 'Finite element analysis of reinforced concrete beams', *Journal of the American Concrete Institute* **64**, 152 163.

Oliver, J. (1996), 'Modelling strong discontinuities in solid mechanics via strain softening constitutive equations. part 2: Numerical simulation', *International Journal for Numerical Methods in Engineering* .

Peirce, D., Shih, C. F. & Needleman, A. (1984), 'A tangent modulus method for rate dependent solids', *Comp. Struct.* **18**, 857–887.

Povirk, G. L. & Needleman, A. (1993), 'Finite elements simulations of fiber pull-out', *Journal of Engineering Materials and Technology* **115**, 286 291.

Rice, J. R. & Ben-Zion, Y. (1996), 'Slip complexity in earthquake fault models', *Proceeding of the national academy of sciences of the United States of America* **93**(9), 3811–3818.

Rice, J. & Ruina, A. L. (1983), 'Stability of steady frictional slipping', *Journal of Applied Mechanics, ASME* **50**, 343–349.

Rots, J. G. (1988), Computational modelling of concrete fracture, PhD thesis, Delft University of Technology, Delft.

Ruina, A. (1981), Friction laws and instabilities: A quasi-static analysis of some dry frictional behavior, PhD thesis, Brown University.

Sridhar, N., Yang, Q. D. & Cox, B. N. (2003), 'Slip, stick, and reverse slip characteristics during dynamic fibre pullout', *Journal of the Mechanics and Physics of Solids* **51**, 1215–1241.

Stang, H. (1996), 'Significance of shrinkage-induced clamping pressure in fiber-matrix bonding in cementitious composite materials', *Advanced cement based materials* **4**, 106–115.

Weiler, B. & Grosse, C. (1996), 'Pullout behaviour of fibers in steel fiber reinforced concrete', *FMPA Journal* pp. 116 127.

Xu, X. & Needleman, A. (1993), 'Void nucleation by inclusion debonding in a crystal matrix', *Modelling Simul. Mater. Sci. Eng.* **1**, 111 132.

Xu, X. & Needleman, A. (1994), 'Numerical simulations of fast crack growth in brittle solids', *Journal of the Mechanics and Physics of Solids* **42**, 1397 1434.

Zhang, J. & Li, V. (2002), 'Effect of inclination angle on fiber rupture load in fiber reinforced cementitous composites', *Composites Science and Technology* **62**, 775–781.

Chapter 5

Strong discontinuities using X-FEM

Contents

5.1 Introduction

Different approaches are considered in order to model the damage and fracture of quasi-brittle materials like concrete. The material failures manifest themselves as fracture process zones, strain localization or discrete crack discontinuities. First, the localization of strains occurs in small zones, and later during the loading process, the integrity is completely lost and displacement discontinuities develop across planes in the material.

Two main approaches are considered for modeling cracking of quasi-brittle materials, the discrete crack model Ngo & Scordelis (1967), and the smeared crack model Rashid (1968). In the discrete crack model, when cracking is going to occur, new degrees of freedom are created and geometrical discontinuities are assumed to occur. In the smeared crack model, the crack process is lumped in the element considered.

The discrete models have been improved by using re-meshing techniques as in (Ingraffea & Saouma 1985), (Carter et al. 1995), (Camacho & Ortiz 1996), the propagation directions are defined using fracture mechanics, and the geometry of the structure is changed according to the new propagation directions.

The discrete models are well suited for highly localized deformations, but not so well suited for more distributed inelastic deformations which may take place in the early stages of failure. Problems arise if the cohesive surfaces are taken to have a non-zero initial compliance, the presence of the cohesive surfaces contributes to the overall compliance of the body. Then, if cohesive surfaces are added between all elements as the computational mesh is refined, the overall compliance depends on the mesh, and an ill-posed problem results. Introducing initially rigid surfaces like in (Camacho & Ortiz 1996) results in other difficulties (Falk et al. 2001).

In the smeared model, the contribution by cracking to the inelastic deformation is represented by cracking strain distributed over a finite volume. The material is then modeled as a continuum. Final fracture is represented by a zone in which the load-bearing capacity is completely lost.

Due to the fact that concrete is not a perfectly brittle material, the material has some residual capacity after reaching the maximum strength. Modifications to the model by Rashid (1968) were introduced to take into account this residual capacity. Additionally, Suidan & Schnobrich (1973) introduced the concept of shear retention factor. To avoid problems related to the direction of the principal stresses that can rotate after cracking, Cope et al. (1980) introduced the rotating crack model.

None of those solutions were able to solve problems of convergence and mesh dependence of the solution. This occurs due to the lack of an internal length scale in the model. Without this factor the boundary problems become ill-posed. To overcome this deficiency, regularization techniques were introduced. These strategies, however, have a major disadvantage: the localization zone must be analyzed with a very fine mesh which is impossible for the analysis of large structures.

The embedded discontinuities can overcome the limitations of the smeared and discrete models. By capturing a crack within an element it is possible to model a discrete or highly localized phenomenon within a continuum approach. The width of the failure zone is less than the width of a single element.

Simo et al. (1993) give a unified framework for the analysis of strong discontinu-

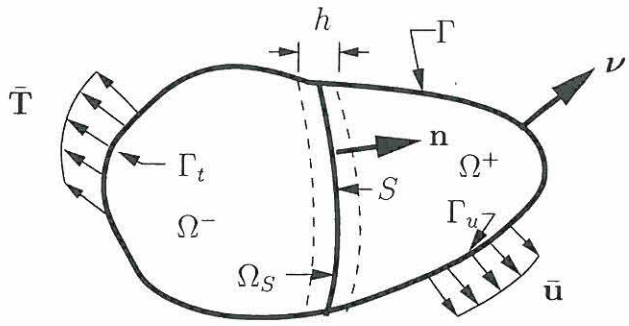

Figure 5.1: The domain Ω crossed by a discontinuity.

ities based on the concept of enrichment of strains. That is under certain conditions, continuum constitutive laws and unbounded strains are compatible. However, stress locking has been reported when elements with embedded discontinuities are used (Wells & Sluys 2000).

An alternative way to embed a discontinuity based on the partition of unity property (Babuška & Melenk 1997) was introduced by Moës et al. (1999) and used with a cohesive model by Wells & Sluys (2001).

In this chapter, the partition of unity property of the finite element method is used to develop finite elements using a cohesive model in a similar way to (Wells & Sluys 2001). The finite elements developed can use a simple cohesive model as in (Wells & Sluys 2001) or a cohesive surface formulation developed by Xu & Needleman (1994).

It is concluded from examples that numerical problems can arise using these elements, and a more robust way to embed the discontinuity is required.

5.2 Strong discontinuities

5.2.1 Kinematics

Considering the domain Ω with boundary Γ shown in figure 5.1. It contains a discontinuity (S) which splits the domain into two parts denoted Ω^+ and Ω^-. The prescribed tractions on Γ_t are denoted $\overline{\mathbf{T}}$ and the prescribed displacements on Γ_u are denoted $\overline{\mathbf{u}}$, where Γ_u and Γ_t are in the external boundary. $\boldsymbol{\nu}$ is a unit normal to the external boundary Γ.

An additional sub-domain $\Omega_S \subset \Omega$ surrounding S is considered, with two arbitrary boundaries behind and ahead of S. The kinematic boundary conditions are defined beyond Ω_S ($\Gamma_u \cap \Omega_S = \emptyset$).

The kinematics of the body exhibiting a discontinuity jump of value $[\![\mathbf{u}]\!]$ in the displacements field, whose normal is $\mathbf{n}$, can be described as:

$$\mathbf{u} = \mathbf{u}_r + \mathrm{H}_S[\![\mathbf{u}]\!] \tag{5.1}$$

where $\mathbf{u}_r$ is the regular (continuous) part of the displacement field. H_S is the step function placed on S, defined as:

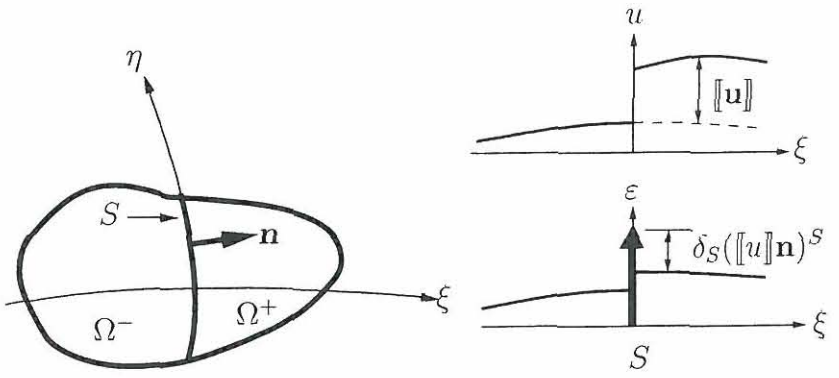

Figure 5.2: The strong discontinuity kinematics.

$$\mathrm{H}_S = \begin{cases} 0 & \text{if } \mathbf{x} \in \Omega^- \\ 1 & \text{if } \mathbf{x} \in \Omega^+ \end{cases} \tag{5.2}$$

where $\mathbf{x}$ denotes the position of a material point.

The strains are:

$$\boldsymbol{\varepsilon} = (\nabla \mathbf{u})^S = \boldsymbol{\varepsilon}_r + \delta_S(\llbracket \mathbf{u} \rrbracket \mathbf{n})^S \tag{5.3}$$

where $\boldsymbol{\varepsilon}$ is the strain tensor, $(\cdot)^S$ stands for the symmetric part of $(\cdot)$, δ_S is Dirac's delta on S obtained by derivation of H_S ($\nabla \mathrm{H}_S(\mathbf{x}) = \delta_S \mathbf{n}$). The regular (bounded) part of the strain is denoted $\boldsymbol{\varepsilon}_r$ and is:

$$\boldsymbol{\varepsilon}_r = (\nabla \mathbf{u}_r)^S + (\mathrm{H}_S(\nabla \llbracket \mathbf{u} \rrbracket))^S \tag{5.4}$$

The kinematics of the strong discontinuity is illustrated in figure 5.2.

5.2.2 Field equations

The field equations governing the boundary value problem can be written as (Oliver 1996):

$$\nabla \boldsymbol{\sigma} + \mathbf{f} = \mathbf{0} \qquad \text{in } \Omega \setminus S \tag{5.5}$$

$$\mathbf{u} = \bar{\mathbf{u}} \qquad \text{in } \Gamma_u \tag{5.6}$$

$$\boldsymbol{\sigma} \cdot \boldsymbol{\nu} = \bar{\mathbf{T}} \qquad \text{in } \Gamma_t \tag{5.7}$$

$$\boldsymbol{\sigma}^+ \cdot \mathbf{n} = \boldsymbol{\sigma}^- \cdot \mathbf{n} \qquad \text{in } S \tag{5.8}$$

$$\mathbf{T}_S = \boldsymbol{\sigma}_S \cdot \mathbf{n} = \boldsymbol{\sigma}^+ \cdot \mathbf{n} \qquad \text{in } S \tag{5.9}$$

where $\boldsymbol{\sigma}$ is the stress tensor, $\mathbf{f}$ are the body forces and $\mathbf{T}_S$ are the tractions across the discontinuity.

Equation (5.5) is the classical equilibrium equation. Equations (5.6) and (5.7) are the essential and natural boundary conditions, respectively. Equations (5.8) and (5.9) state the continuity of the traction vector across the discontinuity S.

Another equation required to solve the problem is the constitutive relations in the form

$$\boldsymbol{\sigma} = \boldsymbol{\sigma}(\boldsymbol{\varepsilon}) \tag{5.10}$$

Consideration of the strong discontinuity leads to the definition of the strain field in terms of the regular part of the displacements $\mathbf{u}_r$, the displacement jump $[\![\mathbf{u}]\!]$ and the normal $\mathbf{n}$

$$\boldsymbol{\varepsilon} = \boldsymbol{\varepsilon}(\mathbf{u}_r, [\![\mathbf{u}]\!], \mathbf{n}) \tag{5.11}$$

$[\![\mathbf{u}]\!]$ and $\mathbf{n}$ are additional unknowns with respect to the standard solid mechanics problem. $\mathbf{n}$ is solved in terms of the stress field, and the jump is found using the traction vector continuity condition (5.9).

Equations (5.5)-(5.11) provide a sufficient and well posed set of equations to solve the problem in terms of $\boldsymbol{\sigma}$, $\boldsymbol{\varepsilon}$, $\mathbf{u}$ and $[\![\mathbf{u}]\!]$.

5.3 Weak formulation

5.3.1 Using the principle of virtual work

Considering the principle of virtual work:

$$\int_\Omega \boldsymbol{\sigma} : (\nabla \delta\mathbf{u})^S d\Omega = \int_\Gamma \bar{\mathbf{T}} \cdot \delta\mathbf{u} d\Gamma + \int_\Omega \mathbf{f} \cdot \delta\mathbf{u} d\Omega \tag{5.12}$$

the left part of (5.12) could be written using the divergence theorem:

$$\begin{aligned} \int_\Omega \boldsymbol{\sigma} : (\nabla \delta\mathbf{u})^S d\Omega &= \int_{\Omega\setminus S} \boldsymbol{\sigma} : (\nabla \delta\mathbf{u})^S d\Omega + \int_{\Omega_S} \boldsymbol{\sigma} : (\nabla \delta\mathbf{u})^S d\Omega \\ &= \int_{\Omega\setminus S} \boldsymbol{\sigma} : (\nabla \delta\mathbf{u})^S d\Omega - \int_S \mathbf{n} \cdot (\boldsymbol{\sigma}^+ - \boldsymbol{\sigma}^-) \cdot \delta\mathbf{u} d\Gamma \end{aligned} \tag{5.13}$$

The virtual work finally looks like:

$$\int_{\Omega\setminus S} \boldsymbol{\sigma} : (\nabla \delta\mathbf{u})^S d\Omega - \int_S \mathbf{n} \cdot (\boldsymbol{\sigma}^+ - \boldsymbol{\sigma}^-) \cdot \delta\mathbf{u} d\Gamma = \int_\Gamma \bar{\mathbf{T}} \cdot \delta\mathbf{u} d\Gamma + \int_\Omega \mathbf{f} \cdot \delta\mathbf{u} S d\Omega \tag{5.14}$$

Integration by parts and again the use of the divergence produce:

$$-\int_{\Omega\setminus S}\nabla\cdot\boldsymbol{\sigma}\cdot\delta\mathbf{u}d\Omega+\int_{\Gamma}\boldsymbol{\nu}\cdot\boldsymbol{\sigma}\cdot\delta\mathbf{u}d\Gamma-\int_{S}\mathbf{n}\cdot(\boldsymbol{\sigma}^{+}-\boldsymbol{\sigma}^{-})\cdot\delta\mathbf{u}d\Gamma = \int_{\Gamma}\bar{\mathbf{T}}\cdot\delta\mathbf{u}d\Gamma+\int_{\Omega}\mathbf{f}\cdot\delta\mathbf{u}Sd\Omega \quad (5.15)$$

Finally

$$-\int_{\Omega\setminus S}(\nabla\cdot\boldsymbol{\sigma}+\mathbf{f})\cdot\delta\mathbf{u}d\Omega+\int_{\Gamma}(\boldsymbol{\nu}\cdot\boldsymbol{\sigma}-\bar{\mathbf{T}})\cdot\delta\mathbf{u}d\Gamma-\int_{S}\mathbf{n}\cdot(\boldsymbol{\sigma}^{+}-\boldsymbol{\sigma}^{-})\cdot\delta\mathbf{u}d\Gamma=0 \quad (5.16)$$

From (5.16) it is obtained that:

$$\nabla\cdot\boldsymbol{\sigma}+\mathbf{f}=0 \quad (5.17)$$

$$\boldsymbol{\sigma}\cdot\boldsymbol{\nu}=\bar{\mathbf{T}} \quad (5.18)$$

$$\boldsymbol{\sigma}^{+}\cdot\mathbf{n}=\boldsymbol{\sigma}^{-}\cdot\mathbf{n} \quad (5.19)$$

This implies that when using the virtual work in this form, (5.5), (5.7) and (5.8) are satisfied in weak form, but the condition corresponding to (5.9) has to be imposed in another form.

5.3.2 Virtual work using a modified $\delta\mathbf{u}$

The variations of displacements according to (5.1) can be decomposed as:

$$\delta\mathbf{u}=\delta\mathbf{u}_{r}+\mathrm{H}_{S}[\![\delta\mathbf{u}]\!] \quad (5.20)$$

then, the strain variations are:

$$\delta\varepsilon=(\nabla\delta\mathbf{u})^{S}=(\nabla\delta\mathbf{u}_{r})^{S}+\mathrm{H}_{S}(\nabla[\![\delta\mathbf{u}]\!])^{S}+\delta_{S}([\![\delta\mathbf{u}]\!]\mathbf{n})^{S} \quad (5.21)$$

Replacing (5.21) in (5.12) and changing the integration domain to eliminate the Heaviside function:

$$\int_{\Omega}\boldsymbol{\sigma}:(\nabla\delta\mathbf{u}_{r})^{S}d\Omega+\int_{\Omega^{+}}\boldsymbol{\sigma}:(\nabla[\![\delta\mathbf{u}]\!])^{S}d\Omega+\int_{\Omega}\boldsymbol{\sigma}:\delta_{S}([\![\delta\mathbf{u}]\!]\mathbf{n})^{S}d\Omega = \int_{\Gamma}\bar{\mathbf{T}}\cdot\delta\mathbf{u}_{r}d\Gamma+\int_{\Gamma^{+}}\bar{\mathbf{T}}\cdot[\![\delta\mathbf{u}]\!]d\Gamma+\int_{\Omega}\mathbf{f}\cdot\delta\mathbf{u}_{r}d\Omega+\int_{\Omega^{+}}\mathbf{f}\cdot[\![\delta\mathbf{u}]\!]d\Omega \quad (5.22)$$

From the properties of the Dirac delta function:

$$\int_{\Omega}\delta_{\Gamma}\phi d\Omega=\int_{\Gamma}\phi d\Gamma \quad (5.23)$$

where ϕ is a continuum function. Then (5.22) is:

$$\int_{\Omega} \boldsymbol{\sigma} : (\nabla \delta \mathbf{u}_r)^S d\Omega + \int_{\Omega^+} \boldsymbol{\sigma} : (\nabla [\![\delta \mathbf{u}]\!])^S d\Omega + \int_S \mathbf{T} \cdot [\![\delta \mathbf{u}]\!] d\Gamma = \int_{\Gamma} \bar{\mathbf{T}} \cdot \delta \mathbf{u}_r d\Gamma + \int_{\Gamma^+} \bar{\mathbf{T}} \cdot [\![\delta \mathbf{u}]\!] d\Gamma + \int_{\Omega} \mathbf{f} \cdot \delta \mathbf{u}_r d\Omega + \int_{\Omega^+} \mathbf{f} \cdot [\![\delta \mathbf{u}]\!] d\Omega \tag{5.24}$$

where:

$$\boldsymbol{\sigma} : ([\![\delta \mathbf{u}]\!] \mathbf{n})^S = \mathbf{T} \cdot [\![\delta \mathbf{u}]\!] \tag{5.25}$$

The weak form of the problem is represented by (5.24). This weak form of the problem will be exploited further, and it has a similar form as the one proposed by Remmers et al. (2003), but the one presented here is derived from the principle of virtual work and includes body forces.

Integration by parts of the terms in the left part of (5.24) produces:

$$\int_{\Omega} \boldsymbol{\sigma} : (\nabla \delta \mathbf{u}_r)^S d\Omega = -\int_{\Omega} \nabla \cdot \boldsymbol{\sigma} \cdot \delta \mathbf{u}_r d\Omega + \int_{\Gamma} \boldsymbol{\sigma} \cdot \boldsymbol{\nu} \cdot \delta \mathbf{u}_r d\Gamma - \int_S \mathbf{n} \cdot (\boldsymbol{\sigma}^+ - \boldsymbol{\sigma}^-) \cdot \delta \mathbf{u}_r d\Gamma \tag{5.26}$$

$$\int_{\Omega^+} \boldsymbol{\sigma} : (\nabla [\![\delta \mathbf{u}]\!])^S d\Omega = -\int_{\Omega^+} \nabla \cdot \boldsymbol{\sigma} \cdot [\![\delta \mathbf{u}]\!] d\Omega + \int_{\Gamma^+} \boldsymbol{\sigma} \cdot \boldsymbol{\nu} \cdot [\![\delta \mathbf{u}]\!] d\Gamma + \int_S \boldsymbol{\sigma}^+ \cdot \mathbf{n} \cdot [\![\delta \mathbf{u}]\!] d\Gamma \tag{5.27}$$

After replacing (5.26), (5.27) and (5.20) in (5.24) and regrouping terms, it is obtained that

$$-\int_{\Omega} (\nabla \cdot \boldsymbol{\sigma} + \mathbf{f}) \cdot \delta \mathbf{u} d\Omega + \int_{\Gamma} (\boldsymbol{\sigma} \cdot \boldsymbol{\nu} - \bar{\mathbf{T}}) \cdot \delta \mathbf{u} d\Gamma - \int_S \mathbf{n} \cdot (\boldsymbol{\sigma}^+ - \boldsymbol{\sigma}^-) \cdot \delta \mathbf{u} d\Gamma + \int_S (\boldsymbol{\sigma}^+ \cdot \mathbf{n} - \mathbf{T}) \cdot [\![\delta \mathbf{u}]\!] d\Gamma = 0 \tag{5.28}$$

this again produces (5.17)-(5.19), but additionally produces:

$$\mathbf{T}_S = \boldsymbol{\sigma} \cdot \mathbf{n} \tag{5.29}$$

5.4 The partition of unity property

The partition of unity property of finite element shape functions (Babuška & Melenk 1997) is used now to simplify the construction of the finite element.

A collection of functions ϕ_i, associated with a node i, forms a partition of unity if

$$\sum_{i=1}^{n} \phi_i(\mathbf{x}) = 1 \tag{5.30}$$

were n is the number of discrete nodal points. For a set of functions ϕ_i, that satisfies (5.30), a field u can be interpolated as follows

$$u(\mathbf{x}) = \sum_{i=1}^{n} \phi_i(\mathbf{x}) \left(\bar{a}_i + \sum_{j=1}^{m} \psi_j(\mathbf{x}) \bar{a}_{ij} \right) \tag{5.31}$$

where $\bar{a}_i$ are the regular nodal degrees of freedom, $\psi_j(\mathbf{x})$ are the enhanced basis terms, and $\bar{a}_{ij}$ are the additional degrees of freedom at node i which represents the amplitude of the jth enhanced basis term $\psi_j(\mathbf{x})$.

The displacement decomposition (5.1) has a structure similar to the interpolation of (5.31). In conventional finite element notation the displacement interpolation is:

$$\mathbf{u}(\mathbf{x}) = \mathbf{N}(\mathbf{x}) \left(\mathbf{v} + \mathbf{H}_s(\mathbf{x})\mathbf{b} \right) = \mathbf{N}(\mathbf{x})\mathbf{v} + \mathbf{N}(\mathbf{x})\mathbf{H}_s(\mathbf{x})\mathbf{b} \tag{5.32}$$

where $\mathbf{N}$ is a matrix containing the usual polynomial shape functions, $\mathbf{v}$ are the usual nodal degrees of freedom, $\mathbf{H}_S$ is a matrix containing enhanced basis terms and $\mathbf{b}$ are the enhanced nodal degrees of freedom representing the magnitudes of the enhanced terms in $\mathbf{H}_S$. The value of the regular degree of freedom is no longer equal to the displacement at the node. The displacement at the node is composed of contributions from the regular and enhanced parts of the interpolation.

Due to the similarity to the decomposition of a discontinuous displacement field according to (5.1), the enhanced matrix $\mathbf{H}_S$ can be replaced by the scalar-valued Heaviside function, leading to

$$\mathbf{u}(\mathbf{x}) = \mathbf{N}(\mathbf{x})\mathbf{v} + \mathrm{H}_S\mathbf{N}(\mathbf{x})\mathbf{b} \tag{5.33}$$

The interpolation in equation (5.33) involves four degrees of freedom per node in two dimensions for nodes whose support is crossed by a discontinuity. Two regular degrees of freedom representing the continuous part of the displacement field in the x and y directions, and two enhanced degrees of freedom representing the discontinuous part of the displacement field in the x and y directions.

5.5 Vector of internal and external forces

In order to develop a finite element with strong discontinuities, the tensors will be replaced by vectors and matrices as used in engineering. The following vectors are defined for a two-dimensional problem in the global coordinate system:

$$\mathbf{u} = \begin{bmatrix} u_1 \\ u_2 \end{bmatrix} \qquad \mathbf{T} = \begin{bmatrix} T_1 \\ T_2 \end{bmatrix} \qquad \bar{\mathbf{T}} = \begin{bmatrix} \bar{T}_1 \\ \bar{T}_2 \end{bmatrix} \qquad \mathbf{f} = \begin{bmatrix} f_1 \\ f_2 \end{bmatrix} \tag{5.34}$$

And in a local coordinate system:

$$\mathbf{u}_l = \begin{bmatrix} u_s \\ u_n \end{bmatrix} \qquad \mathbf{T} = \begin{bmatrix} T_s \\ T_n \end{bmatrix} \tag{5.35}$$

The stress and strain tensors $\boldsymbol{\sigma}$ and $\boldsymbol{\varepsilon}$, respectively, are replaced by the stress and strain vectors defined as:

$$\boldsymbol{\sigma} = \begin{bmatrix} \sigma_{11} \\ \sigma_{22} \\ \sigma_{12} \end{bmatrix} \qquad \boldsymbol{\varepsilon} = \begin{bmatrix} \varepsilon_{11} \\ \varepsilon_{22} \\ 2\varepsilon_{12} \end{bmatrix} \tag{5.36}$$

The regular displacement and jump vectors are:

$$\mathbf{u}_r = \begin{bmatrix} u_{r1} \\ u_{r2} \end{bmatrix} \qquad [\![\mathbf{u}]\!] = \begin{bmatrix} [\![u_1]\!] \\ [\![u_2]\!] \end{bmatrix} \tag{5.37}$$

In the finite element analysis, the vectors defining the displacement will be expressed in terms of nodal degrees of freedom $\mathbf{v}$ and $\mathbf{b}$ using the interpolation functions in $\mathbf{N}$. From (5.1) and (5.33) then:

$$\mathbf{u}_r = \mathbf{N}\mathbf{v} \qquad [\![\mathbf{u}]\!] = \mathbf{N}\mathbf{b} \tag{5.38}$$

and

$$(\nabla \mathbf{u}_r)^S = \mathbf{B}\mathbf{v} \qquad (\nabla [\![\mathbf{u}]\!])^S = \mathbf{B}\mathbf{b} \tag{5.39}$$

Replacing (5.34) - (5.39) in (5.24) the following equation is obtained:

$$\begin{aligned} &\int_\Omega (\mathbf{B}\delta\mathbf{v})^T \boldsymbol{\sigma} d\Omega + \int_{\Omega^+} (\mathbf{B}\delta\mathbf{b})^T \boldsymbol{\sigma} d\Omega + \int_S (\mathbf{N}\delta\mathbf{b})^T \mathbf{T} d\Gamma \\ &\quad = \int_\Gamma (\mathbf{N}\delta\mathbf{v})^T \bar{\mathbf{T}} d\Gamma + \int_{\Gamma^+} (\mathbf{N}\delta\mathbf{b})^T \bar{\mathbf{T}} d\Gamma + \int_\Omega (\mathbf{N}\delta\mathbf{v})^T \mathbf{f} d\Omega + \int_{\Omega^+} (\mathbf{N}\delta\mathbf{b})^T \mathbf{f} d\Omega \end{aligned} \tag{5.40}$$

Define the internal and external forces by:

$$\mathbf{F}^{int} = \mathbf{F}_v^{int} + \mathbf{F}_b^{int} \tag{5.41}$$

$$\mathbf{F}^{ext} = \mathbf{F}_v^{ext} + \mathbf{F}_b^{ext} \tag{5.42}$$

respectively, where

$$\mathbf{F}_v^{ext} = \mathbf{F}_{vT}^{ext} + \mathbf{F}_{vf}^{ext} \qquad \mathbf{F}_b^{int} = \mathbf{F}_{b\sigma}^{int} + \mathbf{F}_{bT}^{int} \tag{5.43}$$

$$\mathbf{F}_b^{ext} = \mathbf{F}_{bT}^{ext} + \mathbf{F}_{bf}^{ext} \tag{5.44}$$

$$\mathbf{F}_v^{int} = \int_\Omega \mathbf{B}^T \boldsymbol{\sigma} d\Omega \qquad \mathbf{F}_{b\sigma}^{int} = \int_{\Omega^+} \mathbf{B}^T \boldsymbol{\sigma} d\Omega \tag{5.45}$$

$$\mathbf{F}_{vT}^{ext} = \int_\Gamma \mathbf{N}^T \bar{\mathbf{T}} d\Gamma \qquad \mathbf{F}_{bT}^{int} = \int_S \mathbf{N}^T \mathbf{T} d\Gamma \tag{5.46}$$

$$\mathbf{F}_{vf}^{ext} = \int_\Omega \mathbf{N}^T \mathbf{f} d\Omega \qquad \mathbf{F}_{bT}^{ext} = \int_{\Gamma^+} \mathbf{N}^T \bar{\mathbf{T}} d\Gamma \tag{5.47}$$

$$\mathbf{F}_{bf}^{ext} = \int_{\Omega^+} \mathbf{N}^T \mathbf{f} d\Omega \tag{5.48}$$

Substitution of equations (5.41) - (5.48) in (5.40) produces

$$\delta \mathbf{v}^T (\mathbf{F}_v^{int} - \mathbf{F}_v^{ext}) + \delta \mathbf{b}^T (\mathbf{F}_b^{int} - \mathbf{F}_b^{ext}) = \mathbf{0} \tag{5.49}$$

The final results are the equilibrium equations in the form:

$$\mathbf{F}_v^{int} = \mathbf{F}_v^{ext} \qquad \mathbf{F}_b^{int} = \mathbf{F}_b^{ext} \tag{5.50}$$

5.6 Constitutive relations

5.6.1 Simple cohesive model

The relation between stresses and strains in rate form is (except in the discontinuity where the strains are unbounded) :

$$\dot{\boldsymbol{\sigma}} = \mathbf{D}\dot{\boldsymbol{\varepsilon}} = \mathbf{D}(\mathbf{B}\dot{\mathbf{v}} + \mathrm{H}_S \mathbf{B}\dot{\mathbf{b}}) \tag{5.51}$$

where an overdot $\dot{()}$ signifies rates, and $\mathbf{D}$ is the tangent stiffness matrix of the bulk material (here rate-independent material behavior is assumed). In case of an elastic isotropic material and in plane stress:

$$\mathbf{D} = \frac{E}{1-\nu^2} \begin{bmatrix} 1 & \nu & 0 \\ \nu & 1 & 0 \\ 0 & 0 & \frac{1}{2}(1-\nu) \end{bmatrix} \tag{5.52}$$

where E is the elastic modulus and ν is Poisson's ratio.

In the discontinuity the tractions are:

$$\mathbf{T}_l = \mathbf{T}_{tl} [\![\mathbf{u}_l]\!] \tag{5.53}$$

where $\mathbf{T}_l$ is the traction vector in the local coordinate system, $[\![\mathbf{u}_l]\!]$ is the jump transformed to the local coordinate system and $\mathbf{T}_{tl}$ is the stiffness of the traction-separation law at the discontinuity, transformed to the element local system.

Remmers et al. (2003) used the cohesive model expressed by the exponential form:

$$T_n = \sigma_u \exp\left(-\frac{\sigma_u}{G_f}\kappa\right) \tag{5.54}$$

where σ_u is the peak stress, G_f is the fracture energy and κ is the maximum value of $[\![u_n]\!]$ in the considered location. In that case:

$$\dot{T}_n = -\frac{\sigma_u^2}{G_f}\exp\left(-\frac{\sigma_u}{G_f}\kappa\right)[\![\dot{u}_n]\!] \tag{5.55}$$

and considering a constant value of T_s

$$\dot{\mathbf{T}}_l = \begin{bmatrix} 0 & 0 \\ 0 & -\frac{\sigma_u^2}{G_f}\exp\left(-\frac{\sigma_u}{G_f}\kappa\right) \end{bmatrix} \begin{bmatrix} [\![\dot{u}_s]\!] \\ [\![\dot{u}_n]\!] \end{bmatrix} \tag{5.56}$$

Transforming (5.56) to the global coordinate system:

$$\dot{\mathbf{T}} = \mathbf{T}_{cz}[\![\dot{\mathbf{u}}]\!] \tag{5.57}$$

where

$$\mathbf{T}_{cz} = \mathbf{R}_2 \begin{bmatrix} 0 & 0 \\ 0 & -\frac{\sigma_u^2}{G_f}\exp\left(-\frac{\sigma_u}{G_f}\kappa\right) \end{bmatrix} \mathbf{R}_2^T \tag{5.58}$$

and

$$\mathbf{R}_2 = \begin{bmatrix} n_1 & -n_2 \\ n_2 & n_1 \end{bmatrix} \tag{5.59}$$

where n_1 and n_2 are the components of the vector $\mathbf{n}$. Finally, it is possible to write:

$$\dot{\mathbf{T}} = \mathbf{T}_{cz}\mathbf{N}\dot{\mathbf{b}} \tag{5.60}$$

5.6.2 The Xu-Needleman cohesive model

This constitutive model is defined in (Xu & Needleman 1993), where the tractions are described as functions of the displacement jump across the interface. The condition that work cannot be extracted from the interface, in a closed cycle for an elastic interface, leads to the existence of a potential ϕ, for which

$$\mathbf{T} = \frac{\partial \phi}{\partial [\![\mathbf{u}]\!]} \tag{5.61}$$

The potential used allows for a shear failure mode in the interfacial region. The dependence on the displacements is given in terms of the normal ($[\![u_n]\!] = \mathbf{n} \cdot [\![\mathbf{u}]\!]$) and tangential ($[\![u_s]\!] = \mathbf{s} \cdot [\![\mathbf{u}]\!]$) displacement jumps, where $\mathbf{n}$ and $\mathbf{s}$ are unit vectors pointing in the normal and tangential direction to the discontinuity, respectively. In particular, ϕ has the form

$$\begin{aligned}\phi([\![\mathbf{u}]\!]) = \phi_n + \phi_n \exp\left(-\frac{[\![u_n]\!]}{\delta_n}\right)\Bigg\{\left(1 - r + \frac{[\![u_n]\!]}{\delta_n}\right)\frac{1-q}{r-1} \\ - \left(q + \frac{r-q}{r-1}\frac{[\![u_n]\!]}{\delta_n}\right)\exp\left(-\frac{[\![u_s]\!]^2}{\delta_s^2}\right)\Bigg\}\end{aligned} \tag{5.62}$$

with

$$q = \frac{\phi_s}{\phi_n} \qquad \text{and} \qquad r = \frac{[\![u_n]\!]^*}{\delta_n} \tag{5.63}$$

where ϕ_n is the work of normal separation, ϕ_s is the work of tangential separation, and $[\![u_n]\!]^*$ is the value of $[\![u_n]\!]$ after complete shear separation under the condition of zero normal tension, $T_n = 0$.

The interfacial tractions are obtained according to (5.61). By differentiation of (5.62), they are::

$$\begin{aligned}T_n = \frac{\phi_n}{\delta_n}\exp\left(-\frac{[\![u_n]\!]}{\delta_n}\right)\Bigg\{\frac{[\![u_n]\!]}{\delta_n}\exp\left(-\frac{[\![u_s]\!]^2}{\delta_s^2}\right) \\ + \frac{1-q}{r-1}\left[1 - \exp\left(-\frac{[\![u_s]\!]^2}{\delta_s^2}\right)\right]\left(r - \frac{[\![u_n]\!]}{\delta_n}\right)\Bigg\}\end{aligned} \tag{5.64}$$

$$T_s = \frac{\phi_n}{\delta_n}\left(2\frac{\delta_n}{\delta_s}\right)\frac{[\![u_s]\!]}{\delta_s}\left\{q + \frac{r-q}{r-1}\frac{[\![u_n]\!]}{\delta_n}\right\}\exp\left(-\frac{[\![u_n]\!]}{\delta_n}\right)\exp\left(-\frac{[\![u_s]\!]^2}{\delta_s^2}\right) \tag{5.65}$$

The maximum value of $|T_s| = \tau_u$ occurs when $|[\![u_s]\!]| = \sqrt{2}\delta_s/2$. The normal and shear work of separation are related to σ_u and τ_u, respectively, by

$$\phi_n = \sigma_u e \delta_n \qquad \phi_s = \sqrt{\frac{e}{2}}\tau_u \delta_s \tag{5.66}$$

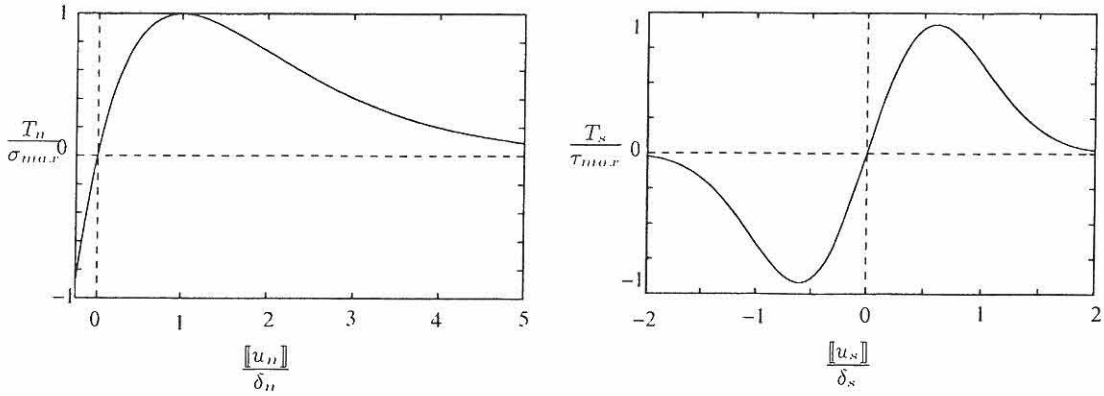

Figure 5.3: The tractions when $\phi_n = \phi_s$ and (a) $[\![u_s]\!] = 0$ or (b) $[\![u_n]\!] = 0$.

where $e = \exp(1)$. For the case $\phi_n = \phi_s$ the tractions are shown in figure 5.3 when only $[\![u_n]\!]$ or $[\![u_s]\!]$ is different from zero.

If it is assumed that $\phi_n = \phi_s$ then $q = 1$. The equations are reduced to:

$$\phi([\![\mathbf{u}]\!]) = \phi_n - \phi_n \exp\left(-\frac{[\![u_n]\!]}{\delta_n}\right)\left(1 + \frac{[\![u_n]\!]}{\delta_n}\right)\exp\left(-\frac{[\![u_s]\!]^2}{\delta_s^2}\right) \tag{5.67}$$

$$T_n = \frac{\phi_n}{\delta_n}\frac{[\![u_n]\!]}{\delta_n}\exp\left(-\frac{[\![u_n]\!]}{\delta_n}\right)\exp\left(-\frac{[\![u_s]\!]^2}{\delta_s^2}\right) \tag{5.68}$$

$$T_t = \left(\frac{\phi_n}{\delta_n}\right)\left(\frac{[\![u_n]\!]}{\delta_n} + 1\right)\left(2\frac{\delta_n}{\delta_s}\right)\frac{[\![u_s]\!]}{\delta_s}\exp\left(-\frac{[\![u_n]\!]}{\delta_n}\right)\exp\left(-\frac{[\![u_s]\!]^2}{\delta_s^2}\right) \tag{5.69}$$

Finally observe that:

$$\dot{\mathbf{T}}_l = \begin{bmatrix}\dot{T}_s \\ \dot{T}_n\end{bmatrix} = \begin{bmatrix}\frac{\partial T_s}{\partial [\![u_s]\!]} & \frac{\partial T_s}{\partial [\![u_n]\!]} \\ \frac{\partial T_n}{\partial [\![u_s]\!]} & \frac{\partial T_n}{\partial [\![u_n]\!]}\end{bmatrix}\begin{bmatrix}[\![\dot{u}_s]\!] \\ [\![\dot{u}_n]\!]\end{bmatrix} \tag{5.70}$$

with the consequence of:

$$\mathbf{T}_{cz} = \mathbf{R}_2\begin{bmatrix}\frac{\partial T_s}{\partial [\![u_s]\!]} & \frac{\partial T_s}{\partial [\![u_n]\!]} \\ \frac{\partial T_n}{\partial [\![u_s]\!]} & \frac{\partial T_n}{\partial [\![u_n]\!]}\end{bmatrix}\mathbf{R}_2^T \tag{5.71}$$

5.7 The tangent stiffness matrix

The rate form of (5.40) is:

$$\int_{\Omega}(\mathbf{B}\delta\mathbf{v})^T\dot{\boldsymbol{\sigma}}d\Omega+\int_{\Omega^+}(\mathbf{B}\delta\mathbf{b})^T\dot{\boldsymbol{\sigma}}d\Omega+\int_S(\mathbf{N}\delta\mathbf{b})^T\dot{\mathbf{T}}d\Gamma$$
$$=\int_{\Gamma}(\mathbf{N}\delta\mathbf{v})^T\dot{\bar{\mathbf{T}}}d\Gamma+\int_{\Gamma^+}(\mathbf{N}\delta\mathbf{b})^T\dot{\bar{\mathbf{T}}}d\Gamma+\int_{\Omega}(\mathbf{N}\delta\mathbf{v})^T\dot{\mathbf{f}}d\Omega+\int_{\Omega^+}(\mathbf{N}\delta\mathbf{b})^T\dot{\mathbf{f}}d\Omega \tag{5.72}$$

replacing the expressions (5.51) and (5.60) in eq. (5.72), and changing the integration limits to eliminate the Heaviside step function, the following equation is obtained:

$$\delta\mathbf{v}^T(\mathbf{K}_{vv}\dot{\mathbf{v}}+\mathbf{K}_{vb}\dot{\mathbf{b}}-\dot{\mathbf{f}}^{ext}_{vT}-\dot{\mathbf{f}}^{ext}_{vf})+\delta\mathbf{b}^T(\mathbf{K}_{bv}\dot{\mathbf{v}}+\mathbf{K}_{bb}\dot{\mathbf{b}}-\dot{\mathbf{f}}^{ext}_{bT}-\dot{\mathbf{f}}^{ext}_{bf})=0 \tag{5.73}$$

where:

$$\mathbf{K}_{vv}=\int_{\Omega}\mathbf{B}^T\mathbf{D}\mathbf{B}d\Omega \qquad \mathbf{K}_{vb}=\mathbf{K}_{bv}=\int_{\Omega^+}\mathbf{B}^T\mathbf{D}\mathbf{B}d\Omega \tag{5.74}$$

$$\mathbf{K}_{bb}=\mathbf{K}_{bb\Omega}+\mathbf{K}_{bb\Gamma} \tag{5.75}$$

$$\mathbf{K}_{bb\Omega}=\int_{\Omega^+}\mathbf{B}^T\mathbf{D}\mathbf{B}d\Omega \qquad \mathbf{K}_{bb\Gamma}=\int_S\mathbf{N}^T\mathbf{T}_t\mathbf{N}d\Gamma \tag{5.76}$$

$$\dot{\mathbf{f}}^{ext}_{vT}=\int_{\Gamma}\mathbf{N}^T\dot{\bar{\mathbf{T}}}d\Gamma \qquad \dot{\mathbf{f}}^{ext}_{vf}=\int_{\Omega}\mathbf{N}^T\dot{\mathbf{f}}d\Gamma \tag{5.77}$$

$$\dot{\mathbf{f}}^{ext}_{bT}=\int_{\Gamma^+}\mathbf{N}^T\dot{\bar{\mathbf{T}}}d\Gamma \qquad \dot{\mathbf{f}}^{ext}_{bf}=\int_{\Omega^+}\mathbf{N}^T\dot{\mathbf{f}}d\Gamma \tag{5.78}$$

From (5.73) the following two equations are obtained:

$$\begin{bmatrix}\mathbf{K}_{vv} & \mathbf{K}_{vb}\\ \mathbf{K}_{bv} & \mathbf{K}_{bb}\end{bmatrix}\begin{bmatrix}\dot{\mathbf{v}}\\ \dot{\mathbf{b}}\end{bmatrix}=\begin{bmatrix}\dot{\mathbf{f}}^{ext}_{v}\\ \dot{\mathbf{f}}^{ext}_{b}\end{bmatrix} \tag{5.79}$$

where

$$\dot{\mathbf{f}}^{ext}_{v}=\dot{\mathbf{f}}^{ext}_{vf}+\dot{\mathbf{f}}^{ext}_{vT} \qquad \text{and } \dot{\mathbf{f}}^{ext}_{b}=\dot{\mathbf{f}}^{ext}_{bf}+\dot{\mathbf{f}}^{ext}_{bT} \tag{5.80}$$

The tangent stiffness matrix is then:

$$\mathbf{K}_T=\begin{bmatrix}\mathbf{K}_{vv} & \mathbf{K}_{vb}\\ \mathbf{K}_{bv} & \mathbf{K}_{bb}\end{bmatrix} \tag{5.81}$$

When a cohesive model is considered and when the force increment is expressed in terms of the external and internal forces, the final result is equal to the one presented by Wells & Sluys (2001):

$$\begin{bmatrix}\mathbf{K}_{vv} & \mathbf{K}_{vb}\\ \mathbf{K}_{bv} & \mathbf{K}_{bb}\end{bmatrix}\begin{bmatrix}\dot{\mathbf{v}}\\ \dot{\mathbf{b}}\end{bmatrix}=\begin{bmatrix}\mathbf{F}^{ext}_{v}\\ \mathbf{F}^{ext}_{b}\end{bmatrix}-\begin{bmatrix}\mathbf{F}^{int}_{v}\\ \mathbf{F}^{int}_{b}\end{bmatrix} \tag{5.82}$$

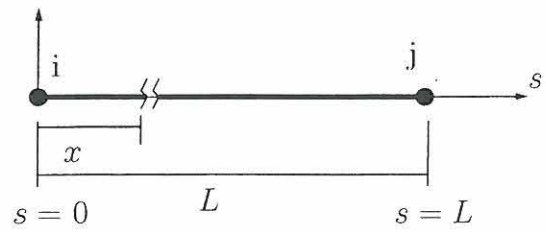

Figure 5.4: Two-node unidimensional finite element with a crack in x.

5.8 One-dimensional element

5.8.1 A bar element with an embedded crack

For the element shown in figure 5.4, using the system of coordinates 's' with origin in the node (i) and a crack at a distance x from (i), the following matrix of shape functions is defined:

$$\mathbf{N} = \frac{1}{L}\begin{bmatrix} L-s & s \end{bmatrix} \qquad \text{and} \qquad \mathbf{B} = \frac{d\mathbf{N}}{ds} = \frac{1}{L}\begin{bmatrix} -1 & 1 \end{bmatrix} \tag{5.83}$$

Therefore,

$$\mathbf{K}_{vv} = \frac{EA}{L}\begin{bmatrix} 1 & -1 \\ -1 & 1 \end{bmatrix} \tag{5.84}$$

For the uncracked bar, the internal and external forces are:

$$\mathbf{F}_{v\sigma}^{int} = \int_0^L \frac{A}{L}\begin{bmatrix} -1 \\ 1 \end{bmatrix} \sigma ds = \begin{bmatrix} -1 \\ 1 \end{bmatrix} A\sigma \tag{5.85}$$

$$\mathbf{F}_{vf}^{ext} = \int_0^L \frac{A}{L}\begin{bmatrix} L-s \\ s \end{bmatrix} f ds = \frac{ALf}{2}\begin{bmatrix} 1 \\ 1 \end{bmatrix} \tag{5.86}$$

respectively. When the bar cracks:

$$\mathbf{K}_{vb} = \mathbf{K}_{bv} = \mathbf{K}_{bb\Omega} = \int_x^L \frac{A}{L}\begin{bmatrix} -1 \\ 1 \end{bmatrix} E\frac{1}{L}\begin{bmatrix} -1 & 1 \end{bmatrix} ds = \frac{AE(L-x)}{L^2}\begin{bmatrix} 1 & -1 \\ -1 & 1 \end{bmatrix} \tag{5.87}$$

If the cohesive model is used:

$$\mathbf{K}_{bb\Gamma} = \int_A \frac{1}{L}\begin{bmatrix} L-x \\ x \end{bmatrix} \mathbf{T}_{cz} \frac{1}{L}\begin{bmatrix} L-x & x \end{bmatrix} dA$$

$$= \frac{A\sigma_u^2 \exp(-\frac{\sigma_u \kappa}{G_f})}{L^2 G_f}\begin{bmatrix} -(x-L)^2 & x(x-L) \\ x(x-L) & -x^2 \end{bmatrix} \tag{5.88}$$

and the internal forces include:

$$\mathbf{F}_{b\sigma}^{int} = \int_x^L \frac{A}{L}\begin{bmatrix}-1\\1\end{bmatrix}\sigma ds = \frac{A\sigma(x-L)}{L}\begin{bmatrix}1\\-1\end{bmatrix} \tag{5.89}$$

$$\mathbf{F}_{bT}^{int} = \int_A \frac{1}{L}\begin{bmatrix}L-x\\x\end{bmatrix} T dA = \frac{TA}{L}\begin{bmatrix}L-x\\x\end{bmatrix} \tag{5.90}$$

If the crack is supposed to occur at the midpoint of the element, the stiffness is:

$$\mathbf{K}_{vb} = \mathbf{K}_{bv} = \mathbf{K}_{bb\Omega} = \int_{L/2}^L \frac{A}{L}\begin{bmatrix}-1\\1\end{bmatrix} E\frac{1}{L}\begin{bmatrix}-1 & 1\end{bmatrix} ds = \frac{AE}{2L}\begin{bmatrix}1 & -1\\-1 & 1\end{bmatrix} \tag{5.91}$$

$$\mathbf{K}_{bb\Gamma} = -\frac{A\sigma_u^2}{4G_f}\exp\left(-\frac{\sigma_u}{G_f}\kappa\right)\begin{bmatrix}1 & 1\\1 & 1\end{bmatrix} \tag{5.92}$$

and the internal forces are:

$$\mathbf{F}_{b\sigma}^{int} = \int_{L/2}^L \frac{A}{L}\begin{bmatrix}-1\\1\end{bmatrix}\sigma ds = \frac{A\sigma}{2}\begin{bmatrix}-1\\1\end{bmatrix} \tag{5.93}$$

$$\mathbf{F}_{bT}^{int} = \int_A \begin{bmatrix}1/2\\1/2\end{bmatrix} T dA = \frac{TA}{2}\begin{bmatrix}1\\1\end{bmatrix} \tag{5.94}$$

If the crack occurs very close to the end of the element (where $s = L$):

$$\mathbf{K}_{bv} = \mathbf{K}_{vb} = \mathbf{K}_{bb\Omega} = \mathbf{0} \tag{5.95}$$

this is because $\Omega^+ \approx 0$. And

$$\mathbf{K}_{bb\Gamma} = \int_A \begin{bmatrix}0\\1\end{bmatrix}\mathbf{T}_{cz}\begin{bmatrix}0 & 1\end{bmatrix} dA = -\frac{A\sigma_u^2}{G_f}\exp(-\frac{\sigma_u}{G_f}\kappa)\begin{bmatrix}0 & 0\\0 & 1\end{bmatrix} \tag{5.96}$$

In this case:

$$\mathbf{f}_b^{int} = TA\begin{bmatrix}0\\1\end{bmatrix} \tag{5.97}$$

5.9 Two-Dimensional implementation

5.9.1 Computation of matrices

The embedded crack element is implemented over a quadrilateral isoparametric element with four nodes based on displacements. The matrices **N** and **B** are the standard matrices for this element. A global system of coordinates $(x_1 - x_2)$ and a

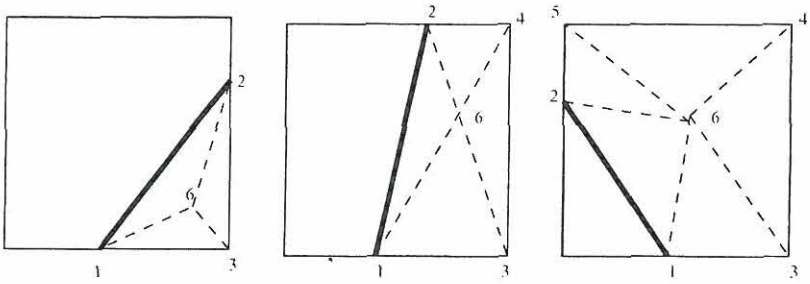

Figure 5.5: Division of the domain Ω^+ in triangular sub-domains

natural system of coordinates $(\xi - \eta)$ are considered. As usual, the derivatives of the shape functions in one system are related to the other system by:

$$\begin{bmatrix} \frac{\partial N}{\partial x_1} \\ \frac{\partial N}{\partial x_2} \end{bmatrix} = \mathbf{J}^{-1} \begin{bmatrix} \frac{\partial N}{\partial \xi} \\ \frac{\partial N}{\partial \eta} \end{bmatrix} \tag{5.98}$$

where $\mathbf{J}$ is the Jacobian matrix. For this element the integration is performed numerically. In that case:

$$\mathbf{K}_{vv} = \int_{\Omega} \mathbf{B}^T \mathbf{D} \mathbf{B} d\Omega = \sum_i \mathbf{B}_i^T \mathbf{D} \mathbf{B}_i t J w_i \tag{5.99}$$

where J is the Jacobian.

The additional parts of the stiffness matrix ($\mathbf{K}_{bv}$, $\mathbf{K}_{vb}$ and $\mathbf{K}_{bb}$) are computed in the same way when the element is not cracked. If the element is cracked, the integration over the sub-domain Ω^+ is required. This is done here dividing the sub-domain into triangles (three cases are considered as shown in figure 5.5).

For a triangle with vertices i, j and k it is possible to map this triangular zone using:

$$\mathbf{x} = \begin{bmatrix} x_1 \\ x_2 \end{bmatrix} = \tilde{\mathbf{N}} \mathbf{c} \tag{5.100}$$

where $\tilde{\mathbf{N}}$ is a matrix containing the shape functions for the triangular element, and $\mathbf{c}$ is the vector of nodal coordinates for the triangle. For an arbitrary function ϕ:

$$\begin{bmatrix} \frac{\partial \phi}{\partial r} \\ \frac{\partial \phi}{\partial s} \end{bmatrix} = \tilde{\mathbf{J}} \begin{bmatrix} \frac{\partial \phi}{\partial x_1} \\ \frac{\partial \phi}{\partial x_2} \end{bmatrix} \tag{5.101}$$

where r and s are local coordinates and $\tilde{\mathbf{J}}$ is the Jacobian matrix considered for mapping the triangle. For this mapping:

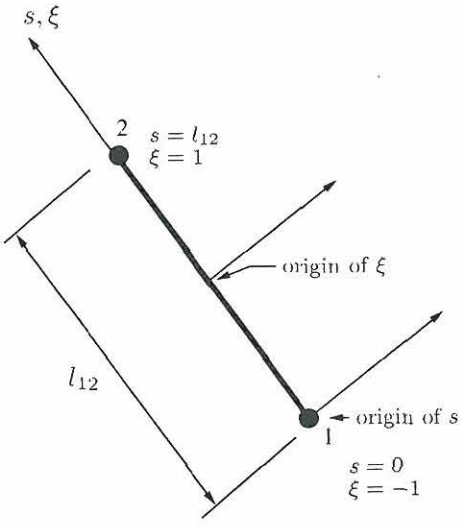

Figure 5.6: Systems of coordinates used along the crack

$$\tilde{\mathbf{J}} = \begin{bmatrix} x_{1j} - x_{1i} & x_{2j} - x_{2i} \\ x_{1k} - x_{1i} & x_{2k} - x_{2i} \end{bmatrix} \tag{5.102}$$

where the first subscript refers to the direction with respect to the global system, and the second subscript is referring to the node of the triangle. The integration in a triangular region is performed using:

$$\int_A t\mathbf{B}^T\mathbf{D}\mathbf{B}dA = \int_{-1}^{1}\int_{-1}^{1} t\mathbf{B}^T\mathbf{D}\mathbf{B}\frac{\tilde{J}}{2}drds = \sum_i t\mathbf{B}_i^T\mathbf{D}\mathbf{B}_i\frac{\tilde{J}}{2}w_i \tag{5.103}$$

where $\tilde{J} = \det(\tilde{\mathbf{J}})$ is the Jacobian. Then the integration process in the sub-domain consists in two steps. First the sub-domain is divided into triangles, and for every triangle the integration is performed using equation (5.103).

Along the crack the integration is performed using the natural coordinate system ξ illustrated in figure 5.6:

$$\xi = \frac{2s}{l_{12}}, \qquad ds = \tfrac{1}{2}l_{12}d\xi \tag{5.104}$$

then:

$$\mathbf{K}_{bb\Gamma} = \int_{l_{12}} t\mathbf{N}^T\mathbf{T}_{cz}\mathbf{N}ds = \int_{-1}^{1} \tfrac{1}{2}t\mathbf{N}^T\mathbf{T}_{cz}\mathbf{N}l_{12}d\xi = \sum_i \tfrac{1}{2}t\mathbf{N}_i^T\mathbf{T}_{czi}\mathbf{N}_i l_{12}w_i \tag{5.105}$$

In a similar way the internal forces are computed using:

$$\mathbf{F}_{b\sigma}^{int} = \int_{\Omega+} \mathbf{B}^T\boldsymbol{\sigma}d\Omega = \sum_i \tfrac{1}{2}t\mathbf{B}_i^T\boldsymbol{\sigma}_i\tilde{J}w_i \tag{5.106}$$

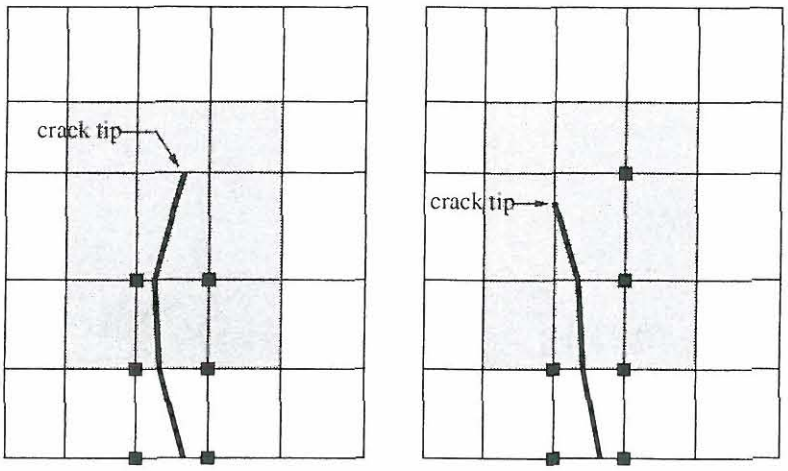

Figure 5.7: Examples of patches of elements showing the nodes with additional (enhanced) degrees of freedom. The patch of elements that could affect the enhanced degrees of freedom for the element containing the crack tip are shaded. The nodes with enhanced degrees of freedom are indicated by solid squares.

and

$$\mathbf{F}_{bT}^{int} = \int_S \mathbf{N}^T \mathbf{T} d\Gamma = \sum_i \tfrac{1}{2} t \mathbf{N}_i^T \mathbf{T}_i l_{12} w_i \tag{5.107}$$

5.9.2 Geometry of the crack

In the element described in section 5.9.1, four Gauss integration points were defined; in each of them the stress is checked. If the stress at one of the points exceeds the maximum stress for the material, a crack is generated.

The crack is generated passing through the integration point at which the maximum principal stress occurs. The direction of the crack is chosen perpendicularly to the maximum stress direction. When the crack grows and the crack tip passes to the neighboring element, then the crack is located in the new cracked element, in such a way, that it continues from the existent crack tip and only the direction is defined in the new cracked element. The new degrees of freedom are then activated in the nodes corresponding to the sub-domain Ω^+ in the cracked element.

Usually, two new nodes with additional degrees of freedom are activated for a new cracked element in the form shown in figure 5.7, in which form the jump at the crack tip is forced to be zero. Nodes in elements not crossed by a discontinuity are not activated because the Heaviside function in these elements is equivalent to a constant, and constant functions form part of the shape functions.

5.9.3 The Xu-Needleman model modified

In order to introduce the discontinuity using the Xu-Needleman model, it is required to modify this model in order to take into account initial values of tractions. This is done here by defining the total jump for the model $\boldsymbol{\Delta}$ as:

$$\boldsymbol{\Delta} = \begin{bmatrix} \Delta_s \\ \Delta_n \end{bmatrix} = \boldsymbol{\Delta}_0 + [\![\mathbf{u}]\!] = \begin{bmatrix} \Delta_{0s} \\ \Delta_{0n} \end{bmatrix} + \begin{bmatrix} [\![u_s]\!] \\ [\![u_n]\!] \end{bmatrix} \tag{5.108}$$

Now the potential is

$$\phi([\![\mathbf{u}_n]\!]) = \phi_n - \phi_n \exp\left(-\frac{\Delta_n}{\delta_n}\right)\left(1 + \frac{\Delta_n}{\delta_n}\right)\exp\left(-\frac{\Delta_s^2}{\delta_s^2}\right) \tag{5.109}$$

and the tractions are:

$$T_n = \frac{\phi_n}{\delta_n}\frac{\Delta_n}{\delta_n}\exp\left(-\frac{\Delta_n}{\delta_n}\right)\exp\left(-\frac{\Delta_s^2}{\delta_s^2}\right) \tag{5.110}$$

$$T_s = \frac{\phi_n}{\delta_n}\left(\frac{\Delta_n}{\delta_n} + 1\right)\left(2\frac{\delta_n}{\delta_s}\right)\frac{\Delta_s}{\delta_s}\exp\left(-\frac{\Delta_n}{\delta_n}\right)\exp\left(-\frac{\Delta_s^2}{\delta_s^2}\right) \tag{5.111}$$

The process after the definition of the crack position consists in defining the initial values of $\boldsymbol{\Delta}_0$. In order to obtain these values first the tractions in a point in the crack are computed as:

$$\mathbf{T} = \mathbf{n} \cdot \boldsymbol{\sigma} \tag{5.112}$$

Second, the equations (5.110) and (5.111) are solved for the values of Δ_n and Δ_s. Taken into account that the first time $[\![\mathbf{u}]\!] = \mathbf{0}$, then $\boldsymbol{\Delta} = \boldsymbol{\Delta}_0$.

5.10 Numerical solution to the non-linear problem

The problem is solved using the arc-length control strategy (Crisfield 1981), (Crisfield 1991), including simple modifications of the standard algorithm due to the inclusion of new degrees of freedom occurring in the cracking process.

The increment in load level is defined as $\Delta\lambda$ and the corresponding increment in nodal displacements is $\Delta\mathbf{P}$. The total of external nodal forces before cracking is represented by the vector $\mathbf{q}_0$ and proportional loading is supposed such that:

$$\mathbf{q} = \lambda\mathbf{q}_0 \qquad \text{and} \qquad \frac{\partial \mathbf{q}}{\partial \lambda} = \mathbf{q}_0 \tag{5.113}$$

where $\mathbf{q}$ is the external load corresponding to the load level λ.

The tangential displacement $\boldsymbol{\delta}_T$ is defined in the form that

$$\Delta\mathbf{P} = \Delta\lambda\boldsymbol{\delta}_T \tag{5.114}$$

Then it is required for equation (5.114) that

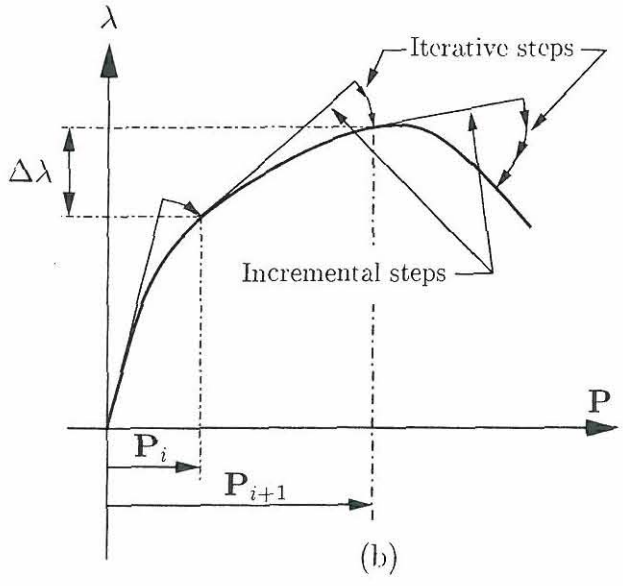

Figure 5.8: (a)Load level vs time, (b) solution sequence.

$$\mathbf{K}\boldsymbol{\delta}_T = \mathbf{f}^* \tag{5.115}$$

where $\mathbf{K}$ is the tangent stiffness matrix, and the load $\mathbf{f}^*$ is defined as:

$$\mathbf{f}^* = (\mathbf{f}^{ext} - \mathbf{f}^{int})/\Delta\lambda \tag{5.116}$$

The solution, disregarding the iterative part, proceeds in the following sequence for the step i:

1. Compute $\mathbf{K}$ and $\mathbf{f}^*$ using the values of variables from step $i-1$.
2. Compute the values of tangential degrees of freedom resulting from equation (5.115).
3. The tangential displacements are then computed as:

$$\boldsymbol{\delta}_T^* = \boldsymbol{\delta}_{Tv} + H_S\boldsymbol{\delta}_{Tb} \tag{5.117}$$

where $\boldsymbol{\delta}_{Tv}$ and $\boldsymbol{\delta}_{Tb}$ are vectors corresponding to the original and additional degrees of freedom in $\boldsymbol{\delta}_T$, respectively.

4. Compute $\Delta\lambda$ by using

$$\Delta\lambda = \pm\frac{\Delta l}{\sqrt{\boldsymbol{\delta}_T^{*T}\boldsymbol{\delta}_T^* + \psi^2\mathbf{q}_0^T\mathbf{q}_0}} \tag{5.118}$$

where the sign depends on the traced branch of the loading path, Δl is the radius of the spherical hyper-surface in the space $(\lambda, \mathbf{u})$, and ψ is a scalar factor which takes into account that λ and $\mathbf{u}$ have different scales.

5. Compute $\Delta\mathbf{P}$ using equation (5.114).
6. If desired, iterate to equilibrium.
7. Update the results using:

$$\mathbf{P}_i = \mathbf{P}_{i-1} + \Delta\mathbf{P} \tag{5.119}$$
$$\lambda_i = \lambda_{i-1} + \Delta\lambda \tag{5.120}$$
$$\boldsymbol{\sigma}_i = \boldsymbol{\sigma}_{i-1} + \Delta\boldsymbol{\sigma} \tag{5.121}$$

The procedure described is repeated until a maximum displacement or a maximum load level is reached.

The iterative process is done in the following sequence:

1. Compute the new stresses in elements using $\mathbf{P}_{i-1} = \mathbf{P}_{n-1} + \Delta\mathbf{P}_{i-1}$ where n is the corresponding step, and i is the corresponding iteration.
2. Compute the new imbalance force $\mathbf{g}$ as:

$$\mathbf{g} = \mathbf{F}^{ext} - \mathbf{F}^{int} = (\lambda_{n-1} + \Delta\lambda_i)\mathbf{F}^{ext} - \mathbf{F}^{int} \tag{5.122}$$

where $\mathbf{F}^{ext}$ is computed at the beginning of every step using equation (5.42)

3. Compute $\delta\mathbf{P}_i$ from $\mathbf{K}_{n-1}\delta\mathbf{P}_i = \mathbf{g}$
4. Compute $\delta\lambda_i$ from

$$a_1\delta\lambda_i^2 + a_2\delta\lambda_i + a_3 = 0 \tag{5.123}$$

where

$$a_1 = \boldsymbol{\delta}_T^{*T}\boldsymbol{\delta}_T^* + \psi^2\mathbf{F}_v^{extT}\mathbf{F}_v^{ext} \tag{5.124}$$
$$a_2 = 2 * \boldsymbol{\delta}_T^{*T}(\Delta\mathbf{P}_0^* + \delta\mathbf{P}_i^*) + 2\Delta\lambda_0\psi^2\mathbf{F}_v^{extT}\mathbf{F}_v^{ext} \tag{5.125}$$
$$a_3 = (\Delta\mathbf{P}_0^* + \delta\mathbf{P}_i^*)^T(\Delta\mathbf{P}_0^* + \delta\mathbf{P}_i^*) - \Delta l^2 + \Delta\lambda_0\psi^2\mathbf{F}_v^{extT}\mathbf{F}_v^{ext} \tag{5.126}$$

and

$$\Delta\mathbf{P}_0^* = \Delta\mathbf{P}_{0v} + H_S\Delta\mathbf{P}_{0b} \tag{5.127}$$
$$\delta\mathbf{P}_i^* = \delta\mathbf{P}_{iv} + H_S\delta\mathbf{P}_{ib} \tag{5.128}$$

Property	Value
E	1×10^8 Pa $= 100$ N/mm^2
ν	0.1
σ_u	1 N/mm^2
G_f	0.2 N mm/mm^2
A	1 mm^2
L	1 mm
P	2 N

Table 5.1: Properties used in the analysis for a single bar.

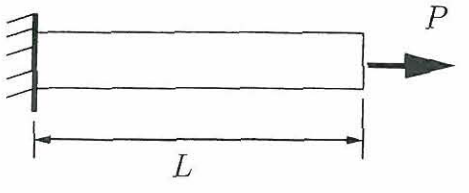

Figure 5.9: A single bar supporting a force P.

5. The new updated quantities are:

$$\Delta \mathbf{P}_i = \Delta \mathbf{P}_0 + \delta \mathbf{P}_i + \delta\lambda_i \boldsymbol{\delta}_T \tag{5.129}$$

$$\Delta\lambda_i = \Delta\lambda_{i-1} + \delta\lambda_i \tag{5.130}$$

6. If converged, stop; otherwise next iteration.

5.11 One-Dimensional examples

5.11.1 A single bar

A single bar which can be cracked at one end is used as a first example. The model consists in only one one-dimensional finite element. The bar has the properties presented in table 5.1, and the bar is shown in figure 5.9. The simple exponential cohesive model will be used, and it will be supposed that the crack occurs at one end of the bar.

In the first step, the following values are obtained:

$$\mathbf{q}_0 = \mathbf{f}^* = [2] \tag{5.131}$$

$$\mathbf{K} = [100] \tag{5.132}$$

therefore

$$\boldsymbol{\delta}_T = \mathbf{K}^{-1}\mathbf{f}^* = [0.02] \tag{5.133}$$

Using $\Delta l = 0.1$, a value of $\Delta\lambda = 0.05$ is computed from equation (5.118). The results for the first step are:

$$\Delta\mathbf{P} = \Delta\lambda\delta_T = 0.001 \tag{5.134}$$

the stress in the bar is:

$$\Delta\boldsymbol{\sigma} = \begin{bmatrix}100\end{bmatrix}\begin{bmatrix}-1 & 1\end{bmatrix}\begin{bmatrix}0\\0.001\end{bmatrix} = 0.1 \tag{5.135}$$

If the value of Δl is kept constant after 10 steps, the following values are obtained:

$$\mathbf{P}_{10} = \begin{bmatrix}0.01\end{bmatrix}, \qquad \lambda_{10} = 0.5, \qquad \sigma_{10} = 1.0 \tag{5.136}$$

At this point, the crack starts with a value of $T = 1\mathrm{N}/\mathrm{mm}^2$. At the beginning of step 11 it is supposed that $\Delta\lambda_{11} = \Delta\lambda_{10} = 0.05$. The global external forces are:

$$\mathbf{F}_v^{ext} = \mathbf{F}_b^{ext} = \mathbf{q}_0(\lambda + \Delta\lambda) = \begin{bmatrix}1.1\end{bmatrix} \tag{5.137}$$

The internal forces in the element are:

$$\mathbf{F}_v^{int} = \begin{bmatrix}-1\\1\end{bmatrix} \qquad \text{and} \qquad \mathbf{F}_b^{int} = \begin{bmatrix}0\\1\end{bmatrix} \tag{5.138}$$

then, the internal global forces are:

$$\mathbf{F}_v^{int} = \mathbf{F}_b^{int} = \begin{bmatrix}1\end{bmatrix} \tag{5.139}$$

producing

$$\mathbf{f}^* = (\mathbf{F}^{ext} - \mathbf{F}^{int})/\Delta\lambda = \begin{bmatrix}2\\2\end{bmatrix} \tag{5.140}$$

The stiffness matrix of the element and the global stiffness matrix are (with $T_{cz} = -5$):

$$\mathbf{K}_e = \begin{bmatrix}100 & -100 & 0 & 0\\ -100 & 100 & 0 & 0\\ 0 & 0 & 0 & 0\\ 0 & 0 & 0 & -5\end{bmatrix} \qquad \mathbf{K} = \begin{bmatrix}100 & 0\\ 0 & -5\end{bmatrix} \tag{5.141}$$

The tangential values of the degrees of freedom are:

$$\boldsymbol{\delta}_T = \begin{bmatrix} \delta_{Tv} \\ \delta_{Tb} \end{bmatrix} = \begin{bmatrix} 0.02 \\ -0.4 \end{bmatrix} \tag{5.142}$$

and the tangential displacement is $\delta_T^* = 0.02 - 0.4 = -0.38$. The new value of $\Delta\lambda = -0.05$. The displacements for this step are:

$$\Delta\mathbf{P} = \Delta\lambda\boldsymbol{\delta}_T = \begin{bmatrix} -9.82 \times 10^{-4} \\ 0.01965 \end{bmatrix}, \qquad \mathbf{P}_{11} = \begin{bmatrix} 0.009018 \\ 0.01965 \end{bmatrix} \tag{5.143}$$

With a jump value of $[\![u]\!] = 0.01965$ the value of T using equation (5.54) is $T = 0.9064\text{N/mm}^2$. The stress is:

$$\sigma_{11} = \sigma_{10} + \Delta\sigma = 1 + 100(-9.82 \times 10^{-4}) = 0.9018\text{N/mm}^2 \tag{5.144}$$

The difference between the value of T and σ is due to the drift error. In figure 5.10(b), the values of T and σ are presented for the case when $\lambda_1 = 0.005$, and values of λ vs displacement are presented in figure 5.10a for the same case. In figure 5.10, iterations have been used in order to reduce the drift error, and then it is possible to observe that the exponential softening is reproduced, as expected from the constitutive model.

5.11.2 Three bars

The system shown in figure 5.11(a) is analyzed using the same kind of elements as in the first example. The properties are the same as in the previous example indicated in table 5.1. The mesh of elements is shown in figure 5.11(b).

The results for this example were here obtained including iterations, and a much better agreement is found between the stresses and the tractions for a smaller number of steps. In figure 5.12(a), the stresses are shown for every bar. In figure 5.12(b), the force-displacement diagram is shown for the node number three. After cracking of the first bar, a change in stiffness occurs, which is shown as a change in the slope of the curve force displacement. The change in the slope of displacements is accompanied by unloading of the cracked bar and of course by unloading of the second one, as is to be seen in figure 5.12(a). Finally, after cracking of the third bar, unloading of the system occurs.

5.11.3 Two bars with cracks at the middle point

Two bars in series are considered as shown in figure 5.13. The properties are the same as in the previous examples, listed in table 5.1. This time a crack is considered to occur at the midpoint of the bar.

The first time the tangent stiffness of the elements are:

$$\mathbf{K}_1 = \mathbf{K}_2 = \begin{bmatrix} 100 & -100 \\ -100 & 100 \end{bmatrix} \tag{5.145}$$

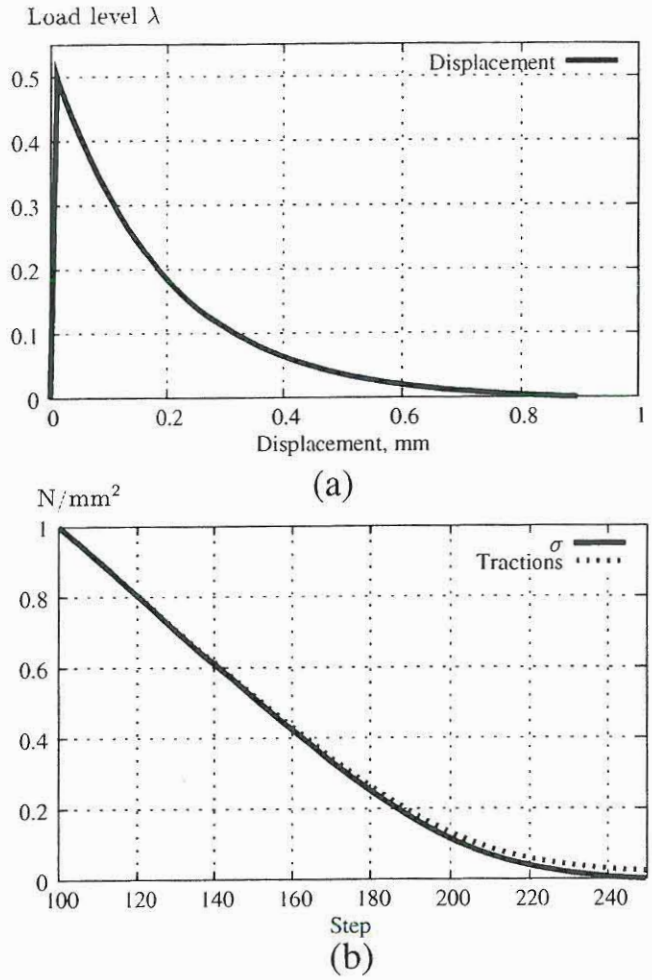

Figure 5.10: (a) λ vs Displacement and (b) Stress or traction vs step for a single bar supporting an axial force.

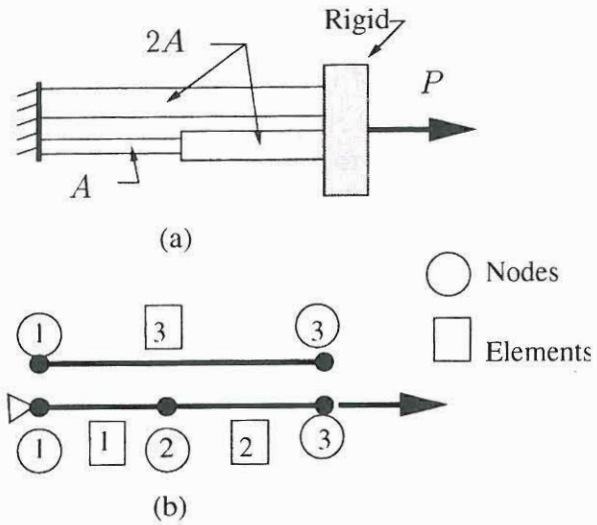

Figure 5.11: (a) The three bar system. (b) Finite element model.

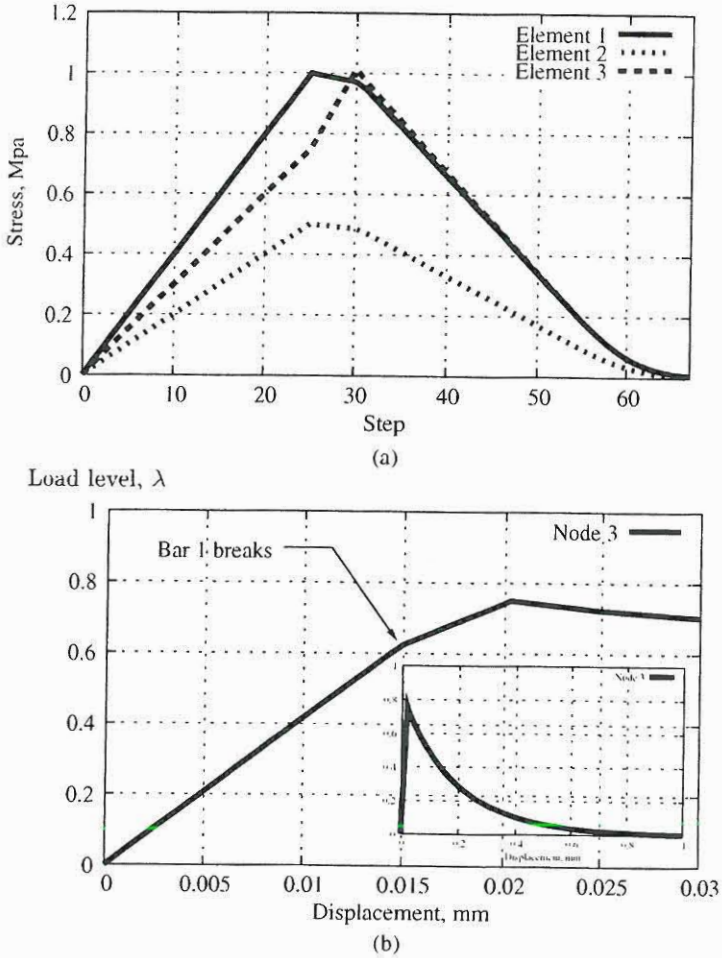

Figure 5.12: (a) Stresses in every bar and (b) Force-displacement diagram for the three bar system.

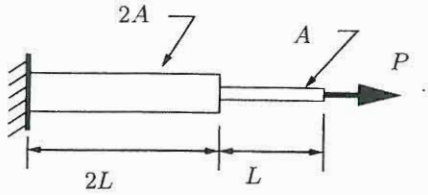

Figure 5.13: System of two bars.

The global stiffness and the load vector are:

$$\mathbf{K} = \begin{bmatrix} 200 & -100 \\ -100 & 100 \end{bmatrix}, \qquad \mathbf{q}_0 = \begin{bmatrix} 0 \\ 2 \end{bmatrix} \tag{5.146}$$

with a value of $\Delta l = 0.1$ then $\Delta\lambda = 0.05$. The tangential displacement and the incremental displacement are:

$$\boldsymbol{\delta}_T = \mathbf{K}^{-1}\mathbf{q}_0 = \begin{bmatrix} 0.02 \\ 0.04 \end{bmatrix}, \qquad \text{and} \qquad \Delta\mathbf{P} = \Delta\lambda\boldsymbol{\delta}_T = \begin{bmatrix} 0.001 \\ 0.002 \end{bmatrix} \tag{5.147}$$

The stresses are computed as:

$$\sigma_{x1} = \tfrac{100}{2}\begin{bmatrix} -1 & 1 \end{bmatrix}\begin{bmatrix} 0 \\ 0.001 \end{bmatrix} = 0.05\text{MPa} \tag{5.148}$$

$$\sigma_{x2} = 100\begin{bmatrix} -1 & 1 \end{bmatrix}\begin{bmatrix} 0.001 \\ 0.002 \end{bmatrix} = 0.1\text{MPa} \tag{5.149}$$

After ten steps with $\Delta l = 0.1$ constant, it is found that:

$$\lambda = 0.5, \qquad \mathbf{P} = \begin{bmatrix} 0.01 \\ 0.02 \end{bmatrix}, \qquad \sigma_{x1} = 0.5\text{MPa}, \qquad \text{and} \qquad \sigma_{x2} = 1\text{Mpa} \tag{5.150}$$

The last result indicates that a crack first appears in the second element in this step. For step number 11:

$$\mathbf{F}^{ext} = (\lambda + \Delta\lambda)\begin{bmatrix} 0 \\ 2 \\ 0 \\ 2 \end{bmatrix} = \begin{bmatrix} 0 \\ 1.1 \\ 0 \\ 1.1 \end{bmatrix} \tag{5.151}$$

where $\lambda = 0.5$ and $\Delta\lambda = 0.05$. The internal forces for every one of the elements are:

$$\mathbf{F}_1^{int} = \begin{bmatrix} -1 \\ 1 \\ 0 \\ 0 \end{bmatrix} \qquad \text{and} \qquad \mathbf{F}_2^{int} = \begin{bmatrix} -1 \\ 1 \\ -\frac{1}{2} + \frac{1}{2} \\ \frac{1}{2} + \frac{1}{2} \end{bmatrix} \tag{5.152}$$

The vector of internal forces, the imbalance vector, and the load vector are:

$$\mathbf{F}^{int} = \begin{bmatrix} 0 \\ 1 \\ 0 \\ 1 \end{bmatrix}, \qquad \mathbf{g} = \mathbf{F}^{ext} - \mathbf{F}^{int} = \begin{bmatrix} 0 \\ 0.1 \\ 0 \\ 0.1 \end{bmatrix} \qquad \text{and} \qquad \mathbf{f}^* = \begin{bmatrix} 0 \\ 2 \\ 0 \\ 2 \end{bmatrix} \tag{5.153}$$

The stiffness matrix for the second element is:

$$\mathbf{K}_2 = \begin{bmatrix} 100 & -100 & 50 & -50 \\ -100 & 100 & -50 & 50 \\ 50 & -50 & 48.75 & -51.25 \\ -50 & 50 & -51.25 & 48.75 \end{bmatrix} \tag{5.154}$$

The stiffness matrix for the first element remains unchanged because the common node is located in the region Ω^-. The global tangential stiffness is then:

$$\mathbf{K} = \begin{bmatrix} 200 & -100 & 50 & -50 \\ -100 & 100 & -50 & 50 \\ 50 & -50 & 48.75 & -51.25 \\ -50 & 50 & -51.25 & 48.75 \end{bmatrix} \tag{5.155}$$

The tangential displacement and the total tangential displacements are:

$$\boldsymbol{\delta}_T = \mathbf{K}^{-1}\mathbf{f}^* = \begin{bmatrix} 0.02 \\ 0.04 \\ -0.4 \\ -0.4 \end{bmatrix}, \quad \text{and} \quad \boldsymbol{\delta}_T^* = \begin{bmatrix} 0.02 \\ -0.36 \end{bmatrix} \tag{5.156}$$

the value of $\Delta\lambda = -0.0492$. The displacement is then

$$\Delta\mathbf{P} = \begin{bmatrix} -0.000984 \\ -0.001968 \\ 0.01968 \\ 0.019684 \end{bmatrix}, \quad \mathbf{P} = \begin{bmatrix} 0.009016 \\ 0.01832 \\ 0.01968 \\ 0.01968 \end{bmatrix} \quad \text{and} \quad \mathbf{P}^* = \begin{bmatrix} 0.009016 \\ 0.03712 \end{bmatrix} \tag{5.157}$$

The stresses are:

$$\Delta\sigma_{x1} = \tfrac{100}{2}\begin{bmatrix} -1 & 1 \end{bmatrix}\begin{bmatrix} 0 \\ -0.000984 \end{bmatrix} = -0.0492\text{MPa} \tag{5.158}$$

$$\Delta\sigma_{x2} = 100(\begin{bmatrix} -1 & 1 \end{bmatrix}\begin{bmatrix} -0.000984 \\ 0.001968 \end{bmatrix} + H_S\begin{bmatrix} -1 & 1 \end{bmatrix}\begin{bmatrix} -0.01968 \\ 0.01968 \end{bmatrix}) = -0.0984\text{MPa} \tag{5.159}$$

The final stress in the second element is $\sigma_{x2} = 1 - 0.0984 = 0.9016$Mpa. Again, a drift error occurs (the traction computed for this element is $T = 0.9063$MPa).

5.11.4 A single bar with a crack in x

The model is the same as used in section 5.11.1, but the crack is located at the position x. In step 11, when the crack starts, it is supposed that $\Delta\lambda_{11} = \Delta\lambda_{10} = 0.05$. The forces are:

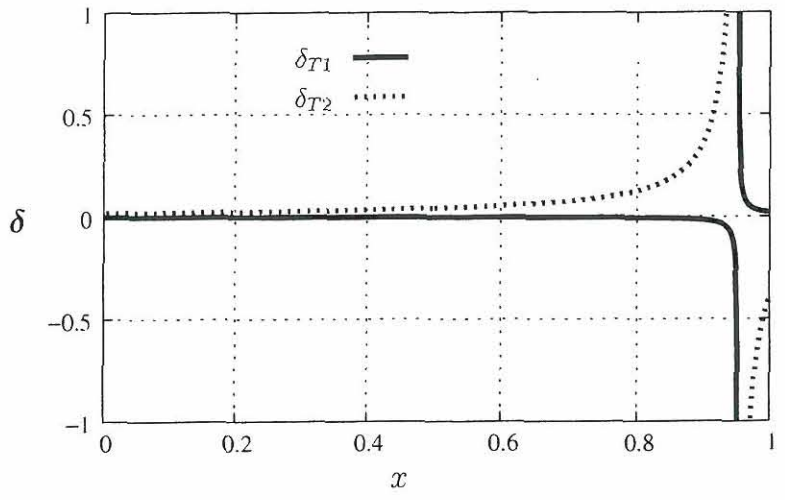

Figure 5.14: Components of $\boldsymbol{\delta}_T$ as functions of x.

$$\mathbf{f}^* = (\mathbf{F}^{ext} - \mathbf{F}^{int})/\Delta\lambda = \begin{bmatrix} 2 \\ 2 \end{bmatrix} \tag{5.160}$$

The stiffness matrix of the element and the global stiffness matrix are (with $T_{cz} = -5$):

$$\mathbf{K}_{vv} = \begin{bmatrix} 100 & -100 \\ -100 & 100 \end{bmatrix} \tag{5.161}$$

$$\mathbf{K}_{bv} = \begin{bmatrix} 100 - 100x & 100x - 100 \\ 100x - 100 & 100 - 100x \end{bmatrix} \tag{5.162}$$

$$\mathbf{K}_{bb\Gamma} = \begin{bmatrix} -5(x-1)^2 & 5x(x-1) \\ 5x(x-1) & -5x^2 \end{bmatrix} \tag{5.163}$$

$$\mathbf{K} = \begin{bmatrix} 100 & 100 - 100x \\ 100 - 100x & 100 - 100x - 5x^2 \end{bmatrix} \tag{5.164}$$

The tangential values of the degrees of freedom are:

$$\boldsymbol{\delta}_T = \begin{bmatrix} \delta_{Tv} \\ \delta_{Tb} \end{bmatrix} = \frac{1}{100x - 105x^2} \begin{bmatrix} -0.1x^2 \\ 2x \end{bmatrix} \tag{5.165}$$

The values of degrees of freedom as a function of x are illustrated in figure 5.14

From figure 5.14 it is observed that a serious problem can arise for these kinds of elements. As can be seen for low values of x, the tangential jump (corresponding to

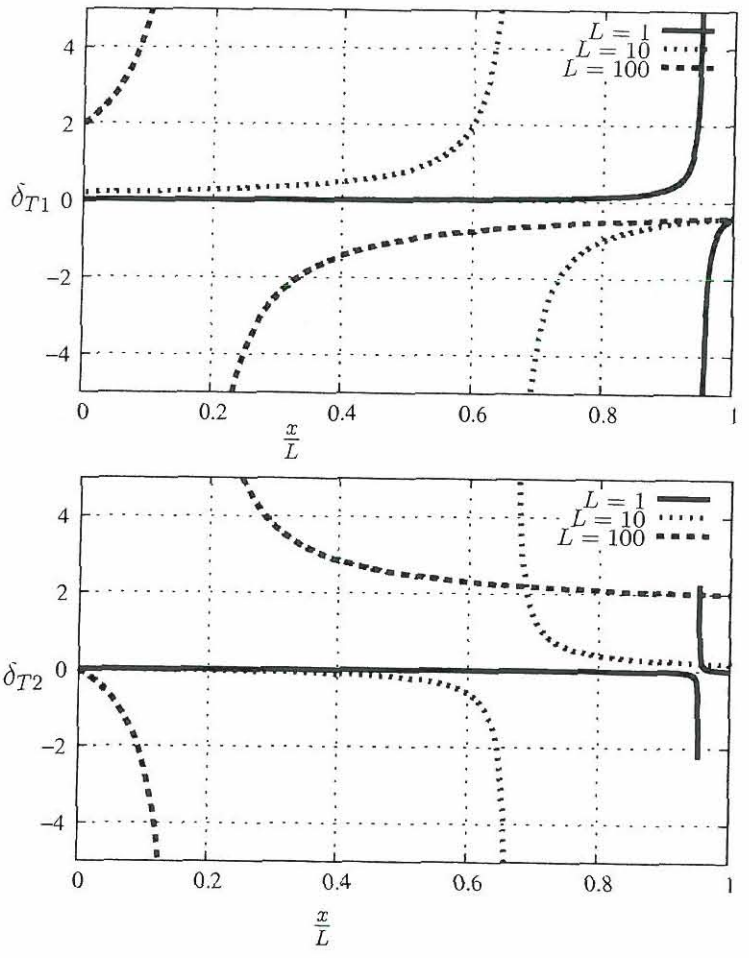

Figure 5.15: Components of $\boldsymbol{\delta}_T$ as functions of x/L for different values of L for the example in section 5.11.4.

δ_{T2}) has a positive value when the increment in the load is positive. This means that an increase of the load is required in order to get an increment in the displacement. This is unphysical, because once the cracking occurs, a softening behavior of the body is expected. This is even worse, there is point x where a singularity occurs. This problem is only a numerical problem, it shall be observed that it is not affecting the results in the example in section 5.11.3, only because in the system of equations producing $\boldsymbol{\delta}_T$, the influence of the stiffness in the first bar removes the problem.

For the single bar with crack in x it is possible to illustrate how $\boldsymbol{\delta}_T$ is affected for different factors. In figure 5.15 the effect of considering different length is illustrated, and in figure 5.16 the effect of changing the value of G_f is illustrated. In general it is observed from this example that a carefully examination of the results is required because the same kind of numerical difficulties can exist in one two or three dimensions.

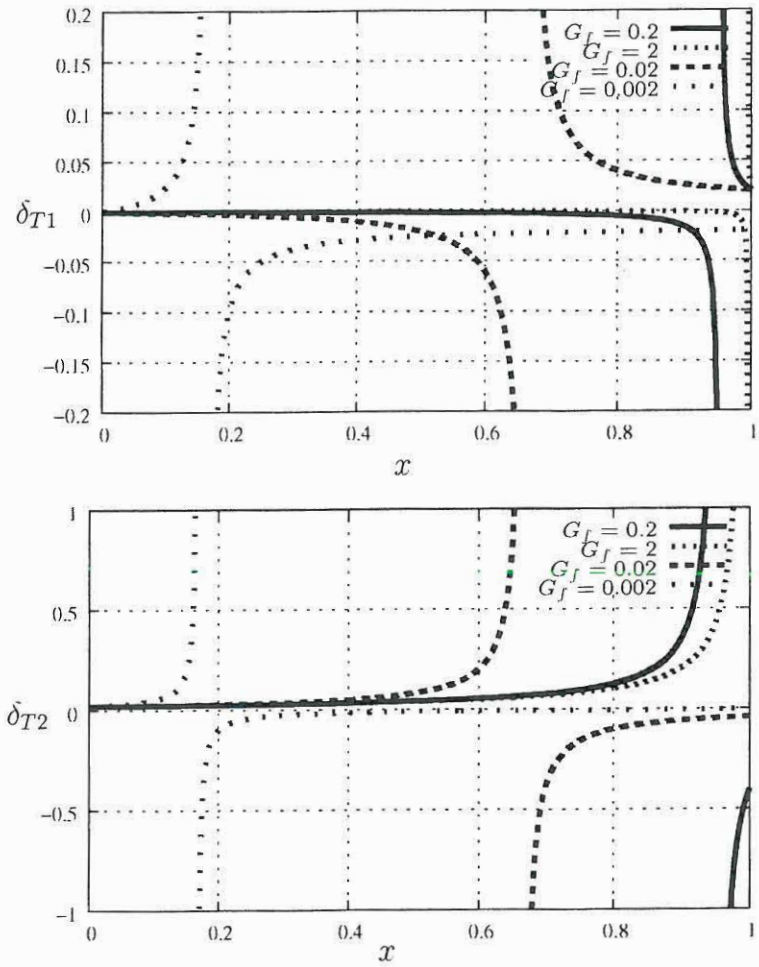

Figure 5.16: Components of $\boldsymbol{\delta}_T$ as functions of x/L for different values of G_f for the example in section 5.11.4.

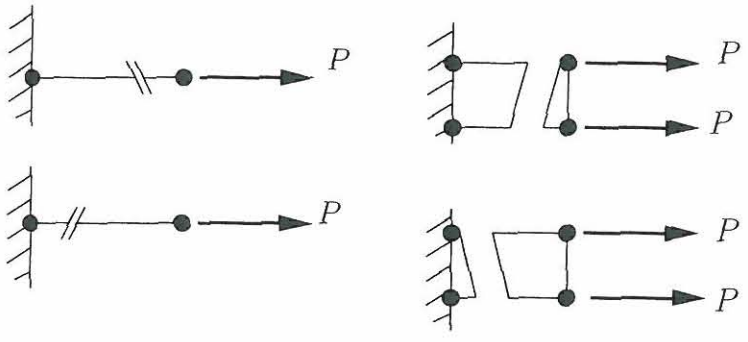

Figure 5.17: Examples of elements with cracks that must produce the same results in the nodes, but produce different results using the implementation developed in this document.

5.12 Conclusions

In this chapter the partition of unity property has been used to create finite elements with embedded cracks. The result is a finite element method where creation of new degrees of freedom is required every time the crack advances into a new element.

Handling of increasing numbers of degrees of freedom, and, of course, a variable number of equations to solve is required. Also integration into sub-domains inside the element is neccessary. The result is an increment in the complexity of the implementation of the method. However, the number of new degrees of freedom are small compared to the total number of degrees of freedom in the system, this fact makes the method reliable and efficient.

The author has found it very difficult to deal with problems involving several cracks at the same time; it is very complex to consider which degrees of freedom are active for an element (the sub-domain Ω^+ for some elements sometimes overlaps with the sub-domain Ω^- in other cracked elements from a neighboring crack) the solution increases in complexity and becomes chaotic.

Finally, it is observed that numerical problems exist as illustrated using the one-dimensional example. It is not possible to find the correct solution using the procedures indicated in this document. The problem occurs because the integration over the sub-domain Ω^+ introduces the position of the crack as a variable in the stiffness matrix of the element. And elements with cracks in different positions can produce different solutions thus losing the solution objectivity, this is the case of the systems illustrated in figure 5.17.

Some implementations of embedded cracks using X-FEM have been reported to be successful, e.g. (Moës et al. 1999), (Wells & Sluys 2001); this means that the problem addressed here has been either unknown, ignored, or only occurs if the implementation is used exactly as presented here.

Bibliography

Babuška, I. & Melenk, J. M. (1997), 'The partition of unit method', *Int. J. Numer. Meth. Engng.* **40**, 727–758.

Camacho, G. T. & Ortiz, M. (1996), 'Computational modeling of impact damage in brittle materials', *Internat. J. Solids Structures* **33**, 2899 2938.

Carter, B., Ingraffea, A. & Bittencourt, T. N. (1995), Topology-controlled modelling of linear and nonlinear 3d crack propagation in geomaterials, *in* 'Fracture of Brittle, Disordered Material', E and FN Spon, London, pp. 301 318.

Cope, R. J., Rao, P. V., Clark, L. A. & Norris, P. (1980), Modelling of reinforced concrete behavior for finite element analysis of bridge slabs, *in* C. Taylor, E. Hinton & D. Owen, eds, 'Numerical methods for nonlinear problems', Swansea: Pineridge Press, pp. 457–470.

Crisfield, M. A. (1981), 'A fast incremental-iterative solution procedure that handles "snap-through"', *Computers and Structures* **13**, 55 62.

Crisfield, M. A. (1991), *Non-linear Finite Element analysis of Solids and Structures*, Vol. Volume 1: essentials, John Wiley and Sons, Chichester.

Falk, M. L., Needleman, A. & Rice, J. (2001), 'A critical evaluation of cohesive zone models of dynamic fracture', *Journal de Physique IV* **11 Pr5**, 43 50.

Ingraffea, A. R. & Sauoma, V. (1985), Numerical modelling of discrete crack propagation in reinforced and plain concrete, *in* 'Fracture mechanics of concrete', Martinus Nijhoff Publishers, Dordrecht, pp. 171 225.

Moës, N., Dolbow, J. & Belitschko, T. (1999), 'A finite element method for crack growth without remeshing', *Int. J. Numer. Meth. Engng.* **46**, 131–150.

Ngo, D. & Scordelis, A. C. (1967), 'Finite element analysis of reinforced concrete beams', *Journal of the American Concrete Institute* **64**, 152 163.

Oliver, J. (1996), 'Modelling strong discontinuities in solid mechanics via strain softening constitutive equations. part 2: Numerical simulation', *International Journal for Numerical Methods in Engineering* .

Rashid, Y. R. (1968), 'Analysis of prestressed concrete pressure vessels', *Nuclear Engineering and Design* **7**(4), 334–355.

Remmers, J. J. C., de Borst, R. & Needleman, A. (2003), 'A cohesive segments method for the simulation of crack growth', *Computational mechanics* **31**(1 2), 69–77.

Simo, J. C., Oliver, J. & Armero, F. (1993), 'An analysis of strong discontinuities induced by strain-softening in rate-independent inelastic solids', *Comp. Mech.* **12**, 277–296.

Suidan, M. & Schnobrich, W. C. (1973), 'Finite element analysis of reinforced concrete', *ASCE J. Struct. Div.* **99**, 2109–2122.

Wells, G. N. & Sluys, L. J. (2000), 'Application of embedded discontinuities for softening solids', *Engineering Fracture Mechanics* **65**, 263–281.

Wells, G. N. & Sluys, L. J. (2001), 'A new method for modelling cohesive cracks using finite elements', *Int. J. Numer. Meth. Engng.* **50**, 2667–2682.

Xu, X. & Needleman, A. (1993), 'Void nucleation by inclusion debonding in a crystal matrix', *Modelling Simul. Mater. Sci. Eng.* **1**, 111–132.

Xu, X. & Needleman, A. (1994), 'Numerical simulations of fast crack growth in brittle solids', *Journal of the Mechanics and Physics of Solids* **42**, 1397–1434.

Chapter 6

Strong discontinuities, an alternative approach

Contents

6.1 Introduction

Different approaches are considered in order to model the damage and fracture of quasi-brittle materials like concrete. The material failures manifest themselves as fracture process zones, strain localization or discrete crack discontinuities. First, the localization of strains occurs in small zones, and later during the loading process, the integrity is completely lost and displacement discontinuities develop across planes in the material.

Two main approaches are considered for modeling cracking of quasi-brittle materials, the discrete crack model Ngo & Scordelis (1967), and the smeared crack model Rashid (1968). In the discrete crack model, when cracking is going to occur, new degrees of freedom are created and geometrical discontinuities are assumed to occur. In the smeared crack model, the crack process is lumped in the element considered.

The discrete models have been improved by using re-meshing techniques (Ingraffea & Saouma 1985), (Carter et al. 1995), (Camacho & Ortiz 1996), the propagation directions are defined using fracture mechanics, and the geometry of the structure is changed according to the new propagation directions.

The discrete models are well suited for highly localized deformations, but not so well suited for more distributed inelastic deformations which may take place at the early stages of failure. An additional problem arises if the cohesive surfaces are taken to have a non-zero initial compliance, the presence of the cohesive surfaces contributes to the overall compliance of the body. Then, if cohesive surfaces are added between all elements as the computational mesh is refined, the overall compliance depends on the mesh, and an ill-posed problem results. Introducing initially rigid surfaces like in (Camacho & Ortiz 1996) presents other difficulties (Falk et al. 2001).

In the smeared model, the contribution by cracking to the inelastic deformation is represented by cracking strain distributed over a finite volume. The material is then modeled as a continuum. Final fracture is represented by a zone in which the load-bearing capacity is completely lost.

Due to the fact that concrete is not a perfectly brittle material, and the material has some residual capacity after reaching the maximum strength, modifications to the model by Rashid (1968) were introduced. Suidan & Schnobrich (1973) introduced the concept of shear retention factor. To avoid problems related with the direction of the principal stresses that can rotate after cracking, Cope et al. (1980) introduced the rotating crack model.

None of these solutions were able to solve problems of convergence and mesh dependence of the solution. This occurs due to the lack of an internal length scale in the model. Without this factor, the boundary problems become ill-posed. To overcome this deficiency, regularization techniques were introduced. These strategies, however, have a major disadvantage: the localization zone must be analyzed using a very fine mesh which is impossible for the analysis of large structures.

The embedded discontinuities can overcome the limitations of the smeared and discrete models. By capturing a crack within an element it is possible to model a discrete or highly localized phenomenon within a continuum approach. The width of the failure zone is less than the width of a single element.

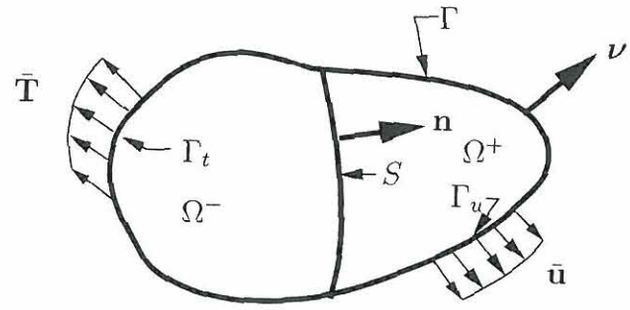

Figure 6.1: The domain Ω crossed by a discontinuity.

Simo et al. (1993) give a unified framework for the analysis of strong discontinuities based on the concept of enrichment of strains. Under certain conditions, continuum constitutive laws and unbounded strains are compatible. However, stress locking has been reported when elements with embedded discontinuities are used (Wells & Sluys 2000).

An alternative way to embed a discontinuity based on the partition of unity property (Babuška & Melenk 1997) was introduced by Moës et al. (1999), and used with a cohesive model by Wells & Sluys (2001).

In chapter 5 it was found that numerical problems can arise if the partition of unity property is used to create the finite elements with embedded cracks. The problem occurs because the position of the crack appears as a new variable in the stiffness matrix.

An alternative approach was first stated by Alfaiate et al. (2003). In this document, a very similar formulation to (Alfaiate et al. 2003) is created. This formulation is constructed incorporating into the principle of virtual work an approximation to the amplitude of the discontinuity. This is done taking into account the kinematics of the discontinuity.

It is found that this method can overcome the numerical difficulties found in the solution based on the partition of unity.

6.2 Strong discontinuities

6.2.1 Kinematics

Considering the domain Ω with boundary Γ shown in figure 6.1. It contains a discontinuity (S) which splits the domain into two parts denoted Ω^+ and Ω^-. The prescribed tractions on Γ_t are denoted $\overline{\mathbf{T}}$ and the prescribed displacements on Γ_u are denoted $\overline{\mathbf{u}}$ where Γ_u and Γ_t are in the external boundary. $\boldsymbol{\nu}$ is a unit normal to the external boundary Γ.

The kinematics of the body exhibiting a discontinuity jump of value $[\![\mathbf{u}]\!]$ in the displacements field, whose normal is $\mathbf{n}$, can be described as:

$$\mathbf{u} = \mathbf{u}_r + \mathrm{H}_S[\![\mathbf{u}]\!] \tag{6.1}$$

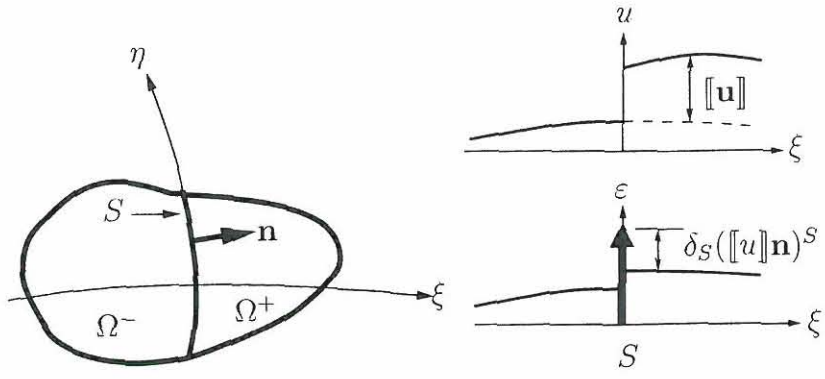

Figure 6.2: The strong discontinuity kinematics.

where $\mathbf{u}_r$ is the regular (continuous) part of the displacement field. H_S is the step function placed on S, defined as:

$$\mathrm{H}_S = \begin{cases} 0 & \text{if } \mathbf{x} \in \Omega^- \\ 1 & \text{if } \mathbf{x} \in \Omega^+ \end{cases} \tag{6.2}$$

where $\mathbf{x}$ denotes the position of a material point.

The strains are:

$$\boldsymbol{\varepsilon} = (\nabla \mathbf{u})^S = \boldsymbol{\varepsilon}_r + (\mathrm{H}_S(\nabla [\![\mathbf{u}]\!])^S) + \delta_S([\![\mathbf{u}]\!]\mathbf{n})^S \tag{6.3}$$

where $\boldsymbol{\varepsilon}$ is the strain tensor, $(\cdot)^S$ stands for the symmetric part of $(\cdot)$, δ_S is Dirac's delta on S obtained by derivation of H_S ($\nabla \mathrm{H}_S(\mathbf{x}) = \delta_S \mathbf{n}$). The regular part of the strain is denoted $\boldsymbol{\varepsilon}_r$ and is:

$$\boldsymbol{\varepsilon}_r = (\nabla \mathbf{u}_r)^S \tag{6.4}$$

The kinematics of the strong discontinuity are illustrated in figure 6.2.

6.2.2 Field equations

The field equations governing the boundary value problem can be written as (Oliver 1996):

$$\nabla \boldsymbol{\sigma} + \mathbf{f} = \mathbf{0} \qquad \text{in } \Omega \setminus S \tag{6.5}$$

$$\boldsymbol{\varepsilon} = (\nabla \mathbf{u})^S \qquad \text{in } \Omega \setminus S \tag{6.6}$$

$$\mathbf{u} = \bar{\mathbf{u}} \qquad \text{in } \Gamma_u \tag{6.7}$$

$$\boldsymbol{\sigma} \cdot \boldsymbol{\nu} = \bar{\mathbf{T}} \qquad \text{in } \Gamma_t \tag{6.8}$$

$$\mathbf{T}^+ = \boldsymbol{\sigma}^+ \cdot \mathbf{n}^+ = \boldsymbol{\sigma}^- \cdot \mathbf{n}^- = -\mathbf{T}^- \qquad \text{in } S \tag{6.9}$$

$$\mathbf{T}_S = \boldsymbol{\sigma}^+ \cdot \mathbf{n}^+ = \mathbf{T}^+ \qquad \text{in } S \tag{6.10}$$

where $\boldsymbol{\sigma}$ is the stress tensor, $\mathbf{f}$ are the body forces and $\mathbf{T}_S$ are the tractions across the discontinuity.

Equation (6.5) is the classical equilibrium equation. Equation (6.6) is the strain displacement relation. Equations (6.7) and (6.8) are the essential and natural boundary conditions, respectively. Equations (6.9) and (6.10) state the continuity of the traction vector across the discontinuity S.

Other equations required to solve the problem are the constitutive relations in the form

$$\boldsymbol{\sigma} = \boldsymbol{\sigma}(\varepsilon) \qquad \text{in } \Omega \setminus S \tag{6.11}$$

$$\mathbf{T}_S = \mathbf{T}_S(\llbracket \mathbf{u} \rrbracket) \qquad \text{in } S \tag{6.12}$$

The consideration of the strong discontinuity leads to the definition of the strain field in terms of the regular part of the displacements $\mathbf{u}_r$, the displacement jump $\llbracket \mathbf{u} \rrbracket$ and the normal $\mathbf{n}$.

$$\varepsilon = \varepsilon(\mathbf{u}_r, \llbracket \mathbf{u} \rrbracket, \mathbf{n}) \tag{6.13}$$

$\llbracket \mathbf{u} \rrbracket$ and $\mathbf{n}$ are additional unknowns with respect to the standard solid mechanics problem. $\mathbf{n}$ is solved in terms of the stress field, and the jump is found using the traction vector continuity condition (6.9).

Equations (6.5)-(6.13) provide a sufficient and well posed set of equations to solve the problem in terms of $\boldsymbol{\sigma}$, ε, $\mathbf{u}$ and $\llbracket \mathbf{u} \rrbracket$.

6.3 Weak formulation

Considering the principle of virtual work:

$$\int_\Omega \boldsymbol{\sigma}(\varepsilon) \colon (\nabla \delta \mathbf{u})^S d\Omega = \int_{\Gamma_t} \bar{\mathbf{T}} \cdot \delta \mathbf{u} d\Gamma + \int_\Omega \mathbf{f} \cdot \delta \mathbf{u} d\Omega \tag{6.14}$$

Considering:

$$\int_\Omega \boldsymbol{\sigma}(\varepsilon) \colon (\nabla \delta \mathbf{u})^S d\Omega = \int_{\Omega \setminus S} \boldsymbol{\sigma}(\varepsilon) \colon (\nabla \delta \mathbf{u})^S d\Omega - \int_S \mathbf{T}_S \delta \llbracket \mathbf{u} \rrbracket d\Gamma \tag{6.15}$$

and replacing (6.1) and (6.15) into (6.14):

$$\begin{aligned} &- \int_{\Omega \setminus S} \boldsymbol{\sigma}(\varepsilon) : (\nabla \delta \mathbf{u}_r)^S d\Omega - \int_{\Omega \setminus S} \boldsymbol{\sigma}(\varepsilon) : \mathrm{H}_S (\nabla \delta \llbracket \mathbf{u} \rrbracket)^S d\Omega + \int_{\Omega \setminus S} \mathbf{f} \cdot \delta \mathbf{u}_r d\Omega \\ &+ \int_{\Omega \setminus S} \mathbf{f} \cdot \mathrm{H}_S \delta \llbracket \mathbf{u} \rrbracket d\Omega + \int_{\Gamma_t} \bar{\mathbf{T}} \cdot \delta \mathbf{u}_r d\Gamma \\ &\qquad + \int_{\Gamma_t} \bar{\mathbf{T}} \cdot \mathrm{H}_S \delta \llbracket \mathbf{u} \rrbracket d\Gamma + \int_S \mathbf{T}_S \cdot \delta \llbracket \mathbf{u} \rrbracket d\Gamma = 0 \end{aligned} \tag{6.16}$$

The weak form of the problem is represented by (6.16). This weak form of the problem will be exploited further, and it has the same form as in (Alfaiate et al. 2003), but the one presented here is derived from the principle of virtual work.

The equation (6.16) can be written as

$$
\begin{aligned}
&-\int_{\Omega\setminus S}\boldsymbol{\sigma}:(\nabla\delta\mathbf{u}_r)^S d\Omega+\int_{\Omega\setminus S}(\boldsymbol{\sigma}-\boldsymbol{\sigma}(\varepsilon)):(\nabla\delta\mathbf{u}_r)^S d\Omega\\
&-\int_{\Omega\setminus S}\boldsymbol{\sigma}:\mathrm{H}_S(\nabla\delta[\![\mathbf{u}]\!])^S d\Omega+\int_{\Omega\setminus S}(\boldsymbol{\sigma}-\boldsymbol{\sigma}(\varepsilon)):\mathrm{H}_S(\nabla\delta[\![\mathbf{u}]\!])^S d\Omega\\
&+\int_{\Omega\setminus S}\mathbf{f}\cdot\delta\mathbf{u}_r d\Omega+\int_{\Omega\setminus S}\mathbf{f}\cdot\mathrm{H}_S\delta[\![\mathbf{u}]\!]d\Omega+\int_{\Gamma_t}\bar{\mathbf{T}}\cdot\delta\mathbf{u}_r d\Gamma\\
&\qquad+\int_{\Gamma_t}\bar{\mathbf{T}}\cdot\mathrm{H}_S\delta[\![\mathbf{u}]\!]d\Gamma+\int_S\mathbf{T}_S\cdot\delta[\![\mathbf{u}]\!]d\Gamma=0
\end{aligned}
\tag{6.17}
$$

Taking the variation of the jump as:

$$
\delta[\![\mathbf{u}]\!]=\delta\mathbf{u}^+-\delta\mathbf{u}^- \quad \text{in } S \tag{6.18}
$$

and defining the variation of strains as:

$$
\delta\boldsymbol{\varepsilon}=(\nabla\delta\mathbf{u}_r)^S+\mathrm{H}_S(\nabla\delta[\![\mathbf{u}]\!])^S \qquad \text{in } \Omega\setminus S \tag{6.19}
$$

the weak form (6.17) can be written as:

$$
\begin{aligned}
&-\int_{\Omega\setminus S}\boldsymbol{\sigma}:(\nabla\delta\mathbf{u})^S d\Omega+\int_{\Omega\setminus S}(\boldsymbol{\sigma}-\boldsymbol{\sigma}(\varepsilon)):\delta\boldsymbol{\varepsilon}d\Omega\\
&\qquad+\int_{\Omega\setminus S}\mathbf{f}\cdot\delta\mathbf{u}d\Omega+\int_{\Gamma_t}\bar{\mathbf{T}}\cdot\delta\mathbf{u}d\Gamma+\int_S\mathbf{T}_S\cdot(\delta\mathbf{u}^+-\delta\mathbf{u}^-)d\Gamma=0
\end{aligned}
\tag{6.20}
$$

Using the divergence theorem in sub-domains Ω^- and Ω^+

$$
\begin{aligned}
\int_{\Omega^-}\boldsymbol{\sigma}:(\nabla\delta\mathbf{u})d\Omega=&-\int_{\Omega^-}(\nabla\cdot\boldsymbol{\sigma})\cdot\delta\mathbf{u}\\
&+\int_{\Gamma_t^-}(\boldsymbol{\sigma}\cdot\boldsymbol{\nu})\cdot\delta\mathbf{u}d\Gamma+\int_S(\boldsymbol{\sigma}^-\cdot\mathbf{n}^-)\cdot\delta\mathbf{u}^-d\Gamma
\end{aligned}
\tag{6.21}
$$

$$
\begin{aligned}
\int_{\Omega^+}\boldsymbol{\sigma}:(\nabla\delta\mathbf{u})d\Omega=&-\int_{\Omega^+}(\nabla\cdot\boldsymbol{\sigma})\cdot\delta\mathbf{u}\\
&+\int_{\Gamma_t^+}(\boldsymbol{\sigma}\cdot\boldsymbol{\nu})\cdot\delta\mathbf{u}d\Gamma+\int_S(\boldsymbol{\sigma}^+\cdot\mathbf{n}^+)\cdot\delta\mathbf{u}^+d\Gamma
\end{aligned}
\tag{6.22}
$$

where $\Gamma_t^+=\Gamma_t\cap\Omega^+$ and $\Gamma_t^-=\Gamma_t\cap\Omega^-$, the following expression is finally produced:

$$\int_{\Omega^-}(\nabla\cdot\boldsymbol{\sigma}+\mathbf{f})\cdot\delta\mathbf{u}d\Omega+\int_{\Omega^+}(\nabla\cdot\boldsymbol{\sigma}+\mathbf{f})\cdot\delta\mathbf{u}d\Omega+\int_{\Omega^-}(\epsilon-(\nabla\mathbf{u})^S):\delta\boldsymbol{\sigma}d\Omega$$
$$+\int_{\Omega^+}(\epsilon-(\nabla\mathbf{u})^S):\delta\boldsymbol{\sigma}d\Omega+\int_{\Gamma_l^-}(\bar{\mathbf{T}}-\boldsymbol{\nu}\cdot\boldsymbol{\sigma})\cdot\delta\mathbf{u}d\Gamma+\int_{\Gamma_l^+}(\bar{\mathbf{T}}-\boldsymbol{\nu}\cdot\boldsymbol{\sigma})\cdot\delta\mathbf{u}d\Gamma$$
$$+\int_{\Omega^-}(\boldsymbol{\sigma}-\boldsymbol{\sigma}(\varepsilon)):\delta\epsilon d\Omega+\int_{\Omega^+}(\boldsymbol{\sigma}-\boldsymbol{\sigma}(\varepsilon)):\delta\epsilon d\Omega$$
$$+\int_S(\mathbf{T}^+-\boldsymbol{\sigma}^+\cdot\mathbf{n}^+)\cdot\delta\mathbf{u}^+d\Gamma+\int_S(\mathbf{T}^--\boldsymbol{\sigma}^-\cdot\mathbf{n}^-)\cdot\delta\mathbf{u}^-d\Gamma=0 \quad (6.23)$$

This implies that using the virtual work in this form, (6.5) to (6.9) and (6.11) are satisfied in weak form. In order to demonstrate that equation (6.10) is satisfied in weak form, first it is necessary to use $\delta[\![\mathbf{u}]\!]=0$ and then $\delta\mathbf{u}_r=0$ in equation (6.16) producing the two following variational statements:

$$-\int_{\Omega\setminus S}\boldsymbol{\sigma}(\varepsilon):(\nabla\delta\mathbf{u}_r)^S d\Omega+\int_{\Omega\setminus S}\mathbf{f}\cdot\delta\mathbf{u}_r d\Omega+\int_{\Gamma_l}\bar{\mathbf{T}}\cdot\delta\mathbf{u}_r d\Gamma=0 \quad (6.24)$$

$$-\int_{\Omega\setminus S}\boldsymbol{\sigma}(\varepsilon):\mathrm{H}_S(\nabla\delta[\![\mathbf{u}]\!])^S d\Omega+\int_{\Omega\setminus S}\mathbf{f}\cdot\mathrm{H}_S\delta[\![\mathbf{u}]\!]d\Omega$$
$$+\int_{\Gamma_l}\bar{\mathbf{T}}\cdot\mathrm{H}_S\delta[\![\mathbf{u}]\!]d\Gamma+\int_S\mathbf{T}_S\cdot\delta[\![\mathbf{u}]\!]d\Gamma=0 \quad (6.25)$$

Applying the divergence theorem to the sub-domain Ω^+ the following is obtained:

$$\int_{\Omega^+}\boldsymbol{\sigma}:(\nabla\delta[\![\mathbf{u}]\!])^S d\Omega=\int_{\Gamma_l^+}\bar{\mathbf{T}}\cdot\delta[\![\mathbf{u}]\!]d\Gamma+\int_S(\mathbf{n}^+\cdot\boldsymbol{\sigma}^+)\cdot\delta[\![\mathbf{u}]\!]-\int_{\Omega^+}(\nabla\cdot\boldsymbol{\sigma})\cdot\delta[\![\mathbf{u}]\!]d\Omega \quad (6.26)$$

Replacing (6.26) in (6.25) produces:

$$\int_S(\mathbf{T}_S-\mathbf{n}\cdot\boldsymbol{\sigma})\cdot\delta[\![\mathbf{u}]\!]d\Gamma=0 \quad (6.27)$$

satisfying (6.10) in weak form.

6.4 Finite element approximation

Here a procedure similar to the one used by Alfaiate et al. (2003) is considered. First, considering a finite element crossed by a discontinuity where the jump occurs along the surface S in the form:

$$[\![\mathbf{u}]\!]=[\![\mathbf{u}(x_s(\mathbf{x}))]\!] \quad (6.28)$$

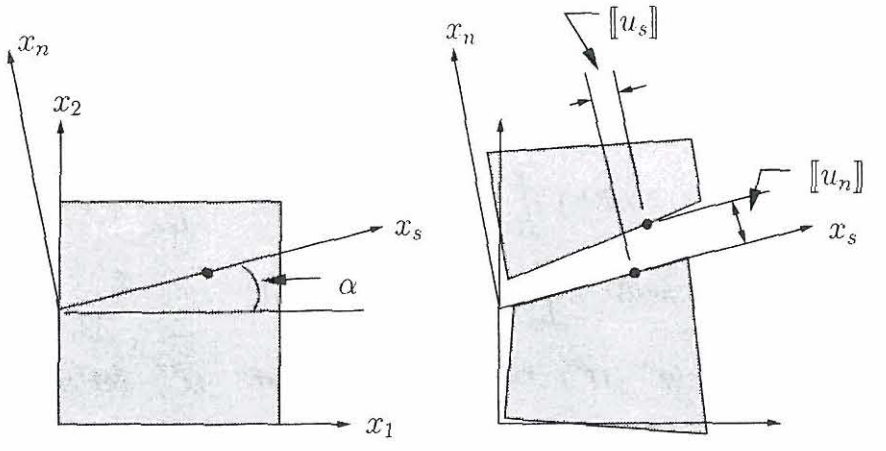

Figure 6.3: Displacement jump in a rectangular element crossed by a discontinuity. The values of the jump for a point in x_s are illustrated

where $x_s(\mathbf{x})$ is the coordinate along S as shown in figure 6.3. It is assumed that the jump is a linear function of x_s given by:

$$[\![\mathbf{u}]\!] = (a_1 + a_2 x_s)\mathbf{n} + (a_3 + a_4 x_s)\mathbf{s} \tag{6.29}$$

where a_1, a_2, a_3 and a_4 are constants and $\mathbf{n}$ and $\mathbf{s}$ are unit vectors along directions n and s, respectively. In this case with the linear function, two additional nodes are required to represent the displacement jump. In general the following approximation of the displacement field is adopted:

$$\mathbf{u}_r = \mathbf{N}\mathbf{v}_r \qquad \text{in } \Omega \setminus S \tag{6.30}$$

$$[\![\mathbf{u}]\!] = \mathbf{N}_b\mathbf{b} \qquad \text{in } S \tag{6.31}$$

where $\mathbf{N}$ is the usual matrix of shape functions, $\mathbf{v}_r$ is the vector of nodal degrees of freedom associated with $\mathbf{u}_r$, $\mathbf{N}_b$ are the shape functions used to approximate the jump and $\mathbf{b}$ are the degrees of freedom associated with $[\![\mathbf{u}]\!]$.

Assuming that the total displacement field $\mathbf{u}$ is approximated by:

$$\mathbf{u} = \mathbf{N}\mathbf{v} \tag{6.32}$$

where $\mathbf{v}$ is the vector of the nodal degrees of freedom associated with the total displacement $\mathbf{u}$. Due to the fact that the displacement field is continuous, the contribution of the jump across discontinuity into $\mathbf{u}$ must also be continuous. This is done by projecting the jump to the original nodes of the element such that:

$$\mathrm{H}_S[\![\mathbf{u}]\!] = \mathbf{N}\mathbf{H}\tilde{\mathbf{v}} \tag{6.33}$$

where $\mathbf{H} = \mathrm{H}_S\mathbf{I}$, $\mathbf{I}$ is the unit matrix and $\tilde{\mathbf{v}}$ are the enhanced degrees of freedom corresponding to the value of the jump in the nodes. The values of $\tilde{\mathbf{v}}$ are given by:

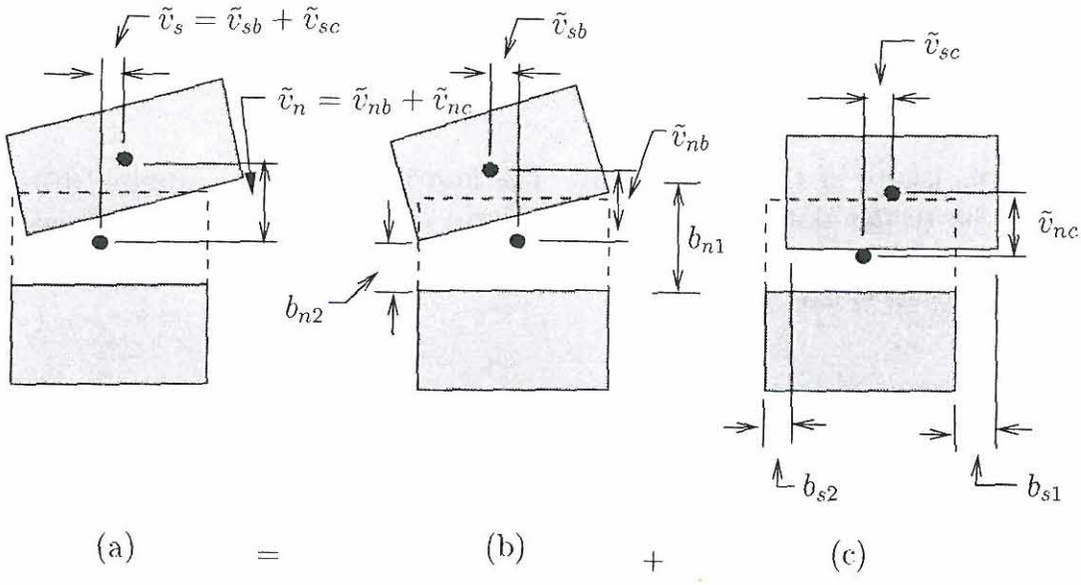

Figure 6.4: The contribution of the jump at a point is illustrated in (a). It is the result of two displacements and a rotation. In (b) the contribution of the normal displacement and rotation is illustrated. In (c) is shown the contribution of the tangential displacement jump.

$$\tilde{\mathbf{v}} = \mathbf{M}\mathbf{b} \tag{6.34}$$

where $\mathbf{M}$ is a matrix of shape functions defined by:

$$\mathbf{M} = \begin{bmatrix} \mathbf{N}_b^{(1)} \\ \mathbf{N}_b^{(2)} \\ \vdots \\ \mathbf{N}_b^{(n_e)} \end{bmatrix} \tag{6.35}$$

and $\mathbf{N}_b^{(i)}$ are the shape functions obtained at $\mathbf{x}_i$, where $\mathbf{x}_i$ are the coordinates of node i, and n_e is the number of nodes in the element.

In figure 6.4 it is illustrated that $\tilde{\mathbf{v}}$ can be obtained for a linear discontinuity as the sum of two effects, the first one produced by the normal components of the jump and the second produced by the tangential components of the jump. In this case for the node (k):

$$\begin{bmatrix} \tilde{v}_s^{(k)} \\ \tilde{v}_n^{(k)} \end{bmatrix} = \begin{bmatrix} b_{s2} - \theta x_n + \Delta x_s \\ b_{n2} + \theta x_s \end{bmatrix} \tag{6.36}$$

where

$$\theta = \frac{b_{n1} - b_{n2}}{l_{12}} \qquad \text{and } \Delta = \frac{b_{s1} - b_{s2}}{l_{12}} \tag{6.37}$$

and l_{12} is the length of the discontinuity. The matrix $\mathbf{M}$ can be computed transforming (6.36) to the global system of coordinates and expressing the equations in terms of $\mathbf{b}$.

The displacement field is written as:

$$\mathbf{u} = \mathbf{N}(\mathbf{v}_r + \mathbf{H}\tilde{\mathbf{v}}) = \mathbf{N}(\mathbf{v}_r + \mathbf{HMb}) \qquad \text{in } \Omega \tag{6.38}$$

$$[\![\mathbf{u}]\!] = \mathbf{N}_b\mathbf{b} \qquad \text{in } S \tag{6.39}$$

The strain field $\boldsymbol{\varepsilon}_r$ is approximated by:

$$\boldsymbol{\varepsilon}_r = \mathbf{LNv}_r = \mathbf{B}(\mathbf{v} - \mathbf{HMb}) \tag{6.40}$$

where $\mathbf{L}$ is the usual differential operator. Finally from (6.38), (6.40), (6.4), (6.33) and (6.34) it is possible to write:

$$\mathbf{u}_r = \mathbf{Nv} - \bar{\mathbf{N}}\mathbf{b} \qquad (\nabla\mathbf{u}_r)^S = \mathbf{Bv} - \bar{\mathbf{B}}\mathbf{b} \tag{6.41}$$

$$\mathrm{H}_S[\![\mathbf{u}]\!] = \mathbf{N}_b\mathbf{b} \qquad \mathrm{H}_S(\nabla[\![\mathbf{u}]\!])^S = \mathbf{B}_b\mathbf{b} \tag{6.42}$$

where

$$\bar{\mathbf{N}} = \mathbf{NHM}, \qquad \bar{\mathbf{B}} = \mathbf{BHM} \qquad \text{and } \mathbf{B}_b = \mathbf{LN}_b \tag{6.43}$$

6.5 Vector of internal and external forces

In order to develop a finite element with strong discontinuities, the tensors in (6.24) and (6.25) will be replaced by vectors and matrices as used in engineering. The following vectors are defined for a two-dimensional problem in the global coordinate system:

$$\mathbf{u} = \begin{bmatrix} u_1 \\ u_2 \end{bmatrix} \qquad \mathbf{T} = \begin{bmatrix} T_1 \\ T_2 \end{bmatrix} \qquad \bar{\mathbf{T}} = \begin{bmatrix} \bar{T}_1 \\ \bar{T}_2 \end{bmatrix} \qquad \mathbf{f} = \begin{bmatrix} f_1 \\ f_2 \end{bmatrix} \tag{6.44}$$

And in a local coordinate system:

$$\mathbf{u}_l = \begin{bmatrix} u_s \\ u_n \end{bmatrix} \qquad \mathbf{T} = \begin{bmatrix} T_s \\ T_n \end{bmatrix} \tag{6.45}$$

The stress and strain tensors $\boldsymbol{\sigma}$ and $\boldsymbol{\varepsilon}$, respectively, are replaced by the stress and strain vectors defined as:

$$\boldsymbol{\sigma} = \begin{bmatrix} \sigma_{11} \\ \sigma_{22} \\ \sigma_{12} \end{bmatrix} \qquad \boldsymbol{\varepsilon} = \begin{bmatrix} \varepsilon_{11} \\ \varepsilon_{22} \\ 2\varepsilon_{12} \end{bmatrix} \tag{6.46}$$

The regular displacement and jump vectors are:

$$\mathbf{u}_r = \begin{bmatrix} u_{r1} \\ u_{r2} \end{bmatrix} \qquad [\![\mathbf{u}]\!] = \begin{bmatrix} [\![u_1]\!] \\ [\![u_2]\!] \end{bmatrix} \tag{6.47}$$

In the finite element analysis, the vectors defining the displacement will be expressed in terms of nodal degrees of freedom $\mathbf{v}$ and $\mathbf{b}$ using the interpolation functions in $\mathbf{N}$. Taking variations of (6.41) and (6.42) produces:

$$\delta\mathbf{u}_r = \mathbf{N}\delta\mathbf{v} - \bar{\mathbf{N}}\delta\mathbf{b} \qquad (\nabla\delta\mathbf{u}_r)^S = \mathbf{B}\delta\mathbf{v} - \bar{\mathbf{B}}\delta\mathbf{b} \tag{6.48}$$

$$\mathrm{H}_S\delta[\![\mathbf{u}]\!] = \mathbf{N}_b\delta\mathbf{b} \qquad \mathrm{H}_S(\nabla\delta[\![\mathbf{u}]\!])^S = \mathbf{B}_b\delta\mathbf{b} \tag{6.49}$$

Introducing (6.48) and (6.49) into (6.24) and (6.25) produces

$$\delta\mathbf{v}^T\left[-\int_\Omega \mathbf{B}^T\boldsymbol{\sigma}d\Omega + \int_\Omega \mathbf{N}^T\mathbf{f}d\Omega + \int_{\Gamma_t} \mathbf{N}^T\bar{\mathbf{T}}d\Gamma\right] + \delta\mathbf{b}^T\left[\int_\Omega \bar{\mathbf{B}}^T\boldsymbol{\sigma}d\Omega - \int_\Omega \bar{\mathbf{N}}^T\mathbf{f}d\Omega + \int_{\Gamma_t} \bar{\mathbf{N}}^T\bar{\mathbf{T}}d\Gamma\right] = 0 \tag{6.50}$$

and

$$\delta\mathbf{b}^T\left[-\int_\Omega \mathbf{B}_b^T\boldsymbol{\sigma}d\Omega + \int_\Omega \mathbf{N}_b^T\mathbf{f}d\Omega + \int_{\Gamma_t} \mathbf{N}_b^T\bar{\mathbf{T}}d\Gamma + \int_S \mathbf{N}_b^T\mathbf{T}_S d\Gamma\right] = 0 \tag{6.51}$$

respectively, where $(\cdot)^T$ means the transpose of $(\cdot)$. The final results are the equilibrium equations in the form:

$$\begin{bmatrix} \mathbf{F}_v^{int} \\ \mathbf{F}_b^{int} \end{bmatrix} = \begin{bmatrix} \mathbf{F}_v^{ext} \\ \mathbf{F}_b^{ext} \end{bmatrix} \tag{6.52}$$

where the internal and external forces are:

$$\mathbf{F}_v^{int} = \int_\Omega \mathbf{B}^T\boldsymbol{\sigma}d\Omega \qquad \mathbf{F}_v^{ext} = \int_{\Gamma_t} \mathbf{N}^T\bar{\mathbf{T}}d\Gamma + \int_\Omega \mathbf{N}^T\mathbf{f}d\Omega \tag{6.53}$$

$$\mathbf{F}_b^{int} = \int_\Omega \bar{\mathbf{B}}^T\boldsymbol{\sigma}d\Omega - \int_S \mathbf{N}_b^T\mathbf{T}_s d\Gamma \qquad \mathbf{F}_b^{ext} = \mathbf{0} \tag{6.54}$$

6.6 Constitutive relations

6.6.1 Simple cohesive model

The relation between stresses and strains in rate form is (except in the discontinuity where the strains are unbounded) :

$$\dot{\boldsymbol{\sigma}} = \mathbf{D}\dot{\boldsymbol{\varepsilon}} = \mathbf{DB}\dot{\mathbf{v}} \tag{6.55}$$

where an overdot ( ) signifies rates, and $\mathbf{D}$ is the tangent stiffness matrix of the bulk material (here rate-independent material behavior is assumed). In case of an elastic isotropic material and in plane stress:

$$\mathbf{D} = \frac{E}{1-\nu^2}\begin{bmatrix} 1 & \nu & 0 \\ \nu & 1 & 0 \\ 0 & 0 & \frac{1}{2}(1-\nu) \end{bmatrix} \tag{6.56}$$

where E is the elastic modulus and ν is Poisson's ratio.

In the discontinuity the tractions are:

$$\mathbf{T}_l = \mathbf{T}_{tl}[\![\mathbf{u}_l]\!] \tag{6.57}$$

where $\mathbf{T}_l$ is the traction vector in the local coordinate system, $[\![\mathbf{u}_l]\!]$ is the jump transformed to the local coordinate system and $\mathbf{T}_{tl}$ is the stiffness of the traction-separation law at the discontinuity, transformed to the element local system.

For elements with strong discontinuities based on the partition of unity method (Remmers et al. 2003) have used the cohesive model expressed by the exponential form:

$$T_n = \sigma_u \exp\left(-\frac{\sigma_u}{G_f}\kappa\right) \tag{6.58}$$

where σ_u is the peak stress, G_f is the fracture energy and κ is the maximum value of $[\![u_n]\!]$ in the considered location. In that case:

$$\dot{T}_n = -\frac{\sigma_u^2}{G_f}\exp\left(-\frac{\sigma_u}{G_f}\kappa\right)[\![\dot{u}_n]\!] \tag{6.59}$$

and considering a constant value of T_s

$$\dot{\mathbf{T}}_l = \begin{bmatrix} 0 & 0 \\ 0 & -\frac{\sigma_u^2}{G_f}\exp\left(-\frac{\sigma_u}{G_f}\kappa\right) \end{bmatrix}\begin{bmatrix} [\![\dot{u}_s]\!] \\ [\![\dot{u}_n]\!] \end{bmatrix} \tag{6.60}$$

Transforming (6.60) to the global coordinate system:

$$\dot{\mathbf{T}} = \mathbf{T}_{cz}[\![\dot{\mathbf{u}}]\!] \tag{6.61}$$

where

$$\mathbf{T}_{cz} = \mathbf{R}_2 \begin{bmatrix} 0 & 0 \\ 0 & -\frac{\sigma_u^2}{G_f} \exp\left(-\frac{\sigma_u}{G_f}\kappa\right) \end{bmatrix} \mathbf{R}_2^T \tag{6.62}$$

and

$$\mathbf{R}_2 = \begin{bmatrix} n_2 & n_1 \\ -n_1 & n_2 \end{bmatrix} \tag{6.63}$$

where n_1 and n_2 are the components of the vector $\mathbf{n}$. Finally, it is possible to write:

$$\dot{\mathbf{T}} = \mathbf{T}_{cz}\mathbf{N}_b\dot{\mathbf{b}} \tag{6.64}$$

6.6.2 The Xu-Needleman cohesive model

This constitutive model is defined in (Xu & Needleman 1993), here the tractions are described as functions of the displacement jump across the interface. The condition that work cannot be extracted from the interface, in a closed cycle for an elastic interface, leads to the existence of a potential ϕ, for which

$$\mathbf{T} = \frac{\partial \phi}{\partial [\![\mathbf{u}]\!]} \tag{6.65}$$

The potential used allows for a shear failure mode in the interface region. The dependence on the displacements is given in terms of the normal ($[\![u_n]\!] = \mathbf{n} \cdot [\![\mathbf{u}]\!]$) and tangential ($[\![u_s]\!] = \mathbf{s} \cdot [\![\mathbf{u}]\!]$) displacement jumps, where $\mathbf{n}$ and $\mathbf{s}$ are unit vectors pointing in the normal and tangential directions to the discontinuity, respectively. In particular ϕ, has the form

$$\phi([\![\mathbf{u}]\!]) = \phi_n + \phi_n \exp\left(-\frac{[\![u_n]\!]}{\delta_n}\right)\left\{\left(1 - r + \frac{[\![u_n]\!]}{\delta_n}\right)\frac{1-q}{r-1} - \left(q + \frac{r-q}{r-1}\frac{[\![u_n]\!]}{\delta_n}\right)\exp\left(-\frac{[\![u_s]\!]^2}{\delta_s^2}\right)\right\} \tag{6.66}$$

with

$$q = \frac{\phi_s}{\phi_n} \qquad \text{and} \qquad r = \frac{[\![u_n]\!]^*}{\delta_n} \tag{6.67}$$

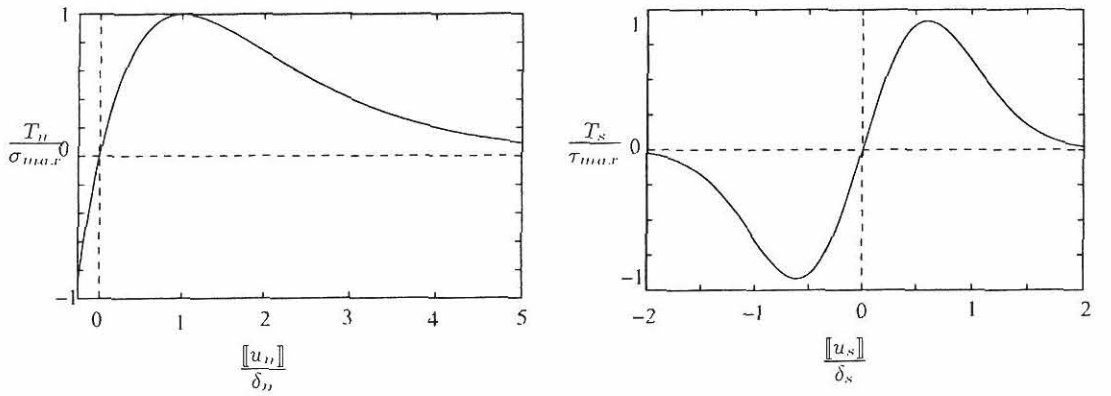

Figure 6.5: The tractions when (a) $[\![u_s]\!] = 0$ or (b) $[\![u_n]\!] = 0$

where ϕ_n is the work of normal separation, ϕ_s is the work of tangential separation, and $[\![u_n]\!]^*$ is the value of $[\![u_n]\!]$ after complete shear separation under the condition of zero normal tension, $T_n = 0$.

According to (6.65), the interface tractions are obtained by differentiation of (6.66):

$$T_n = \frac{\phi_n}{\delta_n}\exp\left(-\frac{[\![u_n]\!]}{\delta_n}\right)\left\{\frac{[\![u_n]\!]}{\delta_n}\exp\left(-\frac{[\![u_s]\!]^2}{\delta_s^2}\right) + \frac{1-q}{r-1}\left[1-\exp\left(-\frac{[\![u_s]\!]^2}{\delta_s^2}\right)\right]\left(r-\frac{[\![u_n]\!]}{\delta_n}\right)\right\} \tag{6.68}$$

$$T_s = \frac{\phi_n}{\delta_n}\left(2\frac{\delta_n}{\delta_s}\right)\frac{[\![u_s]\!]}{\delta_s}\left\{q+\frac{r-q}{r-1}\frac{[\![u_n]\!]}{\delta_n}\right\}\exp\left(-\frac{[\![u_n]\!]}{\delta_n}\right)\exp\left(-\frac{[\![u_s]\!]^2}{\delta_s^2}\right) \tag{6.69}$$

The maximum value of $|T_s| = \tau_u$ occurs when $|[\![u_s]\!]| = \sqrt{2}\delta_s/2$. The normal and shear work of separation are related to σ_u and τ_u, respectively, by

$$\phi_n = \sigma_u e \delta_n \qquad \phi_s = \sqrt{\frac{e}{2}}\tau_u \delta_s \tag{6.70}$$

where $e = \exp(1)$. For the case $\phi_n = \phi_s$, the tractions are shown in figure 6.5 when only $[\![u_n]\!]$ or $[\![u_s]\!]$ is different from zero.

If it is assumed that $\phi_n = \phi_s$ then $q = 1$. The equations are reduced to:

$$\phi([\![\mathbf{u}]\!]) = \phi_n - \phi_n\exp\left(-\frac{[\![u_n]\!]}{\delta_n}\right)\left(1+\frac{[\![u_n]\!]}{\delta_n}\right)\exp\left(-\frac{[\![u_s]\!]^2}{\delta_s^2}\right) \tag{6.71}$$

$$T_n = \frac{\phi_n}{\delta_n}\frac{[\![u_n]\!]}{\delta_n}\exp\left(-\frac{[\![u_n]\!]}{\delta_n}\right)\exp\left(-\frac{[\![u_s]\!]^2}{\delta_s^2}\right) \tag{6.72}$$

$$T_t = \left(\frac{\phi_n}{\delta_n}\right)\left(\frac{[\![u_n]\!]}{\delta_n}+1\right)\left(2\frac{\delta_n}{\delta_s}\right)\frac{[\![u_s]\!]}{\delta_s}\exp\left(-\frac{[\![u_n]\!]}{\delta_n}\right)\exp\left(-\frac{[\![u_s]\!]^2}{\delta_s^2}\right) \tag{6.73}$$

Finally observe that:

$$\dot{\mathbf{T}}_l = \begin{bmatrix} \dot{T}_s \\ \dot{T}_n \end{bmatrix} = \begin{bmatrix} \frac{\partial T_s}{\partial [\![u_s]\!]} & \frac{\partial T_s}{\partial [\![u_n]\!]} \\ \frac{\partial T_n}{\partial [\![u_s]\!]} & \frac{\partial T_n}{\partial [\![u_n]\!]} \end{bmatrix} \begin{bmatrix} [\![\dot{u}_s]\!] \\ [\![\dot{u}_n]\!] \end{bmatrix} \tag{6.74}$$

with the consequence of:

$$\mathbf{T}_{cz} = \mathbf{R}_2 \begin{bmatrix} \frac{\partial T_s}{\partial [\![u_s]\!]} & \frac{\partial T_s}{\partial [\![u_n]\!]} \\ \frac{\partial T_n}{\partial [\![u_s]\!]} & \frac{\partial T_n}{\partial [\![u_n]\!]} \end{bmatrix} \mathbf{R}_2^T \tag{6.75}$$

6.7 The tangent stiffness matrix

Replacing (6.48) and (6.49) into the rate form of (6.24) and (6.25) produce:

$$\begin{aligned} -\int_\Omega (\delta\mathbf{v}^T\mathbf{B}^T - \delta\mathbf{b}^T\bar{\mathbf{B}}^T)\mathbf{D}(\mathbf{B}\dot{\mathbf{v}} - \bar{\mathbf{B}}\dot{\mathbf{b}})d\Omega \\ + \int_\Omega (\delta\mathbf{v}^T\mathbf{N}^T - \delta\mathbf{b}^T\bar{\mathbf{N}}^T)\dot{\mathbf{f}}d\Omega + \int_{\Gamma_l} (\delta\mathbf{v}^T\mathbf{N}^T - \delta\mathbf{b}^T\bar{\mathbf{N}}^T)\dot{\bar{\mathbf{T}}}d\Gamma = 0 \end{aligned} \tag{6.76}$$

and

$$\begin{aligned} \delta\mathbf{b}^T \Bigg[-\int_\Omega \mathbf{B}_b^T\mathbf{D}(\mathbf{B}\dot{\mathbf{v}} - \bar{\mathbf{B}}\dot{\mathbf{b}})d\Omega \\ + \int_\Omega \mathbf{N}_b^T\dot{\mathbf{f}}d\Omega + \int_{\Gamma_l} \mathbf{N}_b^T\dot{\bar{\mathbf{T}}}d\Gamma + \int_S \mathbf{N}_b^T\mathbf{T}_{cz}\mathbf{N}_b\dot{\mathbf{b}}d\Gamma \Bigg] = 0 \end{aligned} \tag{6.77}$$

The following equation is finally obtained:

$$\begin{bmatrix} \mathbf{K}_{vv} & \mathbf{K}_{vb} \\ \mathbf{K}_{bv} & \mathbf{K}_{bb} \end{bmatrix} \begin{bmatrix} \dot{\mathbf{v}} \\ \dot{\mathbf{b}} \end{bmatrix} = \begin{bmatrix} \dot{\mathbf{F}}_v \\ \dot{\mathbf{F}}_b \end{bmatrix} \tag{6.78}$$

where

$$\mathbf{K}_{vv} = \int_\Omega \mathbf{B}^T\mathbf{D}\mathbf{B}d\Omega \qquad \mathbf{K}_{vb} = \mathbf{K}_{bv}^T = -\int_\Omega \mathbf{B}^T\mathbf{D}\bar{\mathbf{B}}d\Omega \tag{6.79}$$

$$\mathbf{K}_{bb} = \int_\Omega \bar{\mathbf{B}}^T\mathbf{D}\bar{\mathbf{B}}d\Omega + \int_S \mathbf{N}_b^T\mathbf{T}_{cz}\mathbf{N}_b d\Gamma \tag{6.80}$$

$$\dot{\mathbf{F}}_v = \int_\Omega \mathbf{N}^T\dot{\mathbf{f}}d\Omega + \int_\Gamma \mathbf{N}^T\dot{\bar{\mathbf{T}}}d\Gamma \qquad \dot{\mathbf{F}}_b = \mathbf{0} \tag{6.81}$$

The tangent stiffness matrix is then:

$$\mathbf{K}_T = \begin{bmatrix} \mathbf{K}_{vv} & \mathbf{K}_{vb} \\ \mathbf{K}_{bv} & \mathbf{K}_{bb} \end{bmatrix} \tag{6.82}$$

When a cohesive model is considered and the force increment is expressed in terms of the external and internal forces, the final result is:

$$\begin{bmatrix} \mathbf{K}_{vv} & \mathbf{K}_{vb} \\ \mathbf{K}_{bv} & \mathbf{K}_{bb} \end{bmatrix} \begin{bmatrix} \dot{\mathbf{v}} \\ \dot{\mathbf{b}} \end{bmatrix} = \begin{bmatrix} \mathbf{F}_v^{ext} \\ \mathbf{F}_b^{ext} \end{bmatrix} - \begin{bmatrix} \mathbf{F}_v^{int} \\ \mathbf{F}_b^{int} \end{bmatrix} \tag{6.83}$$

6.8 The Xu-Needleman model modified

In order to introduce the discontinuity using the Xu-Needleman model, modification of this model is required in order to take into account initial values of tractions. This is done here by defining the total jump for the model $\boldsymbol{\Delta}$ as:

$$\boldsymbol{\Delta} = \begin{bmatrix} \Delta_s \\ \Delta_n \end{bmatrix} = \boldsymbol{\Delta}_0 + [\![\mathbf{u}]\!] = \begin{bmatrix} \Delta_{0s} \\ \Delta_{0n} \end{bmatrix} + \begin{bmatrix} [\![u_s]\!] \\ [\![u_n]\!] \end{bmatrix} \tag{6.84}$$

The potential is now

$$\phi([\![\mathbf{u}_n]\!]) = \phi_n - \phi_n \exp\left(-\frac{\Delta_n}{\delta_n}\right)\left(1 + \frac{\Delta_n}{\delta_n}\right)\exp\left(-\frac{\Delta_s^2}{\delta_s^2}\right) \tag{6.85}$$

and the tractions are:

$$T_n = \frac{\phi_n}{\delta_n}\frac{\Delta_n}{\delta_n}\exp\left(-\frac{\Delta_n}{\delta_n}\right)\exp\left(-\frac{\Delta_s^2}{\delta_s^2}\right) \tag{6.86}$$

$$T_s = \frac{\phi_n}{\delta_n}\left(\frac{\Delta_n}{\delta_n} + 1\right)\left(2\frac{\delta_n}{\delta_s}\right)\frac{\Delta_s}{\delta_s}\exp\left(-\frac{\Delta_n}{\delta_n}\right)\exp\left(-\frac{\Delta_s^2}{\delta_s^2}\right) \tag{6.87}$$

The process after the definition of the crack position consists in defining the initial values of$\boldsymbol{\Delta}_0$. In order to obtain these values: First, the tractions at a point in the crack are computed as:

$$\mathbf{T} = \mathbf{n} \cdot \boldsymbol{\sigma} \tag{6.88}$$

Second, the equations (6.86) and (6.87) are solved for the values of Δ_n and Δ_s, taking into account that the first time $[\![\mathbf{u}]\!] = \mathbf{0}$, then $\boldsymbol{\Delta} = \boldsymbol{\Delta}_0$.

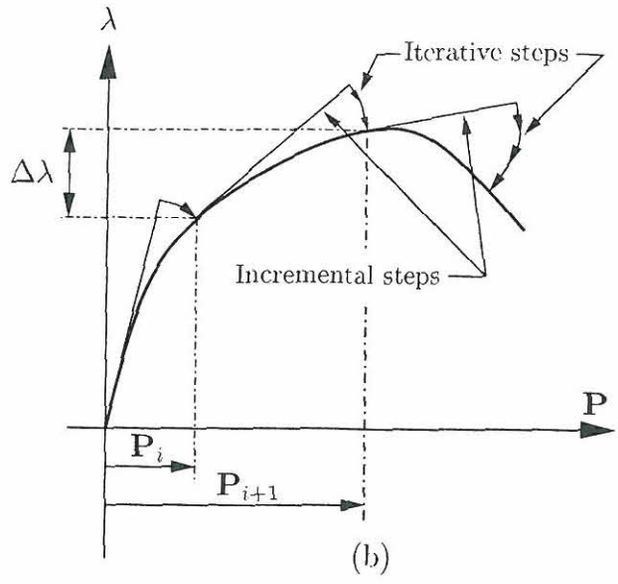

Figure 6.6: (a)Load level vs time, (b) solution sequence.

6.9 Numerical solution to the non-linear problem

The problem is solved using the arc-length control strategy (Crisfield 1981), (Crisfield 1991), including simple modifications of the standard algorithm, because of the inclusion of new degrees of freedom occurring in the cracking process.

The increment in load level is defined as $\Delta\lambda$ and the corresponding increment in nodal displacements is $\Delta\mathbf{P}$. The total of external nodal forces before cracking is represented by the vector $\mathbf{q}_0$ and proportional loading is supposed such that:

$$\mathbf{q} = \lambda \mathbf{q}_0 \qquad \text{and} \qquad \frac{\partial \mathbf{q}}{\partial \lambda} = \mathbf{q}_0 \tag{6.89}$$

where $\mathbf{q}$ is the external load corresponding to the load level λ.

The tangential displacement $\boldsymbol{\delta}_T$ is defined in the form that

$$\Delta\mathbf{P} = \Delta\lambda \boldsymbol{\delta}_T \tag{6.90}$$

and

$$\boldsymbol{\delta}_T = \begin{bmatrix} \boldsymbol{\delta}_{Tv} \\ \boldsymbol{\delta}_{Tb} \end{bmatrix} \tag{6.91}$$

where $\boldsymbol{\delta}_{Tv}$ is the vector of tangential displacements associated with the initial degrees of freedom $\mathbf{v}$ and $\boldsymbol{\delta}_{Tb}$ are the tangential displacements associated with the additional degrees of freedom $\mathbf{b}$.

Then it is required for equation 6.90 that

$$\mathbf{K}\boldsymbol{\delta}_T = \mathbf{f}^* \tag{6.92}$$

where $\mathbf{K}$ is the tangent stiffness matrix, and the load $\mathbf{f}^*$ is defined as:

$$\mathbf{f}^* = (\mathbf{f}^{ext} - \mathbf{f}^{int})/\Delta\lambda \tag{6.93}$$

The solution, disregarding the iterative part, proceeds in the following sequence for step i:

1. Compute $\mathbf{K}$ and $\mathbf{f}^*$ using the values of variables from step $i-1$.
2. Compute the values of tangential degrees of freedom resulting from equation (6.92).
3. Compute $\Delta\lambda$ by using

$$\Delta\lambda = \pm \frac{\Delta l}{\sqrt{\boldsymbol{\delta}_{Tv}^T \boldsymbol{\delta}_{Tv} + w^2 \mathbf{q}_0^T \mathbf{q}_0}} \tag{6.94}$$

   where the sign depends on the traced branch of the loading path, Δl is the radius of the spherical hyper-surface in the space $(\lambda, \mathbf{u})$, and w is a scalar factor which takes into account that λ and $\mathbf{u}$ have different scales.

4. Compute $\Delta\mathbf{P}$ using equation (6.90).
5. If desired, iterate to equilibrium.
6. Update the results using:

$$\mathbf{P}_i = \mathbf{P}_{i-1} + \Delta\mathbf{P} \tag{6.95}$$
$$\lambda_i = \lambda_{i-1} + \Delta\lambda \tag{6.96}$$
$$\boldsymbol{\sigma}_i = \boldsymbol{\sigma}_{i-1} + \Delta\boldsymbol{\sigma} \tag{6.97}$$

The procedure described is repeated until a maximum displacement or a maximum load level is reached.

The iterative process is done in the following sequence:

1. Compute the new stresses in elements using $\mathbf{P}_{i-1} = \mathbf{P}_{n-1} + \Delta\mathbf{P}_{i-1}$ where n is the corresponding step, and i the corresponding iteration.
2. Compute the new imbalance force $\mathbf{g}$ as:

$$\mathbf{g} = \mathbf{F}^{ext} - \mathbf{F}^{int} = (\lambda_{n-1} + \Delta\lambda_i)\mathbf{F}^{ext} - \mathbf{F}^{int} \tag{6.98}$$

   where $\mathbf{F}^{ext}$ is computed at the beginning of every step.

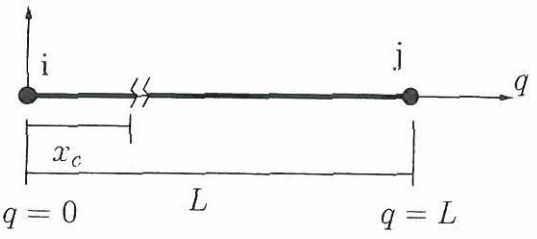

Figure 6.7: Two-node one-dimensional finite element with a crack in x_c.

3. Compute $\delta\mathbf{P}_i$ from $\mathbf{K}_{n-1}\delta\mathbf{P}_i = \mathbf{g}$

4. Compute $\delta\lambda_i$ from

$$a_1\delta\lambda_i^2 + a_2\delta\lambda_i + a_3 = 0 \tag{6.99}$$

where

$$a_1 = \boldsymbol{\delta}_{Tv}\boldsymbol{\delta}_{Tv} + \psi^2\mathbf{F}_v^{extT}\mathbf{F}_v^{ext} \tag{6.100}$$
$$a_2 = 2 * \boldsymbol{\delta}_{Tv}(\Delta\mathbf{P}_{0v} + \delta\mathbf{P}_{iv}) + 2\Delta\lambda_0\psi^2\mathbf{F}_v^{extT}\mathbf{F}_v^{ext} \tag{6.101}$$
$$a_3 = (\Delta\mathbf{P}_{0v} + \delta\mathbf{P}_{iv})^T(\Delta\mathbf{P}_{0v} + \delta\mathbf{P}_{iv}) - \Delta l^2 + \Delta\lambda_0\psi^2\mathbf{F}_v^{extT}\mathbf{F}_v^{ext} \tag{6.102}$$

and $\Delta\mathbf{P}_{0v}$ and $\delta\mathbf{P}_{iv}$ are parts of the increments in displacements associated with the degrees of freedom $\mathbf{v}$

5. The new updated quantities are:

$$\Delta\mathbf{P}_i = \Delta\mathbf{P}_0 + \delta\mathbf{P}_i + \delta\lambda_i\boldsymbol{\delta}_T \tag{6.103}$$
$$\Delta\lambda_i = \Delta\lambda_{i-1} + \delta\lambda_i \tag{6.104}$$

6. If converged, stop; otherwise next iteration.

6.10 One-dimensional implementation

6.10.1 Element matrices

For the element shown in figure 6.7, using the system of coordinates 'q' with origin in the node (i) and a crack at the distance x_c from (i), the following matrix of shape functions is defined:

$$\mathbf{N} = \frac{1}{L}\begin{bmatrix} L-q & q \end{bmatrix} \qquad \text{and} \qquad \mathbf{B} = \frac{d\mathbf{N}}{dq} = \frac{1}{L}\begin{bmatrix} -1 & 1 \end{bmatrix} \tag{6.105}$$

therefore

$$\mathbf{K}_{vv} = \frac{EA}{L}\begin{bmatrix} 1 & -1 \\ -1 & 1 \end{bmatrix} \tag{6.106}$$

For the non-cracked bar, the internal and external forces are:

$$\mathbf{F}_{v\sigma}^{int} = \int_0^L \frac{A}{L}\begin{bmatrix} -1 \\ 1 \end{bmatrix} \sigma dq = \begin{bmatrix} -1 \\ 1 \end{bmatrix} A\sigma \tag{6.107}$$

$$\mathbf{F}_{vf}^{ext} = \int_0^L \frac{A}{L}\begin{bmatrix} L-q \\ q \end{bmatrix} f dq = \frac{ALf}{2}\begin{bmatrix} 1 \\ 1 \end{bmatrix} \tag{6.108}$$

respectively. For this element, the jump is constant, meaning that:

$$\mathbf{N}_b = 1; \qquad \mathbf{M} = \begin{bmatrix} 1 \\ 1 \end{bmatrix} \qquad \text{and } \mathbf{H} = \mathrm{H}_s \begin{bmatrix} 1 & 0 \\ 0 & 1 \end{bmatrix} = \begin{bmatrix} 0 & 0 \\ 0 & 1 \end{bmatrix} \tag{6.109}$$

producing:

$$\bar{\mathbf{N}} = \frac{q}{L} \qquad \text{and} \qquad \bar{\mathbf{B}} = \frac{1}{L} \tag{6.110}$$

When the bar cracks:

$$\mathbf{K}_{vb} = \mathbf{K}_{bv}^T = -\int_0^L \frac{A}{L}\begin{bmatrix} -1 \\ 1 \end{bmatrix} E\frac{1}{L} dq = -\frac{AE}{L}\begin{bmatrix} -1 \\ 1 \end{bmatrix} \tag{6.111}$$

If the simple cohesive model is used:

$$\mathbf{K}_{bb} = \int_0^L A\frac{1}{L}E\frac{1}{L}dq + \int_A \mathbf{1}\left[-\frac{\sigma_u^2}{G_f}\exp\left(-\frac{\sigma_u \kappa}{G_f}\right)\right] dq = \frac{AE}{L} - \frac{A\sigma_u^2}{G_f}\exp\left(-\frac{\sigma_u}{G_f}\kappa\right) \tag{6.112}$$

and the internal forces include:

$$\mathbf{F}_v^{int} = \int_0^L \frac{A}{L}\begin{bmatrix} -1 \\ 1 \end{bmatrix} \sigma dq = A\sigma \begin{bmatrix} -1 \\ 1 \end{bmatrix} \tag{6.113}$$

$$\mathbf{F}_b^{int} = \int_0^L \frac{1}{L}\sigma dq - \int_A [1]\, T_S dA = A(\sigma - T_S) \tag{6.114}$$

Property	Value
E	1×10^8 Pa $= 100$ N/mm^2
ν	0.1
σ_u	1 N/mm^2
G_f	0.2 N mm/mm^2
A	1 mm^2
L	1 mm
P	2 N

Table 6.1: Properties used in the analysis for a single bar.

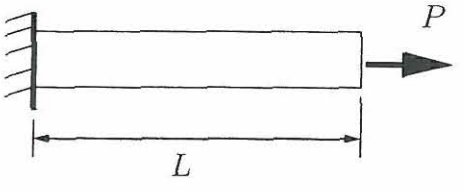

Figure 6.8: A single bar supporting a force P.

6.10.2 Examples

A single bar

A single bar which can crack is used as a first example. The model consists in only one one-dimensional finite element. The bar has the properties presented in table 6.1, and the bar is shown in figure 6.8. The simple exponential cohesive model will be used.

In the first step, the following values are obtained:

$$\mathbf{q}_0 = \mathbf{f}^* = [2] \tag{6.115}$$

$$\mathbf{K} = [100] \tag{6.116}$$

Therefore,

$$\boldsymbol{\delta}_T = \mathbf{K}^{-1}\mathbf{f}^* = [0.02] \tag{6.117}$$

Using $\Delta l = 0.1$ then a value of $\Delta\lambda = 0.05$ is computed from equation (6.94). The results for the first step are:

$$\Delta\mathbf{P} = \Delta\lambda\boldsymbol{\delta}_T = 0.001 \tag{6.118}$$

the stress in the bar is:

$$\Delta\boldsymbol{\sigma} = [100]\begin{bmatrix}-1 & 1\end{bmatrix}\begin{bmatrix}0\\0.001\end{bmatrix} = 0.1 \tag{6.119}$$

If the value of Δl is kept constant and after 10 steps the following values are obtained:

$$\mathbf{P}_{10} = \begin{bmatrix} 0.01 \end{bmatrix}, \qquad \lambda_{10} = 0.5, \qquad \sigma_{10} = 1.0 \tag{6.120}$$

At this point, the crack starts with a value of $T_S = 1\text{N}/\text{mm}^2$. At the beginning of step 11, it is supposed that $\Delta\lambda_{11} = \Delta\lambda_{10} = 0.05$. The global external forces are:

$$\mathbf{F}_v^{ext} = \mathbf{q}_0(\lambda + \Delta\lambda) = \begin{bmatrix} 1.1 \end{bmatrix} \qquad \text{and} \qquad \mathbf{F}_b^{ext} = \mathbf{0} \tag{6.121}$$

The internal forces in the element are:

$$\mathbf{F}_v^{int} = \begin{bmatrix} -1 \\ 1 \end{bmatrix} \qquad \text{and} \qquad \mathbf{F}_b^{int} = \begin{bmatrix} 1 & -1 \end{bmatrix} \tag{6.122}$$

then, the external and internal global forces are:

$$\mathbf{F}^{ext} = \begin{bmatrix} 1.1 \\ 0 \end{bmatrix} \qquad \mathbf{F}^{int} = \begin{bmatrix} 1 \\ 0 \end{bmatrix} \tag{6.123}$$

producing

$$\mathbf{f}^* = (\mathbf{F}^{ext} - \mathbf{F}^{int})/\Delta\lambda = \begin{bmatrix} 2 \\ 0 \end{bmatrix} \tag{6.124}$$

The stiffness matrix of the element and the global stiffness matrix are (with $T_{cz} = -5$):

$$\mathbf{K}_e = \begin{bmatrix} 100 & -100 & 100 \\ -100 & 100 & -100 \\ 100 & -100 & 95 \end{bmatrix} \qquad \mathbf{K} = \begin{bmatrix} 100 & -100 \\ -100 & 95 \end{bmatrix} \tag{6.125}$$

The tangential values of the degrees of freedom are:

$$\boldsymbol{\delta}_T = \begin{bmatrix} \delta_{Tv} \\ \delta_{Tb} \end{bmatrix} = \begin{bmatrix} -0.38 \\ -0.4 \end{bmatrix} \tag{6.126}$$

The new value of $\Delta\lambda = -0.04912$. The displacements for this step are:

$$\Delta\mathbf{P} = \Delta\lambda\boldsymbol{\delta}_T = \begin{bmatrix} 0.01867 \\ 0.01965 \end{bmatrix}, \qquad \mathbf{P}_{11} = \begin{bmatrix} 1.01867 \\ 0.01965 \end{bmatrix} \tag{6.127}$$

With a jump value of $[\![u]\!] = 0.01965$ the value of T using equation (6.58) is $T = 0.9064\text{N}/\text{mm}^2$ The stress is:

$$\sigma_{11} = \sigma_{10} + \Delta\sigma = 1 + 100 \begin{bmatrix} -1 & 1 \end{bmatrix} \left(\begin{bmatrix} 0 \\ 0.01867 \end{bmatrix} - \begin{bmatrix} 0 \\ 1 \end{bmatrix} \begin{bmatrix} 0.01965 \end{bmatrix} \right) = 0.902\text{N}/\text{mm}^2 \tag{6.128}$$

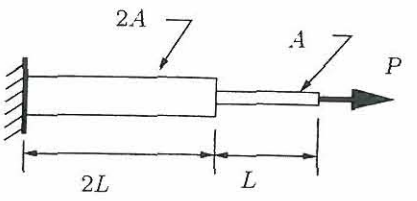

Figure 6.9: System of two bars

Two bars in series

Two bars in series are considered as shown in figure 6.9. The properties are the same as in the previous example, listed in table 6.1. This time is considered that a crack will occur at the midpoint of the bar.

The first time the tangent stiffness of the elements are:

$$\mathbf{K}_1 = \mathbf{K}_2 = \begin{bmatrix} 100 & -100 \\ -100 & 100 \end{bmatrix} \tag{6.129}$$

The global stiffness and the load vector are:

$$\mathbf{K} = \begin{bmatrix} 200 & -100 \\ -100 & 100 \end{bmatrix}, \qquad \mathbf{q}_0 = \begin{bmatrix} 0 \\ 2 \end{bmatrix} \tag{6.130}$$

with a value of $\Delta l = 0.1$, then $\Delta\lambda = 0.05$. The tangential displacement and the incremental displacement are:

$$\boldsymbol{\delta}_T = \mathbf{K}^{-1}\mathbf{q}_0 = \begin{bmatrix} 0.02 \\ 0.04 \end{bmatrix}, \qquad \text{and} \qquad \Delta\mathbf{P} = \Delta\lambda\boldsymbol{\delta}_T = \begin{bmatrix} 0.001 \\ 0.002 \end{bmatrix} \tag{6.131}$$

The stresses are computed as:

$$\sigma_{x1} = \tfrac{100}{2}\begin{bmatrix} -1 & 1 \end{bmatrix}\begin{bmatrix} 0 \\ 0.001 \end{bmatrix} = 0.05\text{MPa} \tag{6.132}$$

$$\sigma_{x2} = 100\begin{bmatrix} -1 & 1 \end{bmatrix}\begin{bmatrix} 0.001 \\ 0.002 \end{bmatrix} = 0.1\text{MPa} \tag{6.133}$$

After ten steps with $\Delta l = 0.1$ constant, it is found that:

$$\lambda = 0.5, \qquad \mathbf{P} = \begin{bmatrix} 0.01 \\ 0.02 \end{bmatrix}, \qquad \sigma_{x1} = 0.5\text{MPa}, \qquad \text{and} \qquad \sigma_{x2} = 1\text{Mpa} \tag{6.134}$$

The last result indicates that a crack appears first in the second element in this step. For step number 11:

$$\mathbf{F}^{ext} = (\lambda + \Delta\lambda) \begin{bmatrix} 0 \\ 2 \\ 0 \end{bmatrix} = \begin{bmatrix} 0 \\ 1.1 \\ 0 \end{bmatrix} \tag{6.135}$$

where $\lambda = 0.5$ and $\Delta\lambda = 0.05$. The internal forces for every one of the elements are:

$$\mathbf{F}_1^{int} = \begin{bmatrix} -1 \\ 1 \end{bmatrix} \qquad \text{and} \qquad \mathbf{F}_2^{int} = \begin{bmatrix} -1 \\ 1 \\ 1 - 1 \end{bmatrix} \tag{6.136}$$

The vector of internal forces, the imbalance vector, and the load vector are:

$$\mathbf{F}^{int} = \begin{bmatrix} 0 \\ 1 \\ 0 \end{bmatrix}, \qquad \mathbf{g} = \mathbf{F}^{ext} - \mathbf{F}^{int} = \begin{bmatrix} 0 \\ 0.1 \\ 0 \end{bmatrix} \qquad \text{and} \qquad \mathbf{f}^* = \begin{bmatrix} 0 \\ 2 \\ 0 \end{bmatrix} \tag{6.137}$$

The stiffness matrix for the second element is:

$$\mathbf{K}_2 = \begin{bmatrix} 100 & -100 & 100 \\ -100 & 100 & -100 \\ 100 & -100 & 95 \end{bmatrix} \tag{6.138}$$

The global tangent stiffness is then:

$$\mathbf{K} = \begin{bmatrix} 200 & -100 & 100 \\ -100 & 100 & -100 \\ 100 & -100 & 95 \end{bmatrix} \tag{6.139}$$

The tangential displacements are:

$$\boldsymbol{\delta}_T = \mathbf{K}^{-1}\mathbf{f}^* = \begin{bmatrix} 0.02 \\ -0.36 \\ -0.4 \end{bmatrix} \tag{6.140}$$

the value of $\Delta\lambda = -0.0492$. The displacements are then

$$\Delta\mathbf{P} = \begin{bmatrix} -0.000984 \\ 0.01771 \\ 0.001968 \end{bmatrix}, \qquad \text{and} \qquad \mathbf{P} = \begin{bmatrix} 0.009016 \\ 0.03771 \\ 0.01968 \end{bmatrix} \tag{6.141}$$

The stresses are:

$$\Delta\sigma_{x1} = \tfrac{100}{2} \begin{bmatrix} -1 & 1 \end{bmatrix} \begin{bmatrix} 0 \\ -0.000984 \end{bmatrix} = -0.0492\text{MPa} \tag{6.142}$$

$$\Delta\sigma_{x2} = 100 \begin{bmatrix} -1 & 1 \end{bmatrix} \left(\begin{bmatrix} -0.000984 \\ 0.01771 \end{bmatrix} - \begin{bmatrix} 0 \\ 1 \end{bmatrix} \begin{bmatrix} 0.01968 \end{bmatrix} \right) = -0.0986\text{MPa} \tag{6.143}$$

The final stress in the second element is finally $\sigma_{x2} = 1 - 0.0986 = 0.9014$Mpa. A drift error occurs (the traction computed for this element is $T = 0.9063$MPa).

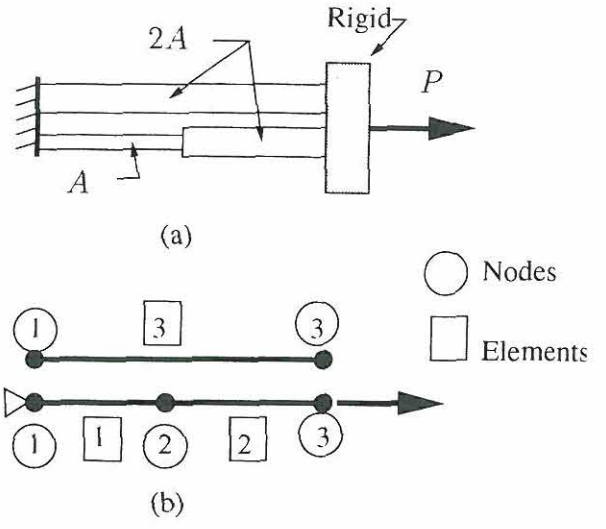

Figure 6.10: (a) The three-bar system. (b) Finite element model.

Three bars

The system shown in figure 6.10(a) is analyzed using the same kind of elements as in the first example. The properties are the same as in the previous example indicated in table 6.1. The mesh of elements is shown in figure 6.10(b).

The results for this example were here obtained including iterations, and a much better agreement is found between the stresses and the tractions for a smaller number of steps. In figure 6.11(a) the stresses are shown for every bar. And in figure 6.11(b) the force-displacements diagram is shown for the node number three. After the cracking of the first bar, a change in stiffness occurs, which is shown as a change in the slope of the curve force displacement. The change in slope in displacements is accompanied by unloading of the cracked bar and, of course, by unloading of the second one, as is to be seen in the stress diagram 6.11(a). Finally, after cracking of the third bar, the unloading of the system occurs.

6.11 Two-dimensional implementation

6.11.1 Computation of matrices

The embedded crack element is implemented over a quadrilateral isoparametric element with four nodes based on displacements. The matrices $\mathbf{N}$ and $\mathbf{B}$ are the standard matrices for this element. A global system of coordinates $(x_1 - x_2)$ and a natural system of coordinates $(\xi - \eta)$ are considered. As usual, the derivatives of the shape functions in one system are related to the other system by:

$$\begin{bmatrix} \frac{\partial N}{\partial x_1} \\ \frac{\partial N}{\partial x_2} \end{bmatrix} = \mathbf{J}^{-1} \begin{bmatrix} \frac{\partial N}{\partial \xi} \\ \frac{\partial N}{\partial \eta} \end{bmatrix} \tag{6.144}$$

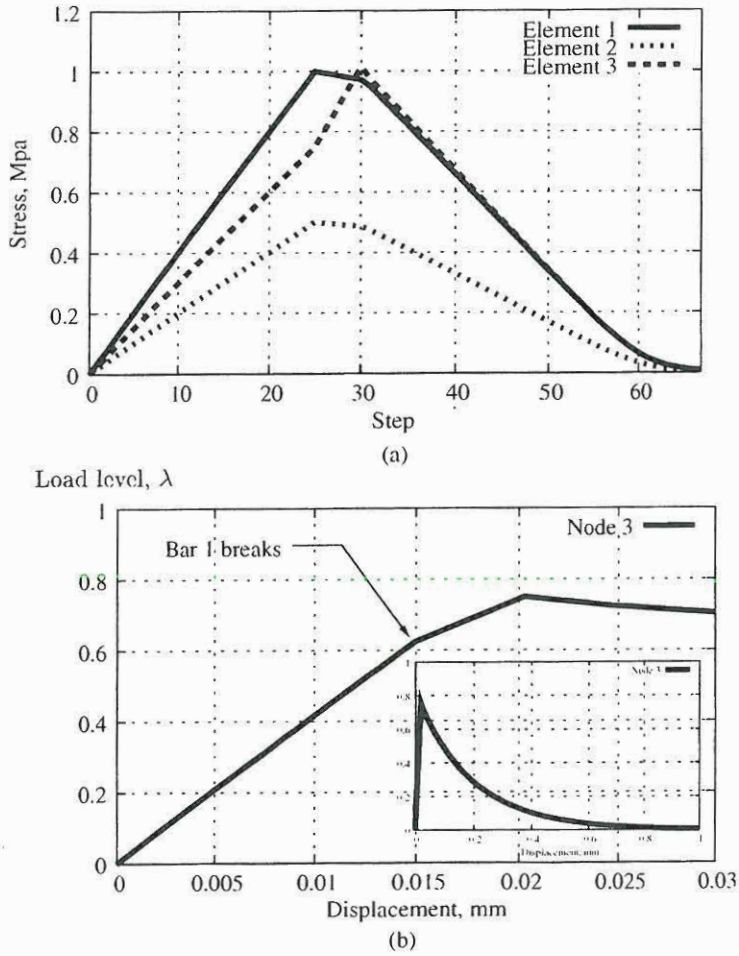

Figure 6.11: (a) Stresses in every bar and (b) Force-displacement diagram for the three-bar system.

where $\mathbf{J}$ is the Jacobian matrix. For this element the integration is performed numerically. In that case:

$$\mathbf{K}_{vv} = \int_{\Omega} \mathbf{B}^T \mathbf{D} \mathbf{B} d\Omega = \sum_i \mathbf{B}_i^T \mathbf{D} \mathbf{B}_i t J w_i \tag{6.145}$$

where J is the Jacobian.

In order to compute the jump, it is necessary to rewrite equation (6.36) in terms of the nodal values of the jump for the node k as:

$$\begin{bmatrix} \tilde{v}_s^{(k)} \\ \tilde{v}_n^{(k)} \end{bmatrix} = \frac{1}{l_{12}} \begin{bmatrix} x_s^{(k)} & -x_n^{(k)} & l_{12} - x_s^{(k)} & x_n^{(k)} \\ 0 & x_s^{(k)} & 0 & l_{12} - x_s^{(k)} \end{bmatrix} \begin{bmatrix} b_{s1} \\ b_{n1} \\ b_{s2} \\ b_{n2} \end{bmatrix} = \mathbf{N}_{bl}^{(k)} \mathbf{b}_l \tag{6.146}$$

Transforming now these quantities to the global system

$$\tilde{\mathbf{v}}^{(k)} = \begin{bmatrix} \tilde{v}_1^{(k)} \\ \tilde{v}_2^{(k)} \end{bmatrix} = \mathbf{R}_2 \mathbf{N}_{bl}^{(k)} \mathbf{R}_4^T \mathbf{b} = \mathbf{N}_b^{(k)} \mathbf{b} \tag{6.147}$$

where

$$\mathbf{R}_4 = \begin{bmatrix} \mathbf{R}_2 & \mathbf{0} \\ \mathbf{0} & \mathbf{R}_2 \end{bmatrix} \tag{6.148}$$

After obtaining the matrix $\mathbf{M}$ and $\mathbf{H}$ the following matrices can be computed:

$$\bar{\mathbf{B}} = \mathbf{B}\mathbf{H}\mathbf{M} \qquad \text{and } \mathbf{N}_b = \mathbf{R}_2 \mathbf{N}_{bl} \mathbf{R}_4^T \tag{6.149}$$

Finally the integration can be performed numerically as:

$$\int_{\Omega} \mathbf{B}^T \mathbf{D} \bar{\mathbf{B}} d\Omega = \sum_i \mathbf{B}_i^T \mathbf{D} \bar{\mathbf{B}}_i t J w_i \tag{6.150}$$

$$\int_S \mathbf{N}_b^T \mathbf{T}_{cz} \bar{\mathbf{N}}_b d\Gamma = \sum_i \tfrac{1}{2} \mathbf{N}_{bi}^T \mathbf{T}_{czi} \bar{\mathbf{N}}_{bi} t l_{12} w_i \tag{6.151}$$

$$\int_{\Omega} \bar{\mathbf{B}}^T \boldsymbol{\sigma} d\Omega = \sum_i \bar{\mathbf{B}}_i^T \boldsymbol{\sigma}_i t J w_i \tag{6.152}$$

$$\int_S \mathbf{N}_b^T \mathbf{T}_S d\Gamma = \sum_i \tfrac{1}{2} \mathbf{N}_{bi}^T \mathbf{T}_S t l_{12} w_i \tag{6.153}$$

6.12 Conclusions

An alternative approach to embed discontinuities in finite elements is presented. The method is different from the one based on the partition of unity property in that the jump is approximated using the kinematics of the jump. The resulting shape functions are not the same shape functions used to approximate the displacement field.

The result is an increase in the complexity of the problem, compared with the solution based on the partition of unity property, because the new degrees of freedom are located along the discontinuity path and not in the existing nodes (as is used in the elements using the partition of unity property).

The resultant stiffness matrix is not dependent on the position of the crack, making this solution objective. This alternative approach can be used in combination with the desired constitutive model; here cohesive models were used.

Bibliography

Alfaiate, J., Simone, A. & Sluys, L. J. (2003), 'Non-homogeneous displacement jumps in strong embedded discontinuities', *International Journal of Solids and Structures* **40**, 5799–5817.

Babuška, I. & Melenk, J. M. (1997), 'The partition of unit method', *Int. J. Numer. Meth. Engng.* **40**, 727 758.

Camacho, G. T. & Ortiz, M. (1996), 'Computational modeling of impact damage in brittle materials', *Internat. J. Solids Structures* **33**, 2899 2938.

Carter, B., Ingraffea, A. & Bittencourt, T. N. (1995), Topology-controlled modelling of linear and nonlinear 3d crack propagation in geomaterials, *in* 'Fracture of Brittle, Disordered Material', E and FN Spon, London, pp. 301 318.

Cope, R. J., Rao, P. V., Clark, L. A. & Norris, P. (1980), Modelling of reinforced concrete behavior for finite element analysis of bridge slabs, *in* C. Taylor, E. Hinton & D. Owen, eds, 'Numerical methods for nonlinear problems', Swansea: Pineridge Press, pp. 457–470.

Crisfield, M. A. (1981), 'A fast incremental-iterative solution procedure that handles "snap-through"', *Computers and Structures* **13**, 55–62.

Crisfield, M. A. (1991), *Non-linear Finite Element analysis of Solids and Structures*, Vol. Volume 1: essentials, John Wiley and Sons, Chichester.

Falk, M. L., Needleman, A. & Rice, J. (2001), 'A critical evaluation of cohesive zone models of dynamic fracture', *Journal de Physique IV* **11 Pr5**, 43–50.

Ingraffea, A. R. & Saouma, V. (1985), Numerical modelling of discrete crack propagation in reinforced and plain concrete, *in* 'Fracture mechanics of concrete', Martinus Nijhoff Publishers, Dordrecht, pp. 171 225.

Moës, N., Dolbow, J. & Belitschko, T. (1999), 'A finite element method for crack growth without remeshing', *Int. J. Numer. Meth. Engng.* **46**, 131–150.

Ngo, D. & Scordelis, A. C. (1967), 'Finite element analysis of reinforced concrete beams', *Journal of the American Concrete Institute* **64**, 152–163.

Oliver, J. (1996), 'Modelling strong discontinuities in solid mechanics via strain softening constitutive equations. part 1: Fundamentals', *International Journal for Numerical Methods in Engineering* .

Rashid, Y. R. (1968), 'Analysis of prestressed concrete pressure vessels', *Nuclear Engineering and Design* **7**(4), 334–355.

Remmers, J. J. C., de Borst, R. & Needleman, A. (2003), 'A cohesive segments method for the simulation of crack growth', *Computational mechanics* **31**(1–2), 69–77.

Simo, J. C., Oliver, J. & Armero, F. (1993), 'An analysis of strong discontinuities induced by strain-softening in rate-independent inelastic solids', *Comp. Mech.* **12**, 277–296.

Suidan, M. & Schnobrich, W. C. (1973), 'Finite element analysis of reinforced concrete', *ASCE J. Struct. Div.* **99**, 2109–2122.

Wells, G. N. & Sluys, L. J. (2000), 'Application of embedded discontinuities for softening solids', *Engineering Fracture Mechanics* **65**, 263–281.

Wells, G. N. & Sluys, L. J. (2001), 'A new method for modelling cohesive cracks using finite elements', *Int. J. Numer. Meth. Engng.* **50**, 2667–2682.

Xu, X. & Needleman, A. (1993), 'Void nucleation by inclusion debonding in a crystal matrix', *Modelling Simul. Mater. Sci. Eng.* **1**, 111–132.

Chapter 7

A computer program for the finite element analysis of cracks

Contents

7.1 Introduction

In order to implement and test some of the techniques used to analyze the process of cracking in structural elements, the computer program CRACK was developed by the author. The program makes use of the finite element method to solve problems where interface elements or elements with embedded discontinuities might be used.

The program, originally conceived to be one single program, was divided into three sub-programs. The first one is a preprocessor program called 'crp', the second, which is a program for processing and solving systems of equations, is called 'crs'. The third program is made for post-processing and producing graphical output and is called 'crg'.

All three sub-programs work on a common database. The input data required can be generated interactively using the program 'crp' or using a single ASCII file with extension '.dat'. This data file can be generated using alternative programs. All of the database used for the program is in ASCII format, so that it can easily be read and modified by the users.

All of the three programs share some common C++ classes and functions, some of these can conform a library by themselves, but here the classes are just included in every one of the three sub-programs.

The program includes different kinds of elements; some of these, however, are not completely implemented because they are not being used by the author as part of the research on material instability. Here, references are made only to the elements that are completely implemented. The program takes advantage of the class definition used in C++. New elements can easily be implemented modifying the class 'elements'.

All of the sub-programs were developed in the computer language C++ using object oriented programming. The sub-programs are copyrighted under the terms of the GNU general public license. The program was developed using the Kdevelop C/C++ Integrated Development Environment which can be found on the site http://www.kdevelop.org. Additionally, the program makes use of the libraries QT and the program Qt designer from Trolltech that can be found on http://www.trolltech.com/qt/. The sub-program 'crg' also uses the library dislin from Helmut Michels (Max-Planck-Institut für Sonnensystemforschung) located at http://www.linmpi.mpg.de/dislin/. All three sub-programs make extensive use of the GNU scientific library, which is used for the implementation and manipulation of matrices and vectors. This library can be found on http://sources.redhat.com/gsl/.

The author has modified and created a C++ class based on the program 'sparse' for solution of sparse matrices created by Kenneth Kundert and Alberto Sangiovanni-Vincentelli from the University of California at Berkeley. The original program 'sparse' can be found on http://www.netlib.org/sparse/index.html.

7.2 The pre-processor 'crp'

The pre-processor program 'crp' allows the interactive creation of the input database required for the crack program including the file `database_name.dat`. The ASCII file `database_name.dat` is the only file required for the program 'crs'. This file can

be created using other programs or a text editor, thus avoiding the need for using this subprogram. To create the file, the instructions in appendix E shall be followed if the program 'crp' is not used.

The sub-program 'crp' is interactive and the user can use it in order to create the database (including the `database_name.dat` file). The program includes options to generate nodes, elements and lists of interface elements along a discontinuity.

7.3 The finite element analysis using the subprogram 'crs'

7.3.1 The solution possibilities

This sub-program is responsible for processing the information and for producing the results corresponding to displacements and stresses. The sub-program 'crs' gets most of the information required from the file `database_name.dat`.

The information in the file `database-name.dat` is sufficient for a linear elastic static analysis. If the analysis is non-linear, then the corresponding options explained in appendix E must be activated.

In case of non-linear analysis, definition of a time curve is required. This time curve is used in case of non-proportional loading. The time curve is constructed by defining a number of points in the curve.

A convergence constant used in the iterative part of the process is required, and so is a number of maximum iterations. Lambda (λ) is defined as the load factor, by default the maximum value of λ is defined as one, but this can be changed in the corresponding option.

When iterations are allowed, the step size (the value of Δl) in the arc-length control strategy can change according to the rule

$$\Delta l_{i+1} = \Delta l_i \sqrt{\frac{I_d}{I_i}} \tag{7.1}$$

where I_d is the number of desired iterations, and I_i is the number of iterations required in step i. However, the following criterion is also applied:

$$\frac{\Delta l_0}{I_{\min}} < \Delta l_{i+1} < \Delta l_0 * I_{\max} \tag{7.2}$$

where $I_{\min}$ and $I_{\max}$ are defined for the user.

The size of Δl in the first step is defined supposing force control (only in the first step). In this force control, the force increment is defined from:

$$\Delta\lambda = \lambda_{\max}/S_d \tag{7.3}$$

where $\lambda_{\max}$ is the maximum value of λ and S_d is the approximate number of steps, both quantities are defined by the user.

The program ends when one of the following criteria is fulfilled: a maximum number of steps defined by the user is reached; a maximum displacement is reached; a maximum value of λ is reached.

Sometimes it is required to restart an analysis after a number of steps have been done. In this case, it is possible to re-start with a step size of different value than the original; in this program it is defined after restart in step $i+1$ that:

$$\Delta l_{i+1} = \Delta l_i * I_f \tag{7.4}$$

where I_f is defined by the user. It is also required to define the value of ψ, where ψ is a constant which takes into account that the displacement and force have different scales. See (Crisfield 1991).

Under normal conditions, the program controls the advancing of the arc-length strategy. This is done by using an energetic criterion which means that the sign of Δl is defined as the one that produces positive external work in the step, i.e.:

$$\Delta W = \mathbf{q}^T \Delta \mathbf{u}_i = \mathbf{q}^T \dot{\mathbf{u}}_i \Delta \lambda_n > 0 \tag{7.5}$$

where W is the external work, $\mathbf{q}$ is the load vector, $\mathbf{u}$ is the displacement vector, and $\dot{\mathbf{u}}$ is the velocity vector.

It is possible to change the advancing criteria in (7.5), and thus control the solution by assuring the advance of a certain degree of freedom.

When cohesive-frictional models are used with interface elements, the transition from cohesive to frictional occurs when:

$$\sqrt{\left(\frac{\Delta u_n}{\delta_n} + 1\right)^2 + \left(\frac{\Delta u_s}{\delta_s}\right)^2} - 1 > 1 \tag{7.6}$$

where Δu_n and Δu_s are the increments in displacement in the normal and tangential directions, respectively, and δ_n and δ_s are the interface characteristic length scales in normal and tangential directions, respectively, according to the Xu-Needleman cohesive model.

7.3.2 Non-linear run possibilities

After defining the time curve and the other parameters required, the problem can be run. The user can choose between different non-linear possibilities. In all cases, the spherical arc-length control solution is used, and details of the general solution can be seen in appendix B, and in (Crisfield 1991). Details specific to the modifications made to the general algorithms for the case of interface elements are found in section 4.5.3 on page 59, and for elements with embedded cracks in sections 5.10 and 6.9 on the pages 98 and 131, respectively.

A non-linear analysis of large displacements can be made if truss elements are defined. If this option is used, the solution is performed efficiently, the stiffness matrix is stored in compact form and a modified Cholesky algorithm is used to

solve the system of equations. In all other cases of non-linear analysis, the matrix is stored as a sparse matrix and the solution is performed using functions developed by Kenneth Kundert from the University of California at Berkeley for the program 'sparse'. These functions allow the solution of systems of equations using sparse matrices. The program 'sparse' has been modified here and a C class has been built for this program. All the functionality of the original program is conserved, so that the matrices can be expanded; the matrices can be symmetric or asymmetric. The solution uses a modified Gauss solution. In the factorization, a relative threshold of 0.001 is chosen (a value of one means complete pivoting, if the value is close to zero, the solution method is Markowitz pivoting without threshold).

7.4 The post-processing program, 'crg'

7.4.1 Introduction

The post-processing sub-program is the sub-program 'crg'. This program is able to present the results of all kinds of analyses made by the program 'crs' graphically. The program is completely interactive, the graphical output is produced using the library 'dislin' from Helmut Michels (Max-Planck-Institut für Sonnensystemforschung) http://www.linmpi.mpg.de/dislin/. The default output is the display of the computer, but it can be redefined to files containing the graphics or the data used to generate the graphics.

It is possible to present the results using different values of the window extension and point of view. The program also has facilities to check the topology of the system before running it using the computer display. It is possible to show the nodes, the mesh, constants (referring them to groups of geometrical parameters), materials, and it is possible to check the restrictions and the position of the forces as well. For the purpose of checking the topology of the system, it is also possible to show the elements in a shrunk form, which is the only way to show the interface elements.

After running the sub-program 'crs' the sub-program 'crg' uses the results to create graphics showing displacements and stresses on the system. The program can show linear graphics presenting displacements, stresses, tractions and friction parameters along selected nodes or elements for specific steps in the analysis.

7.5 Conclusions

A computer program implementation for analysis of cracks using the finite element method was described.

The program has a library of elements that can be combined in order to get the adequate model for various situations. In particular, the program implements interface elements with cohesive and constitutive laws of friction. The program also includes elements with embedded discontinuities based on the partition of unity, and finite elements with embedded discontinuities based on an alternative approach discussed in chapter 6.

All of the relevant options of the program have been presented, and the database used is described in detail in appendix E.

Bibliography

Crisfield, M. A. (1991), *Non-linear Finite Element analysis of Solids and Structures*, Vol. Volume 1: essentials, John Wiley and Sons, Chichester.

Appendix A

Some notes in tensor analysis

Contents

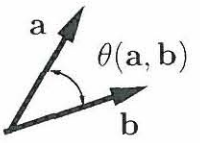

Figure A.1: Two vectors in the space.

A.1 Introduction

This appendix is based principally on (Christoffersen 2001). Other references used to develop this appendix are (Flügge 1972) and (Heinbockel 1996).The motivation of this appendix is to present the notation and general rules used along the thesis related to tensors.

A.2 Vectors and index notation

Vectors are objects which have magnitude and direction. A vector is graphically represented by an arrow, and here symbolically using bold type $\mathbf{a}$. The magnitude is denoted by $|\mathbf{a}|$.

Addition. Let $\mathbf{a}$ and $\mathbf{b}$ be vectors. Then $\mathbf{c} = \mathbf{a} + \mathbf{b}$ is also a vector. The addition is commutative, so that $\mathbf{a}+\mathbf{b} = \mathbf{b}+\mathbf{a}$. The null vector $\mathbf{0}$ is defined so that $\mathbf{a}+\mathbf{0} = \mathbf{a}$.

Multiplication by a scalar. Let $\mathbf{a}$ be a vector and α a scalar. Then $\mathbf{b} = \alpha\mathbf{a}$ is a vector. The direction of $\mathbf{b}$ is parallel to $\mathbf{a}$ and its magnitude is given by $|\mathbf{b}| = \alpha\,|\mathbf{a}|$. The unit vector which is parallel to $\mathbf{a}$ is $\mathbf{n} = \mathbf{a}/|\mathbf{a}|$.

Dot product. Let $\mathbf{a}$ and $\mathbf{b}$ be two vectors. The dot product of $\mathbf{a}$ and $\mathbf{b}$ is a scalar defined by:

$$\mathbf{a} \cdot \mathbf{b} = |\mathbf{a}|\,|\mathbf{b}| \cos\theta(\mathbf{a}, \mathbf{b}) \tag{A.1}$$

where $\theta(\mathbf{a}, \mathbf{b})$ is the angle subtended by $\mathbf{a}$ and $\mathbf{b}$, figure (A.1)

Note that $\mathbf{a} \cdot \mathbf{b} = \mathbf{b} \cdot \mathbf{a}$, and if $|\mathbf{a}| \neq 0$ and $|\mathbf{b}| \neq 0$ then $\mathbf{a} \cdot \mathbf{b} = 0$ if and only if $\mathbf{a}$ and $\mathbf{b}$ are perpendicular.

Cross product. Let $\mathbf{a}$ and $\mathbf{b}$ be two vectors. The cross product of $\mathbf{a}$ and $\mathbf{b}$ is a vector denoted by $\mathbf{c} = \mathbf{a} \times \mathbf{b}$. The direction of $\mathbf{c}$ is perpendicular to $\mathbf{a}$ and $\mathbf{b}$ and is chosen so that $(\mathbf{a}, \mathbf{b}, \mathbf{c})$ form a right handed triad figure (A.2) The magnitude of $\mathbf{c}$ is given by

$$|\mathbf{c}| = |\mathbf{a} \times \mathbf{b}| = |\mathbf{a}|\,|\mathbf{b}| \sin\theta(\mathbf{a}, \mathbf{b}) \tag{A.2}$$

Note that $\mathbf{a} \times \mathbf{b} = -\mathbf{b} \times \mathbf{a}$ and $\mathbf{a} \cdot (\mathbf{a} \times \mathbf{b}) = \mathbf{b} \cdot (\mathbf{a} \times \mathbf{b}) = 0$

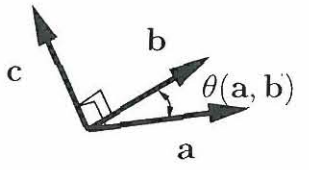

Figure A.2: The cross product.

Any vector **d** can be written as a linear combination of the three vectors **a**, **b** and **c** provided that **a**, **b** and **c** are linearly independent ($\alpha\mathbf{a} + \beta\mathbf{b} + \gamma\mathbf{c} = 0$ only if $\alpha = \beta = \gamma = 0$). In this way any vector **a** can be expressed as:

$$\mathbf{a} = a^1\mathbf{g}_1 + a^2\mathbf{g}_2 + a^3\mathbf{g}_3 = \sum_{i=1}^{3} a^i\mathbf{g}_i = a^i\mathbf{g}_i \tag{A.3}$$

Index notation. In the index notation, the contravariant components of **a** are a^i. The symbol a^i refers to all of the components of **a** simultaneously. The symbol i can have any of the integer values 1, 2 and 3. Whenever there is an expression where the indices occur unrepeated, it is to be understood that each of the subscripts or superscripts can take on any of the integer values $1, 2, \ldots, N$ where N is a specified integer (usually $N = 3$). For example, the expression that defines the Kronecker's delta eq. (A.4)

$$\mathbf{g}^i\mathbf{g}_j = \delta^i_j \tag{A.4}$$

represents nine quantities eq. (A.5). The subscripts i and j occur unrepeated on the left-hand side of the equation, and must also occur on the right-hand side of the equation. These indices are called free indices and can take on any of the values 1, 2 or 3. The nine equations are:

$$\begin{aligned}
&\mathbf{g}^1\mathbf{g}^1 = \delta^1_1 = 1, \quad &&\mathbf{g}^1\mathbf{g}^2 = \delta^1_2 = 0, \quad &&\mathbf{g}^1\mathbf{g}^3 = \delta^1_3 = 0 \\
&\mathbf{g}^2\mathbf{g}^1 = \delta^2_1 = 0, \quad &&\mathbf{g}^2\mathbf{g}^2 = \delta^2_2 = 1, \quad &&\mathbf{g}^2\mathbf{g}^3 = \delta^2_3 = 0 \\
&\mathbf{g}^3\mathbf{g}^1 = \delta^3_1 = 0, \quad &&\mathbf{g}^3\mathbf{g}^2 = \delta^3_2 = 0, \quad &&\mathbf{g}^3\mathbf{g}^3 = \delta^3_3 = 1
\end{aligned} \tag{A.5}$$

Summation convention. The summation convention states that whenever an expression arises where there is an index which occurs twice on the same side of any equation, or term within an equation, it is understood to represent a summation on these repeated indices. (See for example eq. (A.3). The summation convention requires that one must never allow a summation index to appear more than twice in any given expression. Since the summation index no longer appears in the result of such a summation, it does not matter which letter is used for it. Such an index is called a dummy index, and when necessary, we may change the letter used for it from one equation to the next or from the left to the right hand side of one equation.

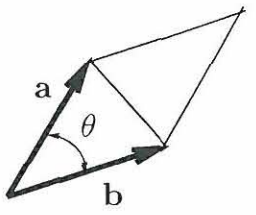

Figure A.3: Parallelogram defined by two vectors.

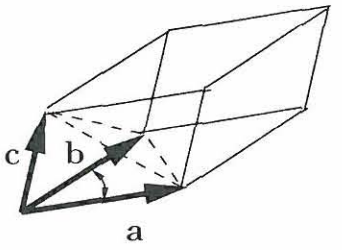

Figure A.4: Parallelopiped defined by three vectors.

Calculating areas. The area of the parallelogram defined by vectors **a** and **b** is $2A$ where A is the area of one of the triangles shown in figure A.3.

$$A = \tfrac{1}{2}\left|\mathbf{a}\times\mathbf{b}\right| \tag{A.6}$$

Calculating volumes The volume of the parallelopiped defined by three vectors **a**, **b** and **c** is figure A.4.

$$V = \left|\mathbf{c}\cdot(\mathbf{a}\times\mathbf{b})\right| \tag{A.7}$$

The volume of the tetrahedron shown in figure A.4 is $V/4$.

Contravariant vectors. Define the covariant independent vectors $\mathbf{g}_1$ and $\mathbf{g}_2$, then the contravariant vector $\mathbf{g}^3$ is orthogonal to the plane in which $\mathbf{g}_1$ and $\mathbf{g}_2$ reside figure A.5 in fact:

$$\begin{aligned}\mathbf{g}^1 &= \tfrac{1}{J}\mathbf{g}_2\times\mathbf{g}_3\\ \mathbf{g}^2 &= \tfrac{1}{J}\mathbf{g}_3\times\mathbf{g}_1\\ \mathbf{g}^3 &= \tfrac{1}{J}\mathbf{g}_1\times\mathbf{g}_2\end{aligned} \tag{A.8}$$

They have all the same value of J, due to eq. (A.5) so that

$$\begin{aligned}\mathbf{g}^1\cdot\mathbf{g}_1 &= \tfrac{1}{J}\mathbf{g}_1\cdot(\mathbf{g}_2\times\mathbf{g}_3) = 1\\ \mathbf{g}^2\cdot\mathbf{g}_2 &= \tfrac{1}{J}\mathbf{g}_2\cdot(\mathbf{g}_3\times\mathbf{g}_1) = 1\\ \mathbf{g}^3\cdot\mathbf{g}_3 &= \tfrac{1}{J}\mathbf{g}_3\cdot(\mathbf{g}_1\times\mathbf{g}_2) = 1\end{aligned} \tag{A.9}$$

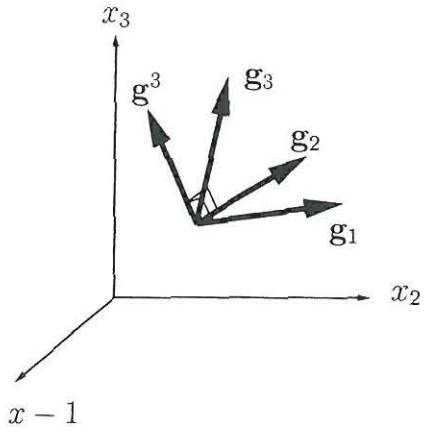

Figure A.5: The contravariant base vector $\mathbf{g}^3$.

and

$$\mathbf{g}_1 \cdot (\mathbf{g}_2 \times \mathbf{g}_3) = \mathbf{g}_2 \cdot (\mathbf{g}_3 \times \mathbf{g}_1) = \mathbf{g}_3 \cdot (\mathbf{g}_1 \times \mathbf{g}_2) \tag{A.10}$$

because they are all the volume of the same parallelopiped. According to eq. (A.7) the volume is:

$$J = \mathbf{g}_1 \cdot (\mathbf{g}_2 \times \mathbf{g}_3) \tag{A.11}$$

where

$$\begin{aligned} \mathbf{g}_1 &= J\mathbf{g}_2 \times \mathbf{g}_3 \\ \mathbf{g}_2 &= J\mathbf{g}_3 \times \mathbf{g}_1 \\ \mathbf{g}_3 &= J\mathbf{g}_1 \times \mathbf{g}_2 \end{aligned} \tag{A.12}$$

The symbol with a subscript $\mathbf{g}_i$ defines covariant base vectors, $\mathbf{g}^i$ defines contravariant base vectors. If a_i are the covariant components of $\mathbf{a}$ and a^i are the contravariant components of $\mathbf{a}$, it is possible to write $\mathbf{a}$ in the following form:

$$\mathbf{a} = a^i \mathbf{g}_i = a_i \mathbf{g}^i \tag{A.13}$$

A.3 Tensors and transformation of coordinates

Tensors are quantities which obey certain transformation laws. Let x^i represent a variable point $(x^1, x^2, \ldots, x^N)$ in an N dimensional space V_N. Another set of N quantities x'^i can be used to represent a variable point $(x'^1, x'^2, \ldots, x'^N)$ in an N dimensional space V'_N. When the x are related to the x' by equations of the form

$$x^i = x^i(x'^1, x'^2, \ldots, x'^N) \tag{A.14}$$

then a transformation is said to exist between the coordinates x^i and x'^i. Whenever the relations eq. (A.14) are functionally independent, single valued and possess partial derivatives such that the Jacobian of the transformation

$$J = \begin{vmatrix} \frac{\partial x^1}{\partial x'^1} & \frac{\partial x^1}{\partial x'^2} & \cdots & \frac{\partial x^1}{\partial x'^N} \\ \vdots & \vdots & & \vdots \\ \frac{\partial x^N}{\partial x'^1} & \frac{\partial x^N}{\partial x'^2} & \cdots & \frac{\partial x^N}{\partial x'^N} \end{vmatrix} \tag{A.15}$$

is different from zero, then an inverse transformation exists

$$x'^i = x'^i(x^1, x^2, \ldots, x^N) \tag{A.16}$$

Definition: Second order contravariant tensor: Whenever N-squared quantities A^{ij} in a coordinate system $(x^1, x^2, \ldots, x^N)$ are related to N-squared quantities A'^{mn} in a coordinate system $(x'^1, x'^2, \ldots, x'^N)$ such that the transformation law

$$A'^{mn}(\mathbf{x}') = A^{ij}(\mathbf{x}) J^W \frac{\partial x'^m}{\partial x^i} \frac{\partial x'^n}{\partial x^j} \tag{A.17}$$

is satisfied, then these quantities are called components of a relative contravariant tensor of second order with weight W. Whenever $W = 0$, these quantities are called the components of an absolute contravariant tensor of second order.

Definition: Second order covariant tensor: Whenever N-squared quantities A_{ij} in a coordinate system $(x^1, x^2, \ldots, x^N)$ are related to N-squared quantities A'_{mn} in a coordinate system $(x'^1, x'^2, \ldots, x'^N)$ such that the transformation law

$$A'_{mn}(\mathbf{x}') = A_{ij}(\mathbf{x}) J^W \frac{\partial x^i}{\partial x'^m} \frac{\partial x^j}{\partial x'^n} \tag{A.18}$$

is satisfied, then these quantities are called components of a relative covariant tensor of second order with weight W. Whenever $W = 0$, these quantities are called the components of an absolute covariant tensor of second order.

Definition: Second order mixed tensor: Whenever N-squared quantities A^i_j in a coordinate system $(x^1, x^2, \ldots, x^N)$ are related to N-squared quantities A'^m_n in a coordinate system $(x'^1, x'^2, \ldots, x'^N)$ such that the transformation law

$$A'^m_n(\mathbf{x}') = A^i_j(\mathbf{x}) J^W \frac{\partial x'^m}{\partial x^i} \frac{\partial x^j}{\partial x'^n} \tag{A.19}$$

is satisfied, then these quantities are called components of a relative mixed tensor of second order with weight W. Whenever $W = 0$ these quantities are called the components of an absolute mixed tensor of second order. It is contravariant of order one and covariant of order one.

Definition: Higher order tensors: Higher order tensors are defined in a similar manner. For example:

$$A'^{m}_{no}(\mathbf{x}') = A^{i}_{jk}(\mathbf{x}) J^{\mathrm{W}} \frac{\partial x'^{m}}{\partial x^{i}} \frac{\partial x^{j}}{\partial x'^{n}} \frac{\partial x^{k}}{\partial x'^{o}} \tag{A.20}$$

this is a relative mixed tensor of order three with weight W. It is contravariant of order one and covariant of order two.

A.4 Properties of tensors

A scalar is a 0-th order tensor, a vector is a first order tensor or a monad, a second order tensor is a dyad, a third order tensor is a triad, and so on. A tensor is defined by a set of scalars and a tensor basis. In a 3-dimensional space, with basis vectors $\mathbf{g}_1$, $\mathbf{g}_2$ and $\mathbf{g}_3$ a tensor $\mathbf{A}$ may be written as

$$\mathbf{A} = A^{ij}\mathbf{g}_i\mathbf{g}_j \tag{A.21}$$

A dyad $\mathbf{ab}$ or $\mathbf{a} \otimes \mathbf{b}$ is formed from the outer or dyad product of two vectors $\mathbf{a}$ and $\mathbf{b}$. A dyad is thus an ordered pair of vectors and then has two directions associated with it. It is another form of a tensor. Dyads obey the following rules if $(\mathbf{A} = \mathbf{ab})$:

$$\mathbf{A} \cdot \mathbf{c} = \mathbf{d} \tag{A.22}$$

where $\mathbf{c}$ and $\mathbf{d}$ are vectors.

$$(\mathbf{ab}) \cdot \mathbf{c} = \mathbf{a}(\mathbf{b} \cdot \mathbf{c}) = \mathbf{d} \tag{A.23}$$

The vector $\mathbf{d}$ has the same direction as $\mathbf{a}$.

$$\mathbf{a} \cdot (\mathbf{bc}) = (\mathbf{a} \cdot \mathbf{b})\mathbf{c} \tag{A.24}$$

If $\mathbf{a}$, $\mathbf{b}$, $\mathbf{c}$, $\mathbf{d}$, $\mathbf{e}$ and $\mathbf{f}$ are vectors, then

$$\mathbf{A} = \mathbf{ab} + \mathbf{cd} + \mathbf{ef} + \ldots \tag{A.25}$$

$$\mathbf{A} = \mathbf{aa} + \mathbf{bb} + \mathbf{cc} \tag{A.26}$$

where $\mathbf{A}$ is a dyad.

$$\mathbf{a}(\alpha\mathbf{b} + \beta\mathbf{c}) = \alpha\mathbf{ab} + \beta\mathbf{ac} \tag{A.27}$$

From eq. (A.25) written for simplicity

$$\mathbf{A} = \mathbf{ab} \tag{A.28}$$

where

$$\mathbf{a} = a^i\mathbf{g}_i, \qquad \text{and} \qquad \mathbf{b} = b^j\mathbf{g}_j \tag{A.29}$$

then

$$\mathbf{A} = a^i b^j \mathbf{g}_i\mathbf{g}_j = A^{ij}\mathbf{g}_i\mathbf{g}_j; \qquad A^{ij} = a^i b^j \tag{A.30}$$

In general:

$$\mathbf{A} = \mathbf{ab} + \mathbf{cd} + \mathbf{ef} + \ldots \tag{A.31}$$

then

$$\mathbf{A} = A^{ij}\mathbf{g}_i\mathbf{g}_j; \qquad A^{ij} = a^i b^j + c^i d^j + \ldots \tag{A.32}$$

Other possibilities are:

$$\mathbf{A} = A^i_j \mathbf{g}_i\mathbf{g}^j \tag{A.33}$$

$$\mathbf{A} = A^j_i \mathbf{g}^i\mathbf{g}_j \tag{A.34}$$

$$\mathbf{A} = A_{ij}\mathbf{g}^i\mathbf{g}^j \tag{A.35}$$

In eq. (A.32) **A** is expressed in contravariant components, in eq. (A.33) and in eq. (A.34) **A** is expressed using mixed components and in eq. (A.35) **A** is expressed in covariant components.

Aa is a triad, **abc** is a triad (a triadic product of **a**, **b** and **c**).

$$(\mathbf{abc}) \cdot \mathbf{d} = \mathbf{ab}(\mathbf{c} \cdot \mathbf{d}) \tag{A.36}$$

If **B** is a triad (a sum of triadic products)

$$\mathbf{B} = B^{ijk}\mathbf{g}_i\mathbf{g}_j\mathbf{g}_k = B^{ij}_k\mathbf{g}_i\mathbf{g}_j\mathbf{g}^k = B^i_{jk}\mathbf{g}_i\mathbf{g}^j\mathbf{g}^k == B_{ijk}\mathbf{g}^i\mathbf{g}^j\mathbf{g}^k \tag{A.37}$$

The permutation tensor. The permutation tensor is defined by the product:

$$e_{ijk} = \mathbf{g}_i \cdot (\mathbf{g}_j \times \mathbf{g}_k) \tag{A.38}$$

Note that

$$\begin{aligned} e_{123} = e_{231} = e_{312} &= J \\ e_{132} = e_{213} = e_{321} &= -J \\ e_{111} = e_{122} = e_{133} = e_{211} = e_{222} = e_{233} = e_{311} = e_{322} = e_{333} &= 0 \\ e^{123} = e^{231} = e^{312} &= 1/J \\ e^{132} = e^{213} = e^{321} &= -1/J \\ e^{111} = e^{122} = e^{133} = e^{211} = e^{222} = e^{233} = e^{311} = e^{322} = e^{333} &= 0 \end{aligned} \tag{A.39}$$

The identity dyad. Defining a vector $\mathbf{a} = a^i \mathbf{g}_i$ then the dot product with the contravariant base vectors $\mathbf{g}^j$ using the definition of Kronecker's delta eq. (A.4) produces:

$$\mathbf{a} \cdot \mathbf{g}^j = a^i \mathbf{g}_i \cdot \mathbf{g}^j = a^i \delta_i^j = a^j \tag{A.40}$$

According to equations eq. (A.40) and eq. (A.24) :

$$\mathbf{a} \cdot \mathbf{g}^j \mathbf{g}_j = a^j \mathbf{g}_j = \mathbf{a} \tag{A.41}$$

Due to the fact that eq. (A.41) is valid for all vectors $\mathbf{a}$, it is concluded that the identity dyad is defined by:

$$\mathbf{g}^j \mathbf{g}_j = \mathbf{1} \tag{A.42}$$

Other useful results. Defining the vector

$$\mathbf{g}^i = g^{ij} \mathbf{g}_j \tag{A.43}$$

Kronecker's delta could be written as:

$$\delta_k^i = \mathbf{g}^i \cdot \mathbf{g}_k = g^{ij} \mathbf{g}_j \cdot \mathbf{g}_k = g^{ij} g_{jk} \tag{A.44}$$

where $g_{jk} = \mathbf{g}_j \cdot \mathbf{g}_k$. Analogously, defining:

$$\mathbf{g}_j = g_{jk} \mathbf{g}^k \tag{A.45}$$

the identity dyad is expressed as:

$$\mathbf{1} = \mathbf{g}^j \mathbf{g}_k = \mathbf{g}^j g_{jk} \mathbf{g}^k = g_{jk} \mathbf{g}^j \mathbf{g}^k = g^{jk} \mathbf{g}_j \mathbf{g}_k \tag{A.46}$$

The vector $\mathbf{a}$ can also be expressed as:

$$\mathbf{a} = a_i \mathbf{g}^j = a_i g^{ij} \mathbf{g}_j = a^j \mathbf{g}_j \tag{A.47}$$

Then it is concluded that:

$$\begin{aligned} a^j &= a_i g^{ij}, \qquad g^{ij} = g^{ji} \\ a^i &= g^{ij} a_j, \qquad a_i = g_{ij} a^j \\ a_i &= g_i^j a_j = \delta_i^j a_j \end{aligned} \tag{A.48}$$

Finally the following identities are also useful

$$\begin{aligned} A^{ij} &= g^{ik} g^{il} A_{kl} \\ A_j^i = g^{ik} g_j^l A_{kl} &= g^{ik} \delta_j^l A_{kl} = g^{ik} A_{kj} \end{aligned} \tag{A.49}$$

A.5 Operations using tensors

Addition and subtraction. Tensors of the same type can be added or subtracted. The result is a tensor of the same order. For example

$$C_{jk}^i = A_{jk}^i + B_{jk}^i \tag{A.50}$$

Multiplication (Outer product). The product of two tensors is also a tensor. The order of the resulting tensor is the sum of the orders of the tensors occurring in the multiplication. For example:

$$C_{jkm}^{il} = A_{jk}^i + B_m^l \tag{A.51}$$

Contraction. The operation of contraction on any mixed tensor of order m is performed when an upper index is set equal to a lower index and the summation convention is invoked. When the summation convention is performed over the repeated indices, the resulting quantity is a tensor of order $(m-2)$. For example:

$$A_{ik}^i = A_{1k}^1 + A_{2k}^2 + \ldots = A_k \tag{A.52}$$

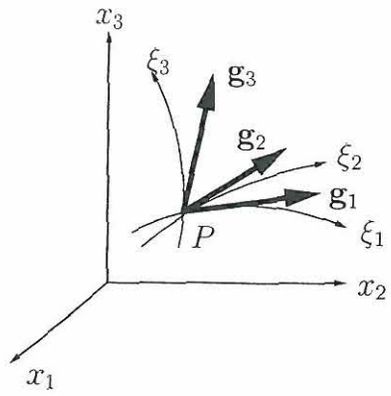

Figure A.6: A curvilinear coordinate system.

Multiplication (inner product). The inner product of two tensors is obtained by:

1. first taking the outer product of the given tensors and
2. performing a contraction on two of the indices.

For example, if A^i and B_j denote the components of two first order tensors, the outer product is:

$$C^i_j = A^i B_j \tag{A.53}$$

The inner product is the scalar

$$C = A^i B_i \tag{A.54}$$

A.6 Metric tensor

In a Cartesian coordinate system there is no distinction between covariant and contravariant components, it is possible to write for this system:

$$\mathbf{g}_i \cdot \mathbf{g}_j = \delta_{ij}, \qquad \mathbf{g}_i = \mathbf{g}^i \tag{A.55}$$

The last equation (eq. (A.55)) is not valid in the general case of a curvilinear coordinate system. Suppose the system shown in figure A.6. Defining the position vector $\mathbf{x} = \mathbf{x}(\xi^1, \xi^2, \xi^3)$ and their derivatives:

$$\mathbf{g}_i = \frac{\partial \mathbf{x}}{\partial \xi^i} = \mathbf{x}_{,i} \tag{A.56}$$

then written:

$$d\mathbf{x} = \mathbf{x}_{,i} d\xi^i = \mathbf{g}_i d\xi^i \tag{A.57}$$

Along the line ξ^1

$$d\xi^2 = d\xi^3 = 0, \qquad d\mathbf{x} = \mathbf{g}_1 d\xi^1 \tag{A.58}$$

and similar relations can be written for the other two directions. Defining now the contravariant base vectors in the same way as in eq. (A.43):

$$\mathbf{g}^i = g^{ij}\mathbf{g}_j, \qquad g^{ik}g_{kj} = \delta^i_j, \qquad g_{ij} = \mathbf{g}_i \cdot \mathbf{g}_j \tag{A.59}$$

It is concluded that it is possible to obtain the covariant base vectors by differentiation of $\mathbf{x}$ eq, (A.56) and contravariant base vectors using eq. (A.59) or alternatively using eq. (A.8). Only if $g_{i,j} = g_{j,i}$, eq. (A.58) is valid because the derivatives of $\mathbf{x}$ can exist. The expression:

$$d\mathbf{x} = \mathbf{g}^i d\xi^i \tag{A.60}$$

is not integrable because $g^i_{,j} \neq g^j_{,i}$ and this is the real difference between the covariant and contravariant bases.

The quantities g_{ij} are called the metrics of the space defined by ξ^i and they define the metric tensor, the quantities g^{ij} are called the conjugate metric components of the space. Another way to understand the meaning of the metrics is to consider the distance ds between two points with coordinates $\mathbf{x}$ and $\mathbf{x} + d\mathbf{x}$:

$$ds^2 = dx^m dx^m \tag{A.61}$$

The differential of each coordinate can be written as:

$$dx^m = x^m_{,i} d\xi^i \tag{A.62}$$

replacing eq. (A.62) in eq. (A.58)

$$ds^2 = x^m_{,i} x^m_{,j} d\xi^i d\xi^j = \mathbf{g}_i \cdot \mathbf{g}_j d\xi^i d\xi^j = g_{ij} d\xi^i d\xi^j \tag{A.63}$$

A.7 Derivatives

A.7.1 Gradient of a scalar field

Let $\mathbf{x}$ be a position vector, then the velocity is its derivative with respect to time (t):

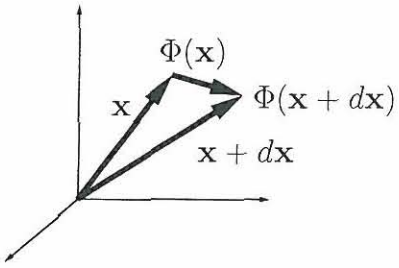

Figure A.7: Two points in a scalar field.

$$\dot{\mathbf{x}} = \mathbf{v} = \frac{d\mathbf{x}}{dt} \tag{A.64}$$

the velocity is usually expressed in contravariant form:

$$d\mathbf{x} = \mathbf{g}_i d\xi^i, \qquad \mathbf{v} = \mathbf{g}_i v^i \tag{A.65}$$

where

$$v^i = \frac{d\xi^i}{dt} \tag{A.66}$$

Let $\Phi = \Phi(\xi^1, \xi^2, \xi^3)$ be a scalar field shown in figure A.7, then the gradient of Φ denoted as $\nabla\Phi$ is such that

$$d\mathbf{x} \cdot \nabla\Phi = \Phi\nabla \cdot d\mathbf{x} = d\Phi \tag{A.67}$$

Using again eq. (A.57) and $d\Phi = \Phi_{,i} d\xi^i$

$$(\Phi\nabla) \cdot \mathbf{g}_i d\xi^i = \Phi_{,i} d\xi^i \tag{A.68}$$

for all $d\xi^i$. Then

$$(\Phi\nabla) \cdot \mathbf{g}_i = \Phi_{,i} \tag{A.69}$$

and using the definition of the identity dyad eq. (A.42), it is possible to obtain the general equation for the gradient of a scalar field:

$$(\Phi\nabla) \cdot \mathbf{g}_i \mathbf{g}^i = \nabla\Phi = \Phi_{,i} \mathbf{g}^i \tag{A.70}$$

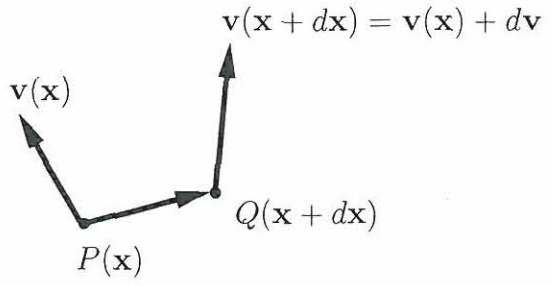

Figure A.8: Variation of $\mathbf{v}$ between two positions.

A.7.2 Gradient of a vector

If it is necessary to obtain the gradient of a vector $\nabla\mathbf{v}$ in rectilinear coordinates, the changes of the vector components indicate the change of the vector. This is no longer the case when the coordinates are curvilinear as in figure A.8 because, even if the vectors are equal, their components could be different in two points.

$$(\mathbf{v}\nabla)\cdot d\mathbf{x} = d\mathbf{x}\cdot(\nabla\mathbf{v}) = d\mathbf{v} \tag{A.71}$$

where the property $\mathbf{A}\cdot\mathbf{b} = \mathbf{b}\cdot\mathbf{A}^T$ was used and $\mathbf{A}$ is a matrix and $\mathbf{b}$ is a vector. Using eq. (A.57)

$$(\mathbf{v}\nabla)\cdot\mathbf{g}_i d\xi^i = \mathbf{v}_{,i}d\xi^i, \qquad \mathbf{g}_i = \mathbf{x}_{,i} \tag{A.72}$$

$$(\mathbf{v}\nabla)\cdot\mathbf{g}_i = \mathbf{v}_{,i} \tag{A.73}$$

analogous to the scalar field is found

$$(\mathbf{v}\nabla)\cdot\mathbf{g}_i\mathbf{g}^i = \mathbf{v}_{,i}\mathbf{g}^i, \qquad \nabla\mathbf{v} = \mathbf{v}_{,i}\mathbf{g}^i \tag{A.74}$$

In order to evaluate eq. (A.74), it is necessary to replace the vector $\mathbf{v}_i$ for its components

$$(v^j\mathbf{g}_j)_{,i}\mathbf{g}^i = v^j_{,i}\mathbf{g}_j\mathbf{g}^i + v^j\mathbf{g}_{j,i}\mathbf{g}^i \tag{A.75}$$

A.7.3 Christoffel symbols

To evaluate eq. (A.75), the following symbols are introduced:

$$\mathbf{g}_{j,i} = \begin{pmatrix} k \\ ji \end{pmatrix}\mathbf{g}_k \tag{A.76}$$

with the following property:

$$\mathbf{g}_{j,i} = \mathbf{x}_{,ji} = \mathbf{x}_{,ij} = \mathbf{g}_{i,j} \tag{A.77}$$

$$\begin{pmatrix} k \\ ji \end{pmatrix} = \begin{pmatrix} k \\ ij \end{pmatrix} \tag{A.78}$$

Using Christoffel symbols it is possible to rewrite eq. (A.75)

$$\mathbf{v}\nabla = v^j_{,i}\mathbf{g}_j\mathbf{g}^i + v^j\begin{pmatrix} k \\ ji \end{pmatrix}\mathbf{g}_k\mathbf{g}^i = v^j_{,i}\mathbf{g}_j\mathbf{g}^i + v^k\begin{pmatrix} j \\ ki \end{pmatrix}\mathbf{g}_j\mathbf{g}^i \tag{A.79}$$

$$\mathbf{v}\nabla = \left[v^j_{,i} + \begin{pmatrix} j \\ ik \end{pmatrix}v^k\right]\mathbf{g}_j\mathbf{g}^i = v^j|_i\mathbf{g}_j\mathbf{g}^i \tag{A.80}$$

where

$$v^j|_i = v^j_{,i} + \begin{pmatrix} j \\ ik \end{pmatrix}v^k \tag{A.81}$$

and $v^j|_i$ is known as the contravariant derivative of v^j with respect to ξ^i.

In an analogous way, but replacing $\mathbf{v}$ by their covariant components in eq. (A.74)

$$\mathbf{v}\nabla = (v_j\mathbf{g}^j)_{,i}\mathbf{g}^i = v_{j,i}\mathbf{g}^j\mathbf{g}^i + v_j\mathbf{g}^j_{,i}\mathbf{g}^i \tag{A.82}$$

where

$$(\mathbf{g}^j\mathbf{g}_j)_{,i} = (\mathbf{1})_{,i} = \mathbf{g}^j_{,i}\mathbf{g}_j + \mathbf{g}^j\mathbf{g}_{j,i} = \mathbf{0} \tag{A.83}$$

then

$$\mathbf{g}^j_{,i}\mathbf{g}_j = -\mathbf{g}^j\begin{pmatrix} k \\ ij \end{pmatrix}\mathbf{g}_k = -\mathbf{g}^k\begin{pmatrix} j \\ ik \end{pmatrix}\mathbf{g}_j \tag{A.84}$$

multiply by $\mathbf{g}^l$

$$\mathbf{g}^j_{,i}\mathbf{g}_j \cdot \mathbf{g}^l = -\mathbf{g}^k\begin{pmatrix} j \\ ik \end{pmatrix}\mathbf{g}_j \cdot \mathbf{g}^l = -\mathbf{g}^k\begin{pmatrix} j \\ ik \end{pmatrix}\delta^l_j \tag{A.85}$$

then

$$\mathbf{g}^l_{,i} = -\begin{pmatrix} l \\ ik \end{pmatrix}\mathbf{g}^k \tag{A.86}$$

is found. Replacing (eq.A.86) in eq. (A.82) produces

$$\mathbf{v}\nabla = \left[v_{j,i} - \begin{pmatrix} k \\ ij \end{pmatrix} v_k\right]\mathbf{g}^j\mathbf{g}^i = v_j|_i\mathbf{g}^j\mathbf{g}^i \tag{A.87}$$

where $v_j|_i$ is the covariant derivative of v_j with respect to ξ^i. The dot product of eq. (A.76) with $\mathbf{g}^l$ produces

$$\mathbf{g}^l \cdot \mathbf{g}_{i,j} = \begin{pmatrix} k \\ ij \end{pmatrix}\mathbf{g}^l \cdot \mathbf{g}_k = \begin{pmatrix} k \\ ij \end{pmatrix}\delta^l_k \tag{A.88}$$

then the result is the following formula for the Christoffel symbol:

$$\begin{pmatrix} k \\ ij \end{pmatrix} = \mathbf{g}^k \cdot \mathbf{g}_{i,j} \tag{A.89}$$

or

$$\begin{pmatrix} k \\ ij \end{pmatrix} = \mathbf{g}^k \cdot \mathbf{1} \cdot \mathbf{g}_{i,j} = \mathbf{g}^k \cdot \mathbf{g}^l\mathbf{g}_l \cdot \mathbf{g}_{i,j} = \mathbf{g}^{kl}\mathbf{g}_l \cdot \mathbf{g}_{i,j} \tag{A.90}$$

then

$$\begin{pmatrix} k \\ ij \end{pmatrix} = \tfrac{1}{2}g^{kl}(\mathbf{g}_l \cdot \mathbf{g}_{i,j} + \mathbf{g}_{l,j} \cdot \mathbf{g}_i + \mathbf{g}_l \cdot \mathbf{g}_{j,i} + \mathbf{g}_{l,i} \cdot \mathbf{g}_j - \mathbf{g}_{j,l} \cdot \mathbf{g}_i - \mathbf{g}_{i,l} \cdot \mathbf{g}_j) \tag{A.91}$$

Finally, another formula for Chistoffel symbols is found:

$$\begin{pmatrix} k \\ ij \end{pmatrix} = \tfrac{1}{2}g^{kl}(g_{li,j} + g_{lj,i} - g_{ij,l}) \tag{A.92}$$

A.7.4 Gradient of a second order tensor

Let $\mathbf{A}$ be a second order tensor

$$\mathbf{A} = A^{ij}\mathbf{g}_i\mathbf{g}_j \tag{A.93}$$

The gradient of $\mathbf{A}$ is :

$$\mathbf{A}\nabla = A^{ij}_{,k}\mathbf{g}^k\mathbf{g}_i\mathbf{g}_j + A^{ij}\mathbf{g}_{i,k}\mathbf{g}_j + A^{ij}\mathbf{g}_i\mathbf{g}_{j,k} = A^{ij}|_k\mathbf{g}_i\mathbf{g}_j\mathbf{g}^k \tag{A.94}$$

where

$$A^{ij}|_k = A^{ij}_{,k} + \begin{pmatrix} i \\ kl \end{pmatrix} A^{lj} + \begin{pmatrix} j \\ kl \end{pmatrix} A^{il} \tag{A.95}$$

Using the covariant form:

$$\mathbf{A}\nabla = (A_{ij}\mathbf{g}^i\mathbf{g}^j)_{,k}\mathbf{g}^k = A_{ij}|_k\mathbf{g}^i\mathbf{g}^j)_{,k} \tag{A.96}$$

where

$$A_{ij}|_k = A_{ij,k} - \begin{pmatrix} l \\ ik \end{pmatrix} A_{lj} - \begin{pmatrix} l \\ jk \end{pmatrix} A_{il} \tag{A.97}$$

A.7.5 Divergence of a vector

The divergence of a vector is:

$$\nabla \cdot \mathbf{v} = \mathbf{v} \cdot \nabla = v_i|_j\mathbf{g}^i \cdot \mathbf{g}^j = v_i|_j g^{ij} = (g^{ij}v_i)|_j - g^{ij}|_j v_i \tag{A.98}$$

Due to:

$$\nabla\mathbf{1} = \nabla g_{ij}\mathbf{g}^i\mathbf{g}^j = 0 \tag{A.99}$$

then

$$g_{ij}|_k = 0 \tag{A.100}$$

The divergence of a vector is:

$$\nabla \cdot \mathbf{v} = (g^{ij}v_i)|_j = v^j|_j \tag{A.101}$$

where $v^j|_j$ is the divergence of v_j.

The equations of equilibrium of stresses can be expressed in this way and the results are:

$$\sigma^{ij}|_i + p^j = 0 \tag{A.102}$$

The Lagrange strains are:

$$\varepsilon_{ij} = \tfrac{1}{2}(u_i|_j + u_j|_i + g^{kl}u_k|_i u_l|_j) \tag{A.103}$$

A.8 Invariants and physical components

A.8.1 Invariants

Invariants are obtained when a contraction of indices is performed. Examples of invariants are:

$$\sigma_{ij} = g_{ij}\sigma^{ij} \tag{A.104}$$

$$\sigma^{ij}\sigma_{ij} = g^{ik}g_{jl}\sigma^{ij}\sigma_{kl} \tag{A.105}$$

$$I_1 = \sigma_{ii} \tag{A.106}$$

$$I_2 = \tfrac{1}{2}(\sigma_{ik}\sigma_{ki} - \sigma_{ii}\sigma_{kk}) \tag{A.107}$$

$$I_3 = \tfrac{1}{6}e_{ijk}e_{pqr}\sigma_{ip}\sigma_{jq}\sigma_{kr} \tag{A.108}$$

the elastic strain work is an invariant

$$W_e = \tfrac{1}{2}\sigma^{ij}\varepsilon_{ij} \tag{A.109}$$

The von Mises invariant is:

$$\sigma_e = \sqrt{\tfrac{3}{2}s^{ij}s_{ij}} \tag{A.110}$$

where

$$s^{ij} = \sigma^{ij} - \tfrac{1}{3}g^{ij}\sigma_{kk} \tag{A.111}$$

then

$$\sigma_e = \sqrt{\tfrac{3}{2}(\sigma^{ij}\sigma_{ij}) - \tfrac{1}{3}\sigma^i_i\sigma^j_j} \tag{A.112}$$

Other related invariants are

$$J_1 = s_{ii} = 0 \tag{A.113}$$

$$J_2 = \tfrac{1}{2}(s_{ik}s_{ki} - s_{ii}s_{kk}) \tag{A.114}$$

$$J_3 = \tfrac{1}{6}e_{ijk}e_{pqr}s_{ip}s_{jq}s_{kr} \tag{A.115}$$

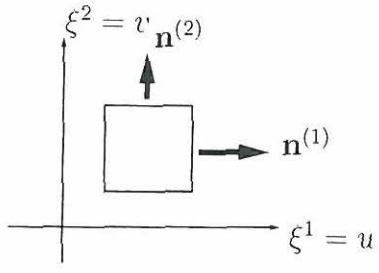

Figure A.9: Normal vectors in orthogonal directions.

A.8.2 Physical components

Physical components are invariant combinations of tensors. In orthogonal coordinates, $g_{ij} = 0$ if $i \neq j$. The physical components of a tensor can be obtained finding the projection of the tensor in the desired direction. Referring to figure A.9 $n^{(i)}$ is a vector in the direction ξ^i, and the physical components of a second order tensor $\boldsymbol{\sigma}$ are:

$$\begin{aligned} \sigma_{uu} &= \sigma^{ij}\mathbf{n}_i^{(1)}\mathbf{n}_j^{(1)} \\ \sigma_{uv} &= \sigma^{ij}\mathbf{n}_i^{(1)}\mathbf{n}_j^{(2)} \end{aligned} \tag{A.116}$$

where

$$\mathbf{n}^{(1)} = \lambda^{(1)}\mathbf{g}^1, \qquad \mathbf{n}^{(1)} \cdot \mathbf{n}^{(1)} = 1, \qquad \lambda^{(1)} > 0 \tag{A.117}$$

$$1 = [\lambda^{(1)}]^2\mathbf{g}^1, \cdot \mathbf{g}^1 = [\lambda^{(1)}]^2 g^{11} \tag{A.118}$$

then

$$\lambda^{(1)} = \frac{}{\sqrt{g^{11}}} = \sqrt{g_{11}} \tag{A.119}$$

due to the orthogonality of the coordinate system. This implies

$$\sigma_{uu} = (\boldsymbol{\sigma} \cdot \mathbf{n}^{(1)}) \cdot \mathbf{n}^{(1)} = \mathbf{n}^{(1)} \cdot \boldsymbol{\sigma}) \cdot \mathbf{n}^{(1)} = [\lambda]^2\mathbf{g}^1 \cdot \boldsymbol{\sigma} \cdot \mathbf{g}^1 = g_{11}\mathbf{g}^1 \cdot \boldsymbol{\sigma} \cdot \mathbf{g}^1 \tag{A.120}$$

$$\sigma_{uu} = g_{11}\sigma^{11} \tag{A.121}$$

$$\sigma_{uv} = \mathbf{n}^{(1)} \cdot \boldsymbol{\sigma}) \cdot \mathbf{n}^{(2)} = \lambda^{(1)}\lambda^{(2)}\mathbf{g}^1 \cdot \boldsymbol{\sigma} \cdot \mathbf{g}^2 = \sqrt{g_{11}g_{22}}\sigma^{12} \tag{A.122}$$

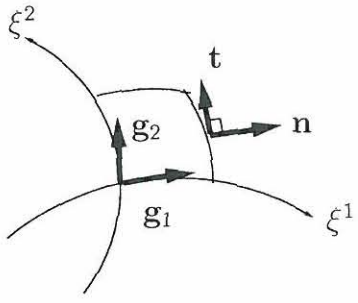

Figure A.10: Normal and tangent vectors in a curvilinear coordinate system.

In a curvilinear coordinate system, figure A.9, the normal and tangential components of the tensor $\boldsymbol{\sigma}$ are:

$$\begin{aligned} \sigma &= \mathbf{n} \cdot \boldsymbol{\sigma}\mathbf{n} = n_i \sigma^{ij} n_j \\ \tau &= \mathbf{n} \cdot \boldsymbol{\sigma}\mathbf{t} = n_i \sigma^{ij} t_j \end{aligned} \tag{A.123}$$

Defining $\mathbf{t} = \mu \mathbf{g}_2$, and $\mathbf{n} = \lambda \mathbf{g}^1$ analogously to eq. (A.118)

$$\mu = \frac{1}{\sqrt{g_{22}}}, \qquad \mathbf{t} = \frac{1}{\sqrt{g_{22}}} \mathbf{g}_2 \tag{A.124}$$

$$\lambda = \frac{1}{\sqrt{g^{11}}}, \qquad \mathbf{n} = \frac{1}{\sqrt{g^{11}}} \mathbf{g}^1 \tag{A.125}$$

the vectors $\mathbf{t}$ and $\mathbf{n}$ are orthogonal

$$\mathbf{n} \cdot \mathbf{t} = \lambda \nu \mathbf{g}^1 \cdot \mathbf{g}_2 = 0 \tag{A.126}$$

and finally the physical components are

$$\begin{aligned} \sigma &= \frac{1}{g^{11}} \mathbf{g}^1 \cdot \boldsymbol{\sigma} \mathbf{g}^1 = \frac{\sigma^{11}}{g^{11}} \\ \tau &= \frac{1}{\sqrt{g^{11} g_{22}}} \mathbf{g}^1 \cdot \boldsymbol{\sigma} \mathbf{g}_2 = \frac{\sigma^1_2}{\sqrt{g^{11} g_{22}}} \end{aligned} \tag{A.127}$$

In general, $\sigma_{uv} \neq \sigma_{vu}$ because the normal and tangent vectors have different orientation between these two faces.

Bibliography

Christoffersen, J. (2001), 'Tensor analysis'. Unpublished notes from a course on Tensor Analysis at Aalborg University.

Flügge, W. (1972), *Tensor analysis and Continuum Mechanics*, Springer-Verlag.

Heinbockel, J. H. (1996), *Introduction to Tensor Calculus and continuum Mechanics*, Published in electronic media www.math.odu.edu/ jhh/counter2.html.

Appendix B

Solution schemes in nonlinear finite element analysis

Contents

B.1 Introduction

Since the early 1960s; the problem of solving the systems of equations produced by the Finite Element Method (FEM) has been an important part of the FEM technology. At the beginning, from 1960 until around 1975, much research was oriented towards obtaining correct and implementable non-linear finite element equations. The art of solving these equations in a reliable and efficient manner was neglected. The solutions produced were usually based on purely incremental methods. Corrective methods of the Newton type got attention since the early 1970s, and these were principally used for geometrically non-linear problems.

Problems with smooth non-linearities are highly developed, incremental steps have been corrected with corrective iterations, conventional and modified Newton methods are used in the corrective phase, and, more recently, variants of the conjugate-gradient and quasi-Newton methods have been used.

While problems with smooth non-linearities are characterized by continuous, path independent non-linear relation at the local level (geometric non-linearities, non-linear elasticity, follower forces), rough non-linearities (for example flow-rule plasticity, contact, friction) are characterized by a non-smooth local response, and those are more difficult to solve. The main difficulty comes from the fact that conventional solution procedures based on Taylor expansions may fail, because such Taylor expansions need not exist. For rough non-linearities, incremental methods, as opposed to incremental iterative methods, dominate.

The full Newton-Raphson technique has a high cost, modified Newton-Raphson technique has a low cost but it has a slower convergence. The quasi-Newton techniques represents a compromise. The major difficulties found here are related to the behavior of these techniques in limit points. Arc-length techniques are developed to pass some of these points.

Due to the fact that load and displacement are adjusted during the iteration process, the arc-length control technique is robust and suitable for automatic selection of increments. In this document Newton-Raphson techniques and modified Newton-Raphson techniques are discussed respect to the arc-length control.

The arc-length techniques are based on the work by Riks (1979) and Wempner (1971). The original technique was elaborated further and made suitable for implementation by Crisfield (1981). The arc-length techniques are now presented in most of the books on non-linear analysis, for example: (Crisfield 1991), (Belytschko, Liu & Moran 2000), (Bittnar & Sejnoha 1996), and (Krenk 1993).

B.2 Terminology

Equilibrium path A graphical representation of a response diagram, the one most used is the load deflection response diagram.

Response diagram A diagram that shows the relation between inputs and outputs. For structures, the most common inputs are the forces and the most common outputs are the displacements or deflections. This type of response should not be confused with the response time history used in dynamics (which involves time).

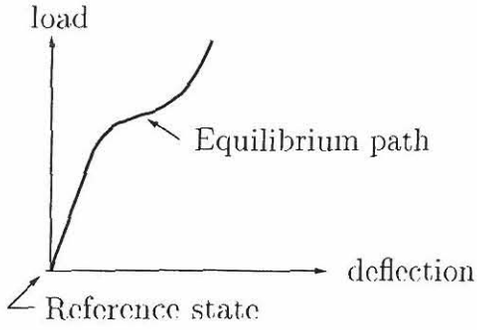

Figure B.1: A load-deflection response diagram.

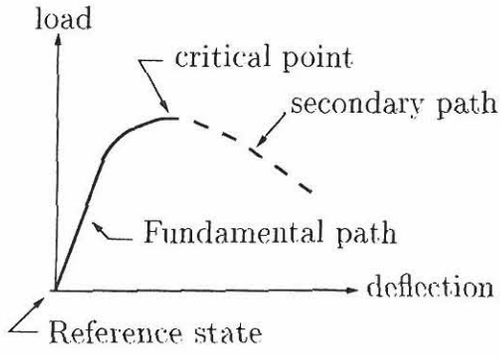

Figure B.2: Fundamental and secondary equilibrium paths.

Equilibrium path A smooth curve in a load-deflection diagram is called a path. If the path represents configurations of equilibrium, it is called an equilibrium path. The fundamental path passes through the reference state, as in figure B.1. Any path that is not a fundamental path but connects with it at a critical point is called a secondary path (figure B.2).

Critical points There are two types: Limit points, at which the tangent to the equilibrium path is horizontal, and bifurcation points, at which two or more equilibrium paths cross.

Turning points Points at which the tangent to the equilibrium path is vertical.

Failure points Points at which a path suddenly stops or breaks because of physical failure.

Tangent stiffness The tangent to an equilibrium path is the tangent stiffness and is the limit of the ratio:

$$\frac{\text{Force increment}}{\text{Displacement increment}} \tag{B.1}$$

The reciprocal ratio is the flexibility or compliance.

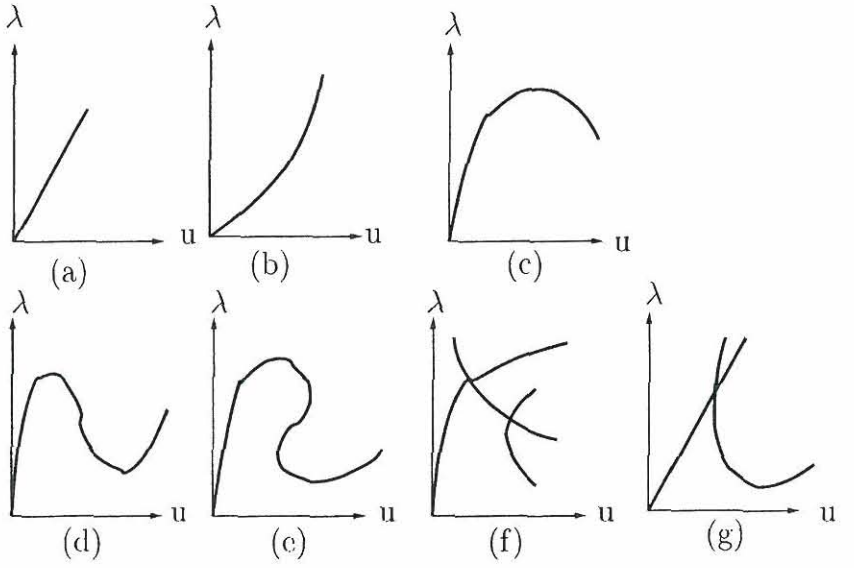

Figure B.3: Flavors of non-linear response: (a) linear until brittle fracture, (b) stiffening or hardening, (c) softening, (d) snap-through, (e) snap-back, (f) bifurcation, (g) bifurcation combined with limit points and snap-back.

Generalized response The load-deflection curve can be generalized to a control state response in which the control parameter, called λ, is plotted along the vertical axis versus the state parameter, called u plotted along the horizontal axis. The term *response* is used in a generalized sense to refer to the control state response. In practice, the control parameter is often a load amplitude or load factor, whereas the state parameter is a displacement amplitude. Some kinds of response are illustrated in figure B.3.

Residual force equations The residual force equations, or residual equations for short, is the algebraic system representing equilibrium of forces at the discrete level. More specifically, for a discrete model coming from the displacement FEM, the equilibrium of nodal forces.

B.3 Residual force equations

B.3.1 Equilibrium equations

Discrete equilibrium equations resulting from non-linear static structural analysis can be presented in compact form as force residual:

$$\mathbf{r}(\mathbf{u}, \lambda) = \mathbf{0} \tag{B.2}$$

The dependence of $\mathbf{r}$ on $\mathbf{u}$ and λ is assumed to be piece-wise smooth so that the first and second derivatives exist (except possibly at critical points). If the system is conservative, $\mathbf{r}$ is the gradient of the total potential energy $\Pi(\mathbf{u}, \lambda)$ for fixed λ:

$$\mathbf{r} = \frac{\partial \Pi}{\partial \mathbf{u}} \tag{B.3}$$

An alternative version of eq. (B.2) is the force-balance form:

$$\mathbf{p}(\mathbf{u}) = \mathbf{f}(\mathbf{u}, \lambda) \tag{B.4}$$

where $\mathbf{p}$ are the configuration-dependent internal forces, and $\mathbf{f}$ are the control-dependent external forces, which may also be configuration-dependent. The residual is:

$$\mathbf{r} = \mathbf{p} - \mathbf{f} \tag{B.5}$$

Expression (B.5) states that the internal forces $\mathbf{p}$ balance the applied forces $\mathbf{f}$.

B.3.2 Stiffness matrix and rate forms

Varying the vector $\mathbf{r}$ with respect to the components of $\mathbf{u}$ while keeping λ fixed, yields the Jacobian matrix $\mathbf{K}$:

$$\mathbf{K} = \frac{\partial \mathbf{r}}{\partial \mathbf{u}} \tag{B.6}$$

The matrix $\mathbf{K}$ is the tangent stiffness matrix. Varying the negative of $\mathbf{r}$ with respect to λ while keeping $\mathbf{u}$ fixed produce:

$$\mathbf{q} = -\frac{\partial \mathbf{r}}{\partial \lambda} \tag{B.7}$$

which is the incremental load vector.

Parametric representation of $\mathbf{u}$ and λ is useful in the description of the solution methods. The general form is:

$$\mathbf{u} = \mathbf{u}(t), \qquad \text{and} \qquad \lambda = \lambda(t) \tag{B.8}$$

where t is a non-dimensional time-like parameter. Derivatives with respect to t will be denoted by superposed dots, as in real dynamics. The first two derivatives of the residual using the chain rule are:

$$\dot{\mathbf{r}} = \mathbf{K}\dot{\mathbf{u}} - \mathbf{q}\dot{\lambda} \tag{B.9}$$

$$\ddot{\mathbf{r}} = \mathbf{K}\ddot{\mathbf{u}} + \dot{\mathbf{K}}\dot{\mathbf{u}} - \mathbf{q}\ddot{\lambda} - \dot{\mathbf{q}}\dot{\lambda} \tag{B.10}$$

The rate forms of eq. (B.2) are obtained by equating (B.9) and (B.10) to zero producing:

$$\mathbf{K}\dot{\mathbf{u}} = \mathbf{q}\dot{\lambda} \tag{B.11}$$

$$\mathbf{K}\ddot{\mathbf{u}} + \dot{\mathbf{K}}\dot{\mathbf{u}} = \mathbf{q}\ddot{\lambda} + \dot{\mathbf{q}}\dot{\lambda} \tag{B.12}$$

At *regular points* of the $(\mathbf{u}, \lambda)$ space, the tangent stiffness is non-singular, then it is possible to solve eq. (B.11) for $\dot{\mathbf{u}}$:

$$\dot{\mathbf{u}} = \mathbf{K}^{-1}\mathbf{q}\dot{\lambda} = \mathbf{v}\dot{\lambda} \tag{B.13}$$

where

$$\mathbf{v} = \mathbf{K}^{-1}\mathbf{q} = \frac{\partial \mathbf{u}}{\partial \lambda} = \mathbf{u}' \tag{B.14}$$

is the incremental velocity vector.

B.4 Solution methods

B.4.1 Introduction

Methods for tracing equilibrium paths are called continuation methods, the basic idea is to follow the equilibrium response of the structure as the control and state parameters vary by small amounts.

The general idea is to divide the task into two stages: incremental steps and iterative steps. If only the incremental steps are present, the method is called a predictor-only method, otherwise it will be called a predictor-corrector method or incremental iterative method.

The predictor always advances in the solution, in the correction phase the drifting error is eliminated or reduced.

Purely corrective methods can be used (without using the predictor phase), if there is only interest in the final results, but the increments can have another purpose, in particular:

1. Help convergence. In order to succeed in the correction, it is necessary to have a good initial guess. The initial guess is given by the predictor, and can be improved by reducing the increment.

2. Avoid extraneous roots. The solution process starts from an easily computable solution, and then it tries to follow the behavior of the system. Small actions applied to the system produce small changes in small steps (the increments). The previous solution is then used as a new starting point for the iterative solution procedure. The underlying prescription is: follow the physics.

3. Insight into structural behavior. The knowledge of the equilibrium path can teach more about the structural behavior than simply knowing the final solution.

4. Critical points may occur before the final solution.

5. Path dependence. The presence of path-dependent effects restricts incremental sizes because of history-tracing constraints. For example, in plasticity analysis, stress states must not be allowed to stay too far outside of the yield surface.

B.4.2 The increment control

Given the solution to the incremental step n, in order to calculate the solution to the step $n+1$, it is necessary to obtain:

$$\Delta \mathbf{u}_n = \mathbf{u}_{n+1} - \mathbf{u}_n, \qquad \Delta\lambda_n = \lambda_{n+1} - \lambda_n \tag{B.15}$$

satisfying the residual equilibrium equations (B.2) to the requested accuracy. The problem is not complete due to the fact that there are less equations than unknowns, which makes the incremental size indeterminate. The problem is closed by adopting an incremental control strategy, expressed as a constraint condition.

$$c(\Delta \mathbf{u}_n, \Delta\lambda_n) = 0 \tag{B.16}$$

A rate form of the constraint equation is obtained by differentiation with respect to t:

$$\dot{c} = \mathbf{a}^T \dot{\mathbf{u}} + g\dot{\lambda} = 0 \tag{B.17}$$

where

$$\mathbf{a}^T = \frac{\partial c}{\partial \mathbf{u}} \qquad \text{and} \qquad g = \frac{\partial c}{\partial \lambda} \tag{B.18}$$

Then, a non-dimensional scalar l is defined that characterizes the size of the increment:

$$c(\Delta \mathbf{u}_n, \Delta\lambda_n) = \Delta\lambda_n - l_n = 0 \tag{B.19}$$

this is called λ-control. When the parameter λ is a loading amplitude, this is called load control. For this case:

$$\mathbf{a}^T = \mathbf{0}, \qquad g = 1 \tag{B.20}$$

B.4.3 Forward Euler integration

From eq. (B.9) when $t \equiv \lambda$:

$$\mathbf{r}' = \mathbf{K}\mathbf{u}' - \mathbf{q} = \mathbf{0} \tag{B.21}$$

where primes denote differentiation with respect to λ. Solving for $\mathbf{u}'$:

$$\mathbf{u}' = \frac{d\mathbf{u}}{d\lambda} = \mathbf{K}^{-1}\mathbf{q} = \mathbf{v} \tag{B.22}$$

given the initial condition

$$\mathbf{u} = \mathbf{u}_0 \qquad \text{at} \qquad \lambda = 0 \tag{B.23}$$

The exact integration of (B.22) into the initial conditions (B.23) is

$$\mathbf{r}(\mathbf{u}, \lambda) = \mathbf{r}_0 = \mathbf{r}(\mathbf{u}_0, 0) \tag{B.24}$$

thus an initial error does not decay, producing the so-called drifting error. The error committed at each step moves the equilibrium point to a neighboring curve.

Using the forward Euler integrator:

$$\mathbf{u}_{n+1} = \mathbf{u}_n + \Delta\lambda\mathbf{u}' \tag{B.25}$$

yields the scheme:

$$\Delta\mathbf{u}_n = \mathbf{K}_n^{-1}\mathbf{q}_n\Delta\lambda_n = \mathbf{v}_n\Delta\lambda_n \tag{B.26}$$

$$\mathbf{u}_{n+1} = \mathbf{u}_n + \Delta\mathbf{u}_n \tag{B.27}$$

B.4.4 Newton methods

Introduction

The purely incremental methods (for example the forward Euler) compute a sequence of values such as: $(\mathbf{u}_0, \lambda_0, \mathbf{u}_1, \lambda_1, \ldots \mathbf{u}_n, \lambda_n, \ldots)$. The corrective methods implement a phase in which one iterates for equilibrium while satisfying the increment constraint. The starting point is the solution predicted by the incremental method.

If the last accepted solution from the incremental step is $(\mathbf{u}_n, \lambda_n)$, the objective is to compute the solution $(\mathbf{u}_{n+1}, \lambda_{n+1})$ that satisfies the non-linear algebraic system

$$\mathbf{r}(\mathbf{u}_{n+1}, \lambda_{n+1}) = \mathbf{0} \tag{B.28}$$

$$c(\Delta\mathbf{u}_n, \Delta\lambda_n) = 0 \tag{B.29}$$

where

$$\Delta \mathbf{u}_n = \mathbf{u}_{n+1} - \mathbf{u}_n, \qquad \Delta \lambda_n = \lambda_{n+1} - \lambda_n \tag{B.30}$$

The predicted solution resulting from the predictor phase is:

$$\mathbf{u}^0_{n+1}, \qquad \lambda^0_{n+1} \tag{B.31}$$

Now, for simplicity, the subscripts will be omitted from the formulas. The conventional Newton method generates a sequence of iterates $\mathbf{u}^k, \lambda^k$, where $k = 1, 2, \ldots$ is an iteration step index.

The conventional Newton method is based on the truncated Taylor expansion of the system $\mathbf{r} = \mathbf{0}$, $c = 0$ about $(\mathbf{u^k}, \lambda^{\mathbf{k}})$:

$$\mathbf{r}^{k+1} = \mathbf{r}^k + \frac{\partial \mathbf{r}}{\partial \mathbf{u}}(\mathbf{u}^{k+1} - \mathbf{u}^k) + \frac{\partial \mathbf{r}}{\partial \lambda}(\lambda^{k+1} - \lambda^k) + O(2) = \mathbf{0} \tag{B.32}$$

$$c^{k+1} = c^k + \frac{\partial c}{\partial \mathbf{u}}(\mathbf{u}^{k+1} - \mathbf{u}^k) + \frac{\partial c}{\partial \lambda}(\lambda^{k+1} - \lambda^k) + O(2) = \mathbf{0} \tag{B.33}$$

where $O(2)$ denotes higher order terms (quadratic or higher in $\mathbf{u}^{k+1} - \mathbf{u}^k$ and $\lambda^{k+1} - \lambda^k$), and all derivatives are evaluated at $(\mathbf{u}^k, \lambda^k)$. Discarding the higher order terms, the linear algebraic system is obtained:

$$\begin{bmatrix} \mathbf{K} & -\mathbf{q} \\ \mathbf{a}^T & g \end{bmatrix} \begin{bmatrix} \mathbf{d} \\ \eta \end{bmatrix} = - \begin{bmatrix} \mathbf{r} \\ c \end{bmatrix} \tag{B.34}$$

where

$$\mathbf{d} = \mathbf{u}^{k+1} - \mathbf{u}^k, \qquad \eta = \lambda^{k+1} - \lambda^k, \qquad \mathbf{K} = \frac{\partial \mathbf{r}}{\partial \mathbf{u}}, \tag{B.35}$$

$$\mathbf{q} = -\frac{\partial \mathbf{r}}{\partial \lambda}, \qquad \mathbf{a}^T = \frac{\partial c}{\partial \mathbf{u}}, \qquad g = \frac{\partial c}{\partial \lambda} \tag{B.36}$$

From eq. (B.34), it is possible to obtain the following scalar equation for η:

$$(g + \mathbf{a}^T \mathbf{K}^{-1} \mathbf{q})\eta = -c + \mathbf{a}^T \mathbf{K}^{-1} \mathbf{r} \tag{B.37}$$

Then

$$\eta = -\frac{c + \mathbf{a}^T \mathbf{d}_r}{g + \mathbf{a}^T \mathbf{d}_q}, \qquad \mathbf{d} = \mathbf{d}_r + \eta \mathbf{d}_q \tag{B.38}$$

where

$$\mathbf{K}\mathbf{d}_r = -\mathbf{r}, \qquad \text{and} \qquad \mathbf{K}\mathbf{d}_q = \mathbf{q} \tag{B.39}$$

The ordinary Newton method and modifications

The ordinary Newton method corresponds to the case of λ or load control. if λ is kept constant, the incremental step constraint is $\Delta\lambda_n = l_n$. System (B.34) reduces to:

$$\begin{bmatrix} \mathbf{K} & -\mathbf{q} \\ \mathbf{0} & 1 \end{bmatrix} \begin{bmatrix} \mathbf{d} \\ \eta \end{bmatrix} = - \begin{bmatrix} \mathbf{r} \\ 0 \end{bmatrix} \tag{B.40}$$

where $c = 0$ because the constraint is satisfied exactly. The Newton iteration reduces to:

$$\mathbf{u}^{k+1} = \mathbf{u}^k - (\mathbf{K}^k)^{-1}\mathbf{r}^k \tag{B.41}$$

$$\lambda^{k+1} = \lambda^k = \lambda_n + l_n \qquad \text{(kept fixed)} \tag{B.42}$$

This method has a high cost, because the tangent stiffness matrix $\mathbf{K}^k$ has to be formed and factored at each iteration step. The method has a low reliability because the desired solution is not guaranteed unless the initial estimate is sufficiently close.

The problem of high cost per step can be alleviated if the same stiffness matrix is maintained for several iteration steps. This general class of methods is known as chord methods, and is based on the iteration scheme:

$$\begin{bmatrix} \bar{\mathbf{K}} & -\bar{\mathbf{q}} \\ \mathbf{0} & 1 \end{bmatrix} \begin{bmatrix} \mathbf{d} \\ \eta \end{bmatrix} = - \begin{bmatrix} \mathbf{r} \\ 0 \end{bmatrix} \tag{B.43}$$

where $\bar{\mathbf{K}}$ and $\bar{\mathbf{q}}$ denote an approximation to $\mathbf{K}$ and $\mathbf{q}$ in some sense, which is kept fixed for several or all iteration steps.

The modified Newton method results when $\bar{\mathbf{K}} = \mathbf{K}_n$, which is the stiffness matrix at the start of the increment.

The quasi-Newton methods emerge when the stiffness $\bar{\mathbf{K}}$ is updated at each iteration step with rank one or rank two matrices built up from information from the previous iteration. In this way a better approximation of the actual stiffness matrix is obtained while still avoiding re-evaluation and factorization.

Newton method in the context of a dynamic system

The process of finding approximations to the equilibrium path has been viewed as a process in which first every incremental step is followed by corrective steps to eliminate the drift error (see figure B.4).

The incremental phase is driven by the rate form $\dot{\mathbf{r}} = \mathbf{0}$. If the drift error is penalized by adding a term proportional to the residual $\mathbf{r}$:

$$\dot{\mathbf{r}} + \mathbf{W}\mathbf{r} = \mathbf{0} \tag{B.44}$$

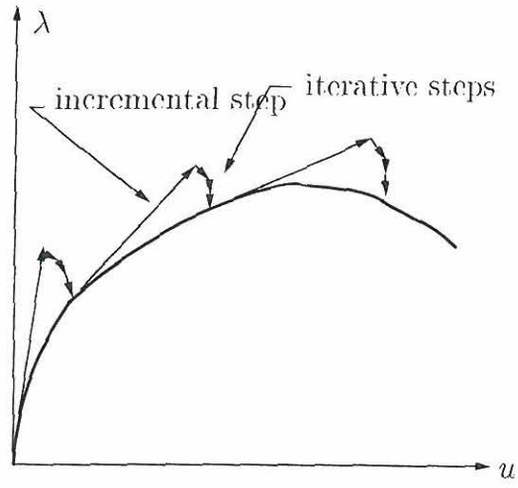

Figure B.4: An incremental iterative solution method.

where $\mathbf{W}$ is a positive definite residual weighting matrix. The job of the penalty term $\mathbf{Wr}$ is to force the solution trajectories to approach $\mathbf{r} = \mathbf{0}$ as the corrective steps are performed.

Inserting eq. (B.9) in (B.44) and recalling eq. (B.17), the corrective equation can be generalized as:

$$\begin{bmatrix} \mathbf{K}\dot{\mathbf{u}} + \mathbf{W}\mathbf{r} \\ \mathbf{a}^T\dot{\mathbf{u}} + g\dot{\lambda} \end{bmatrix} = \begin{bmatrix} \mathbf{q}\dot{\lambda} \\ 0 \end{bmatrix} \tag{B.45}$$

with the forward Euler integrator:

$$\mathbf{u}^{k+1} = \mathbf{u}^k + h^k\dot{\mathbf{u}}^k, \qquad \lambda^{k+1} = \lambda^k + h\dot{\lambda}^k \tag{B.46}$$

where h is the integration step length. Integrating (B.45) into (B.46), followed by setting $\mathbf{W} = \mathbf{I}$ and $h = 1$, yields the conventional Newton method. The reason to variate the value of h is to accelerate the convergence to equilibrium, schemes that utilize non-unitary step sizes are called accelerators.

Termination tests

Several convergence criteria can be applied to the Newton method; some of these are:

1. Displacement convergence test: The change in the last correction $\mathbf{d}$ of the state vector $\mathbf{u}$ should not exceed a given tolerance ϵ_d for example:

$$\|\mathbf{d}\| = \sqrt{\mathbf{d}^T\mathbf{d}} \leq \epsilon_d \tag{B.47}$$

2. Residual convergence test:

$$\|\mathbf{r}\| \leq \epsilon_r \tag{B.48}$$

3. Combining the last two criteria using 'and' or 'or'.

4. Combining both tests in the form of a work change criterion:

$$|\mathbf{r}^T\mathbf{d}| \leq \epsilon_d\epsilon_r \tag{B.49}$$

Since $\mathbf{d}$ and $\mathbf{r}$ usually have physical dimensions, so do necessarily ϵ_d and ϵ_r. It is desirable to work with ratios that render the ϵ_d and ϵ_r non-dimensional, for example:

$$\frac{\|\mathbf{r}\|}{\|\mathbf{r}^0\|} \leq \epsilon_r, \qquad \text{and} \qquad \frac{\|\mathbf{d}\|}{\|\mathbf{u}^0\|} \leq \epsilon_d \tag{B.50}$$

where $\mathbf{r}^0$ is the residual after the predictor step, and $\mathbf{u}^0$ is the total or accumulated displacement.

The Newton iteration is not guaranteed to converge, divergence will be diagnosed if either of the following inequalities occurs:

$$\frac{\|\mathbf{r}\|}{\|\mathbf{r}^0\|} \geq g_r, \qquad \text{and} \qquad \frac{\|\mathbf{d}\|}{\|\mathbf{u}^0\|} \geq g_d \tag{B.51}$$

where g_r and g_d are divergence factors. For example $g_r = g_d = 1000$.

Occasionally the iterations will neither diverge nor converge, so it is a good practice to define a maximum number of iterations into each step.

B.4.5 Arc-length control

Introduction

In section B.4.2 it was stated that in order to solve the problem, it was necessary to adopt an incremental control strategy, expressed as a constraint condition eq. (B.16). The load control was presented in that section. Other alternatives of control can be seen in figure B.5 for the special case of a sigle degree of freedom problem.

Before stating the mathematics of this control strategy, it is necessary to introduce the scaling used. There are two reasons for scaling the equations: first, because $\mathbf{r}$ has two types of arguments: $\mathbf{u}$ and λ, the first has physical dimensions, the second is non-dimensional; second, because $\mathbf{u}$ may have heterogeneous physical dimensions -for example translations and rotations.

A scaling of the vector $\mathbf{u}$ to make it non-dimensional is:

$$\tilde{\mathbf{u}} = \mathbf{S}\mathbf{u} \tag{B.52}$$

where $\mathbf{S}$ is a diagonal matrix, and a superposed $\tilde{()}$ identifies a scaled quantity.

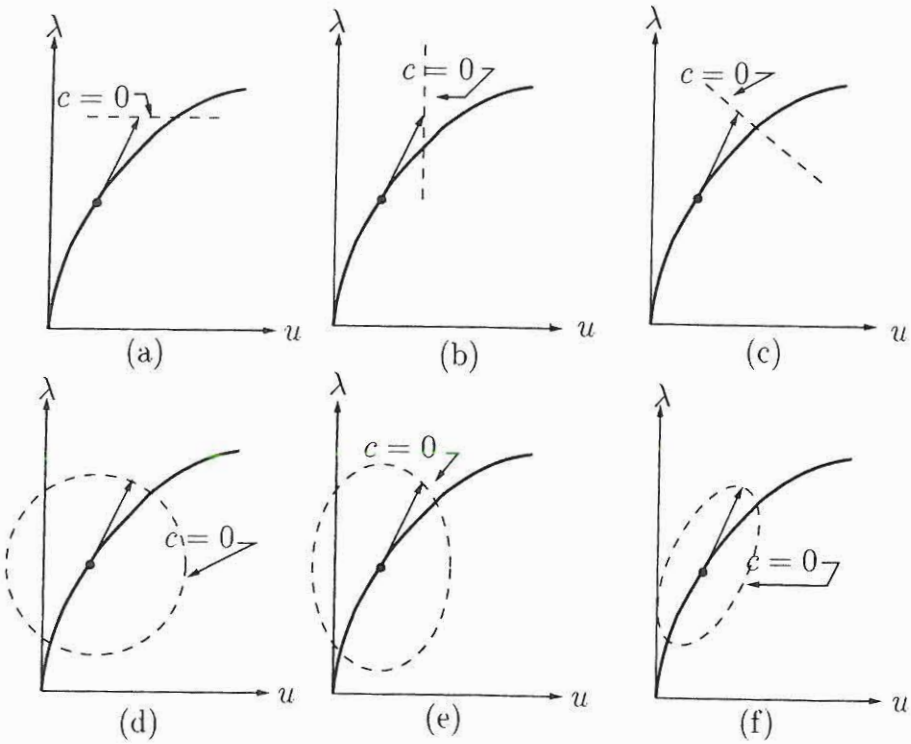

Figure B.5: Geometric representation of constraints for a single degree of freedom, problem. (a)load control, (b) state control, (c) arc-length control, (d) hyper spherical control, (e) global hyper elliptical control, and(f) local hyper elliptic control.

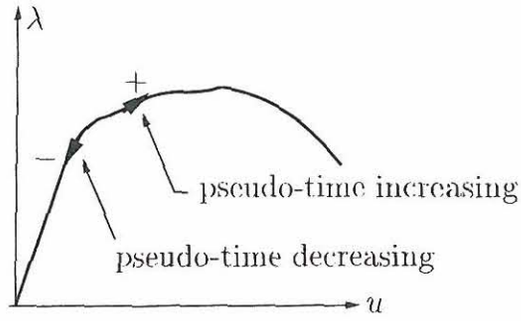

Figure B.6: Positive and negative traverse senses on a path.

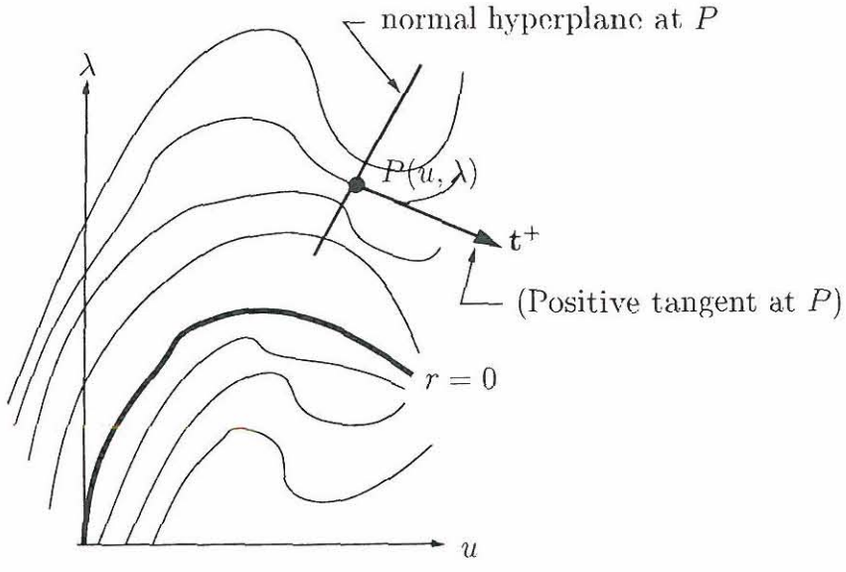

Figure B.7: A family of constant residual trajectories.

Geometry of incremental flow

Considering the fundamental path in a response curve, it is possible to observe that it can be traversed in two directions, see figure B.6. The positive direction is the one associated with increasing values of pseudo-time, when the path is parametrically described as $\mathbf{u} = \mathbf{u}(t)$ and $\lambda = \lambda(t)$.

Considering the perturbed equilibrium path described by the residual equation:

$$\mathbf{r}(\mathbf{u}, \lambda) = \mathbf{r}_c \tag{B.53}$$

where $\mathbf{r}_c$ is a constant vector. The vector $\mathbf{r}_c$ is obtained as the solution of $\dot{\mathbf{r}} = \mathbf{0}$. The residual paths are illustrated in figure B.7. A family of constant residual trajectories is collectively known as incremental flow.

At a point P not necessarily on the equilibrium path, the normalized unit tangent vector $\mathbf{t}$ is defined as:

$$\mathbf{t} = \frac{1}{f}\begin{bmatrix}\mathbf{v}\\ 1\end{bmatrix} \tag{B.54}$$

where f is the scaling factor:

$$f = \sqrt{1 + \mathbf{v}^T\mathbf{v}} \tag{B.55}$$

The hyper plane normal to $\mathbf{t}$ at $P(\mathbf{u}, \lambda)$ is:

$$\mathbf{v}^T\Delta\mathbf{u} + \Delta\lambda = 0 \tag{B.56}$$

where $\Delta\mathbf{u} = \mathbf{u} - \mathbf{u}_P$ and $\Delta\lambda = \lambda - \lambda_P$ are increments from P. Dividing these increments by Δt and passing to the limit:

$$\mathbf{v}^T\dot{\mathbf{u}} + \dot{\lambda} = 0 \tag{B.57}$$

the left-hand side of eq. (B.56) normalized on dividing through by f is:

$$\Delta s = \frac{1}{f}(\mathbf{v}^T\Delta\mathbf{u} + \Delta\lambda) \tag{B.58}$$

where Δs is the signed distance from the normal hyper plane at P to a point $Q(\delta\mathbf{u}, \Delta\lambda)$. For small increments Δs may be considered an approximation of the arc-length s of the path that passes through P because

$$ds = \frac{1}{f}(\mathbf{v}^T d\mathbf{u} + d\lambda) \tag{B.59}$$

The scaled versions of the quantities defined for the arc-legnth are:

$$\Delta\tilde{\mathbf{u}} = \mathbf{S}\Delta\mathbf{u} \qquad \tilde{\mathbf{q}} = \mathbf{s}^{-1}q \qquad \tilde{\mathbf{K}} = \mathbf{S}^{-1}\mathbf{K}\mathbf{S}^{-1} \tag{B.60}$$

$$\tilde{\mathbf{v}} = \mathbf{S}\mathbf{v} \qquad \tilde{f} = \sqrt{1 + \tilde{\mathbf{v}}^T\tilde{\mathbf{v}}} \qquad \tilde{\mathbf{t}} = \frac{1}{\tilde{f}}\begin{bmatrix}\tilde{\mathbf{v}}\\ 1\end{bmatrix} \tag{B.61}$$

$$\Delta\tilde{s} = \frac{1}{\tilde{f}}(\tilde{\mathbf{v}}^T\Delta\tilde{\mathbf{u}} + \Delta\lambda) \tag{B.62}$$

Constraint strategies

The state control consists of specifying a norm of $\Delta \mathbf{u}_n$, for example:

$$c(\Delta \mathbf{u}_n) = \Delta \mathbf{u}_n^T \Delta \mathbf{u}_n - l_n u^2 = 0 \tag{B.63}$$

or using the scaled increment:

$$\Delta \tilde{\mathbf{u}}_n^T \Delta \tilde{\mathbf{u}}_n - l_n = 0 \tag{B.64}$$

consequently:

$$\mathbf{a}^T = 2\Delta \mathbf{u}_n, \qquad g = 0. \tag{B.65}$$

Arc-length control consists of specifying a distance $\|\Delta s\| = l$ along the path tangent. The constraint is:

$$c(\Delta \mathbf{u}_n, \Delta \lambda_n) = |\Delta s_n| - l_n = \frac{1}{f_n} |\mathbf{v}_n^T \Delta \mathbf{u} + \Delta \lambda_n| - l_n = 0 \tag{B.66}$$

using the forward Euler method, substitution in equation (B.26) yields

$$\Delta \lambda_n^0 = \pm \frac{l_n}{f_n}, \qquad \Delta \mathbf{u}_n^0 = \pm \frac{\mathbf{v}_n l_n}{f_n} \tag{B.67}$$

and produces:

$$\mathbf{a}^T = \frac{\mathbf{v}_n}{f_n}, \qquad g = \frac{1}{f_n} \tag{B.68}$$

Geometrically this equation represents a hyper plane normal to $\mathbf{t}$, located at a distance l_n from the last solution point. The scaled form is:

$$\Delta \tilde{s} - l_n = 0 \tag{B.69}$$

and

$$\mathbf{a}^T = \frac{\mathbf{v}_n \mathbf{S}^2}{\tilde{f}_n}, \qquad g = \frac{1}{\tilde{f}_n} \tag{B.70}$$

The global hyper-elliptic control uses the constraint

$$a_n^2 \Delta \tilde{\mathbf{u}}_n^T \Delta \tilde{\mathbf{u}}_n + b_n^2 (\Delta \lambda_n)^2 = l_n^2 \tag{B.71}$$

where a and b are scalars which may not be zero simultaneously.

The arc-length control solution

The following forward Euler incremental scheme is obtained from section B.4.5:

$$\begin{aligned}
\mathbf{v}_n &= \mathbf{K}_n^{-1}\mathbf{q}_n \\
f_n &= \sqrt{1+\mathbf{v}_n^T\mathbf{v}_n} \\
\Delta\lambda_n &= \pm\frac{l_n}{f_n} \\
\mathbf{u}_{n+1} &= \mathbf{u}_n + \mathbf{v}_n\delta\lambda_n \\
\lambda_{n+1} &= \lambda_n + \Delta\lambda_n
\end{aligned}$$

Then it is possible to obtain two solutions, depending on the sign of $\Delta\lambda$, the ambiguity comes from the fact that the tangent at a point in an equilibrium path can have two directions, and these can intersect the constraint hyper-surface at minimum in two points. Two different strategies to choose the sign are proposed: the first requires that the external work over the predictor step is positive

$$\Delta W = \mathbf{q}^T\Delta\mathbf{u}_n^0 = \mathbf{q}^T\mathbf{v}_n\Delta\lambda_n > 0 \tag{B.72}$$

i.e., $\Delta\lambda$ should have the sign of $\mathbf{q}^T\mathbf{v} = \mathbf{q}^T\mathbf{K}^{-1}\mathbf{q}$.

The second criterion appears because sometimes it is necessary for the structure to release external work to continue along the equilibrium path. In that case, a condition on the angle of the prediction vector is more effective; therefore choose the positive sense so that:

$$\mathbf{t}_n^T\mathbf{t}_{n-1} > 0 \tag{B.73}$$

To set the magnitude of l_n, two possibilities exist. Either l_n is kept constant equal to l_0, or it may be automatically adjusted, Crisfield (1991) recommends:

$$l_n = l_{n-1}\left(\frac{I_d}{I_{n-1}}\right)^{1/2} \tag{B.74}$$

where I_d is the input desired number of iterations in the corrective phase, and I_{n-1} is the number of iterations required in the corrective phase in the last step. It is also recommended that a minimum and a maximum arc-length condition be defined such that:

$$l_{\min} \le l_n \le l_{\max} \tag{B.75}$$

It is possible to use:

$$l_{\min} = \frac{l_0}{l_{fac}}, \qquad l_{\max} = l_0 l_{fac} \tag{B.76}$$

At $\lambda = 0$ it is known that $\mathbf{u} = \mathbf{u}_0$. It is desired to advance until the norm of $\mathbf{u}$ exceeds $u_{\max}$, the magnitude of λ exceeds $\lambda_{\max}$, the number of incremental steps exceeds $n_{\max}$ or an impassable bifurcation point is reached. Parameter l_0 is specified. Set $n = 0$ and perform the following steps:	
Step 1	Form and factor $\mathbf{K}_n$. If the factorization fails, perturb $\mathbf{u}$ by a tiny amount and repeat. If this failure repeats after a certain number of tries, stop.
Step 2	Form $\mathbf{q}_n$, and solve $\mathbf{K}_n\mathbf{v}_n = \mathbf{q}_n$. Form f_n.
Step 3	Adjust l_n (or keep $l_n = l_0$). Set $\Delta\lambda_n = l_n/f_n$, give the sign of $\mathbf{q}_n^T\mathbf{v}_n$
Step 4	Compute $\Delta\mathbf{u}_n = \mathbf{v}_n\Delta\lambda_n$. Advance $\mathbf{u}_{n+1} = \mathbf{u}_n + \Delta\mathbf{u}_n$ and $\lambda_{n+1} = \lambda_n + \delta\lambda_n$.
Step 5	If $\lvert\mathbf{u}_{n+1}\rvert > u_{\max}$, or $\lvert\lambda_{n+1} > \lambda_{\max}$, or $n > n_{\max}$, stop. Else set $n \leftarrow n+1$ and return to Step 1.

Table B.1: Arc - length controlled Incremental Solution. Forward Euler Procedure.

where l_{fac} is typically 1 to 20.

The algorithm for the solution for the predictor phase using the Forward Euler Procedure is shown in table B.1.

In order to determine l_0, a possibility is to start with a load controlled step, and from the output estimate a suitable l_0.

Bibliography

Belytschko, T., Liu, w. K. & Moran, B. (2000), *Nonlinear finite elements for continua and structures*, John Wiley, New York.

Bittnar, Z. & Sejnoha, J. (1996), *Numerical methods in structural mechanics*, ASCE press, Thomas telford.

Crisfield, M. A. (1981), 'A fast incremental-iterative solution procedure that handles "snap-through"', *Computers and Structures* **13**, 55–62.

Crisfield, M. A. (1991), *Non-linear Finite Element analysis of Solids and Structures*, Vol. Volume 1: essentials, John Wiley and Sons, Chichester.

Krenk, S. (1993), *Non-Linear Analysis with finite elements*, Aalborg University, Aalborg, Denmark.

Riks, E. (1979), 'An incremental approach to the solution of snapping and buckling problems', *Int. J. Solids and Structs* **15**, 529–551.

Wempner, G. A. (1971), 'Discrete approximations related to nonlinear theories of solids', *Int. J. Solids and structs* **7**, 1581–1599.

Appendix C

Review of some documents on higher-order theories

Contents

C.1 Introduction

This document presents a review of papers read by the author as part of his Ph.D. studies related to higher-order theories used in elasticity and plasticity. Here the term Higher-Order theories will be used to refer to the group of theories that in some way introduce an explicit length scale in the continuum mechanics theory.

C.2 Roderick Lakes

Roderick Lakes has written several papers related to non-local theories. Lakes works with the Department of Engineering Physics, of the Engineering Mechanics Program at the University of Wisconsin-Madison.

C.2.1 Experimental methods for the study of Cosserat elastic solids and other generalized continua

The author found this article (Lakes 1995) useful as a point of departure to study non-local theories in that it presents a comparison of different non-local theories relevant to elasticity, giving emphasis on differences between those theories and classical elasticity. Lakes presents possible strategies to experimentally obtain the necessary elastic constants.

The treatment presented in Lakes's paper is restricted to elastic behavior.

Constitutive equations

From the point of view of elasticity, he presents the constitutive equations:

Uniconstant elasticity. This theory by Navier was used in the early days of the theory of elasticity. The constitutive equation is:

$$\sigma_{kl} = G\varepsilon_{rr}\delta_{kl} + 2G\varepsilon_{kl} \tag{C.1}$$

where σ_{ij} is the stress tensor, ε_{ij} is the strain tensor, G is the shear elastic modulus and δ_{kl} is Kronecker's delta.

Classical Elasticity. The constitutive equation is:

$$\sigma_{kl} = \lambda\varepsilon_{rr}\delta_{kl} + \mu\varepsilon_{kl} \tag{C.2}$$

where λ an μ are the Lame constants.

Cosserat(micropolar) Elasticity. The Cosserat theory (Cosserat & Cosserat 1909) incorporates a local rotation of points as well as the translation; and a couple stress (a torque per unit area) as well as the force stress. The idea of a couple stress could be traced to Voigt (1887) and Voigt (1894). In more recent years, theories incorporating couple stresses were developed (Eriksen & Truesdell 1958); (Grioli 1960); (Aero & Kuvshinskii 1961); (Toupin 1962); (Mindlin & Tiersten 1962); (Mindlin 1965*b*); (Eringen 1968); (Nowacki 1970). A survey of the interrelation between generalized continuum analysis and material defects, dislocations and other inhomogeneities was presented by Kunin (1982), Kunin (1983) and Eringen (1968). Lakes indiscriminately uses the terms Cosserat elasticity and micropolar elasticity.

In the isotropic Cosserat solid there are six elastic constants. The constitutive equations using the symbols by Eringen (1968) are:

$$\sigma_{kl} = \lambda\varepsilon_{rr}\delta_{kl} + (2\mu + \kappa)\varepsilon_{kl} + \kappa\varepsilon_{klm}(r_m - \phi_m) \tag{C.3}$$

$$m_{kl} = \alpha\phi_{r,r}\delta_{kl} + \beta\phi_{k,l} + \gamma\phi_{l,k} \tag{C.4}$$

where m_{ij} are the couple stress and λ, μ, κ, α, β and γ are elastic constants. In eq.(C.3) σ_{kl} is asymmetric. The microrotation ϕ_k is distinct from the macrorotation $r_k = (e_{klm}u_{m,l})/2$ obtained from the displacement gradient. The following technical constants are more beneficial in terms of physical insight (Gauthier & Jahsman 1975):

Young's modulus $E = (2\mu + \kappa)(3\lambda + 2\mu + \kappa)/(2\lambda + 2\mu + \kappa)$
Shear modulus $G = (2\mu + \kappa)/2$
Poisson's ratio $\nu = \lambda/(2\lambda + 2\mu + \kappa)$
Characteristic length for torsion $l_t = [(\beta + \gamma)/(2\mu + \kappa)]^{1/2}$
Characteristic length for bending $l_b = [\gamma/2(2\mu + \kappa)]^{1/2}$
Coupling number $N = [\kappa/2(\mu + \kappa]^{1/2}$
Polar ratio $\Psi = (\beta + \gamma)/(\alpha + \beta + \gamma)$

The case N=1 (its upper bound) is known as "couple stress theory" (Mindlin & Tiersten 1962); (Cowin 1970) the limit $\kappa \to 0$ presents physical difficulties (Lakes 1985).

Void elasticity. This theory is relevant for the work of Lakes because his main work is in analysis of foams, and in this context, this theory could be important. Constitutive equations (Cowin & Nunziato 1983):

$$\sigma_{kl} = \lambda\varepsilon_{rr}\delta_{kl} + 2\mu\varepsilon_{kl} + \beta\phi\delta_{kl} \tag{C.5}$$

$$h_k = \alpha\phi_{,k} \tag{C.6}$$

$$g = -\xi\phi - \beta\varepsilon_{rr} \tag{C.7}$$

where h_k is the equilibrated stress vector, λ and μ are the classical Lame elastic constants, g is the intrinsic equilibrated body force, ϕ change of volume fraction, which can be interpreted as a dilatation of points in the continuum.

Nonlocal Elasticity. The points can only undergo translational motion as in the classical case, but the stress at a point depends on the strain in a region near that point (Kröner 1967), (Eringen 1972). Constitutive equations in terms of the position vector $\mathbf{x}$:

$$\sigma_{ij}(\mathbf{x}) = \int_V \Big[\lambda(|\mathbf{x}' - \mathbf{x}|)\varepsilon_{rr}(\mathbf{x}')\delta_{ij} + 2\mu(|\mathbf{x}' - \mathbf{x}|)\varepsilon_{ij}(\mathbf{x}')\Big] dV(\mathbf{x}') \tag{C.8}$$

where $\mathbf{x}'$ is the position of all points around $\mathbf{x}$.

A simpler alternative representation is (Eringen 1981):

$$\sigma_{ij}(\mathbf{x}) = \int_V \alpha(|\mathbf{x}' - \mathbf{x}|)[\lambda\varepsilon_{rr}(\mathbf{x}')\delta_{ij} + 2\mu\varepsilon_{ij}(\mathbf{x}')dV(\mathbf{x}') \tag{C.9}$$

with the nonlocal kernel $\alpha(|\mathbf{x}|)$ subject to:

$$\int_V \alpha(|\mathbf{x}|)dV = 1 \tag{C.10}$$

Characteristic lengths can be defined in nonlocal elasticity, in terms of the effective range associated with a Kernel. (A modified kernel is presented in section C.10).

Microstructure (micromorphic) Elasticity. (Mindlin 1965*b*) (Eringen 1968), the points can deform microscopically as well as translate and rotate. There are 18 elastic constants in the isotropic case.

The constitutive equations are:

$$\tau_{pq} = \lambda\delta_{pq}\varepsilon_{ij} + 2\mu\varepsilon_{pq} + g_1\delta_{pq}\gamma_{ii} + g_2(\gamma_{pq} + \gamma_{qp}) \tag{C.11}$$

$$\sigma_{pq} = g_1\delta_{pq}\gamma_{ii} + 2g_2\varepsilon_{pq} + b_1\delta_{pq}\gamma_{ii} + b_2\gamma_{pq} + b_3\gamma_{pq} \tag{C.12}$$

$$\begin{aligned}\mu_{pqr} = {} & a_1(\xi_{iip}\delta_{qr} + \xi_{rii}\delta_{pq}) + a_2(\xi_{iiq}\delta_{pr} + \xi_{iri}\delta_{pq}) + \\ & + a_3\xi_{iir}\delta_{pq} + a_4\xi_{pii}\delta_{qr} + a_5(\xi_{qii}\delta_{pr} + \xi_{ipi}\delta_{qr}) + a_8\xi_{iqi}\delta_{pr} + \\ & + a_{10}\xi_{pqr} + a_{11}(\xi_{rpq} + \xi_{qrp}) + a_{13}\xi_{prq} + a_{14}\xi_{qpr} + a_{15}\xi_{rqp}\end{aligned} \tag{C.13}$$

where τ_{pq} is the symmetric Cauchy stress, σ_{pq} is the asymmetric relative stress, and μ_{pqr} is the double stress. The asymmetric part with respect to the last two indices of the double stresses represents the couple stresses. γ is the macrodeformation minus the microdeformation, ξ is the microgradient of microdeformation, the asymmetric part of which corresponds to rotation gradient in Cosserat's theory.

Microstructure elasticity includes Cosserat elasticity and the theory of voids as special cases.

Consequences of constitutive equations

The uniconstant theory predicts a Poisson ratio of $1/4$ for all materials, this theory was rejected based on experimental measurements of Poisson's ratio.

Classical elasticity predicts:

1. The rigidity of circular cylindrical bars of diameter d in tension goes as d^2, in bending and in torsion goes as d^4.
2. Plane waves in an unbound medium propagate without dispersion.
3. There is no length scale, the effect of inhomogeneities only depends on the shape of the inhomogeneity, not on its size.
4. Poisson's ratio can have values in the range $-1 < \nu < 1/2$

Cosserat elasticity has the following consequences:

1. A size effect is predicted in torsion of circular cylinders, slender cylinders appear more stiff than expected classically. A similar effect is predicted in bending of plates and beams. No size effect is predicted in tension.
2. The stress concentration factor for a circular hole is smaller than the classical value. Stress concentration around a rigid inclusion is greater.
3. Dilatational waves propagate without dispersion, shear waves propagate dispersively. A new kind of wave associated with the microrotation exists.
4. The mode structure of vibrating bodies is modified.
5. Poisson's ratio can have values in the range $-1 < \nu < 1/2$
6. In noncentrosymmetric (or Chiral) bodies, a rod under tensile load deforms in torsion. Wave speed depends on the wave of polarization.

Void elasticity gives rise to the following:

1. Size effects are predicted in bending of rods, but not in torsion or tension.
2. The stress concentration factor for a hole is greater than the classical value.
3. Dilatational waves propagate dispersively. Shear waves exhibit no dispersion.

Microstructure elasticity gives rise to the following:

1. Dispersion of dilatational and shear waves occurs.
2. The stress concentration factor for a hole can be greater than the classical value.

Nonlocal elasticity gives rise to the following:

1. The stress concentration near a crack is alleviated.

2. Dispersion of elastic waves is predicted.

3. Size effects are predicted in tension and bending. For certain short range nonlocal behaviors, these size effects can be thought of as surface or "skin" effects.

Further consequences of constitutive equations

Cosserat solid. Considering bending of a Cosserat beam, size effects are predicted in which slender bars are stiffer than expected using classical elasticity (in bending).

Nonlocal solid. According to Chirita (1978), for both tension and bending, the displacement field is identical to the classical one. Nonlocal elasticity predicts no shape changes in comparison with classical elasticity for bending.

Lakes developed the problem of simple tension. He found: To first order there is no size effect in tension, however, to second order there will be a size effect as a result of influence of the boundaries. When Lakes considered the problem of a unidimensional bending, he found that there is a surface layer of depth a in which the stress is less than $E\varepsilon$. Such a surface effect has a negligible effect on the rigidity if $a \ll W$ where a is characteristic length and W is the depth of the cross-section of the bar. This effect becomes progressively more important for thinner slabs, since the stiffness is smaller for a slender specimen than for a thick one. Depending on the kernel, it is deduced from the equations presented by Lakes that the size effects could produce softening or stiffening effects on thin specimens.

In bending, nonlocal size effects are encountered as linear, while in Cosserat solids, size effect is not linear in bending.

Physical causes of mechanical behavior

The couple stresses in Cosserat and microstructure elasticity represent spatial averages of distributed moments per unit area. Such moments can occur as a result of the fact that interatomic forces propagate further than one atomic spacing (Kröner 1967). Such effects occur in *all* solids, but the corresponding characteristic lengths would be of atomic scale and not amenable to macroscopic mechanical experiment. Moments may also be transmitted on a much larger scale through fibers in fiber reinforced materials, or in the cell ribs or walls in cellular solids. The Cosserat characteristic lengths would then be associated with the physical size scales in the microstructure, and be sufficiently large to observe experimentally.

The nonlocal theory incorporates long-range interactions between particles in a continuum model. Such long-range interactions occur between charged atoms or molecules in a solid. Long-range forces may also be considered to propagate along fibers or laminae in composite material.

The final part of this paper is dedicated to the study of experimental procedures for Cosserat elastic solids. Lakes presents possible ways to obtain the elastic constants and characteristic lengths experimentally.

Discussion

Continuum theories are available with a range of complexity. The degree of complexity, which, is appropriate, depends on what kinds of experiments are done and how carefully we wish to examine the material response. Size effects predicted by Cosserat theory can involve apparent torsional or bending stiffness tending to infinity as the specimen thickness tends to zero. It is possible that a new, additional freedom of the microstructure theory would be required for a better description of bending.

Conclusions

Size effects for Cosserat and nonlocal elastic solids are predicted to differ.

The continuum theory of voids does not adequately describe the microelastic effects observed in cellular solids with solid volume fraction less than 0.5.

C.2.2 Lakes and Benedict, 1982

A solid which is isotropic with respect to coordinate rotations but not with respect to inversions is called noncentrosymmetric, acentric, or chiral (Lakes & Benedict 1982). In Cosserat elasticity, chirality has an effect. A chiral Cosserat solid has 9 elastic constants. The chiral Cosserat solid is predicted to undergo torsional deformation when subjected to tensile load. Thus chiral solids have mechanical behavior which is different from solids with a center of symmetry.

Introduction

Common to generalized continuum mechanics theories is the assumption of couple stress and the associated asymmetry of the force stress tensor. The predictions of size effects in the apparent stiffness of a cylindrical member in torsion and in bending are of particular interest. Usually, material isotropy is assumed, but some materials are not invariant to coordinate inversion, structural noncentrosymmetry is characteristic of bone (material investigated by Lakes) as well as synthetic composites containing twisted fibers.

Noncentrosymmetric micropolar theory

In classical elasticity, inversion symmetry has no effects as shown:

$$C_{ijkl} = \frac{\partial x_m}{\partial x_i}\frac{\partial x_n}{\partial x_j}\frac{\partial x_o}{\partial x_k}\frac{\partial x_p}{\partial x_l}C_{mnop} \tag{C.14}$$

$$C_{ijkl} = (-1)\delta_{im}(-1)\delta_{jn}(-1)\delta_{ok}(-1)\delta_{pl}C_{mnop} = (-1)^4 C_{ijkl} = C_{ijkl} \tag{C.15}$$

Tensors of odd rank are zero if there is inversion symmetry, and can only be nonzero if there is handedness. Examples include strain gradient elastic theories which are governed by a fifth order tensor.

In an anisotropic Cosserat solid, the constitutive equations correspond to eq. (C.3) and eq. (C.4).

The microrotation ϕ_k is kinematically distinct from the macrorotation $r_k = (e_{klm}u_{m,l})/2$ the first refers to the rotation of points themselves, while the second refers to the rotation associated with movement of nearby points.

The free energy density for general anisotropy is:

$$Y = A_o + A_{kl}e_{kl} + \tfrac{1}{2}A_{klmn}e_{kl}e_{mn} + B_{kl}\phi_{k,l} + \tfrac{1}{2}B_{klmn}\phi_{k,l}\phi_{m,n} + C_{klmn}e_{kl}\phi_{m,n} \quad \text{(C.16)}$$

$$e_{kl} = e_{kl} + e_{klm}(r_m - \phi_m) \quad \text{(C.17)}$$

Rewriting eq. (C.3) and eq. (C.4) in terms of the macrostrain for the noncentrosymmetric but isotropic material:

$$\sigma_{kl} = \lambda e_{rr}\delta_{kl} + (2\mu + \kappa)e_{kl} + \kappa e_{klm}(r_m - \phi_m) + \\ + C_1\frac{\partial \phi_r}{\partial x_r}\delta_{kl} + C_2\frac{\partial \phi_k}{\partial x_l} + C_3\frac{\partial \phi_l}{\partial x_k} \quad \text{(C.18)}$$

$$m_{kl} = \alpha\frac{\partial \phi_r}{\partial x_r}\delta_{kl} + \beta\frac{\partial \phi_k}{\partial x_l} + \gamma\frac{\partial \phi_l}{\partial x_k} + C_1 e_{rr}\delta kl + \\ + (C_2 + C_3)e_{kl} + (C_3 - C_2)e_{klm}(r_m - \phi_m) \quad \text{(C.19)}$$

Elastic constants C_1, C_2 and C_3 are associated with noncentrosymmetry; if these vanish, the equations (C.3) and (C.4) of isotropic micropolar elasticity are recovered.

Restrictions on micropolar elastic moduli

It is necessary that the internal energy be nonnegative, this produces limitations on the coefficients. The C coefficients associated with a noncentrosymmetry are bound by products of combinations of classical elastic and micropolar coefficients.

Simple tension

Consider a cylindrical rod of radius R, of a noncentrosymmetric micropolar elastic solid. This cylinder is subjected to a force F, and free of rotational constraint. The following field of displacement and microrotation gives rise to a solution. Here I is the modified Bessel function of first order.

Displacement field:

$$u_z = ez \quad \text{(C.20)}$$

$$u_r = -e\left(V_o r + A_9\left[C_1 + C_2 + \frac{C_3}{e(\lambda - 2\mu + \kappa)I_1(pr)}\right]\right) \tag{C.21}$$

$$\phi_z = b_o r z \tag{C.22}$$

Microrotation field:

$$\phi_z = b_o z \tag{C.23}$$

$$\phi_r = A_9 I_1(pr) - b_o(r/2) \tag{C.24}$$

$$\phi_\theta = 0 \tag{C.25}$$

where e, b_0 and A_9 are constants and

$$p^2 = \frac{\kappa}{\alpha + \beta + \gamma}\frac{1}{1/k_0^2} \tag{C.26}$$

with

$$K_0^2 = \frac{(C_1 + C_2 - C_3)^2}{(\alpha + \beta + \gamma)\lambda + 2\mu + \kappa} \tag{C.27}$$

Physical interpretation

The quantities l_0 - l_4 have dimensions of length and may be referred to as characteristic lengths. The noncentrosymmetric theory is intended for solids containing twisted or spiraling fibers, in which one direction of twist of spiral predominates. They can exhibit torsional deformation when stretched.

Experiments based on the results are capable of detecting micropolar behavior, but calculation of the nine elastic constants will be less than straightforward.

C.2.3 Other papers by Lakes

This is extracted from Lakes's own review, presented on his website.

Lakes, 1982

In (Lakes 1982), the presence of couple stress effects implies a reduction in the stress concentration factor around holes, particularly small holes.

Yang and Lakes, 1982

In (Yang & Lakes 1982): such theories (referring to Cosserat theories) are thought to be applicable to materials with a fibrous or granular structure.

Lakes, 1993

In (Lakes 1993): Cosserat solids have a characteristic length which is greater than zero. Strongly elastic Cosserat materials are considered to be those materials for which the Cosserat characteristic length is substantially greater than the structure size and for which the coupling number is large. Such materials are predicted to exhibit superior toughness.

C.3 Christoffersen, 2000

The following review is based on a draft (Christoffersen 2000).

C.3.1 Introduction

C.3.2 Symmetry properties of modulus tensors

In this section, Christoffersen presents the necessity to introduce the spin to take into account phenomena like magnetic dipoles, which cannot be treated using classical continuum mechanics.

It is customary to state constitutive equations for time-independent materials, in a form such as

$$\check{\tau}_{ij} = \mathcal{L}_{ijkl}\varepsilon_{lk} \tag{C.28}$$

where ε_{ij} is the strain rate, and $\check{\tau}_{ij}$ is an objective stress rate. The modulus tensor $\mathcal{L}_{ijkl}$ may change with deformation but it is independent or a 0th order homogeneous function of the strain rate. The modulus tensor is symmetric, motivated in the indicial symmetry of the strain rate tensor $\varepsilon_{ij} = \varepsilon_{ji}$, and this condition follows from the balance of moments. Christoffersen follows with a discussion about the history of the elastic constants, rigid-body movements supposition, and singularities.

Electric and magnetic dipoles account for mechanical moments distributed over a volume. This leads to nonsymmetric stress and objective stress rate tensors, but there are no means of accommodating them because of the constitutive equations. There is no other option but to abandon the notion of symmetry in the constitutive equations. The symmetry of the strain rate becomes inadmissible, so it is necessary to introduce the spin.

The new spin must be controlled by physical rules, this calls for a further set of field equations, and appropriate constitutive equations. The gradient of the spin will be called the material bending rate.

Continuum mechanics holds its stand as an effective means of accounting for the average outcome of complicated interatomic interactions. Nothing in modern

physics discourages the introduction of couple stresses in a continuum mechanical theory.

C.3.3 Balance equations: total forms

Christoffersen obtains the differential equilibrium equations for the body with couple stresses, these are:

$$\sigma_{ij,i} + p_j = 0 \tag{C.29}$$

$$\mu_{ij,i} + e_{jkl}\sigma_{kl} + q_j = 0 \tag{C.30}$$

where σ_{ij} is the direct stress tensor, p_j are body forces, μ_{ij} is the couple stress tensor, q_j is the body couple loading and e_{ijk} is the permutation tensor.

C.3.4 Work of forces and couples

It is possible to obtain the equation for work considering that the spins ω_j perform work with the couples and the displacements with the forces:

$$W = \int (\sigma_{ij}\varepsilon_{ji} + \mu_{ij}\kappa_{ji})dV \tag{C.31}$$

Here

$$\varepsilon_{ij} = v_{i,j} - e_{ikj}\omega_k \tag{C.32}$$

$$\kappa_{ij} = \omega_{i,j} \tag{C.33}$$

Strain and bending rates are subject to the compatibility conditions

$$e_{ijkl}\varepsilon_{jl,k} + \delta_{ij}\kappa_{kk} - \kappa_{ij} = 0 \tag{C.34}$$

$$e_{ikl}\kappa_{jl,k} = 0 \tag{C.35}$$

where δ_{ij} is Kronecker's delta.

C.3.5 Balance equations: rate forms

In this part of the paper, Christoffersen rewrites the equilibrium equations including rates of the tractions, traction couples, body forces and body couples. To represent these material rates, he introduces a dot attached to a symbol. For example, the rate of body forces is denoted:

$$\hat{p}_j = \frac{(p_j dV)^{\cdot}}{dV} \tag{C.36}$$

The rate form of the equilibrium equations is finally:

$$\hat{s}_{ij,i} + \hat{p}_j = 0 \tag{C.37}$$

$$\hat{m}_{ij,i} + e_{jkl}(\hat{s}_{kl} + v_{k,i}\sigma_{il}) + \hat{q}_j = 0 \tag{C.38}$$

C.3.6 Conservative loading

Christoffersen presents a rate form of the principle of virtual work equating two expressions of the bilinear forms, see eq. (C.39) and eq. (C.40):

$$L^{\alpha\beta} = \int (\hat{T}_j^{\alpha} v_j^{\beta} + \hat{Q}_j^{\alpha}\omega_j^{\beta} - \tfrac{1}{2}e_{jkl}\omega_k^{\alpha}Q_l\omega_j^{\beta})dS + \\ + \int (\hat{p}_j^{\alpha} v_j^{\beta} + \hat{q}_j^{\alpha}\omega_j^{\beta} - \tfrac{1}{2}e_{jkl}\omega_k^{\alpha}q_l\omega_j^{\beta})dV \tag{C.39}$$

$$L^{\alpha\beta} = \int \Big(\tilde{\tau}_{ij}^{\alpha}\varepsilon_{ji}^{\beta} + \tilde{\nu}_{ij}^{\alpha}\kappa_{ji}^{\beta} - \sigma_{ik}e_{klj}(\omega_l^{\alpha}\varepsilon_{ji}^{\beta} + \omega_l^{\beta}\varepsilon_{ji}^{\alpha}) - \\ - \tfrac{1}{2}\mu_{ik}e_{klj}(\omega_l^{\alpha}\kappa_{ji}^{\beta} + \omega_l^{\beta}\kappa_{ji}^{\alpha}) + \omega_i^{\alpha}\sigma_{jj}\omega_i^{\beta} - \tfrac{1}{2}\omega_i^{\alpha}(\sigma_{ij} + \sigma_{ji}\omega_j^{\beta}) \Big) dV \tag{C.40}$$

with

$$\tilde{\tau}_{ij} = \dot{\sigma}_{ij} + \sigma_{ij}v_{k,k} - v_{i,k}\sigma_{kj} + \sigma_{ik}e_{klj}\omega_l \tag{C.41}$$

$$\tilde{\nu}_{ij} = \dot{\mu}_{ij} + \mu_{ij}v_{k,k} - v_{i,k}\mu_{kj} + \mu_{ik}e_{klj}\omega_l \tag{C.42}$$

It was shown in (Christoffersen 1989) that the form $L^{\alpha\beta}$ is symmetric, then:

$$\int (\tilde{\tau}_{ij}^{\alpha}\varepsilon_{ji}^{\beta} + \tilde{\nu}_{ij}^{\alpha}\kappa_{ji}^{\beta}))dV = \int (\tilde{\tau}_{ij}^{\beta}\varepsilon_{ji}^{\alpha} + \tilde{\nu}_{ij}^{\beta}\kappa_{ji}^{\alpha}))dV \tag{C.43}$$

C.3.7 Rate constitutive equations

Elastic materials will be defined by:

$$\tilde{\tau}_{ij} = A_{ijkl}\varepsilon_{lk} + B_{ijkl}\kappa_{lk} \tag{C.44}$$

$$\tilde{\nu}_{ij} = C_{ijkl}\varepsilon_{lk} + D_{ijkl}\kappa_{lk} \tag{C.45}$$

where the modulus tensors A_{ijkl}, B_{ijkl}, C_{ijkl} and D_{ijkl} may vary with the deformation, but not depend on the strain or bending rates.

C.3.8 Centrosymmetric materials

The most general isotropy of the material is centrosymmetric (isotropic with respect to a point of reflection). In these materials with the rotation and reflection, $\tilde{\tau}_{ij}$ and ε_{ij} retain their signs, while $\tilde{\nu}_{ij}$ and κ_{ij} change theirs. Rates of direct stress cannot, therefore, depend on the bending rate. Consequently, $B_{ijkl} = 0$ and $C_{ijkl} = 0$ for centrosymmetric materials.

Homogeneous and isotropic materials are necessarily centrosymmetric.

C.3.9 Homogeneous states

In this section, Christoffersen presents the consequences of a homogeneous state in which A_{ijkl}, B_{ijkl}, C_{ijkl} and D_{ijkl} are homogeneous throughout the body together with the stresses σ_{ij} and μ_{ij}. This necessitates vanishing body forces. And with a homogeneous field of displacements, $v_{i,j}$ and ω_i are constant throughout the body.

Christoffersen explains through the study of an homogeneous state that modulus tensors B_{ijkl}, C_{ijkl} and D_{ijkl}, as well as parts of A_{ijkl} are inaccessible through mechanical experiments involving only these homogeneous states. Bending and torsion experiments then become important.

C.3.10 Relation to the Cosserat theory

In this section Christoffersen presents the relations between the Cosserat theory and his work, relating the gradient stresses to the quantities in the original theory by Cosserat.

C.3.11 Initial isotropic materials

In the context of micropolar materials involving couple stresses, two basically different models have been proposed. In the original Cosserat version, the spin is an independent parameter. Another form that has been investigated by Koiter (1964) it has been assumed that the spin is:

$$\omega_j = \tfrac{1}{2}e_{jkl}v_{l,k} \tag{C.46}$$

Although Koiter refers to the Cosserat work, Christoffersen believes that Koiter's theory is not a special case of the Cosserat model, it is rather a model in its own right.

Christoffersen concludes that Koiter's model is appropriate as a Cosserat theory for the case of small deformations, provided the material is isotropic.

C.3.12 Bending of strips

In this section, Christoffersen presents the results of bending for a homogeneous beam. He makes reference to the fact that the fiber in bending not only stretched but also bent. The consequences are investigated in an homogeneous centrosymmetric beam. The field of displacements proposed is:

$$v_1 = -\kappa x_1 x_2, \qquad v_2 = \tfrac{1}{2}\kappa x_1^2 + \tfrac{1}{2} c x_2^2, \qquad \omega_3 = \kappa x_1 \tag{C.47}$$

where κ and c are constants to be determined. The constitutive equations are written as:

$$\begin{aligned}
\dot{\sigma}_{11} &= F_{11}\varepsilon_{11} + F_{12}\varepsilon_{22} \\
\dot{\sigma}_{21} &= G_{21}\varepsilon_{21} + G_{22}\varepsilon_{12} \\
\dot{\sigma}_{12} &= G_{11}\varepsilon_{21} + G_{12}\varepsilon_{12} \\
\dot{\sigma}_{22} &= F_{21}\varepsilon_{11} + F_{22}\varepsilon_{22} \\
\dot{\mu}_{13} &= H_1\kappa_{31} \\
\dot{\mu}_{23} &= H_2\kappa_{32}
\end{aligned} \tag{C.48}$$

where F_{ij} and G_{ij} are elastic constants. The final equations obtained are:

$$c = \frac{F_{21}}{F_{22}}\kappa \tag{C.49}$$

$$\dot{\sigma}_{11} = -E_1 \kappa x_2 \tag{C.50}$$

$$\dot{\mu}_{13} = H_1 \kappa \tag{C.51}$$

where

$$E_1 = F_{11} - \frac{F_{12}F_{21}}{F_{22}} \tag{C.52}$$

The rate of sectional bending moment per unit width of the strip is

$$\dot{M} = -\int_{-h/2}^{h/2} \dot{\sigma}_{11} x_2 dx_2 + \int_{-h/2}^{h/2} \dot{\mu}_{13} dx_2 \tag{C.53}$$

or

$$\dot{M} = (\frac{1}{12} E_1 h^3 + H_1 h)\kappa \tag{C.54}$$

The structure will stiffen up by introduction of a new degree of freedom, the material spin. The characteristic length of the structure is $\sqrt{H_1/E_1}$ for the material considered.

C.3.13 Torsion of circular cylindrical rods

Assuming a centrosymmetric material with the constitutive equations:

$$\tilde{\tau}_{uv} = A_{uvrr}\varepsilon_{rr} + A_{uv\theta\theta}\varepsilon_{\theta\theta} + A_{uv\theta z}\varepsilon_{z\theta} + A_{uvz\theta}\varepsilon_{\theta z} + A_{uvzz}\varepsilon_{zz} \tag{C.55}$$

$$\tilde{\nu}_{uv} = D_{uvrr}\kappa_{rr} + D_{uv\theta\theta}\kappa_{\theta\theta} + D_{uvzz}\kappa_{zz} \tag{C.56}$$

with $(uv) \in (rr, \theta\theta, zz, \theta z, z\theta, zz)$. The simple problem in which the material is homogeneous isotropic and large enough to admit neglecting. The convection and rotation terms have the following results:

$$\begin{aligned}
A_{rrrr} &= A_{\theta\theta\theta\theta} = A_{zzzz} = F_0 \\
A_{rr\theta\theta} &= A_{\theta\theta zz} = A_{zz\theta\theta} = F_1 \\
A_{\theta\theta rr} &= A_{zz\theta\theta} = A_{\theta\theta zz} = F_1 \\
A_{\theta z\theta z} &= A_{z\theta z\theta} = G_0 \\
A_{\theta zz\theta} &= A_{z\theta\theta z} = G_1 \\
D_{rrrr} &= D_{\theta\theta\theta\theta} = D_{zzzz} = H_0 \\
D_{rr\theta\theta} &= D_{\theta\theta zz} = D_{zz\theta\theta} = H_1 \\
D_{\theta\theta rr} &= D_{zz\theta\theta} = D_{\theta\theta zz} = H_1
\end{aligned} \tag{C.57}$$

The stresses are:

$$\dot{\sigma}_{z\theta} = \left(\frac{G_0 + G_1}{2} r + \frac{G_0 - G_1}{2} \frac{\frac{1-\eta}{\lambda} I_1(\lambda r)}{I_0(\lambda R) - \frac{1-\eta}{\lambda R} I_1(\lambda R)}\right)\alpha \tag{C.58}$$

and

$$\dot{\mu}_{zz} = H_0 \frac{1-\eta}{2}\left(\frac{\eta I_0(\lambda r)}{I_0(\lambda R) - \frac{1-\eta}{\lambda R} I_1(\lambda R)} + 1\right)\alpha \tag{C.59}$$

The rate of torque is:

$$\dot{M}_t = \left(\frac{G_0 + G_1}{2}\frac{\pi}{2}R^4 + \frac{H_0 - H_1}{2}\Phi(\eta;\rho)\pi R^2\right)\alpha \tag{C.60}$$

where

$$\rho = \lambda R \tag{C.61}$$

$$\Phi(\eta;\rho) = \frac{I_2(\rho) + \frac{2\eta}{\rho} I_1(\rho) + 1}{I_0(\rho) - \frac{1-\eta}{\rho} I_1(\rho)} \tag{C.62}$$

$$\eta = \frac{H_1}{H_0} \tag{C.63}$$

where I represents Bessels functions. For very large values of ρ, where most of the torque is carried by shear stresses the stiffness is proportional to R^4, while for very small values of ρ, where couple stresses account for most of the torque, it is proportional to R^2. (The same result was presented by Lakes in section C.2.1)

C.4 Hutchinson, J. W.

C.4.1 Plasticity at the micron scale Hutchinson, 2000

In this paper (Hutchinson 2000) presents some size effects associated with hardness data, torsion, tension and bending in metals. Size effects are found at the micron scale. The problem is that conventional plasticity does not incorporate size effects, and the effects are too large to be analyzed using discrete dislocation mechanics.

Size-dependence at the micron scale

Indentation tests are a common means of assessing material yield strength. At present instruments exist that can measure indentation hardness at the micron and nano scale. A large size-dependence is observed in indentation tests of metals. The hardness increases with decrease in indent size. Torsional test of copper wires, tensile test of the same wires, and bending of micron thick films also detect large apparent strengthening of thinner films or wires over the thicker ones. The size dependence yield strength is believed to be associated with geometrically necessary dislocations generated by non-uniform straining. Geometrically necessary dislocations are by

definition the definite density of dislocations ρ_G required to produce plastic deformation. Geometrically necessary dislocations accumulate in proportion to the strain gradient so that $\partial\dot{\varepsilon}^p/\partial x \propto \dot{\rho}_G b$. The length scale at which plastic strain gradients significantly influence flow stress increments via Taylor's relation is denoted L, which also depends on the statistically stored dislocations ρ_S. Statistically stored dislocations are imagined to be dependent on the plastic strains ε^p.

To produce a continuum formulation, (Fleck, Muller, Ashby & Hutchinson 1994) imagine that the dislocation density increases in proportion to the measure $((\varepsilon^p)^\lambda + (l\partial\varepsilon^p/\partial x)^\lambda)^{1/\lambda}$ where l is the new constitutive length scale. Gao & Nix (1998) take the flow stress dependence to be $\sqrt{f(\varepsilon^p)^2 + l\partial\varepsilon^p/\partial x}$ (see section C.6.1).

Phenomenological theory of strain gradient plasticity: applications at the micron scale

Sketch of the theory and constitutive length parameters. In this section, Hutchinson presents a generalization of J_2 flow theory which will be denominated J_2SGP theory; the presentation is not detailed, Hutchinson refers to the article (Fleck & Hutchinson 1997).

The theory has a deformation version and an incremental version with a yield surface and provision for loading and unloading. The strain measure is defined by:

$$E_e^2 = \tfrac{2}{3}\varepsilon'_{ij}\varepsilon'_{ij} + l_1^2\eta'^{(1)}_{ijk}\eta'^{(1)}_{ijk} + l_2^2\eta'^{(2)}_{ijk}\eta'^{(2)}_{ijk} + l_3^2\eta'^{(3)}_{ijk}\eta'^{(3)}_{ijk} \tag{C.64}$$

where ε'_{ij} is the deviatoric strain, $\eta_{ijk} = u_{k,ij}$ is the strain gradient and η'_{ijk} is its deviator. The stresses are:

$$\sigma_{ij} = \frac{\partial W}{\partial \varepsilon_{ij}} \tag{C.65}$$

$$\tau_{ijk} = \frac{\partial W}{\partial \eta_{ijk}} \tag{C.66}$$

The deformation version falls within the class of solids considered by Toupin (1962) and Mindlin (1965*a*) (Microstructure or micromorphic solids according to section C.2.1). The virtual work statement of equilibrium is:

$$\int_V (\sigma_{ij}\delta\varepsilon_{ij} + \tau_{ijk}\delta\eta_{ijk})dV = \int_A (t_{ij}\delta u_{ij} + r_i\eta_j\delta u_{i,j})dA \tag{C.67}$$

where η_i is the outward unit normal to the surface, $r_i = \eta_j\eta_k\tau_{jki}$ is the double stress acting on the surface, and the surface traction is:

$$t_k = \eta_i(\sigma_{ij} - \tau_{ijk,j}) + \eta_i\eta_j\tau_{ijk}(D_p\eta_p) - D_j(\eta_i\tau_{ijk}) \tag{C.68}$$

the surface gradient being $D_j = (\delta_j k - \eta_j \eta_k)\partial_k$. Second and third invariants of the strain gradient in eq. (C.64) depend only on the rotation gradient $\chi_{ij} = \theta_{i,j} = e_{ipk}\varepsilon_{kj,p'}$ where the rotation is $\theta_i = e_{ijk}u_{k,j}/2$. The equivalent strain is taken to be

$$E_e^2 = \tfrac{2}{3}\varepsilon'_{ij}\varepsilon'_{ij} + l_1^2\eta'^{(1)}_{ijk}\eta'^{(1)}_{ijk} + \tfrac{2}{3}(2l_2^2 + \tfrac{12}{5}l_3^2)\chi_{ij}\chi_{ij} + \tfrac{2}{3}(2l_2^2/\tfrac{12}{5}l_3^2)\chi_{ij}\chi_{ji} \qquad \text{(C.69)}$$

Solutions suggest that the last term plays an unessential role in most problems. Effective strain is taken to be:

$$E_e^2 = \tfrac{2}{3}\varepsilon'_{ij}\varepsilon'_{ij} + l_{SG}^2\eta'^{(1)}_{ijk} + \tfrac{2}{3}l_{RG}^2\chi_{ij}\chi_{ij} \qquad \text{(C.70)}$$

There has already been some progress in identifying the constitutive length parameters for a few materials. Based on experimental data available at the present time, it appears that there is not a large variation in the constitutive length parameters from metal to metal, Hutchinson concludes:

$$l_{SG} \approx 0.25 \quad \text{to} \quad 1\mu\text{m} \qquad l_{RG} \approx 5\mu\text{m} \qquad \text{(C.71)}$$

Applications and implications of strain gradient plasticity As long as the length scale of the deformation field is long compared to the constitutive length parameters, there will be no size effects, because the theory reduces to the conventional theory in this limit. The size depends on the problem.

The theory has important implications for void growth, thin films and crack growth. Some of these applications are discussed by Hutchinson.

Bonded ceramic particles in a metal matrix induce gradients in plastic strain in the vicinity of the particle when the composite is subject to overall plastic strain. Results from this theory show strengthening due to smaller particles. Void growth in a solid undergoing plastic strain is interesting and potentially important to the understanding of ductile fracture. Void growth involves nearly irrotational deformations and, consequently, only the stretch gradient length parameter l_{SG} has any significant influence. It is found that the smaller the void, the more resistant it will be to growth. The elevation in stress due to plastic strain gradients observed in indentation, bending, and torsion, is expected to have a profound effect on fracture models when the size of the fracture process zone is sub-micron. Now, the length scale parameters for some of these problems are found. Plasticity in very thin metal films, particularly those grown epitaxially, with thickness less than about a hundred nanometers lie outside the scope of continuum theory. Thick films with thickness in the micron range are candidates for strain gradient plasticity.

Is a higher order theory necessary?

Acharya & Bassani (1996) followed by Dai & Parks (1998), proposed a version of strain gradient theory which retains lower order formulation. These authors adopt the conventional equilibrium equations and boundary conditions, but take the incremental tangent moduli to be functions of the strains and strain gradients:

$$\dot{\sigma_{ij}} = L_{ijkl}(\varepsilon, \eta)\dot{\varepsilon_{kl}} \tag{C.72}$$

This approach has not been developed nor explored to the same extent as J_2SGP theory, and it still remains to be seen if this theory can adequately reproduce observed size effects. A more fundamental issue is whether higher order stresses and boundary conditions should be brought into the picture along with strain gradients. The answer now is that there are important physical consequences that follow from higher order theories which are absent in lower order theories.

Concluding remarks

Strain gradient theories are motivated by the gap between conventional plasticity and dislocation mechanics. They need new length constitutive parameters. In J_2SGP theory, two length parameters have been identified, one tied to the stretch gradient (l_{SG}) and the other to rotation gradients (l_{RG}).

There are a number of open questions in connection with strain gradient plasticity formulations which require resolution. These include the issue of whether a higher order formulation is necessary and the problem of the most effective way to combine the strains and strain gradients in a phenomenological theory.

C.4.2 Fleck and Hutchinson, 1997

Fleck & Hutchinson (1997) develop a phenomenological strain gradient theory, this is an extension of the previous theory presented by Fleck & Hutchinson (1993).

Introduction

Dislocation theory suggests that the plastic flow strength of a solid depends on strain gradients in addition to strains. In general, strain gradients are inversely proportional to the length scale over which plastic deformation occurs, so they are important at small scales. Experimental evidence suggests that flow strength increases with diminishing size.

The theory that is proposed in the paper fits within the Toupin-Mindlin strain gradient framework, which involves all components of the strain gradient tensor, and work-conjugated higher-order stresses in the form of couple stresses and double stresses.

The underlying idea in this theory is that material flow strength is controlled by the total density of dislocations stored (the focus will be on a large number of dislocations, not on individual dislocation interactions). Dislocations accumulated by random trapping are called statistically stored dislocations with density ρ_S. Dislocations stored that are produced by gradients of plastic strain are called geometrically necessary dislocations with density ρ_G. The geometrically necessary dislocations ρ_G can be calculated if the gradient of plastic slip on crystal planes is known. To define ρ_G for the case of a single slip system, if slip occurs in direction s aligned with x_1 axis, and the normal to the slip plane is along x_2 axis, a gradient of slip $\partial\gamma/\partial x_1$, gives rise to a density

$$\frac{1}{b}\frac{\partial \gamma}{\partial x_1} \tag{C.73}$$

where b is the Burgers vector. The simplest possible dimensionally correct relationship between the flow strength τ_y on the slip plane and the total dislocation density is:

$$\tau_y = CGb\sqrt{\rho_S + \rho_G} \tag{C.74}$$

where G is the shear modulus, and C is a constant taken to be 0.3 by Ashby (1970). Other couplings between ρ_S and ρ_G are possible.

Survey of Strain Gradient Plasticity: Formulations and Phenomena

Higher-order continuum theories of elasticity were promulgated in the 1960s culminating with the major contributions by Koiter (1964), Mindlin (1965*a*) and Toupin (1962). No experimental corroboration of these theories was achieved, and in due course it was generally accepted that the phenomena being addressed in these works should be expected to come into play only at scales comparable to atomic lattice spacing.

Higher-order effects can be expected to come into play in conventional linear elastic solids when the representative length scale of the deformation field becomes comparable to a micro-structural length scale. While gradient effects in an elastic single crystal of pure metal become significant only for deformation fields with wavelengths on the order of the atomic spacing, when plastic deformation occurs, gradient effects can become important at much larger scales.

The representative length scale of the deformation fields sets the magnitude of plastic strain gradients compared with the magnitude of the average plastic strains. A small representative length scale implies the presence of large strain gradients relative to strains, and consequently, a large density of geometrically necessary dislocations relative to statistically stored dislocations.

Rotation gradients: couple stress theory Fleck & Hutchinson (1993) have developed a phenomenological theory of strain gradient plasticity based on gradients of rotations which fits with the framework of couple stress theory. The yield strength of the solid is taken to depend upon both strain ε and curvature ξ. The strain tensor $\boldsymbol{\varepsilon}$ is related to the material displacement $\mathbf{u}$ via $\varepsilon_{ij} = (u_{i,j} + u_{j,i})/2$, and the curvature $\boldsymbol{\xi}$ is the spatial gradient of the material rotation $\boldsymbol{\theta}$:

$$\xi_{ip} = \theta_{i,p} = \tfrac{1}{2} e_{ijk} u_{k,jp} = e_{ijk}\varepsilon_{kp,j} \tag{C.75}$$

where e_{ijk} is the permutation tensor. The strain energy density w of an incompressible solid is taken to depend upon the second Von Mises invariant of strain $\varepsilon_e = \sqrt{\frac{2}{3}\varepsilon_{ij}\varepsilon_{ij}}$ and the analogous second invariant of the curvature $\xi_e = \sqrt{\frac{2}{3}\xi_{ij}\xi_{ij}}$.

Fleck & Hutchinson (1993) assumed that the strain energy density w depends only upon the overall effective strain quantity ϵ_{CS} where

$$\epsilon_{CS} = \sqrt{\varepsilon_e^2 + l_{CS}^2 \xi_e^2} \tag{C.76}$$

The material length scale l_{CS} has been introduced as required for dimensional consistency, and the subscript 'CS' is short for 'couple stress'. A generalization of eq. (C.76) used to assess the sensitivity of predictions to the way in which ε_e and ξ_e are combined is:

$$\epsilon_{CS} = [\varepsilon_e^\mu + l_{CS}^\mu \xi_e^\mu]^{1/\mu} \tag{C.77}$$

where an additional parameter μ has been introduced.

Rotation and stretch gradients: Toupin-Mindlin theory. In this framework, the generalized strain variables are the symmetric strain tensor ε_{ij} and the second gradient of displacement $\eta_{ijk} = u_{k,ij}$. The work increment per unit volume w due to an arbitrary variation of displacement $\mathbf{u}$ is

$$\delta w = \sigma_{ij}\delta\varepsilon_{ij} + \tau_{ijk}\delta\eta_{ijk} \tag{C.78}$$

where τ_{ijk} is the higher-order stress tensor. Then eq. (C.78) implies that $\sigma_{ij} = \partial w/\partial\varepsilon_{ij}$ and $\tau_{ijk} = \partial w/\partial\eta_{ijk}$. Toupin (1962) and Mindlin (1965*a*) showed that the strain energy density w depends upon $\boldsymbol{\epsilon}$ and $\boldsymbol{\eta}$ in the manner

$$w = \tfrac{1}{2}\lambda\varepsilon_{ii}\varepsilon_{ii} + \mu\varepsilon_{ij}\varepsilon_{ij} + a_1\eta_{ijj}\eta_{ikk} + a_2\eta_{iik}\eta_{kjj} + a_3\eta_{iik}\eta_{jjk} + a_4\eta_{ijk}\eta_{ijk} + a_5\eta_{ijj}\eta_{kji} \tag{C.79}$$

where λ and μ are the standard Lame constants and a_n are additional stiffness constants. For the special case of an incompressible solid, w simplifies to

$$w = \mu\varepsilon'_{ij}\varepsilon'_{ij} + a_3\eta'_{iik}\eta'_{jjk} + a_4\eta'_{ijk}\eta'_{ijk} + a_5\eta'_{ijj}\eta'_{kji} \tag{C.80}$$

where the superscript $(')$ is introduced to emphasize that the strain quantities are derived for an incompressible displacement field. Introducing the fully symmetric tensor $\boldsymbol{\eta}$ where

$$\eta'^S_{ijk} = \tfrac{1}{3}[\eta'_{ijk} + \eta'_{jki} + \eta'_{kij}] \tag{C.81}$$

The orthogonal decomposition of $\boldsymbol{\eta}$ into three tensors is given by:

$$\eta'^{(1)}_{ijk} = \eta'^S_{ijk} - \tfrac{1}{5}[\delta_{ij}\eta'^S_{kpp} + \delta_{jk}\eta'^S_{ipp} + \delta_{ki}\eta'^S_{jpp}] \tag{C.82}$$

$$\eta'^{(2)}_{ijk} = \tfrac{1}{6}[e_{ikp}e_{jlm}\eta'_{lpm} + e_{jkp}e_{ilm}\eta'_{lpm} + 2\eta'_{ijk} - \eta'_{jki} - \eta'_{kij}] \tag{C.83}$$

$$\eta'^{(3)}_{ijk} = \tfrac{1}{6}[-e_{ikp}e_{jlm}\eta'_{lpm} - e_{jkp}e_{ilm}\eta'_{lpm} + 2\eta'_{ijk} - \eta'_{jki} - \eta'_{kij}] + \\ + \tfrac{1}{5}[\delta_{ij}\eta'^{S}_{kpp} + \delta_{jk}\eta'^{S}_{ipp} + \delta_{ki}\eta'^{S}_{jpp}] \tag{C.84}$$

The combined strain quantity ϵ can be written using eq. (C.81) to eq. (C.84) after some lengthy manipulation as:

$$\epsilon^2 = \tfrac{2}{3}\varepsilon'_{ij}\varepsilon'_{ij} + l_1^2\eta'^{(1)}_{ijk}\eta'^{(1)}_{ijk} + l_2^2\eta'^{(2)}_{ijk}\eta'^{(2)}_{ijk} + l_3^2\eta'^{(3)}_{ijk}\eta'^{(3)}_{ijk} \tag{C.85}$$

Eq. (C.85) is the defining relation for ϵ. This equation can be rewritten in terms of the three invariants $\xi'_{ij}\xi'_{ij}$, $\xi'_{ij}\xi'_{ji}$ and $\eta'^{(1)}_{ijk}\eta'^{(1)}_{ijk}$ as:

$$\epsilon^2 = \tfrac{2}{3}\varepsilon'_{ij}\varepsilon'_{ij} + l_1^2\eta'^{(1)}_{ijk}\eta'^{(1)}_{ijk} + (\tfrac{4}{3}l_2^2 + \tfrac{8}{5}l_3^2)\xi'_{ij}\xi'_{ij} + (\tfrac{4}{3}l_2^2 + \tfrac{8}{5}l_3^2)\xi'_{ij}\xi'_{ji} \tag{C.86}$$

For simplicity, a power law dependence of the strain energy density w on the effective strain ϵ of the form

$$w = \frac{n}{n+1}\Sigma_0\epsilon_0\left(\frac{\epsilon}{\epsilon_0}\right)^{(n+1)/n} \tag{C.87}$$

is assumed where Σ_0, ϵ_0 and the strain-hardening exponent n are taken to be material constants.

Phenomena influenced by plastic strain gradients

In this section, Fleck & Hutchinson (1997) present a series of problems which are analyzed using this theory. Examples include: Torsion of thin wires; the grain size effect on polycrystalline yield strength; the strengthening of metal matrices by rigid particles; the effect of void size in void growth and softening; cavitation instabilities; indentation hardness testing; the study of stress field in the vicinity of a sharp crack tip.

The framework for strain gradient theory

Toupin-Mindlin theory Following Toupin (1962), Mindlin (1965*a*) the work increment for a volume V is:

$$\int_V [\delta w]dV = \int_V [\sigma_{ij}\delta\varepsilon_{ij} + \tau_{ijk}\delta\eta_{ijk}]dV \tag{C.88}$$

Using the divergence theorem and Stokes's surface divergence theorem, the principle of virtual work is written

$$\int_V [\sigma_{ij}\delta\varepsilon_{ij} + \tau_{ijk}\delta\eta_{ijk}]dV = \int_V [f_k\delta u_k]dV + \int_S [t_k\delta u_k]dS + \int_S [r_k(D\delta u_k)]dS \quad \text{(C.89)}$$

where f_k is the body force, t_k is the surface traction, r_k is the double stress traction, and D is the normal gradient operator is defined as

$$D = n_k()_{,k} \quad \text{(C.90)}$$

The equilibrium relation in V is:

$$f_k + (\sigma_{ik} - \tau_{ijk,j})_{,i} = 0 \quad \text{(C.91)}$$

and t_k is:

$$t_k = n_i(\sigma_{ik} - \tau_{ijk,j}) + n_i n_j \tau_{ijk} D_p n_p - D_j(n_i\tau_{ijk}) \quad \text{(C.92)}$$

where the surface gradient operator is:

$$D_j = (\delta_{jk} - n_j n_k)()_{,k} \quad \text{(C.93)}$$

other parts of this section present the relation between this theory and the couple stress theory.

Flow theory

The current strength of the solid is dependent upon the accumulated strain and strain gradient. The theory predicts the existence of boundary layers of deformation close to stiff interfaces An alternative is to assume that the current tangent-hardening modulus is increased by the presence of accumulated strain gradients. The resulting formulation does not require additional boundary conditions or boundary layers near to interfaces.

The strain gradient version of J_2 flow theory is generated by the following prescription. In the absence of higher-order stresses $\boldsymbol{\tau}$, the deviatoric, symmetric Cauchy stress $\boldsymbol{\sigma}'$ may be represented by a five-dimensional vector. When higher-order stresses are present, the role of $\boldsymbol{\sigma}'$ is replaced by that of the 23-dimensional vector $\boldsymbol{\Sigma} = (\boldsymbol{\sigma}', \boldsymbol{\tau}')$; $\boldsymbol{\Sigma}$ is made up of the five symmetric components of $\boldsymbol{\sigma}'$, the eight independent components of couple stress $\boldsymbol{\tau}'^A$ and the ten independent components of double force per unit area $\boldsymbol{\tau}'^S$, where it is considered that the higher-order stress tensor $\boldsymbol{\tau}$ can be split into a symmetric tensor $\boldsymbol{\tau}^S$ and a remainder $\boldsymbol{\tau}^A$:

$$\tau_{ijk} = \tau^S_{ijk} + \tau^A_{ijk} \quad \text{(C.94)}$$

where

$$\tau^S_{ijk} = \tfrac{1}{3}(\tau_{ijk} + \tau_{jki} + \tau_{kij}) \tag{C.95}$$

$$\tau^A_{jqr} = \tfrac{1}{4}e_{iqr}m_{ji} + \tfrac{1}{4}e_{ijr}m_{qi} \tag{C.96}$$

where $\mathbf{m}$ is the couple stress tensor.

In the same manner, the deviatoric stress tensor ϵ' is replaced by the 23-dimensional vector $\epsilon = (\epsilon, \boldsymbol{\eta}')$.

The elastic modulus Υ is defined as

$$\Upsilon_{ijkl} = \frac{E}{2(1+\nu)}\left(\frac{2\nu}{1+2\nu}\delta_{ij}\delta_{kl} + \delta_{ik}\delta_{jl} + \delta_{il}\delta_{jk}\right) \tag{C.97}$$

The plastic strain rate $\dot{\epsilon}^{pl}$ is replaced by the 23-dimensional vector $\dot{\epsilon}^{pl} = (\dot{\epsilon}^{pl}, \dot{\boldsymbol{\eta}}^{pl})$. The yield surface generalized to

$$\Phi(\Sigma, Y) = \Sigma - Y = 0 \tag{C.98}$$

The overall effective stress sigma is defined by

$$\Sigma^2 = \tfrac{3}{2}\sigma'_{ij}\sigma'_{ij} + \sum_{I=1}^{3}\left[l_I^{-2}\tau'^{(I)}_{ijk}\tau'^{(I)}_{ijk}\right] = \sigma_e^2 + \sum_{I=1}^{3}\left[\left(\frac{\tau_e^{(I)}}{l_I}\right)^2\right] \tag{C.99}$$

where σ_e is the usual von Mises effective stress

$$\sigma_e = \sqrt{\tfrac{2}{3}\sigma'_{ij}\sigma'_{ij}} \tag{C.100}$$

and τ_e is the higher order effective stress defined by

$$\tau_e^{(I)} = \sqrt{\tau^{(I)}_{ijk}\tau^{(I)}_{ijk}} \qquad \text{(no sumation on } I\text{)} \tag{C.101}$$

The effective plastic strain gradient rates are

$$\dot{\eta}_e^{(I)^{pl}} = \sqrt{\dot{\eta}^{(I)^{pl}}_{ijk}\,\dot{\eta}^{(I)^{pl}}_{ijk}} \qquad \text{(no summation on } I\text{)} \tag{C.102}$$

and the overall effective plastic strain rate is:

$$\dot{\epsilon}^{pl} = \sqrt{\tfrac{2}{3}\dot{\epsilon}^{pl}_{ij}\dot{\epsilon}^{pl}_{ij} + \sum_{I=1}^{3}[l_I^2\dot{\eta}^{(I)^{pl}}_{ijk}\,\dot{\eta}^{(I)^{pl}}_{ijk}]} \tag{C.103}$$

Plastic strain is assumed to be normal to the yield surface and the plastic-strain rate is taken to be linear in the stress rate, then the plastic strain generalizes to

$$\dot{\epsilon}^{pl} = \frac{1}{h(\Sigma)} \frac{\partial \Phi}{\partial \Sigma} \dot{\sigma} \tag{C.104}$$

where the hardening rate h is chosen such that the uniaxial tensile response is reproduced

Summary of elastic-plastic constitutive relations Plastic flow is normal to the yield surface such that

$$\dot{\varepsilon}_{ij}^{pl} = \frac{3}{2h} \frac{\sigma'_{ij}}{\Sigma} \dot{\Sigma} \tag{C.105}$$

and

$$\dot{\eta}_{ijk}^{pl} = \frac{\dot{\Sigma}}{h} \frac{\partial \Phi}{\partial \tau_{ijk}} = \frac{\dot{\Sigma}}{h\Sigma} \sum_{I=1}^{3} [l_I^{-2} \tau_{ijk}^{\prime(I)}] \tag{C.106}$$

The rate of overall effective stress is given by the rate form of eq. (C.99)

$$\dot{\Sigma} = \frac{3}{2\Sigma} \sigma'_{ij} \dot{\sigma}'_{ij} + \frac{1}{\Sigma} \sum_{I=1}^{3} [l_I^{-2} \tau_{ijk}^{\prime(I)} \dot{\tau}_{ijk}^{\prime(I)}] \tag{C.107}$$

The elastic strain rates are

$$\dot{\varepsilon}_{ij}^{el} = M_{ijkl} \dot{\sigma}_{kl} \tag{C.108}$$

and

$$\dot{\eta}_{ijk}^{el} = K_{ijklmn} \dot{\tau}_{lmn} \tag{C.109}$$

where $\mathbf{K} = \boldsymbol{\Upsilon}^{-1}$ and

$$M_{ijkl} = \frac{1+\nu}{2E} (\delta_{ik}\delta_{jl} + \delta_{il}\delta_{jk}) - \frac{\nu}{E} \delta_{ij}\delta_{kl} \tag{C.110}$$

where E is Young's modulus and ν is Poisson's ratio.

Minimum principles The theory satisfies the generalized Drucker stability postulates

$$\dot{\sigma}_{ij}\dot{\varepsilon}^{pl}_{ij} + \dot{\tau}_{ijk}\dot{\eta}^{pl}_{ijk} \geq 0 \tag{C.111}$$

for a stress rate $(\dot{\boldsymbol{\sigma}}, \dot{\boldsymbol{\tau}})$ corresponding to a plastic strain rate $(\dot{\boldsymbol{\varepsilon}}^{pl}, \dot{\boldsymbol{\eta}}^{pl})$, and

$$(\sigma_{ij} - \hat{\sigma}_{ij})\dot{\varepsilon}^{pl}_{ij} + (\tau_{ijk} - \hat{\tau}_{ijk})\dot{\eta}^{pl}_{ijk} \geq 0 \tag{C.112}$$

for a stress state $(\boldsymbol{\sigma}, \boldsymbol{\tau})$ associated with a plastic strain rate $(\dot{\boldsymbol{\varepsilon}}^{pl}, \dot{\boldsymbol{\eta}}^{pl})$, and any other stress state $(\hat{\boldsymbol{\sigma}}, \hat{\boldsymbol{\tau}})$ on or whiting the yield surface.

Minimum principle for the displacement rate. The functional $F(\dot{\mathbf{u}})$ is minimized by the exact solution $(\dot{\mathbf{u}}, \dot{\boldsymbol{\varepsilon}}, \dot{\boldsymbol{\sigma}}, \dot{\boldsymbol{\tau}})$

$$F(\dot{\mathbf{u}}) = \tfrac{1}{2}\int_V [\dot{\sigma}_{ij}\dot{\varepsilon}_{ij} + \dot{\tau}_{ijk}\dot{\eta}_{ijk}]dV - \int_S [\dot{t}^0_i\dot{u}_i + \dot{r}^0_i D\dot{u}_i]dS \tag{C.113}$$

Minimum principle for the stress rate The functional $H(\dot{\boldsymbol{\sigma}}, \dot{\boldsymbol{\tau}})$ is minimized by the exact solution$(\dot{\mathbf{u}}, \dot{\boldsymbol{\varepsilon}}, \dot{\boldsymbol{\sigma}}, \dot{\boldsymbol{\tau}})$

$$H(\dot{\boldsymbol{\sigma}}, \dot{\boldsymbol{\tau}}) = \tfrac{1}{2}\int_V [\dot{\sigma}_{ij}\dot{\varepsilon}_{ij} + \dot{\tau}_{ijk}\dot{\eta}_{ijk}]dV - \int_S [\dot{t}^0_i\dot{u}_i + \dot{r}^0_i D\dot{u}_i]dS \tag{C.114}$$

C.4.3 Fleck and Hutchinson, 2001

Fleck & Hutchinson (2001) present another version of a phenomenological strain gradient theory. This version is formulated to accommodate three length parameters, it is similar to the theory proposed by Aifantis (1984). This theory is simpler to implement into a finite element analysis, and produces better results when the plastic deformations are close to the elastic deformation than does the previous theory by Fleck & Hutchinson (1997).

Introduction

In most of the theories to incorporate the role of gradient strains in the increasing effective flow strength of metals, it is possible to identify only three phenomenological approaches. One type of theory Acharya & Bassani (2000) incorporates a dependence on plastic strain gradients into the incremental or tangential moduli. This theory has standard boundary conditions and introduces no higher order stresses. There are examples that illustrate the necessity of additional boundary conditions in small-scale plasticity.

The second type of theory is that first proposed by Aifantis (1984). This theory has extra boundary conditions and possesses higher order stress quantities. The

simplest version of the theory introduces one material length scale and employs as its measure of strain gradients the magnitude of the gradient of the amplitude of the plastic strain. A disadvantage is its inability, as formulated, to address a range of problems that appear to require more than just one material length parameter.

The third type of theory is the class of higher-order theories proposed and applied by Fleck & Hutchinson (1997). The theory proposed in this paper produces similar predictions in the plastic range to the theory by Fleck & Hutchinson (1997).

Measures of gradients of plastic strain rate

The Aifantis theory makes use of an effective plastic strain rate defined by

$$\dot{E}_p^2 = \dot{\varepsilon}_p^2 + l_*^2 \dot{\varepsilon}_{p,i} \dot{\varepsilon}_{p,i} \tag{C.115}$$

where the conventional effective plastic strain rate is $\dot{\varepsilon}_p = \sqrt{2\dot{\varepsilon}_{ij}^p \dot{\varepsilon}_{ij}^p/3}$ and l_* is a length parameter required for dimensional consistency.

In order to generalize this theory, the plastic strain gradient is introduced as

$$\rho_{ijk} = \rho_{jki} = \dot{\varepsilon}_{ij,k}^p \tag{C.116}$$

A unique orthogonal decomposition for third order tensors produce

$$\rho_{ijk} = \rho_{ijk}^{(1)} + \rho_{ijk}^{(2)} + \rho_{ijk}^{(3)} \tag{C.117}$$

with

$$\rho_{ijk}^{(1)} = \rho_{ijk}^S - \tfrac{1}{5}(\delta_{ij}\rho_{kpp}^S + \delta_{ik}\rho_{jpp}^S + \delta_{jk}\rho_{ipp}^S) \tag{C.118}$$

$$\rho_{ijk}^{(2)} = \tfrac{1}{3} e_{kip} \xi_{pj}^S + \tfrac{1}{3} e_{kjp} \xi_{pi}^S \tag{C.119}$$

$$\rho_{ijk}^{(3)} = \tfrac{1}{3} e_{kip} \xi_{pj}^A + \tfrac{1}{3} e_{kjp} \xi_{pi}^A + \tfrac{1}{5}(\delta_{ij}\rho_{kpp}^S + \delta_{ik}\rho_{jpp}^S + \delta_{jk}\rho_{ipp}^S) \tag{C.120}$$

where

$$\begin{aligned} &\rho_{ijk}^S = \tfrac{1}{3}(\rho_{ijk} + \rho_{jki} + \rho_{kij}), \qquad \xi_{ij} = e_{iqr}\rho_{jrq} \\ &\xi_{ij}^S = \tfrac{1}{2}(\xi_{ij} + \xi_{ji}) \qquad \text{and} \qquad \xi_{ij}^A = \tfrac{1}{2}(\xi_{ij} - \xi_{ji}) \end{aligned} \tag{C.121}$$

Fleck & Hutchinson (2001) take the measure of a generalized effective plastic strain rate to have the same form as the effective strain by Fleck & Hutchinson (1997)

$$\dot{E}_p^2 = \dot{\varepsilon}_p^2 + l_1^2 \rho_{ijk}^{(1)} \rho_{ijk}^{(1)} + 4 l_2^2 \rho_{ijk}^{(2)} \rho_{ijk}^{(2)} + \tfrac{8}{3} l_3^2 \rho_{ijk}^{(3)} \rho_{ijk}^{(3)} \tag{C.122}$$

where $\dot{\varepsilon}_p^2 = 2\dot{\varepsilon}_{ij}^p \dot{\varepsilon}_{ij}^p/3$. The generalized effective plastic strain is intended as a phenomenological measure of the total dislocation density. The contribution depending on l_1 measures stretch rate gradients as well as rotation gradients. The variety of small-scale plasticity phenomena dictates the necessity of more than one length parameter in the gradient description.

Generalization of classical J_2 theory

The flow theory The elastic and plastic parts of the strains are denoted ε_{ij}^e and ε_{ij}^p. The elastic properties of the material are taken to be isotropic with Young's modulus E and Poisson's ratio ν, and with the moduli tensor C_{ijkl}. The tangent hardening quantitity is $h(\varepsilon_p) = d\sigma/d\varepsilon_p$ where $\varepsilon_p = \int \dot{\varepsilon}_p dt$ and $\dot{\varepsilon}_p = \sqrt{2\dot{\varepsilon}_{ij}^p \dot{\varepsilon}_{ij}^p/3}$. The conventional plastic flow condition is assumed such that with the yield condition satisfied and $\dot{\varepsilon}_p \geq 0$,

$$\dot{\varepsilon}_{ij} = \dot{\varepsilon}_p m_{ij} \tag{C.123}$$

where $m_{ij} = (3/2)s_{ij}/\sigma_e$; s_{ij} are the deviatoric stress components and $\sigma_e = \sqrt{3 s_{ij} s_{ij}/2}$ is the conventional effective stress.

The internal virtual work increment, IVW, is assumed to take the form

$$IVW = \int_V [-\sigma_{ij,j}\delta u_i + (Q - \sigma_e - \tau_{i,j})\delta\varepsilon_p] dV + \int_S [\sigma_{ij} n_j \delta u_i + \tau_i n_i \delta\varepsilon_p] dS \tag{C.124}$$

where n_i is the unit outward normal to S, Q is defined as the work conjugate to the plastic strain ε_p, and the vector quantity τ_i is the higher order stress working through the plastic strain gradient $\varepsilon_{p,i}$

The principle of virtual work for incremental problems reads

$$\int_V [\dot{\sigma}_{ij}\delta\dot{\varepsilon}_{ij}^e + \dot{Q}\delta\dot{\varepsilon}_p + \dot{\tau}_i \delta\dot{\varepsilon}_{p,i}] dV = \int_V [\dot{\sigma}_{ij}\delta\dot{\varepsilon}_{ij} + \dot{\tau}_{i,i}\delta\dot{\varepsilon}_p + \dot{\tau}_i\delta\dot{\varepsilon}_{p,i}] dV = \int_S [\dot{T}_i \delta\dot{u}_i + \dot{t}\delta\dot{\varepsilon}_p] dS \tag{C.125}$$

where T_i and t are traction quantities on the boundary S.

The expression (C.122) can be recast as

$$\dot{E}_p^2 = \dot{\varepsilon}_p^2 + A_{ij}\dot{\varepsilon}_{p,i}\dot{\varepsilon}_{p,j} + B_i \dot{\varepsilon}_{p,i}\dot{\varepsilon}_p + C\dot{\varepsilon}_p^2 \tag{C.126}$$

where the three explicit expresions for A_{ij}, B_i and C depend on the three material length parameters.

The incremental boundary value problem can be stated as a minimum principle $\delta I = 0$ with

$$I(\dot{u}_i, \dot{\varepsilon}_p) = \frac{1}{2}\int_V [C_{ijkl}(\dot{\varepsilon}_{ij} - \dot{\varepsilon}_p m_{ij})(\dot{\varepsilon}_{kl} - \dot{\varepsilon}_p m_{kl}) + h(E_p)E_p^2]dV - \int_{S_T} [\dot{T}_i^0 \dot{u}_i + \dot{t}^0 \dot{\varepsilon}_p]dS \tag{C.127}$$

where $\dot{T}_i^0$ and $\dot{t}^0$ are prescribed traction rates on S_T and $E_p = \int \dot{E}_p dt$ is the accumulated effective plastic strain. By identifying $\dot{Q} = \dot{\sigma}_e + \dot{\tau}_{i,i}$ the constitutive equations governing plastic loading ($\dot{Q} = \dot{Q}_Y$) are obtained as

$$\dot{Q}_Y = h(E_p)(\dot{\varepsilon}_p + \tfrac{1}{2}B_i \dot{\varepsilon}_{p,i} + C\dot{\varepsilon}_p) \tag{C.128}$$

$$\dot{\tau}_i = h(E_p)(A_{ij}\dot{\varepsilon}_{p,j} + \tfrac{1}{2}B_i \dot{\varepsilon}_p) \tag{C.129}$$

The deformation theory. To define the deformation theory, let $\varepsilon_{ij}^p = \varepsilon_p m_{ij}$. The generalized total effective strain using eq. (C.122) but now in terms of the total plastic strain and their gradients, $\rho_{ijk} = \varepsilon_{ij,k}^p = \varepsilon_{p,k} m_{ij} + \varepsilon_p m_{ij,k}$ are

$$E_p^2 = \varepsilon_p^2 + A_{ij}\varepsilon_{p,i}\varepsilon_{p,j} + B_i \varepsilon_{p,i}\varepsilon_p + C\varepsilon_p^2 \tag{C.130}$$

A potential energy functional is

$$\Phi(u_i, \varepsilon_p) = \int_V \left[\tfrac{1}{2}C_{ijkl}(\varepsilon_{ij} - \varepsilon - p m_{ij})(\varepsilon_{kl} - \varepsilon_p m_{kl}) + \int_0^{E_p} \sigma(\tilde{\varepsilon}_p)d\tilde{\varepsilon}_p\right]dV - \int_{S_T} [T_i^0 u_i + t^0 \varepsilon_p]dS \tag{C.131}$$

The field equations and boundary conditions associated with $\delta\Phi = 0$ are obtained. The principle of virtual work is recovered as used in eq. (C.124) with the constitutive statements,

$$Q = \frac{\sigma(E_p)}{E_p}(\varepsilon_p + \tfrac{1}{2}B_i \varepsilon_{p,i} + C\varepsilon_p) \tag{C.132}$$

$$\tau_i = \frac{\sigma(E_p)}{E_p}(A_{ij}\varepsilon_{p,j} + \tfrac{1}{2}B_i \varepsilon_p) \tag{C.133}$$

According to Fleck & Hutchinson (2001), it is possible to show that the solution of the boundary value problem for the deformation theory coincides with the solution for the corresponding flow theory when the deformation theory solution obeys proportional stressing. For all but a very few problems, however, the presence of elasticity prevents the precise satisfaction of proportional stressing.

Solution to problems and their implications

Three problems are presented, in each one a Ramberg-Osgood curve is used to characterize the uniaxial tensile stress-strain curve of the solid.

Shearing of a sandwich layer between two substrates. Strain gradients come into play only if the boundaries are assumed to constrain the plastic flow. In the solution the plastic shear strain distribution displays a boundary layer which occupies a diminishing fraction of the layer thickness and decreases as l/L decreases, where the height of the layer is $2L$.

Wire torsion. The first length parameter is found to be unimportant. In wire torsion l_2 is the controlling parameter.

Size effects in void growth. It is found that l_1 is far more important that l_3 in setting the influence of strain gradients in void growth. This might be from the fact that the spherically symmetric expansion involves only stretch gradients and no rotation gradients.

Implications from experimental observations

Size effects in wire torsion are controlled by l_2, while l_1 is the important length parameter in void growth. Indentation is similar to void growth in that stretch gradients are dominant with l_1 playing the primary role. The distinct difference between the size effects in wire torsion, indentation and void growth is problematic for a one-parameter formulation. It seems unlikely that the various phenomena reviewed could be subsumed under a theory that invokes only one length parameter. In an attemp to reduce the number of necessary length parameters from three to two, Begley & Hutchinson (1998) proposed to neglect the contributions of the invariant quantity, $\xi_{ij}\xi_{ij}$ in eq. (C.122). With

$$l_2 = \tfrac{1}{2} l_{CS}, \qquad l_3 = \sqrt{\tfrac{5}{24}} l_{CS} \tag{C.134}$$

the effective plastic strain rate becomes

$$\dot{E}_p^2 = \dot{\varepsilon}_p^2 + l_1^2 \eta_{ijk}^{(1)} \eta_{ijk}^{(1)} + \tfrac{2}{3} l_{CS}^2 \xi_{ij} \xi_{ij} \tag{C.135}$$

where l_{CS} is the length parameter introduced by Fleck et al. (1994)

Relations of the present theory to previous higher order theories

Deformation theory and flow theory extension of J_2 theory to account for strain gradient effects were proposed earlier by Fleck & Hutchinson (1997). This previous deformation theory incorrectly introduces a dependence on strain gradients in the linear elastic range, producing nonphysical dependence of the initial slope of the torque-twist relations on l_2. As the plastic strain becomes large compared to the elastic strains, the solutions to the earlier deformation theory become asymptotic to the solutions produced by the new deformation theory.

C.5 Pamin, 1994

This reference corresponds to the Ph.D. thesis by Pamin (1994), the work is devoted to the study of localization phenomena using gradient dependent plasticity.

C.5.1 Introduction

Strain localization is a notion describing a deformation mode, in which the whole deformation of a material specimen occurs in one or more narrow bands, while the rest of the specimen usually exhibits unloading.

Material heterogeneity induces a strongly nonlinear behavior and local weakness of the material. As a result of the inhomogeneous deformations, a softening response at the structural level is observed.

Classical constitutive models embody an implicit assumption that the deformation of the specimen varies in a sufficiently smooth manner. The further consequence is a spurious discretization sensitivity in numerical simulations of localization and softening problems.

Scope and objectives

Pamin developed his work for frictional materials, and incorporates a higher-order strain gradient in his model. The gradient dependence of the yield function has the consequence of producing a differential equation for the plastic consistency condition, which is an algebraic equation in the classical theory.

Assumptions and contents

The main assumption is the static loading and small deformations of the analyzed configurations.

C.5.2 Strain localization in softening media

Background and problem statement

A concentration of deformations in small zones by material effects is called strain localization.

In a body subjected to loads and boundary conditions such that the resulting deformation is homogeneous, localization occurs suddenly at a certain point of the load history when the whole of the further deformation is confined in narrow band-shaped parts of the body (shear bands). The gradual decrease of stiffness and load-carrying capacity with the increase of deformation is called softening. Softening is a structural property, it is a manifestation of the fact that the deformation of the body is highly inhomogeneous.

The width of the shear bands is small, but finite, and depends on the material. Apparently a characteristic length parameter exists that sets the size of the bands.

At the meso-level of observation, every material is inhomogeneous and, due to the presence of microvoids and microcraks, it is also discontinuous. If the characteristic

deformation scale is much larger than the characteristic size of the material heterogeneity, the microstructural contributions to the deformation vanish, and it can be assumed that the material behaves like a classical continuum. In softening, the characteristic deformation scale and the microstructure size become comparable. In the presence of large deformation gradients, the relative motion of the microstructure becomes comparable to the length scale in the deformation pattern, which means that the state of the material at a point depends on the deformation history of a certain neighborhood of this point.

Material instability and loss of ellipticity. In classical continuum, the stress tensor depends only on the deformation history of the point. The functional dependence is only through the first order deformation gradient F_{ij}

$$\sigma_{ij}(\xi_k, t) = \psi_{ij}(\xi_k, F_{lm}(\xi_k, t-\tau)) \tag{C.136}$$

where ξ_k are the material coordinates, F_{ij} is defined in terms of the motion functions $x_i = x_i(\xi_j, t)$ written in terms of the coordinates x_i

$$F_{ij} = \frac{\partial x_i}{\partial \xi_j} \tag{C.137}$$

with the displacement vector $u_i = x_i - \xi_i$

$$F_{ij} = \frac{\partial u_i}{\partial \xi_j} + \delta_{ij} \tag{C.138}$$

The rate of deformation gradient is:

$$\dot{F}_{ij} = \frac{\partial \dot{u}_i}{\partial \xi_j} = \frac{\partial \dot{u}_i}{\partial x_k} F_{kj} \tag{C.139}$$

With the assumption of small deformations $F_{ij} = \delta_{ij}$ and then:

$$\dot{F}_{ij} = \frac{\partial \dot{u}_i}{\partial x_j} \tag{C.140}$$

To eliminate rotation effects, taking the symmetric part of F_{ij} and defining the strain tensor as:

$$\dot{\varepsilon}_{ij} = \tfrac{1}{2}\left(\frac{\partial \dot{u}_i}{\partial x_j} + \frac{\partial \dot{u}_j}{\partial x_i}\right) \tag{C.141}$$

Recalling the classical notion of *material instability* (Hill 1958), (Maier & Hueckel 1979), a material is defined as stable if its constitutive relationship fulfills the condition of a second order work density $\dot{\varepsilon}_{ij}\dot{\sigma}_{ij} > 0$ and in a volume V:

$$\int_V \dot{\varepsilon}_{ij}\dot{\sigma}_{ij}dV > 0 \tag{C.142}$$

Using incrementally linear constitutive equations, the occurrence of material instability is indicated by the loss of definiteness of the material tangent stiffness tensor D_{ijkl}:

$$\dot{\varepsilon}_{ij}D_{ijkl}\dot{\varepsilon}_{kl} = 0 \tag{C.143}$$

For a symmetric tangent stiffness tensor, the loss of material stability coincides with the limit point ($\dot{\sigma}_{ij} = D_{ijkl}\dot{\varepsilon}_{kl} = 0$) and loss of uniqueness. For a nonsymmetric tangent stiffness tensor, loss of material stability may be encountered prior to the limit point and loss of uniqueness.

For a discrete mechanical system with the nonsymmetric stiffness matrix $\mathbf{K}$, the structural instability condition can be written as:

$$\left|\mathbf{K} + \mathbf{K}^T\right| = 0 \tag{C.144}$$

In this case Pamin demonstrates that the bifurcation point is detected when the smallest eigenvalue of the tangent operator $\mathbf{K}$ becomes negative. Then it is concluded that for a symmetric tangent operator, loss of structural stability coincides with the loss of solution uniqueness. For a nonsymmetric tangent stiffness, the structural stability may be lost before the loss of uniqueness.

Pamin considers a homogeneous and homogeneously deformed body, and investigates the possibility of a discontinuity in the deformation gradient produced by a further increment of deformation. He found the following condition:

$$(v_i D_{ijkl} v_l)\mu_k = 0 \tag{C.145}$$

in which the jump of the displacement gradient has the form $[\![u_{i,j}]\!] = v_i\mu_j$ for an arbitrary vector μ_i. The quantity $Q_{jk} = v_i D_{ijkl} v_l$ is called the acoustic tensor. When the determinant of the acoustic tensor is equal to zero there is a singularity, and this corresponds to the loss of ellipticity of the rate equilibrium equations. Ellipticity is one of the necessary conditions for well-posedness of the rate boundary value problem. The emergence of the discontinuities has traditionally been identified by strain localization (localization has been understood as a bifurcation in the macroscopic constitutive description of the material).

Implications for softening and non-associated plasticity Pamin considers a bilinear stress-strain relationship composed of a linear-elastic branch and a linear softening branch. In the post peak regime $\varepsilon = \varepsilon^e + \varepsilon^p$ and the plastic strains are determined from:

$$\sigma = \sigma_y + h\varepsilon^p \tag{C.146}$$

where h is a negative softening modulus. The strain rate may be calculated from:

$$\dot{\sigma} = \frac{Eh}{h+E}\dot{\varepsilon} \tag{C.147}$$

When the hardening modulus h is non-positive material stability and ellipticity are lost.

In a three-dimensional elastic body, the constitutive relations take the form:

$$\dot{\boldsymbol{\sigma}} = \mathbf{D}^e(\dot{\boldsymbol{\varepsilon}} - \dot{\lambda}\mathbf{m}) \tag{C.148}$$

where $\dot{\lambda}$ determines the magnitude and $\mathbf{m}$ the direction of the plastic flow. The plastic flow is governed by the consistency condition

$$\dot{F} = \mathbf{n}^T\dot{\boldsymbol{\sigma}} - h\dot{\lambda} = 0 \tag{C.149}$$

The gradient to the yield function is:

$$\mathbf{n} = \frac{\partial F}{\partial \boldsymbol{\sigma}} \tag{C.150}$$

Using these equations, it is possible to obtain the tangential stiffness relation:

$$\dot{\boldsymbol{\sigma}} = \left[\mathbf{D}^e - \frac{\mathbf{D}^e\mathbf{m}\mathbf{n}^T\mathbf{D}^e}{h + \mathbf{n}^T\mathbf{D}^e\mathbf{m}}\right]\dot{\boldsymbol{\varepsilon}} \tag{C.151}$$

Finally, it is possible to investigate the material stability replacing the non-symmetric elasto-plastic stiffness matrix from eq. (C.151) in the matrix form of (eq.C.143). For $\mathbf{n} = \mathbf{m}$ (associated plasticity) the loss of material stability is possible when h is zero or negative. There is a critical strain rate $\dot{\boldsymbol{\varepsilon}} = \dot{\alpha}\mathbf{n}$ with a scalar $\dot{\alpha}$, for which the product $\dot{\boldsymbol{\varepsilon}}^T\dot{\boldsymbol{\sigma}} \leq 0$. For $\mathbf{n} \neq \mathbf{m}$ (non associated plasticity) the loss of material stability may occur even if the hardening modulus is positive. The nonsymmetry of the tangent operator is thus a destabilizing factor.

Substituting the stiffness matrix of eq. (C.151) into the definition of the acoustic tensor eq. (C.145), it is possible to find the critical values of h and the direction vector $\mathbf{v}$ normal to the discontinuity plane (Rudnicki & Rice 1975). However, an assessment of the post-critical behavior of the system is impossible since well-posedness of the boundary value problem is lost.

Mesh sensitivity of results for classical continuum Pamin presents a series of results of finite element analysis using the theory presented above. The shear bands are produced by the inclusion of an imperfection in the mesh. After the peak load the solutions are all unstable, the strains have a tendency to concentrate in the smallest possible area. Pamin notices that in the absence of a physically motivated length scale which would govern the width of the localization zone, such a scale is

introduced into the problem by the discretization (element size). He proposes then to incorporate an internal length in the continuum description.

Another observation from the examples presented by Pamin is that shear bands have the incorrect tendency to follow the mesh lines, since in this direction they can be narrower.

Therefore, it has been suggested as solutions to enrich the strain interpolation by incompatible assumed strain functions (Ortiz et al. 1987) and to use an adaptative mesh refinement (Ortiz & Quigley 1990). While the former enhancement improves the element kinematics and the latter is obviously advisable in the presence of large strain gradients, none of them remove the fundamental difficulty associated with the loss of ellipticity.

Related work and possible solution approaches

Discountinuum versus continuum modeling. Two possible approaches have been proposed: discontinuum modeling and enhanced continuum modeling. In the first one, the softening is attributed to discrete cracks, in which continuity of deformation is abandoned. In the second approach an internal length scale is introduced in the continuum description.

In the discontinuum modeling, interface elements are introduced between continuum elements. The difficulty of discontinuum modeling lies in the fact that either the morphology of the cracks must be known a priory, or the interfaces must be assumed between all continuum elements in the potential fracture zone, or frequent remeshing must be performed during the analysis. (Larsson 1992).

It is convenient to remain within the continuum description and use the classical quantities of stress and strain, having now modified definitions in order to better reproduce the physical reality in degrading materials. It is possible to relate the classical softening model to the fracture energy treated as a material constant (Bažant & Oh 1983), (William 1984):

$$G_t = w \int \sigma d\varepsilon \tag{C.152}$$

where w is the width of the localization zone, which is related to the finite element size to remedy the mesh dependence of the load deformation response. Consequently, the softening diagram must be adjusted for each finite element mesh.

The results are mesh insensitive and the size effect can be reproduced, but the fracture energy release still takes place in a different area for each mesh, since the loss of ellipticity is not prevented.

In an enhanced continuum approach, either the continuum kinematics must incorporate the evolution of microstructures or the macroscopic constitutive relations must be nonlocal (De Borst, Sluys, Muhlhaus & Pamin 1993). It is necessary to admit that the stress tensor at a material point $\boldsymbol{\xi}$ depends on the motion history of all the material points $\boldsymbol{\eta}$ in a certain neighborhood of the point ξ:

$$\boldsymbol{\sigma}(\boldsymbol{\xi}, t) = \boldsymbol{\psi}(\boldsymbol{\xi}, \mathbf{x}(\boldsymbol{\eta}, t - \tau)) \tag{C.153}$$

where ψ is a nonlocal constitutive functional. ψ only depends on the relative motion of the points η and ξ which can be approximated by a Tailor series around ξ:

$$\mathbf{x}(\eta,t)-\mathbf{x}(\xi,t)=\mathbf{F}(\xi,t)(\eta-\xi)+\tfrac{1}{2}\mathbf{F}_2(\xi,t)(\eta-\xi)^2+\cdots+\tfrac{1}{n!}\mathbf{F}_n(\xi,t)(\eta-\xi)^n \quad \text{(C.154)}$$

where $\mathbf{F}_n$ is the n-th order deformation gradient. Three enhanced continuum approaches have so far proven to be successful:

1. Cosserat (micropolar) continuum.
2. Nonlocal (integral) model.
3. Higher-order gradient continuum

Micropolar continuum. Pamin presents the idea of couple stress, and microcurvatures defined in the plane case as:

$$\kappa_{zx}=\frac{\partial\omega_z}{\partial x}, \qquad \kappa_{zy}=\frac{\partial\omega_z}{\partial y} \quad \text{(C.155)}$$

The couple stress μ_{ij} are proportional to the microcurvatures, in the plane case:

$$\mu_{zx}=Gl^2\kappa_{zx}, \qquad \mu_{zy}=Gl^2\kappa_{zy} \quad \text{(C.156)}$$

where G is the elastic shear modulus and l is an internal length for the material. The presence of microrotations is specially relevant for granular materials, and the internal length has been shown to determine the thickness of shear bands (Mühlhaus & Vardoulakis 1987).

It is assumed that the microrotations are equal to the local rigid rotations (Mindlin 1962) (In section C.3.11 Christoffersen attributes this relation to Koiter eq. (C.46)):

$$\omega_z=\tfrac{1}{2}\left(\frac{\partial v}{\partial x}-\frac{\partial u}{\partial y}\right) \quad \text{(C.157)}$$

From eq. (C.157) eq. (C.155) and again eq. (C.156) it is founded that second order deformation gradients are incorporated in the formulation, and therefore, such a micropolar continuum is a special case of a grade-2 continuum.

Nonlocal integral models The nonlocal continuum approach is based on spatial averaging of tensor or scalar state variables in a certain neighborhood of a given point. With the aid of a weighting function $g(\mathbf{s})$ a nonlocal quantity Y is defined as:

$$\bar{Y}(\mathbf{x})=\frac{1}{V_g}\int_V Y(\mathbf{x}+\mathbf{s})g(\mathbf{s})dV, \qquad V_g=\int_V g(\mathbf{s})dV \quad \text{(C.158)}$$

where the weighting function is normalized with its integral so that $\bar{Y} = Y$ if $Y(\mathbf{x})$ is constant. The weighting function is for instance taken as the Gauss error function

$$g(\mathbf{s}) = \exp\left(\frac{-|s|^2}{2l^2}\right) \tag{C.159}$$

The parameter l plays the role of an internal length scale.

In finite element implementation, an additional loop over the elements is required to determine the nonlocal quantity, but standard C^0 continuous elements can be used. If the averaging domain extends to the outside of the given body, the problem of additional boundary conditions occurs.

The nonlocal approach is appealing from a physical point of view and has a convincing micromechanical motivation (Bažant 1994). A general constitutive law as follows is considered:

$$\Delta\boldsymbol{\sigma} = \mathbf{D}^e \Delta\varepsilon - \Delta\bar{\mathbf{S}} \tag{C.160}$$

where $\Delta\bar{\mathbf{S}}$ is a spatial averaging of the inelastic stress increment tensor $\Delta\mathbf{S}$ according to eq. (C.158). It has been proved (Carmeliet & De Borst 1994) that the incorporation of a localization limiter is necessary to avoid the spurious discretization sensitivity.

C.5.3 Gradient-dependent softening plasticity theory

Essentials of the theory

Pamin focuses on the development of a gradient-dependent continuum formulation. Incorporation of the gradient-dependence into plasticity theory has been made plausible by consideration of dislocation motion and evolution (Aifantis 1984), (Aifantis 1987). The second order derivative of an accumulated shear strain $\bar{\gamma}$ has been included in the shear stress-strain rate equation (Coleman & Hodgon 1985):

$$\tau = \left(\bar{\tau}(\bar{\gamma}) - c\frac{d^2\bar{\gamma}}{dx^2}\right)\frac{\dot{\gamma}}{|\dot{\gamma}|} \tag{C.161}$$

where τ is the shear stress, $\dot{\gamma}$ the shear strain rate, $\bar{\tau}(\bar{\gamma})$ is the yield stress and c is a positive phenomenological constant.

In a more general approach, the Laplacian of an effective deformation measure γ has been included in the yield condition (Zbib & Aifantis 1997) which has been written as:

$$\tau = \bar{\tau}(\gamma) - c\nabla^2\gamma \tag{C.162}$$

where τ is the second invariant of the deviatoric stress tensor and $\bar{\tau}(\gamma)$ is the hardening law.

In his thesis Pamin makes use of a gradient-dependent plasticity theory (De Borst & Muhlhaus 1991) (De Borst & Muhlhaus 1992) in which the yield condition is similar to eq. (C.162):

$$\phi(\boldsymbol{\sigma}) = \bar{\sigma}(\kappa) - g\nabla^2\kappa \tag{C.163}$$

where $\phi(\boldsymbol{\sigma})$ is an equivalent stress ($\sqrt{3J_2}$ for Huber-Mises plasticity), κ is an invariant plastic strain measure, $\bar{\sigma}$ is the yield strength and g is positive coefficient with the dimension of force. The gradient term is negligible if strains vary slowly in space, but has a significant influence on the presence of strain localization.

Analytical solution for a one-dimensional case. Before presenting the general theory, Pamin illustrates the introduction of second order gradient using a simple uniaxial problem. He starts developing the function $\varepsilon^p(x+s)$ in a Taylor series around $s = 0$:

$$\tilde{\varepsilon^p}(x) = \frac{1}{a}\int_{-a/2}^{a/2}[\varepsilon^p(x) + \varepsilon'^p(x)s + \tfrac{1}{2}\varepsilon''^p(x)s^2 + \ldots]ds \approx \varepsilon^p(x) + \tfrac{a^2}{24}\varepsilon''^p(x) \tag{C.164}$$

where $'$ denotes differentiation with respect to x. Defining $l^2 = a^2/24$ and using eq. (C.146), the gradient dependent yield condition is obtained:

$$\sigma = \sigma_y + h\varepsilon^p + hl^2\varepsilon''^p \tag{C.165}$$

It is possible to observe that eq. (C.165) has the same form as eq. (C.163) with $g = -hl^2$.

Assuming localization of plastic strains within a length w at the center of the bar, using the boundary condition $\varepsilon^p = 0$ for $x = \pm w/2$ and assuming symmetry respect to $x = 0$, the inhomogeneous second order differential equation eq. (C.165) can be derived as:

$$\varepsilon^p = \frac{\sigma - \sigma_y}{h}\left[1 - \frac{\cos(x/l)}{\cos(w/2l)}\right] \tag{C.166}$$

Calculating the average strain $\bar{\varepsilon}$ in w and looking for the most critical solution produce:

$$\bar{\varepsilon} = \frac{\sigma}{E} + \frac{\sigma - \sigma_y}{h}\frac{2\pi l}{L} \tag{C.167}$$

where L is the length of the bar. The slope of the post-peak branch is:

$$\frac{d\bar{\varepsilon}}{d\sigma} = \frac{1}{E} + \frac{2\pi}{h}\frac{l}{L} \tag{C.168}$$

Material stability and ellipticity. Writing the assumed yield condition eq. (C.163) in the form:

$$F = \phi(\boldsymbol{\sigma}) - \bar{\sigma}(\kappa) + g\nabla^2\kappa = 0 \tag{C.169}$$

the consistency argument yields the following equation:

$$\dot{F} = \mathbf{n}^T\dot{(\boldsymbol{\sigma})} - h\dot{\lambda} + g\nabla^2\dot{\kappa} = 0 \tag{C.170}$$

where $\mathbf{n}$ and h are defined as eq. (C.150):

$$\mathbf{n} = \frac{\partial F}{\partial \boldsymbol{\sigma}} = \frac{\partial \phi}{\partial \boldsymbol{\sigma}} \tag{C.171}$$

$$h = -\frac{\dot{\kappa}}{\dot{\lambda}}\frac{\partial F}{\partial \kappa} = \frac{\dot{\kappa}}{\dot{\lambda}}\frac{\partial \bar{\sigma}}{\partial \kappa} \tag{C.172}$$

Calculation of $\dot{\lambda}$ from eq. (C.170) substitution into the constitutive relation eq. (C.148) and using the Sherman-Morrison formula, the modified elasto-plastic stress-strain relation can be written as:

$$\dot{\boldsymbol{\sigma}} = \mathbf{D}^{ep}\dot{\boldsymbol{\varepsilon}} + \mathbf{g}\nabla^2\dot{\kappa} \tag{C.173}$$

with

$$\mathbf{D}^{ep} = \mathbf{D}^e - \frac{\mathbf{D}^e\mathbf{m}\mathbf{n}^T\mathbf{D}^e}{h + \mathbf{n}^T\mathbf{D}^e\mathbf{m}}, \qquad \mathbf{g} = -g\frac{\mathbf{D}^e\mathbf{m}}{h + \mathbf{n}^T\mathbf{D}^e\mathbf{m}} \tag{C.174}$$

Considering the possibility of emergence of a discontinuity across the plane with a normal v_i, which involves a jump in the deformation gradient eq. (C.175) and in the second order gradient eq. (C.176) with an arbitrary vector α_k

$$[\![\varepsilon_{ij}]\!] = \frac{1}{2}(v_i\mu_j + v_j\mu_i) \tag{C.175}$$

$$[\![\nabla^2\dot{\kappa}]\!] = v_k\alpha_k \tag{C.176}$$

where $[\![]\!]$ denotes a jump of a quantity. Using the fact that the equilibrium condition requires the continuity of tractions across the discontinuity plane, and the elastoplastic constitutive relation eq. (C.173), it is possible to write:

$$[\![\dot{t_j}]\!] = v_i[\![\dot{\sigma_{ij}}]\!] = (v_iD_{ijkl}v_l)\mu_k + (v_ig_{ij}v_k)\alpha_k = 0 \tag{C.177}$$

where $\dot{t_j}$ are the traction rates across the discontinuity. Emergence of the discontinuity is possible only if, for arbitrary μ_k and α_k, both contributions in eq. (C.177) vanish simultaneously. This does not normally happen. Since violation of the bifurcation condition eq. (C.175) guarantees ellipticity, it is possible to conclude that the gradient dependence has a regularizing effect.

Rate boundary value problem

Under the assumption of small deformations and static loading, Pamin presents the following equations for an elasto-plastic body:

$$\mathbf{L}^T\dot{\boldsymbol{\sigma}} + \dot{\mathbf{b}} = \mathbf{0} \tag{C.178}$$

$$\dot{\boldsymbol{\varepsilon}} = \mathbf{L}\dot{\mathbf{u}} \tag{C.179}$$

$$\dot{\boldsymbol{\sigma}} = \mathbf{D}^e(\dot{\boldsymbol{\varepsilon}} - \dot{\lambda}\mathbf{m}) \tag{C.180}$$

where $\mathbf{L}$ is a differential operator matrix, $\mathbf{b}$ is a body force vector and $\mathbf{D}^e$ is the elastic stiffness matrix. The flow rule is:

$$\dot{\boldsymbol{\varepsilon}}^p = \dot{\lambda}\mathbf{m}, \qquad \mathbf{m} = \frac{\partial G}{\partial \boldsymbol{\sigma}} \tag{C.181}$$

where $\mathbf{m}$ is derived from a plastic potential function $G = G(\boldsymbol{\sigma})$.

The gradient dependence is included in the definition of the yield function F:

$$F = \phi(\sigma) - \bar{\sigma}_g(\kappa, \nabla^2\kappa) \tag{C.182}$$

where $\bar{\sigma}_g$ is gradient dependent and $\kappa = \eta\dot{\lambda}$ is an invariant plastic strain measure. The plastic consistency condition $\dot{F} = 0$ becomes a differential equation:

$$\left(\frac{\partial F}{\partial \boldsymbol{\sigma}}\right)^T \dot{\boldsymbol{\sigma}} + \frac{\partial F}{\partial \kappa}\dot{\kappa} + \frac{\partial F}{\partial \nabla^2\kappa}\nabla^2\dot{\kappa} = 0 \tag{C.183}$$

Using the gradient of the yield function eq. (C.171) , the variable hardening modulus eq. (C.172) and the gradient influence variable g

$$g(\kappa) = \frac{\dot{\kappa}}{\dot{\lambda}}\frac{\partial F}{\partial \nabla^2\kappa} = \eta\frac{\partial \bar{\sigma}_g}{\partial \nabla^2\kappa} \tag{C.184}$$

it is possible to write eq. (C.183) in the form:

$$\mathbf{n}^T\dot{\boldsymbol{\sigma}} - h\dot{\lambda} + g\nabla^2\dot{\lambda} = 0 \tag{C.185}$$

The problem of solving eq. (C.185) is thus characteristic for the present theory.

Weak form of field equations

Multiplying eq. (C.185) by a variation of the plastic multiplier $\delta\dot{\lambda}$ and integrating over the plastic volume of the body, it is possible to write:

$$\int_V \delta\dot{\lambda}(\mathbf{n}^T\dot{\boldsymbol{\sigma}} - h\dot{\lambda} + g\nabla^2\dot{\lambda}) = 0 \tag{C.186}$$

After substitution of the relation between the stress and elastic strain rate eq. (C.180) and after integration by parts the following is obtained:

$$\int_V \delta\dot{\lambda}[\mathbf{n}^T\mathbf{D}^e\dot{\boldsymbol{\varepsilon}} - (h + \mathbf{n}^T\mathbf{D}^e\mathbf{m})\dot{\lambda}]dV - \int_V g(\nabla\delta\dot{\lambda})^T(\nabla\dot{\lambda})dV + \int_S g\delta\dot{\lambda}(\nabla\dot{\lambda})^T\mathbf{v}_\lambda dS = 0 \tag{C.187}$$

where $\mathbf{v}_\lambda$ defines the outward normal to the boundary of the plastic part of the body. The eq. (C.187) leads to a symmetric matrix problem. In this case, standard C^0 continuous shape functions suffice for both $\dot{\mathbf{u}}$ and $\dot{\lambda}$.

The next part of this reference corresponds to the finite element implementation of the problem according to eq. (C.187) and discussion of the results obtained in localization problems.

C.6 Gao and Nix

C.6.1 Gao and Nix, 1998

Gao & Nix (1998) present the concept of geometrically necessary dislocations, and use this concept to model the indentation test in metals, the results are compared with experimental results.

Introduction

A number of experiments have shown that the flow properties of crystalline solids can be dependent not only on the strain but also on the strain gradient. Fleck et al. (1994) have pointed out that the hardness is observed to increase with decreased indentation size. Large strain gradients that are present in small indentation test lead to geometrically necessary dislocations that cause enhanced hardening.

To account for these effects, Fleck & Hutchinson (1993) have developed a phenomenological theory of plasticity, using a single, constant, material length scale, l, within the general framework of couple stress theory. This theory bears some resemblance to the early work of Kröner (1963). A more general formulation of the phenomenological theory, which involves up to three independent material length scales, has been developed by Fleck & Hutchinson (1997).

Model

Gao & Nix (1998) developed a model of geometrically necessary dislocations based on De Guzman, Neubauer, Flinn & Nix (1993). The model is based on an indentation test which supposes a rigid cone. To estimate the deformation resistance, Gao & Nix (1998) make use of Taylor's relation to find the shear strength as:

$$\tau = \alpha\mu b\sqrt{\rho_T} = \alpha\mu b\sqrt{\rho_G + \rho_s} \tag{C.188}$$

where ρ_T is the total dislocation density in the indentation, ρ_S is the density of statistically stored dislocations, ρ_G is the density of geometrically necessary dislocations, μ is the shear modulus, b is Burgers' vector and α is a constant to be taken as 0.5. While ρ_S is not expected to depend on the depth of indentation, it depends on the average strain in the indentation, which is related to the shape of the indent.

Comparison with indentation test

Gao & Nix (1998) compare results using the geometrically necessary dislocation model with results obtained experimentally. They observe excellent agreement between the model and the tests.

A law for gradient plasticity

Using the model for geometrically necessary dislocations, Gao & Nix (1998) derive a law for strain gradient plasticity. For the indentation problem, a measure of the strain gradient is:

$$\xi = \frac{\tan(\theta)}{a} \tag{C.189}$$

where a is the contact radius and θ is the angle between the conical indenter and the plane of the surface. Using eq. (C.189) and eq. (C.188), together with the von Mises flow rule, the expression for the depth dependence of the hardness is:

$$\left(\frac{\sigma}{\sigma_0}\right)^2 = 1 + \tfrac{9}{8}b\xi\left(\frac{\mu}{\sigma_0}\right)^2 \tag{C.190}$$

or more simply,

$$\left(\frac{\sigma}{\sigma_0}\right)^2 = 1 + b\left(\frac{\mu}{\sigma_0}\right)^2\xi \tag{C.191}$$

where σ is the effective flow stress in the presence of a strain gradient and σ_0 is the flow stress in the absence of a gradient. The quantity

$$\hat{l} = b\left(\frac{\mu}{\sigma_0}\right)^2 \tag{C.192}$$

is a length scale to which any strain gradient must be compared to determine the effect of the strain gradient on the flow stress. $\hat{l}$ depends on the mean spacing between dislocations and the Burgers vector.

Strain gradient plasticity

The indentation experiments suggest a strain gradient plasticity law of the form:

$$\sigma^2 = \sigma_0^2 + \mu^2 b\xi \tag{C.193}$$

where ξ measures the strain gradient. Considering the usual power hardening law in the absence of a strain gradient:

$$\sigma_0 = \sigma_{\text{ref}}\varepsilon^{1/n} \tag{C.194}$$

where n is a hardening exponent and σ_{ref} is a reference stress taken to be a measure of the yield stress. Inserting eq. (C.193) into eq. (C.194) yields a strain gradient plasticity law with a strain-independent material length scale:

$$\left(\frac{\sigma}{\sigma_{\text{ref}}}\right)^2 = \varepsilon^{2/n} + b\left(\frac{\mu}{\sigma_{\text{ref}}}\right)^2 \xi \tag{C.195}$$

This can be compared to the corresponding law in the Fleck & Hutchinson (1997) strain gradient plasticity framework, in the case of a single material length scale:

$$\left(\frac{\sigma}{\sigma_{\text{ref}}}\right)^2 = \left(\varepsilon^\beta + (l\xi)^\beta\right)^{2/(n\beta)} \tag{C.196}$$

where l is a phenomenological length scale, β is an exponent usually taken to be 2 ((Fleck & Hutchinson 1993)). The effective strain ε and the effective strain gradient ξ are related to the tensor components by:

$$\varepsilon = \sqrt{\tfrac{2}{3}\varepsilon_{ij}\varepsilon_{ij}}, \qquad \xi = \sqrt{\tfrac{2}{3}\xi_{ij}\xi_{ij}} \tag{C.197}$$

where ξ_{ij} is the so-called curvature tensor, which is related to the third order strain gradient tensor by:

$$\xi_{ij} = e_{ikl}\varepsilon_{jk,l} \tag{C.198}$$

where e_{ikl} is the permutation tensor.

The effective gradient ξ corresponds to the invariant of the curvature tensor ξ_{ij}.

The strain gradient law eq. (C.195) exactly matches the Fleck-Hutchinson phenomenological law eq. (C.196) only under the following conditions:

$$n = 2, \qquad \beta = 1, \qquad l = b\left(\frac{\mu}{\sigma_{\text{ref}}}^2\right) = \hat{l}\left(\frac{\sigma_0}{\sigma_r e f}\right)^2 \tag{C.199}$$

The phenomenological length scale l of Fleck and Hutchinson is now related to measurable physical parameters, and to the microstructural length scale $\hat{l}$. Serious numerical problems are observed and reported when the value of β approaches 1 (Fleck & Hutchinson 1997). Apparently, further developments of the strain gradient plasticity theory are required.

C.6.2 Gao, Huang and Nix 1999

In this paper Gao, Huang & Nix (1999) present a theory called mechanism-based strain gradient plasticity (MSG) which connects microscale dislocation interaction to mesoscale plasticity.

Introduction

The classical continuum plasticity theory cannot predict the size dependence of material behavior observed at the micrometer scale because their constitutive models possess no internal material length scale. Strain gradient plasticity represents such a theory which connects classical plasticity to dislocation mechanics.

Dislocations become stored for one of two reasons: they accumulate by trapping each other in a random way, or they are required for compatible deformation between various parts of the material. Plastic strain gradients appear either because of the loading geometry or because of inhomogeneous deformation in the material.

Fleck & Hutchinson (1993) developed a phenomenological theory of strain gradient plasticity. Dimensional consideration has demanded a constitutive length parameter, l, which is thought of as an internal material length related to the storage of geometrically necessary dislocations. Its prediction of micro and nanoindentation hardness falls short of agreement with the significant increase observed in the micro and nano indentation tests. To resolve this inconsistency Fleck & Hutchinson (1997) have proposed an extended theory of strain gradient plasticity that introduces two additional material lengths.

Recently the development on strain gradient plasticity has focused on two questions:

1. What is the physical interpretation of the constitutive length parameters l?
2. Is it possible to develop a theory of mesoscale plasticity directly based on microscale dislocation mechanics?

Gao & Nix (1998) have shed light on these questions. They started from Taylor's relationship between the shear strength and total dislocations density. The density of geometrically necessary dislocations is related to an effective strain gradient ξ by $\rho_G = \eta/b$, b is the Burgers vector, and ρ_G is the density of geometrically necessary dislocations. In the absence of a strain gradient term, the density of statistically

stored dislocations ρ_S is obtained from the uniaxial power law stress relationship eq. (C.194), the flow stress is obtained as eq. (C.195). Using a different notation, eq. (C.195) is written as:

$$\sigma = \sigma_{\text{ref}}\sqrt{\varepsilon^{2N} + l\eta} \tag{C.200}$$

where $N = 1/n$, $\eta = \xi$ and

$$l = \bar{M}^2\alpha^2(\mu/\sigma_{\text{ref}})^2\bar{r}b \tag{C.201}$$

is identified as the intrinsic material parameter for strain gradient plasticity. $\bar{M}$ is the Taylor factor and $\bar{r}$ is the Nye factor introduced by Arsenlis & Parks (1999) to reflect the scalar measure of geometrically necessary dislocation density resulting from macroscopic plastic strain gradients.

If the representative length of nonuniform deformation is much larger than l, strain gradients effects are negligible. It is important to note that l is a natural combination of the elastic modulus μ, the plastic stress σ_{ref} and the atomic Burgers vector b. Gao & Nix (1998) have estimated the macroindentation hardness based on eq. (C.200). They found that the strain gradient law implies that the square of indentation hardness depends linearly on $1/h$, where h is the depth of indentation. The phenomenological theories of strain gradient plasticity fail to explain such behavior. This motivates an alternative formulation in which the Taylor hardening model is adopted as a founding principle. The resulting theory (MSG) is based on a multiscale hierarchical framework linking the microscale notion to the mesoscale notion. In the microscale, the Taylor hardening model in dislocation mechanics is used to characterize dislocation interactions and their effect on the flow of stress. On the mesoscale, the constitutive equations are constructed by averaging microscale plasticity laws over a representative cell. The mathematical structure is similar to the phenomenological theory proposed by Fleck & Hutchinson (1997).

C.6.3 Geometrically necessary dislocations

Geometrically necessary dislocations are dislocations which are necessary to accommodate the geometry of plastic deformation. The presence of these dislocations causes additional storage of defects and increases the deformation resistance by acting as obstacles to the statistically stored dislocations. The gradient of plastic strain corresponds to the density of geometrically necessary dislocations.

From the continuum plasticity point of view, it is necessary to link the density of geometrically necessary dislocations to deformation curvature $\eta_{ijk} = u_{k,ij}$ where u_k are the displacements. In MSG plasticity:

$$\rho_G b = \sqrt{c_1\eta_{iik}\eta_{jjk} + c_2\eta_{ijk}\eta_{ijk} + c_3\eta_{ijk}\eta_{kji}} \tag{C.202}$$

The three constants c_1, c_2 and c_3 scale the three quadratic invariants to the incompressible third order tensor η_{ijk} and are determined from three distinct dislocation models consisting of plane strain bending, pure torsion and two dimensional

axisymmetric void growth (Gao, Huang, Nix & Hutchinson 1999). The results produce $c_1 = 0$, $c_2 = 1/4$ and $c_3 = 0$ which suggest that including the Nye factor:

$$\rho_G = \frac{\bar{r}}{2b}\sqrt{\eta_{ijk}\eta_{ijk}} \tag{C.203}$$

The Taylor hardening model

In the Taylor model the interaction of a group of statistically stored dislocations which trap each other in a random way is considered. If the mean dislocation space is L, the critical stress required to induce significant plastic deformation is defined as the Taylor flow stress:

$$\tau_G = \alpha\mu/L = \alpha\mu b\sqrt{\rho} \tag{C.204}$$

where $\rho = 1/L^2$ is the dislocation density.

Mechanism-based strain gradient plasticity

Multiscale, Hierarchical Framework. On the microscale, the scale of analysis is small compared with the length over which the strain field varies. The microscale flow stress is governed by the dislocation motion, and it obeys the Taylor hardening relationship. Stresses and strains at the microscale are denoted $\hat{\sigma}_{ij}$ and $\hat{\varepsilon}_{ij}$, respectively. Flow stress is defined as the critical stress to move a glide dislocation through a forest of obstacles.

On mesoscale, a continuum plasticity theory is constructed to represent the collective behavior of dislocations on the microscale. In MSG plasticity, higher order stresses and strain gradients are introduced to ensure that the constitutive model satisfies the essential thermodynamic restrictions. The generalized strain measures are strains ε_{ij} and strain gradients $\eta_{ijk} = u_{k,ij}$. The stress measures are stresses σ_{ij} and higher order stresses τ_{ijk}.

The micro and meso scales are related by equality of virtual work at the two scales:

$$\int_{V_{cell}} \hat{\sigma}_{ij}\delta\hat{\varepsilon}_{ij}dV = (\sigma_{ij}\delta\varepsilon_{ij} + \tau_{ijk}\delta\eta_{ijk})V_{cell} \tag{C.205}$$

where V_{cell} is the volume of the mesoscale cell. Strains and strain gradients are related by the kinematic relationship $\delta\hat{\varepsilon}_{ij} = \delta\varepsilon_{ij} + \frac{1}{2}(\delta\eta_{kij} + \delta\eta_{kji})x_k$ where x_k are coordinates centered in the mesoscale cell.

The equilibrium equation in MSG plasticity is:

$$\sigma_{ik,i} - \tau_{ijk,ij} = 0 \tag{C.206}$$

Constitutive relations in MSG plasticity The Taylor hardening model at the microscale and the multiscale gives the mesoscale constitutive relationship on MSG plasticity:

$$\sigma_{ij} = K\varepsilon_{kk}\delta_{ij} + \frac{2}{3}\frac{\sigma}{\varepsilon}\varepsilon'_{ij} \tag{C.207}$$

$$\tau_{ijk} = l_\varepsilon^2\left[\frac{1}{6}K\eta^H_{ijk} + \frac{\sigma}{\varepsilon}(\Lambda_{ijk} - \Pi_{ijk}) + \frac{N\sigma_{\text{ref}}^2\varepsilon^{2N-1}}{\sigma}\Pi_{ijk}\right] \tag{C.208}$$

where K is the elastic bulk modulus, ε_{kk} and ε'_{ij} are the volume and deviatoric strains, $\varepsilon = (2\varepsilon'_{ij}\varepsilon'_{ij}/3)^{1/2}$ is the effective strain, σ is the flow stress in eq. (C.200), η^H_{ijk} is the volumetric part of strain gradients η_{ijk}, and Λ_{ijk} and Π_{ijk} depend on the deviatoric parts of strain and strains gradients (Gao, Huang, Nix & Hutchinson 1999). $l_\varepsilon = \beta b\mu/\sigma_{\text{ref}}$ where β is of the order of 10.

Experimental validation

Excellent agreement is observed between the numerically predicted microindentation hardness based on MSG and the experimental data. The comparison in the torsional case seems to be quite reasonable.

C.7 Geers M.G.D.

The following is extracted from the review of the book by Geers (Geers 1997), this author has not read the book itself.

It has been recognized that the mathematically consistent description of failure and the accompanying localization of deformation require higher order continuum models. If such an enhancement is not made, ill posed boundary value problems may result. The enhancement introduces one or more additional material parameters. Inevitably, a material parameter is introduced that has the dimension of length, and which is related to the dimensions of the localization zone.

An experimental problem resides in the determination of the characteristic length, it cannot be measured by simple tests, since it depends intrinsically on the local deformation behavior of the material.

The constant gradient damage method (CGD) suffers from some inherent deficiencies which render the method incapable of describing a discontinuous crack. The damage computed by the CGD-method propagates in a direction normal to the crack, which causes a widening of the damage zone. This shortcoming limits the applicability of the CGD method to problems where only small strains occur and no macroscopic cracks arise.

C.8 W Ehlers, P.Ellsiepen W. Volk

This corresponds to (Ehlers, Ellsiepen & Volk 2001). The authors are part of the Institut für Mechanik (Bauwesen), Universität Stuttgart, Germany.

The original article was not revised by this author, only the abstract. From this abstract the following is extracted:

Shear band phenomena occur as a result of local concentration of plastic strains in small bands of finite width (shear bands). It is well known that the numerical description of shear-band phenomena, e.g. in the framework of the finite element method, leads to an ill-posed problem, when the type of the governing differential equation changes from elliptic to hyperbolic. The direction and the width of the shear band strongly depend on the discretization.

Micropolarity includes additional material parameters (e.g. the internal length scale), which can be used for an implicit determination of the shear-band width independently of the mesh size.

C.9 Lages, Paulino, Menezes, and Silva

This corresponds to (Lages, Paulino, Menezes & Silva 1999).

The original article was not revised by the author, only the abstract; from this abstract and representative results the following is extracted:

The inclination of the post-peak branch in the study of localization phenomena using FEM shows reduced sensitivity to mesh refinement, especially for the finer meshes. The results are presented in graphics force displacement for variable meshes, and in deformed configurations presented by the authors.

C.10 Web page on nonlocal elasticity of the Rensselaer Polytechnic Institute

C.10.1 Introduction

Experimental results have shown a significant size effect in mechanical properties when the dimensions of the specimen or the probed material become small. The classical theories lack the capability of representing such effects, these theories are expected to fail when the specimen size or the wavelength of the perturbation become comparable with the internal length scale(s) of the material.

Several modifications of the classical elasticity theory have been proposed, their predictions reduce to those of local continuum theories when the specimen size is much larger than the internal length scale.

In the nonlocal elasticity due to Eringen (1972), the constitutive equation is expressed in terms of a non-local kernel. The stress at point $\mathbf{x}$ is a function of the strain at all points $\mathbf{y}$ in the body, through a weighting kernel α:

$$\sigma_{ij}(\mathbf{x}) = \int_V \alpha(|\mathbf{x}-\mathbf{y}|)t_{ij}(\mathbf{y})dV(\mathbf{y}) \tag{C.209}$$

(compare with equation (C.8)).

The kernel is often assumed to be Gaussian.

$$\alpha(|\mathbf{x}-\mathbf{y}|) = \alpha_0 exp[-(|\mathbf{x}-\mathbf{y}|/mb)^2] \tag{C.210}$$

mb is an intrinsic length scale, and α_0 is found from the normalization condition:

$$\int_V \alpha(|\mathbf{x}-\mathbf{y}|)dV(\mathbf{y}) = 1 \tag{C.211}$$

to be

$$\alpha_0 = \frac{1}{\pi\sqrt{x}m^3} \tag{C.212}$$

The selection of the internal length scale mb is still a controversial issue.

C.10.2 A new nonlocal elasticity kernel

In the original local kernel, the actual interatomic interactions are not directly represented. Even with the largest parameter suggested, $m = 0.5$, the kernel is so short ranged that a displacement of a first neighbor located at a distance b from the representative atom, has no effective influence on the central atom. There are suggestions that the actual kernel should change sign at a distance corresponding to the inflection point of the interatomic potential. Then it is necessary to change the definition of the kernel.

The functional form of the new suggested kernel is:

$$\alpha(|\mathbf{x}-\mathbf{y}|) = \alpha_0(1 = n(|\mathbf{x}-\mathbf{y}|/b)^2)exp[-(|\mathbf{x}-\mathbf{y}|/mb)^2] \tag{C.213}$$

where n is a second nondimensional non-locality parameter.

C.11 Discussion

In this paper, a general presentation of some of the available higher-order available theories in continuum mechanics are included. Every one of the authors presents a different motivation to develop or use these theories. For Lakes (section C.2), the motivation was to develop models for foam materials (like human bone); for Christoffersen (section C.3), it was to model problems involving nonsymmetry of the stress tensor like in magnetic dipole problems. The motivation for Hutchinson (section C.4), is the necessity to include scale factors in continuum mechanics, because it is necessary to include these factors to obtain agreement with experimental data of indentation, torsion of wires and other scale sensitive test. Pamin (section C.5), needs to include higher order theories to avoid numerical problems (for example mesh sensitivity in FEM) that are found using classical theories in the problem of strain localization. Gao and Nix (section C.6) are also motivated by the necessity of modeling indentation tests.

Common to all the theories is that they include a dependence of strain in strain gradients. This means that in all higher-order theories presented, the state of strain and stress at a point strongly depends on their neighborhood on a length scale associated with the microstructure of the material. These length scales could be of micrometers in metals, but could be greater depending on the material. Another common point is that these theories introduce length scale factors. When these theories are used in problems involving sizes much greater than the length scale factors, the theories reduce to the classical theory.

Lakes (1995) catalogs these theories into four groups: Cosserat theories, explicitly incorporating a local rotation of points. According to Christoffersen (2000), this rotation was an independent quantity in the original theory, but a relation between this rotation and gradient of displacements is proposed by Koiter (1964) eq. (C.46); the second one is the void theory; third non-local theory based on Eringen & Edelen (1972). And finally microstructure theories based on Mindlin (1965*a*). The Cosserat theory could be understood as a special case of microstructure theory.

Strain gradient theories (microstructure theories according to Lakes (1995)) are divided into three types by Fleck & Hutchinson (2001): theories based on Acharya & Bassani (2000) that incorporate the dependence on strain gradients in the tangent moduli. The second type of theory as proposed by Aifantis (1984). The work by Pamin (1994) could be considered in this group of theories which is characterized by the use of a hardening equation of the form eq. (C.163) involving the laplacian of the effective plastic strain rate as the starting point. The theory proposed by Fleck & Hutchinson (2001) is a theory of the same type, but the laplacian emerges as a byproduct of the more fundamental role of the plastic strain gradients. The third type of theory is the phenomenological theory proposed by Fleck & Hutchinson (1997) which is an extension of Fleck & Hutchinson (1993). These theories are the product of considering the concept of geometrically necessary dislocations. Gao & Nix (1998) developed another theory of this third type starting from the concept of geometrically necessary dislocations with eq. (C.195) as a yield strain plasticity law.

The theories based on the concept of necessary geometrically dislocations can be understood as theories linking classical plasticity and dislocation mechanics. It is important to these theories to diferentiate between microscale, in which dislocation mechanics works ($< 1\mu m$), and mesoscale, at which plasticity theory is formulated.

Every one of the higher order theories was developed to fulfill specific physical phenomena. Some of the applications mentioned here include modeling of foams (Lakes 1995), solids including twisting or spiraling fibers (Lakes & Benedict 1982), piezoelectric response (Lakes 2001), localization phenomena (Pamin 1994), (Ehlers et al. 2001), (Lages et al. 1999), (Geers 1997), size effects in material properties (Hutchinson 2000), (Fleck & Hutchinson 1997), (Fleck & Hutchinson 2001), (Gao & Nix 1998), (Gao, Huang & Nix 1999), mechanics of random structure materials (Warren & Byskov 2000).

In the present paper, the most elaborated theories are those presented by Fleck & Hutchinson (1997) and Fleck & Hutchinson (2001), both theories include three length parameters. The three length scale parameters seem to be necessary to accommodate a large number of problems using the same theory. It is found that

usually only one or two of the three length scale parameters govern in specific applications. Both theories converge to the same value when the plastic strain is large. The expected results of the first one are incorrect in the elastic range due to the artificially presented length parameters in the elastic range. The simplicity of the first theory permits closed forms solutions to basic problems. The second theory is easier to implement using finite element analysis than the first one.

Apparently, the easiest theory to implement into finite element analysis is a theory with only one length scale parameter, like the one proposed by Gao, Huang & Nix (1999) or Pamin (1994). The theory by Gao, Huang & Nix (1999) was compared with results of indentation tests by the authors producing acceptable agreement, but the same comparison with torsion of wires was not satisfactory.

C.12 Conclusions

An increasing number of higher-order theories exist in continuum mechanics. These theories can be used to find solutions to problems which involve length scales in continuum mechanics. The length scales are a natural part of higher-order theories, but at present it is unknown how many scale factors are really necessary for a general theory and which is their physical interpretation. The theories came from the necessity to solve specific problems and were usually developed for specific applications. The length scale parameters are usually obtained from experimental data.

In the elastic range, the characteristic lengths would normally be of atomic scale, but in materials with fibers or in cellular solids, these lengths are much bigger and experimentally observable. In plasticity, these scale effects are also observable.

Higher-order theories could have consequences in the study of structures made with materials like fiber-reinforced concrete, wood, fiber-reinforced plastics and others materials. The solution of simple problems like simple tension, pure bending, torsion, etc. could be used to obtain the additional elastic constants and length scales from testing.

C.13 Notes about the references

The references cited here by Lakes in (Lakes 1995) are (Lakes 1985), (Cosserat & Cosserat 1909), (Voigt 1887), (Voigt 1894), (Eriksen & Truesdell 1958), (Grioli 1960), (Aero & Kuvshinskii 1961), (Toupin 1962), (Mindlin & Tiersten 1962), (Mindlin 1965*b*), (Eringen 1968), (Eringen 1972), (Nowacki 1970), (Kunin 1982), (Kunin 1983), (Gauthier 1982), (Cowin 1970), (Cowin & Nunziato 1983), (Kröner 1967) and (Chirita 1978).

The references (Lakes 1982), (Yang & Lakes 1982), (Lakes & Benedict 1982) and (Lakes 1993) are cited by Lakes on his webpage.

The reference (Geers 1997) is cited on a review in the author web page.

The references (Koiter 1964) and (Christoffersen 1989) are cited by Christoffersen in
(Christoffersen 2000).

The references (Fleck et al. 1994), (Gao & Nix 1998), (Toupin 1962), (Mindlin 1965*a*), (Acharya & Bassani 1996), (Dai & Parks 1998) and (Fleck & Hutchinson 1997) are cited in (Hutchinson 2000).

The references (Hill 1958), (Maier & Hueckel 1979), (Rudnicki & Rice 1975), (Ortiz et al. 1987), (Ortiz & Quigley 1990), (Larsson 1992), (Bažant & Oh 1983), (William 1984), (De Borst et al. 1993), (Mühlhaus & Vardoulakis 1987), (Mindlin 1962), (Bažant 1994), (Carmeliet & De Borst 1994), (Aifantis 1984), (Aifantis 1987), (Coleman & Hodgon 1985), (Zbib & Aifantis 1997), (De Borst & Muhlhaus 1991), (De Borst & Muhlhaus 1992) are cited by Pamin in (Pamin 1994).

The references (Fleck et al. 1994), (Fleck & Hutchinson 1993), (Kröner 1963), (Fleck & Hutchinson 1997) and (De Guzman et al. 1993) are cited by Gao & Nix (1998).

The references (Fleck & Hutchinson 1993), (Fleck & Hutchinson 1997), (Gao & Nix 1998), (Arsenlis & Parks 1999), (Gao, Huang, Nix & Hutchinson 1999) are cited in (Gao, Huang & Nix 1999)

The references (Fleck & Hutchinson 1993), (Koiter 1964), (Mindlin 1965*a*) and (Toupin 1962) are cited in (Fleck & Hutchinson 1997)

The references (Acharya & Bassani 2000), (Aifantis 1984), (Fleck & Hutchinson 1997), (Begley & Hutchinson 1998) and (Fleck et al. 1994) are cited in (Fleck & Hutchinson 2001)

Bibliography

Acharya, A. & Bassani, J. L. (1996), On non-local flow theories that preserve the classical structure of incremental boundary value problems, *in* 'IUTAM Symp. on michromechanics of plasticity and damage', Kluwer Academic Publisher, pp. 3–10.

Acharya, A. & Bassani, J. L. (2000), 'Lattice incompatibility and a gradient theory of crystal plasticity', *J. Mech. Phys. Solids* **48**, 1565 1595.

Aero, E. L. & Kuvshinskii, E. V. (1961), *Fundamentals equations of the theory of elastic media with rotationally interacting particles*, Vol. 2, pp. 1272–1281. Fizika Tverdogo Tela, 2, 1399-1409, 1960.

Aifantis, E. C. (1984), 'On the microstructural origin of certain inelastic models', *J. Eng. Mater. Technol.* **106**, 326–330.

Aifantis, E. C. (1987), 'The physics of plastic deformation', *Int. J. Plasticity* **3**, 211–247.

Arsenlis, A. & Parks, D. M. (1999), 'Crystallographic aspects of geometrically-necessary and statistically-stored dislocation density', *Acta Mater* **47**, 1597–1611.

Ashby, M. F. (1970), 'The deformation of plastically non-homogeneous alloys', *Philos. Mag.* **21**, 399–424.

Bažant, Z. P. (1994), 'Nonlocal damage theory based on micromechanics of crack interactions', *ASCE J. Eng. Mech.* **120**, 593 617.

Bažant, Z. P. & Oh, B. (1983), 'Crack band theory for fracture of concrete', *RILEM Materials and structures* **16**, 155–177.

Begley, M. R. & Hutchinson, J. W. (1998), 'The mechanics of size-dependent indentation', *J. Mech. Phys. Solids* **46**, 2049 2068.

Carmeliet, J. & De Borst, R. (1994), Nonlocal damage and random fields, *in* H. e. a. Mang, ed., 'Proc. EURO-C 1994 Int. Conf. Computer Modelling of Concrete Structures', Pineridge Press, Swansea, pp. 73 82.

Chirita (1978), 'Saint venant's problem in nonlocal elasticity', *Analele stiintifice ale Universitatii 'Al. I. Cuza' Iasi* **24**, 147–156.

Christoffersen, J. (1989), 'When is a moment conservative?', *J. Appl. mech.* **56**, 299–301.

Christoffersen, J. (2000), Material curvature. Unpublished notes on Nonlinear Micropolar Theories.

Coleman, B. D. & Hodgon, M. L. (1985), 'On shear bands in ductile materials', *Arch. Ration. Mech. Anal.* **90**, 219 247.

Cosserat, E. & Cosserat, F. (1909), *Theorie des Corps Deformables*, Hermann et Fils,, Paris.

Cowin, S. C. (1970), 'An incorrect inequality in micropolar elasticity theory', *J. appl. Math. Phys. (ZAMP)* **21**, 494–497.

Cowin, S. C. & Nunziato, J. W. (1983), 'Linear elastic materials with voids', *J. Elasticity* **13**.

Dai, H. & Parks, D. M. (1998), Geometrically-necessary dislocation density in continuum plasticity theory and fem implementation. Unpublished.

De Borst, R. & Muhlhaus, H. B. (1991), Continuum models for discontinuos media, *in* van Mier G. J. M. et all, ed., 'Fracture Processes in Concrete, Rock and Ceramics', E and FN Spon/Chapman and Hall, London, pp. 601–618.

De Borst, R. & Muhlhaus, H. B. (1992), 'Gradient dependent plasticity: Formulation and algorithmic aspects', *Int. J. Num. Meth. Eng.* **35**, 521–539.

De Borst, R., Sluys, L. J., Muhlhaus, H. B. & Pamin, J. (1993), 'Fundamental issues in finite element analyses of localization of deformation', *Eng. Comput.* **10**, 99 121.

De Guzman, M. S., Neubauer, G., Flinn, P. & Nix, W. D. (1993), The role of indentation depth on the measured hardness of materials, *in* 'Materials Research Symposium Proceedings', Vol. 308, pp. 613 618.

Ehlers, W., Ellsiepen, P. & Volk, W. (2001), 'Localization phenomena in saturated and empty frictional porous materials computed by time and space-adaptative methods'.

Eriksen, J. L. & Truesdell, C. (1958), 'Exact theory of stress and strain in rods and shells', *Arch. Rational Mech. Anal.* **1**, 295–323.

Eringen, A. C. (1968), *Theory of micropolar elasticity*, Vol. 1, Academic Press.

Eringen, A. C. (1972), 'Linear theory of nonlocal elasticity and dispersion of plane waves', *Int. J. Engng. Sci.* **10**, 425–435.

Eringen, A. C. & Edelen, D. G. B. (1972), 'On nonlocal elasticity', *Int. J. Engng. Sci.* **10**, 233–248.

Fleck, N. A. & Hutchinson, J. W. (1993), 'A phenomenological theory for strain gradient effects in plasticity', *J. Mech. Phys. of Solids* **41**, 1825 1857.

Fleck, N. A. & Hutchinson, J. W. (1997), Strain gradient plasticity, *in* 'Adv. in Applied Mechanics', Vol. 33, Hutchinson, J. W., Wu T.T., pp. 295–361.

Fleck, N. A. & Hutchinson, J. W. (2001), 'A reformulation of strain gradient plasticity', *J. Mech. Phys. of Solids* **49**, 2245 – 2271.

Fleck, N. A., Muller, G. M., Ashby, M. F. & Hutchinson, J. W. (1994), 'Strain gradient plasticity theory and experiment', *Acta. Met. Mater* **42**, 475–487.

Gao, H., Huang, Y. & Nix, W. D. (1999), 'Modeling plasticity at the micrometer scale', *Naturwissenschaften* **86**, 507 515.

Gao, H., Huang, Y., Nix, W. D. & Hutchinson, J. W. (1999), 'Mechanism-based strain gradient plasticity i theory', *J. Mech. Phys Solids* **47**, 1239 1263.

Gao, H. & Nix, W. D. (1998), 'Identation size effects in crystalline materials: A law for strain gradient plasticity', *J. Mech. Phys. Solids* **46**, 411–425.

Gauthier, R. D. (1982), *Experimental investigations of micropolar media*, ed. Brulin R. K. T. Hsich, World Scientific, 1982.

Gauthier, R. D. & Jahsman, W. E. (1975), 'A quest for micropolar elastic constants', *J. Applied Mechanics* **42**, 369–374.

Geers, M. G. D. (1997), *Experimental analysis and Computational Modelling of Damage and Fracture*, Eindhoven University of Technology, Eindhoven.

Grioli, G. (1960), 'Elastiita asimmetrica', *Annali di Matematica pura e dapplicata, Ser IV* **50**, 389 417.

Hill, R. (1958), 'A general theory of uniqueness and stability in elastic-plastic solids', *J. Mech. Phys. Solids* **6**, 236–249.

Hutchinson, J. W. (2000), 'Plasticity at the micron scale', *Int. J. of Solids and Structures* **37**, 225–238.

Koiter, W. T. (1964), Couple stresses in the theory of elasticity, I and II, *in* 'Proc. Ned. Acad. Wet. (B)', Vol. 67, pp. 17–44.

Kröner, E. (1963), 'On the physical reality of torque stresses in continuum mechanics', *Int. J. Engineering Science* **1**, 261 278.

Kröner, E. (1967), 'Elasticity theory of materials with long range cohesive forces', *Int. J. Solids and Structures* **3**, 731 742.

Kunin, I. A. (1982), *Elastic media with microstructure I*, Springer Verlag, Berlin.

Kunin, I. A. (1983), *Elastic media with microstructure II*, Springer Verlag, Berlin.

Lages, E. N., Paulino, G. H., Menezes, I. F. M. & Silva, R. R. (1999), 'Nonlinear finite element analysis using an object-oriented philosophy application to beam elements and to the cosserat continuum', *Engineeering with Computers* **15**, 73 89.

Lakes, R. (1985), 'A pathological situation in micropolar elasticity', *J. Applied Mechanics* **52**, 234–235.

Lakes, R. (1995), Experimental methods for study of cosserat elastic solids and other generalized continua, *in* H. J. Muhlhaus, ed., 'Continuum models for materials with micro-structure.', J. Wiley, N.Y., pp. 1–22.

Lakes, R. (2001), 'Elastic and viscoelastic behavior of chiral materials', *Int. J. of Mech. Sciences* **43**, 1579 1589.

Lakes, R. & Benedict, R. (1982), 'Noncentrosymmetry in micropolar elasticity', *Int. J. of Engineering Science* **29(10)**, 1161 1167.

Lakes, R. S. (1982), 'Dynamical study of couple stress effect in human compact bone', *Journal of biomechanical Engineering* **104**, 6–11.

Lakes, R. S. (1993), 'Strongly cosserat elastic lattice and foam materials for enhanced toughness', *Cellular Polymers* **12**, 17–30.

Larsson, R. Runesson, K. (1992), Plastic localisation captured by discontinuous displacement approximation, *in* D. R. J. O. et al, ed., 'Proc. third Int. Conf. Computational Plasticity: Fundamentals and Applications', Pineridge Press, Swansea, pp. 605–616.

Maier, G. & Hueckel, T. (1979), 'Nonassociated and coupled flow rules of elastoplasticity for rock-like materials', *Int. J. Rock Mech. Min. Sci. and Geomech. Abstr.* **16**, 77 92.

Mindlin, R. D. (1962), 'Influence of couple-stresses on stress concentrations', *Exp. Mech.* **3**, 1–7.

Mindlin, R. D. (1965*a*), 'Second gradient of strain and surface-tension in linear elasticity', *Int. J. Solids Struct.* **1**, 417–438.

Mindlin, R. D. (1965*b*), 'Stress functions for a cosserat continuum', *Int. J. Solids and Structures* **1**, 265–271.

Mindlin, R. D. & Tiersten, H. F. (1962), 'Effect of couple stresses in linear elasticity', *Arch. Rational Mech, Analy* **11**, 415–448.

Mühlhaus, H. B. & Vardoulakis, I. (1987), 'The thickness of shear bands in granular materials', *Geotechnique* **37**, 271–283.

Nowacki, W. (1970), *Theory of micropolar elasticity*, Poznan.

Ortiz, M., Leroy, Y. & Needleman, A. (1987), 'A finite element method for localized failure analysis', *Comp. Meth. Appl. Mech. Eng.* **61**, 189–214.

Ortiz, M. & Quigley, J. J. (1990), 'Adaptive mesh refinement in strain loacalization problems', *Comp. Meth. Appl. Mech. Eng.* **90**, 781 804.

Pamin, J. K. (1994), Gradient dependent plasticity in numerical simulation of localization phenomena, PhD thesis, Technissche Universiteit Delft.

Rudnicki, J. W. & Rice, J. R. (1975), 'Conditions for the localization of deformation in pressure-sensitive dilatant materials', *J. Mech. Phys. Solids* **23**, 371–394.

Toupin, R. A. (1962), 'Elastic materials with couple stress', *Arch. Rational Mech. Anal.* **11**, 385–414.

Voigt, W. (1887), 'Theoretische studien uber die elastizitatsverhaltnisse der krystalle', *Abh. Ges. Wiss. Gottingen* **34**.

Voigt, W. (1894), 'Uber mediem ohne innere krafte und eine durch sie gelieferte mechanische deutung der maxwell-hertzchen gleichungen', *Gott.Abh.* pp. 72–79.

Warren, W. E. & Byskov, E. (2000), Three-fold symmetry restrictions on two-dimensional micropolar materials, Structural and Solid Mechanics 1, Aalborg University, Dept. of Building Technology and Structural Engineering.

William, K. J. (1984), Experimental and computational aspects of concrete fracture, *in* F. e. a. Damjanic, ed., 'Proc. Int. conf. Computer Aided Analysis an Design of Concrete Structures', Pineridge Press, Swansea, pp. 33 70.

Yang, J. F. C. & Lakes, R. S. (1982), 'Experimental study of micropolar and couple stress elasticity in bone in bending', *Journal of Biomechanics* **15**, 91 98.

Zbib, H. M. & Aifantis, E. C. (1997), 'On the localization and postlocalization behavior of plastic deformation, i, ii, iii', *Res. Mechanica* **23**, 261 277, 279 292, 293–305.

Appendix D

Simple problems using higher-order theories

Contents

D.1 Introduction

Several higher-order theories have been developed to take into account the effect of strain gradients in strains and to introduce scale length parameters in continuum mechanics. The first theory by Cosserat & Cosserat (1909) introduces the concept of couple stresses and spins in the continuum. In the original theory by Cosserat, the spin is an independent parameter, but Koiter (1964) investigated the special case in which the spin is related to displacements according to eq. (D.1) (Christoffersen 2000)

$$\omega_j = \tfrac{1}{2} e_{jkl} v_{l,k} \tag{D.1}$$

where e_{jkl} is the permutation tensor, ω_j is the spin and v_i are the displacements. The contributions by Toupin (1962) and Mindlin (1965*b*) are very important. The theory by Mindlin (1965*a*) and Cowin (1970) is known as "Couple stress theory". Mindlin (1965*b*) and Eringen (1968) proposed a microstructure theory in which the points can deform microscopically as well as rotate and translate.

In the theory by Kröner (1967) and Eringen (1972), known as non-local theory, the points can only undergo translational motion, but the stress at a point depends on the strain in a region near the point.

More recently Aifantis (1984), has proposed a theory which introduces one material length scale. A theory of this type has been used to study the problem of localization of deformation (see for example (Pamin 1994)). Theories of this type have been developed to include three length scales by Fleck & Hutchinson (2001).

Fleck & Hutchinson (1993), based on the previous work by Toupin (1962) and Mindlin (1965*a*), developed a phenomenological theory that includes a single scale length parameter, and this theory was extended by Fleck & Hutchinson (1997) to include three length scale parameters.

In order to compare some of these theories, the author presents some simple problems solved using some of these theories including the classical theory of elasticity and plasticity.

D.2 Axial force

A bar subjected to axial force will be considered, the cross-section of the bar is constant. The bar is driven by an external force F and the material is considered elastic.

D.2.1 Classical theory

The balance equations are (Byskov 1999), (Chakrabarty 1987):

$$\sigma_{ij,i} + p_j = 0 \tag{D.2}$$

where σ_{ij} is the stress tensor and p_j are the body forces. In this particular case all stresses are considered to vanish except the normal stress σ_{11}. (Eq.D.2) reduces to:

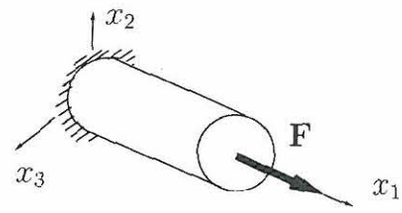

Figure D.1: Bar under axial force.

$$\sigma_{11,1} = 0 \tag{D.3}$$

The constitutive equations are (Byskov 1999):

$$\sigma_{ij} = L_{ijkl}\varepsilon_{kl} \tag{D.4}$$

where L_{ijkl} is the tensor of elastic constants and ε_{ij} is the symmetric strain tensor. For this case these equations are:

$$\begin{aligned}
\sigma_{11} &= L_{1111}\varepsilon_{11} + L_{1122}\varepsilon_{22} + L_{1133}\varepsilon_{33} \\
0 &= L_{2211}\varepsilon_{11} + L_{2222}\varepsilon_{22} + L_{2233}\varepsilon_{33} \\
0 &= L_{3311}\varepsilon_{11} + L_{3322}\varepsilon_{22} + L_{3333}\varepsilon_{33}
\end{aligned} \tag{D.5}$$

where it is supposed that in the material the shear strains do not have influence over normal stresses. Defining

$$\begin{aligned}
D = L_{1111}L_{2222}L_{3333} + L_{1122}L_{2233}L_{3322} + L_{1133}L_{2211}L_{3311} \\
- L_{3311}L_{2222}L_{1133} - L_{3322}L_{2233}L_{1111} - L_{3333}L_{2211}L_{1122}
\end{aligned} \tag{D.6}$$

the relation between strains and stresses is:

$$\begin{aligned}
\varepsilon_{11} &= \sigma_{11}(L_{2222}L_{3333} - L_{3322}L_{1133})/D \\
\varepsilon_{22} &= \sigma_{11}(L_{2233}L_{3311} - L_{3333}L_{2211})/D \\
\varepsilon_{33} &= \sigma_{11}(L_{3311}L_{2222} - L_{2211}L_{3322})/D
\end{aligned} \tag{D.7}$$

The equations relating strains and displacements are (Byskov 1999):

$$\varepsilon_{ij} = \tfrac{1}{2}(v_{i,j} + v_{j,i}) \tag{D.8}$$

where v_i is the displacement vector. In this case eq. (D.8) produces:

$$\varepsilon_{11} = v_{1,1}, \qquad \varepsilon_{22} = v_{2,2}, \qquad \varepsilon_{33} = v_{3,3} \tag{D.9}$$

Replacing eq. (D.7) into eq. (D.9) produces

$$v_{1,11} = \frac{\sigma_{11}}{E} \tag{D.10}$$

where E is the elastic modulus $E = D/(L_{2222}L_{3333} - L_{3322}L_{1133})$. The first derivative of eq. (D.10) produces the differential equation:

$$v_{1,11} = \frac{\sigma_{11,1}}{E} = 0 \tag{D.11}$$

The solution is:

$$v_1 = C_1 x + C_2 \tag{D.12}$$

with the boundary conditions

$$\begin{aligned} v_1 &= 0 = C_2 \qquad \text{if} \qquad x = 0 \\ v_1 &= v_L = C_1 L \qquad \text{if} \qquad x = L \end{aligned} \tag{D.13}$$

The solution $v_1 = (v_L/L)x$ produces ε_{11} constant. According to eq. (D.5) the stress σ_{11} is also constant and according to eq. (D.10) and eq. (D.13)

$$\sigma_{11} = E\frac{v_L}{E} \tag{D.14}$$

Using now

$$\int_A \sigma_{11} dA = F \tag{D.15}$$

produces

$$v_L = \frac{FL}{AE} \tag{D.16}$$

The final solution is then

$$v_1 = \frac{Fx}{AE} \qquad \varepsilon_{11} = \frac{F}{AE} \qquad \sigma_{11} = \frac{F}{A} \tag{D.17}$$

D.2.2 Micropolar elasticity

The equilibrium equations are (Christoffersen 2000):

$$\sigma_{ij,i} + p_j = 0 \tag{D.18}$$

$$\mu_{ij,i} + e_{jkl}\sigma_{kl} + q_j = 0 \tag{D.19}$$

where q_j are the body couple loading, μ_{ij} is the couple stress tensor and e_{ijk} is the permutation tensor. The constitutive equations are:

$$\sigma_{ij} = A_{ijkl}\varepsilon_{kl} + B_{ijkl}\kappa_{kl} \tag{D.20}$$

$$\mu_{ij} = C_{ijkl}\varepsilon_{kl} + D_{ijkl}\kappa_{kl} \tag{D.21}$$

where A_{ijkl}, B_{ijkl}, C_{klij} and D_{ijkl} are tensors of elastic constants. According to Christoffersen (2000) for elastic materials, $A_{ijkl} = A_{klij}$, $B_{ijkl} = C_{klij}$ and $D_{ijkl} = D_{klij}$, it is possible to write eq. (D.21) as:

$$\mu_{ij} = B_{klij}\varepsilon_{kl} + D_{ijkl}\kappa_{kl} \tag{D.22}$$

The relations between strains and displacements are (Christoffersen 2000):

$$\varepsilon_{ij} = v_{i,j} - e_{ikj}\omega_k \tag{D.23}$$

$$\kappa_{ij} = \omega_{i,j} \tag{D.24}$$

Here the relation between the microrotation ω_i and displacements eq. (D.1) are not considered. In order to find the solution to the problem, the bar is supposed to be of cylindrical shape and the following displacement and microrotation field is assumed:

$$\begin{aligned} v_z &= \epsilon z \\ v_\theta &= \alpha r z \\ v_r &= \xi r \end{aligned} \tag{D.25}$$

$$\begin{aligned} \omega_z &= \alpha z \\ \omega_\theta &= 0 \\ \omega_r &= g(r) \end{aligned} \tag{D.26}$$

where α, ϵ, ξ and $g(r)$ are unknown quantities. The equilibrium equations in cylindrical coordinates are:

$$\begin{aligned}
&\sigma_{rr,r} + \frac{1}{r}\sigma_{\theta r,\theta} + \sigma_{zr,z} + \frac{\sigma_{rr} - \sigma_{\theta\theta}}{r} + p_r = 0 \\
&\sigma_{r\theta,r} + \frac{1}{r}\sigma_{\theta\theta,\theta} + \sigma_{z\theta,z} + \frac{2\sigma_{r\theta}}{r} + p_\theta = 0 \\
&\sigma_{rz,r} + \frac{1}{r}\sigma_{\theta z,\theta} + \sigma_{zz,z} + \frac{\sigma_{rz}}{r} + p_z = 0
\end{aligned} \tag{D.27}$$

$$\begin{aligned}
&\mu_{rr,r} + \frac{1}{r}\mu_{\theta r,\theta} + \mu_{zr,z} + \frac{\mu_{rr} - \mu_{\theta\theta}}{r} + \sigma_{\theta z} - \sigma_{z\theta} + q_r = 0 \\
&\mu_{r\theta,r} + \frac{1}{r}\mu_{\theta\theta,\theta} + \mu_{z\theta,z} + \frac{2\mu_{r\theta}}{r} + \sigma_{rz} - \sigma_{zr} + q_\theta = 0 \\
&\mu_{rz,r} + \frac{1}{r}\mu_{\theta z,\theta} + \mu_{zz,z} + \frac{\mu_{rz}}{r} + \sigma_{r\theta} - \sigma_{\theta r} + q_z = 0
\end{aligned} \tag{D.28}$$

The strain displacement relations in cylindrical coordinates are:

$$\begin{aligned}
\varepsilon_{rr} &= v_{r,r} & \kappa_{rr} &= \omega_{r,r} \\
\varepsilon_{\theta\theta} &= \tfrac{1}{r}v_{\theta,\theta} + \tfrac{1}{r}v_r & \kappa_{\theta\theta} &= \tfrac{1}{r}\omega_{\theta,\theta} + \tfrac{1}{r}\omega_r \\
\varepsilon_{zz} &= v_{z,z} & \kappa_{zz} &= \omega_{z,z} \\
\varepsilon_{r\theta} &= \tfrac{1}{r}v_{r,\theta} - \tfrac{1}{r}u_\theta + \omega_z & \kappa_{r\theta} &= \tfrac{1}{r}\omega_{r,\theta} - \tfrac{1}{r}\omega_\theta \\
\varepsilon_{\theta z} &= v_{\theta,z} + \omega_r & \kappa_{\theta z} &= \omega_{\theta,z} \\
\varepsilon_{z\theta} &= \tfrac{1}{r}v_{z,\theta} - \omega_r & \kappa_{z\theta} &= \tfrac{1}{r}\omega_{z,\theta} \\
\varepsilon_{\theta r} &= v_{\theta,r} - \omega_z & \kappa_{\theta r} &= \omega_{\theta,r} \\
\varepsilon_{rz} &= v_{r,z} - \omega_\theta & \kappa_{rz} &= \omega_{r,z} \\
\varepsilon_{zr} &= v_{z,r} + \omega_\theta & \kappa_{zr} &= \omega_{z,r}
\end{aligned} \tag{D.29}$$

The strains and curvatures are obtained replacing eq. (D.25) and eq. (D.26) in eq. (D.29)

$$\begin{aligned}
\varepsilon_{rr} &= \xi & \kappa_{rr} &= g'(r) \\
\varepsilon_{\theta\theta} &= \xi & \kappa_{\theta\theta} &= \tfrac{1}{r}g(r) \\
\varepsilon_{zz} &= \epsilon & \kappa_{zz} &= \alpha \\
\varepsilon_{r\theta} &= 0 & \kappa_{r\theta} &= 0 \\
\varepsilon_{\theta z} &= \alpha r + g(r) & \kappa_{\theta z} &= 0 \\
\varepsilon_{z\theta} &= -g(r) & \kappa_{z\theta} &= 0 \\
\varepsilon_{\theta r} &= 0 & \kappa_{\theta r} &= 0 \\
\varepsilon_{rz} &= 0 & \kappa_{rz} &= 0 \\
\varepsilon_{zr} &= 0 & \kappa_{zr} &= 0
\end{aligned} \tag{D.30}$$

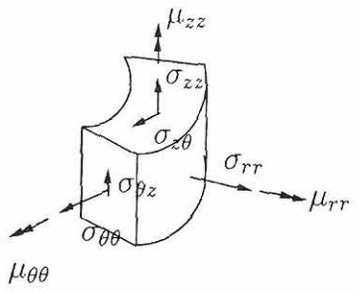

Figure D.2: stresses allowed at a point of the cylindrical bar.

Now inserting eq. (D.30) into eq. (D.20) and eq. (D.22),

$$\begin{aligned}\sigma_{uv} &= A_{uvrr}\xi + A_{uv\theta\theta}\xi + A_{uvzz}\epsilon + A_{uv\theta z}(\alpha r + g(r)) - A_{uvz\theta}g(r) + \\ &\quad + B_{uvrr}g'(r) + B_{uv\theta\theta}\tfrac{1}{r}g(r) + B_{uvzz}\alpha \\ \mu_{uv} &= B_{rruv}\xi + B_{\theta\theta uv}\xi + B_{zzuv}\epsilon + B_{\theta zuv}(\alpha r + g(r)) - B_{z\theta uv}g(r) + \\ &\quad + D_{uvrr}g'(r) + D_{uv\theta\theta}\tfrac{1}{r}g(r) + D_{uvzz}\alpha\end{aligned} \tag{D.31}$$

The possible stresses present in the problem are shown in figure D.2.
The following stresses vanish:

$$\begin{aligned}&\sigma_{r\theta} = \sigma_{\theta r} = \sigma_{zr} = \sigma_{rz} = 0 \\ &\mu_{r\theta} = \mu_{rz} = \mu_{\theta r} = \mu_{\theta z} = \mu_{zr} = \mu_{z\theta} = 0\end{aligned} \tag{D.32}$$

The equilibrium equations reduced to:

$$\begin{aligned}&\sigma_{rr,r} + \frac{\sigma_{rr} - \sigma_{\theta\theta}}{r} = 0 \\ &\mu_{rr,r} + \frac{\mu_{rr} - \mu_{\theta\theta}}{r} + \sigma_{\theta z} - \sigma_{z\theta} = 0\end{aligned} \tag{D.33}$$

Replacing eq. (D.31) into eq. (D.33) and assuming that shear strains have no effect over normal strains the following is produced:

$$a_1 g''(r) + \frac{b_1}{r}g'(r) + \frac{c_1}{r^2}g(r) + \frac{d_1}{r} = 0 \tag{D.34}$$

$$a_2 g''(r) + \frac{b_2}{r}g'(r) + (\frac{c_2}{r^2} + e)g(r) + \frac{d_2}{r} + fr = 0 \tag{D.35}$$

where

$$
\begin{aligned}
a_1 &= B_{rrrr} \\
b_1 &= B_{rr\theta\theta} + B_{rrrr} - B_{\theta\theta rr} \\
c_1 &= -B_{\theta\theta\theta\theta} \\
d_1 &= \alpha(B_{rrzz} - B_{\theta\theta zz}) + \epsilon(A_{rrzz} - A_{\theta\theta zz}) + \xi(A_{rrrr} + A_{rr\theta\theta} - A_{\theta\theta rr} - A_{\theta\theta\theta\theta}) \\
a_2 &= D_{rrrr} \\
b_2 &= D_{rr\theta\theta} + D_{rrrr} - D_{\theta\theta rr} \\
c_2 &= -D_{\theta\theta\theta\theta} \\
d_2 &= \alpha(D_{rrzz} - D_{\theta\theta zz}) + \epsilon(B_{zzrr} - B_{zz\theta\theta}) + \xi(B_{rrrr} + B_{\theta\theta rr} - B_{rr\theta\theta} - B_{\theta\theta\theta\theta}) \\
e &= A_{\theta z\theta z} - A_{\theta zz\theta} - A_{z\theta\theta z} + A_{z\theta z\theta} \\
f &= \alpha(A_{\theta z\theta z} - A_{z\theta\theta z})
\end{aligned}
\tag{D.36}
$$

If the material is centrosymmetric $B_{ijkl} = 0$ (Christoffersen 2000). Therefore, it is impossible that axial forces produce torsion on the bar made of centrosymmetric material and the solution reduces to the classical one. Otherwise, if the material is non-centrosymmetric, shear stresses and couple stresses appear in the solution.

D.2.3 Theory by Aifantis

For a unidimensional lateral constrained problem defined by

$$v_1 = v_1(x), \qquad v_2 = v_3 = 0 \tag{D.37}$$

the field equations of this gradient elasticity theory become (Altan, Evensen & Aifantis 1996)

$$\varepsilon_{11} = v_{1,1}, \text{all others zero} \tag{D.38}$$

$$\sigma_{11} = (\lambda + 2\mu)(\varepsilon_{11} - c\varepsilon_{11,11}) \tag{D.39}$$

$$\sigma_{22} = \sigma_{33} = \lambda(\varepsilon_{11} - c\varepsilon_{11,11}) \tag{D.40}$$

The equilibrium equations correspond to eq. (D.2). Replacing eq.(D.39) into eq. (D.2) produces the following equation

$$\varepsilon_{11,1} - c\varepsilon_{11,111} = 0 \tag{D.41}$$

The general solution of eq. (D.41) is

$$\varepsilon_{11} = D_1 + D_2 e^{-\frac{x_1}{\sqrt{c}}} + D_3 e^{\frac{x_1}{\sqrt{c}}} \tag{D.42}$$

and

$$\sigma_{11} = (\lambda + 2\mu) D_1 \tag{D.43}$$

For a bar under constant axial force using eq. (D.15)

$$F = \int_A \sigma_{11} dA = (\lambda + 2\mu) D_1 A, \qquad D_1 = \frac{F}{A} \frac{1}{(\lambda + 2\mu)} \tag{D.44}$$

To solve the general problem it is necessary to use boundary conditions for ε_{11}, for example if it is supposed that $\varepsilon_{11}(0) = \varepsilon_{11}(L) = K$ where L is the length of the bar and K is a constant

$$D_2 = -(K - D_1) \frac{1 - e^{\frac{L}{\sqrt{c}}}}{2 \sinh(\frac{L}{\sqrt{c}})} \tag{D.45}$$

$$D_3 = (K - D_1) \left(1 + \frac{1 - e^{\frac{L}{\sqrt{c}}}}{2 \sinh(\frac{L}{\sqrt{c}})} \right) \tag{D.46}$$

and

$$\varepsilon_{11} = \frac{F}{A} \frac{1}{(\lambda + 2\mu)} + \left(K - \frac{F}{A} \frac{1}{(\lambda + 2\mu)} \right) \left(\frac{1 - e^{\frac{L}{\sqrt{c}}}}{\sinh(\frac{L}{\sqrt{c}})} \sinh(\frac{x_1}{\sqrt{c}}) + e^{-\frac{x_1}{\sqrt{c}}} \right) \tag{D.47}$$

A graph comparing the effect of two different values of c on a bar of unit length is shown in figure (D.3). In the graph a value of $K = 0.9 D_1$ is used.

D.3 Torsion

D.3.1 Classical theory

Considering only the case of a cylindrical shaft driven by a torsional moment (see figure D.4), longitudinal displacements and forces are supposed to be null on this bar.

In elasticity analysis of pure torsion over cylindrical bars it is considered that $\sigma_{r\theta} = \sigma_{\theta r} = 0$, $\sigma_{rr} = \sigma_{\theta\theta} = \sigma_{zz} = 0$ and $\sigma_{\theta z} = \sigma_{z\theta} = \tau \neq 0$. If the stress varies linearly from 0 to $\tau_{\max}$ along the radius:

$$\tau = \frac{r \tau_{\max}}{R} \tag{D.48}$$

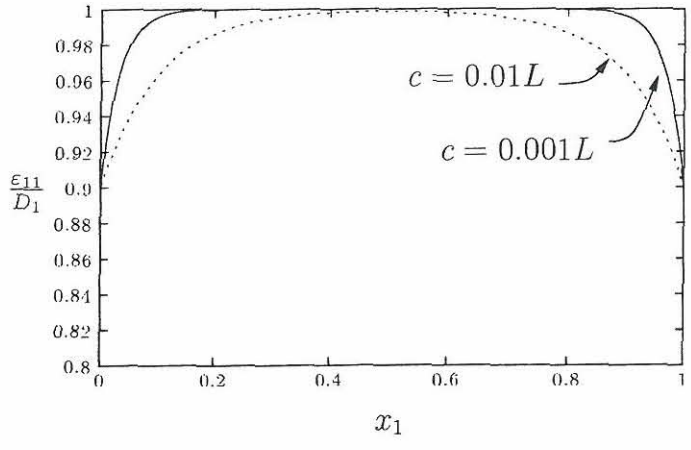

Figure D.3: The effect of constant axial force against the longitudinal position (x_1) for Aifantis theory. It is used that $K = 0.9D_1$ and $L = 1$.

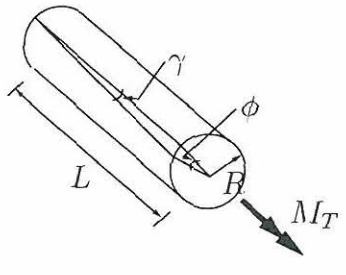

Figure D.4: Deformation by torsion in a cylindrical bar.

Equilibrium equations reduce to

$$\tfrac{1}{r}\tau_{,z} = 0 \tag{D.49}$$

The relation between the torsional moment M_T and stresses is from equilibrium:

$$M_T = \int_A \tau r dA = \int_A \frac{r^2 \tau_{\max}}{R} dA = \frac{\tau_{\max} J}{R} \tag{D.50}$$

where J is the polar inertia of the section. Replacing eq. (D.50) into eq. (D.48) the following is obtained:

$$\tau = \frac{M_T r}{J} \tag{D.51}$$

From (figure D.4) it is possible to write:

$$\gamma dz = r d\phi \tag{D.52}$$

if the material is ortotropic or isotropic the relation between γ and τ is:

$$\gamma = 2\varepsilon_{\theta z} = \frac{\tau}{G} \tag{D.53}$$

where G is the shear modulus of the material. Replacing eq. (D.52) and eq. (D.53) into eq. (D.51), the following equation is obtained:

$$\frac{d\phi}{dz} = \frac{M_T}{JG} \tag{D.54}$$

Using the displacement field by eq. (D.25) $\epsilon = \xi = 0$ and $\alpha = M_T/(JG)$ are found.

D.3.2 Micropolar elasticity

The problem of torsion has been solved as a part of the general problem of axial force, equations of section D.2.2 are completely valid for torsion. When the material is centrosymmetric, $B_{ijkl} = 0$ and eq. (D.34) vanishe. If the material is isotropic

$$\begin{aligned}
&A_{rrrr} = A_{\theta\theta\theta\theta} = A_{zzzz} = F_0 \\
&A_{rr\theta\theta} = A_{\theta\theta zz} = A_{zz\theta\theta} = A_{\theta\theta rr} = F_1 \\
&A_{\theta z\theta z} = A_{z\theta z\theta} = G_0 \\
&A_{\theta zz\theta} = A_{z\theta\theta z} = G_1 \\
&D_{rrrr} = D_{\theta\theta\theta\theta} = D_{zzzz} = H_0 \\
&D_{rr\theta\theta} = D_{\theta\theta zz} = D_{zz\theta\theta} = D_{\theta\theta rr} = H_1
\end{aligned} \tag{D.55}$$

Introducing eq. (D.55) into eq. (D.35) produces:

$$H_0(g''(r) + \tfrac{1}{r}g'(r) - \tfrac{1}{r^2}g(r)) - 2(G_0 - G_1)g(r) = (G_0 - G_1)\alpha r \tag{D.56}$$

Replacing the boundary condition $\mu_{rr} = 0$ for $r = R$ into eq. (D.31) the following boundary condition for $g(r)$ is obtained:

$$H_0 g'(R) + \tfrac{H_1}{R}g(R) + H_1\alpha = 0 \tag{D.57}$$

The differential equation (D.56) was solved by Christoffersen (2000). The solution in terms of Bessel functions is:

$$g(r) = \frac{\alpha}{2}\left(\frac{\frac{1-\eta}{\lambda}I_1(\lambda r)}{I_0(\lambda R) - \frac{1-\eta}{\lambda R}I_1(\lambda R)} - r\right) \tag{D.58}$$

where

$$\lambda = \sqrt{2\frac{G_0 - G_1}{H_0}} \qquad \eta = \frac{H_1}{H_0} \tag{D.59}$$

If the axial force F is not null, from eq. (D.31):

$$\begin{aligned} 2F_1\xi + f_0\epsilon &= \sigma_{zz} \\ F_0\xi + F_1\xi + F_1\epsilon &= 0 \end{aligned} \tag{D.60}$$

and

$$\int_A \sigma_{zz} dA = F \tag{D.61}$$

Producing:

$$\epsilon = \frac{F}{A}\left(\frac{F_0 + F_1}{2F_1^2 + F_0^2 + F_0F_1}\right), \qquad \xi = \frac{F}{A}\left(\frac{2F_1^2}{2F_1^2 + F_0^2 + F_0F_1}\right) \tag{D.62}$$

In case of torsional moment acting on the bar

$$\int_A (\sigma_{z\theta} r + \mu_{zz}) dA = M_T \tag{D.63}$$

It is possible to find the stresses and couple stresses $\sigma_{z\theta}$ and μ_{zz} using eq. (D.31), and the results are:

$$\sigma_{z\theta} = \left(\frac{G_0 + G_1}{2} + \frac{G_0 - G_1}{2} \frac{\frac{1-\eta}{\lambda} I_1(\lambda r)}{I_0(\lambda R) - \frac{1-\eta}{\lambda R} I_1(\lambda R)} \right) \alpha \tag{D.64}$$

$$\mu_{zz} = H_0 \frac{1-\eta}{2} \left(\frac{\eta I_0(\lambda r)}{I_0(\lambda R) - \frac{1-\eta}{\lambda R} I_1(\lambda R)} + 1 \right) \alpha \tag{D.65}$$

With eq. (D.64) and eq. (D.65) the result of eq. (D.63) is:

$$M_T = \left(\frac{G_0 + G_1}{2} J + \frac{H_0 + H_1}{2} \Phi(\eta, \lambda R) \pi R^2 \right) \alpha \tag{D.66}$$

where

$$\Phi(\eta, \lambda R) = \left(\frac{I_2(\lambda R) + \frac{2\eta}{\lambda R} I_1(\lambda R) + 1}{I_0(\lambda R) - \frac{1-\eta}{\lambda R} I_1(\lambda R)} \right) \alpha \tag{D.67}$$

The function $\Phi(\eta, \lambda R)$ tends to be 1 for large values of R, and tends to be equal to 2 for small values of R. From eq. (D.66) it can be observed that for very small values of R, the torque is proportional to R^2, and for large values of R, the torque tends to be the classical value as a function of J.

D.3.3 Micropolar theory using the rotations defined by Koiter

Using the relation between displacements an rotations eq. (D.1), the relation between displacements and strains eq. (D.23) in polar coordinates are:

$$\begin{aligned}
\varepsilon_{rr} &= v_{r,r} \\
\varepsilon_{\theta\theta} &= \tfrac{1}{r}(v_r + v_{\theta,\theta}) \\
\varepsilon_{zz} &= v_{z,z} \\
\varepsilon_{r\theta} &= \varepsilon_{\theta r} = \tfrac{1}{2r}(v_{r,\theta} - v_\theta + r v_{\theta,r}) \\
\varepsilon_{\theta z} &= \varepsilon_{z\theta} = \tfrac{1}{2r}(v_{z,\theta} + r v_{\theta,z}) \\
\varepsilon_{rz} &= \varepsilon_{zr} = \tfrac{1}{2}(v_{r,z} + v_{z,r})
\end{aligned} \tag{D.68}$$

The relation between curvatures and displacements is established by eq. (D.1) and eq. (D.24). In cylindrical coordinates

$$
\begin{aligned}
\kappa_{rr} &= \tfrac{1}{2r^2}(rv_{z,\theta r} - v_{z,\theta} - r^2 v_{\theta,zr}) \\
\kappa_{\theta\theta} &= -\tfrac{1}{2r^2}(v_{z,\theta} - rv_{\theta,z} + rv_{r,z\theta} - rv_{z,r\theta}) \\
\kappa_{zz} &= \tfrac{1}{2r}(v_{\theta,z} - v_{r,\theta z} + rv_{\theta,rz}) \\
\kappa_{r\theta} &= \tfrac{1}{2r^2}(rv_{z,r} - rv_{r,z} + v_{z,\theta\theta} - rv_{\theta,z\theta}) \\
\kappa_{\theta z} &= \tfrac{1}{2}(v_{r,zz} - v_{z,rz}) \\
\kappa_{z\theta} &= \tfrac{1}{2r^2}(v_{\theta,\theta} - v_{r,\theta\theta} + rv_{\theta,r\theta}) \\
\kappa_{\theta r} &= \tfrac{1}{2}(v_{r,zr} - v_{z,rr}) \\
\kappa_{rz} = \kappa_{zr} &= \tfrac{1}{2r}(v_{z,\theta z} - rv_{\theta,zz})
\end{aligned}
\tag{D.69}
$$

Assuming the displacement field according to eq. (D.25), the strains and curvatures are:

$$
\begin{aligned}
\varepsilon_{rr} &= \xi, & \kappa_{rr} &= -\tfrac{1}{2}\alpha \\
\varepsilon_{\theta\theta} &= \xi, & \kappa_{\theta\theta} &= -\tfrac{1}{2}\alpha \\
\varepsilon_{zz} &= \epsilon, & \kappa_{zz} &= \alpha \\
\varepsilon_{r\theta} &= \varepsilon_{\theta r} = 0, & \kappa_{r\theta} &= \kappa_{\theta r} = 0 \\
\varepsilon_{\theta z} &= \varepsilon_{z\theta} = \tfrac{1}{2}\alpha r, & \kappa_{\theta z} &= \kappa_{z\theta} = 0 \\
\varepsilon_{rz} &= \varepsilon_{zr} = 0, & \kappa_{rz} &= \kappa_{zr} = 0
\end{aligned}
\tag{D.70}
$$

Replacing eq. (D.70) into equations (D.20) and (D.21), these are reduced to:

$$
\begin{aligned}
\sigma_{uv} = (A_{uvrr} + A_{uv\theta\theta})\xi + A_{uvzz}\epsilon + \frac{\alpha r}{2}(A_{uv\theta z} + A_{uvz\theta}) + \\
+ \frac{\alpha}{2}(B_{uvrr} + B_{uv\theta\theta}) + B_{uvzz}\alpha \\
\mu_{uv} = (B_{rruv} + B_{\theta\theta uv})\xi + B_{zzuv}\epsilon + \frac{\alpha r}{2}(B_{\theta zuv} + B_{z\theta uv}) + \\
+ \frac{\alpha}{2}(D_{uvrr} + D_{uv\theta\theta}) + D_{uvzz}\alpha
\end{aligned}
\tag{D.71}
$$

If the material is centrosymmetric and isotropic, using eq. (D.55):

$$
\begin{aligned}
\sigma_{rr} &= \sigma_{\theta\theta} = (F_0 + F_1)\xi + F_1\epsilon \\
\sigma_{z\theta} &= \sigma_{\theta z} = \frac{\alpha}{2}(G_0 + G_1)r \\
\sigma_{zz} &= 2F_1\xi + F_0\epsilon \\
\mu_{rr} &= \mu_{\theta\theta} = \tfrac{\alpha}{2}(H_1 - H_0) \\
\mu_{zz} &= \tfrac{\alpha}{2}(H_0 - H_1)
\end{aligned}
\tag{D.72}
$$

the torsional moment is related to α through eq. (D.63). Using the values from eq. (D.72):

$$M_T = \tfrac{1}{2}(G_1 + G_0)\alpha J_0 - (H_1 - H_0)\alpha\pi R^2 \tag{D.73}$$

where $H_1 < H_0$. The solution has the same form as eq. (D.67), again for small values of R the torque is proportional to R^2.

D.3.4 Theory by Fleck and Hutchinson, 1997

In this theory, the relation between displacements and strains corresponds to eq. (D.8). The symbol κ is used to represent the spatial gradient of the material rotation, where the material rotation is defined as eq. (D.1):

$$\kappa_{ij} = \omega_{i,j} = \tfrac{1}{2}e_{ipq}v_{q,pj} = e_{ipq}\varepsilon_{qj,p} \tag{D.74}$$

The strain displacement relations in cylindrical coordinates are:

$$\begin{aligned}
&\varepsilon_{rr} = v_{r,r}, && \varepsilon_{r\theta} = \varepsilon_{\theta r} = \tfrac{1}{2}(\tfrac{1}{r}v_{r,\theta} + v_{\theta,r} - \tfrac{1}{r}v_\theta)\\
&\varepsilon_{rz} = \varepsilon_{zr} = \tfrac{1}{2}(v_{r,z} + v_{z,r}), && \varepsilon_{\theta,\theta} = \tfrac{1}{r}v_{\theta,\theta} + \tfrac{1}{r}v_r\\
&\varepsilon_{\theta z} = \varepsilon_{z\theta} = \tfrac{1}{2}(v_{\theta,z} + \tfrac{1}{r}v_{z,\theta}), && \varepsilon_{zz} = v_{z,z}
\end{aligned} \tag{D.75}$$

Using the displacement field of eq. (D.25) the strains are:

$$\begin{aligned}
&\varepsilon_{rr} = \varepsilon_{\theta\theta} = \xi\\
&\varepsilon_{rz} = \varepsilon_{zr} = \varepsilon_{\theta r} = \varepsilon_{r\theta} = 0\\
&\varepsilon_{\theta z} = \varepsilon_{z\theta} = \tfrac{1}{2}\alpha r\\
&\varepsilon_{zz} = \epsilon
\end{aligned} \tag{D.76}$$

The curvatures are the same as in the Koiter theory eq. (D.69) and produce:

$$\begin{aligned}
&\kappa_{rr} = -\tfrac{1}{2}\alpha\\
&\kappa_{\theta\theta} = -\tfrac{1}{2}\alpha\\
&\kappa_{zz} = \alpha\\
&\kappa_{r\theta} = \kappa_{\theta r} = 0\\
&\kappa_{\theta z} = \kappa_{z\theta} = 0\\
&\kappa_{rz} = \kappa_{zr} = 0
\end{aligned} \tag{D.77}$$

The second gradient of displacement η_{ijk} is defined as:

$$\eta_{ijk} = u_{k,ij} \tag{D.78}$$

In cylindrical coordinates, eq. (D.78) is:

$$
\begin{aligned}
\eta_{zzz} &= v_{z,zz}, & \eta_{\theta zz} &= \tfrac{1}{r} v_{z,z\theta} \\
\eta_{zz\theta} &= \tfrac{1}{r} v_{z\theta z}, & \eta_{z\theta z} &= v_{\theta,zz} \\
\eta_{rzz} &= v_{z,rr}, & \eta_{\theta z\theta} &= \frac{1}{r^2}(r v_{z,r} + v_{z,\theta\theta}) \\
\eta_{zzr} &= v_{z,rz}, & \eta_{\theta\theta z} &= \tfrac{1}{r}(v_{r,z} + v_{\theta,z\theta}) \\
\eta_{z\theta\theta} &= \tfrac{1}{r}(v_{r,z} + v_{\theta,\theta z}), & \eta_{zrz} &= v_{rzz} \\
\eta_{rz\theta} &= \frac{1}{r^2}(r v_{z,\theta r} - v_{z,\theta}), & \eta_{\theta zr} &= \frac{1}{r^2}(r_{z,r\theta} - v_{z,\theta}) \\
\eta_{r\theta z} &= v_{\theta,rr}, & \eta_{\theta\theta\theta} &= \frac{1}{r^2}(2v_{r,\theta} - v_\theta + r v_{\theta,r} + v_{\theta,\theta\theta}) \\
\eta_{z\theta r} &= v_{\theta,rz}, & \eta_{\theta rz} &= \tfrac{1}{r}(v_{r,z\theta} - v_{\theta,z}) \\
\eta_{zr\theta} &= \tfrac{1}{r}(v_{r,\theta z} - v_{\theta,z}), & \eta_{rzr} &= v_{z,rr} \\
\eta_{r\theta\theta} &= \frac{1}{r^2}(r v_{r,r} - v_{\theta,\theta} - v_r + r v_{\theta,\theta r}), & \eta_{\theta\theta r} &= \frac{1}{r^2}(r v_{r,r} - v_{\theta,\theta} - v_r + r v_{\theta,r\theta}) \\
\eta_{rrz} &= v_{r,rr}, & \eta_{\theta r\theta} &= \frac{1}{r^2}(r v_{r,r} - 2v_{\theta,\theta} - v_r + v_{r,\theta\theta}) \\
\eta_{zrr} &= v_{r,rz}, & \eta_{r\theta r} &= v_{\theta,rr} \\
\eta_{rr\theta} &= \frac{1}{r^2}(v_\theta - v_{r,\theta} - r v_{\theta,r} + r v_{r,\theta r}), & \eta_{\theta rr} &= \frac{1}{r^2}(v_\theta - v_{r,\theta} - r v_{\theta,r} + r v_{r,r\theta}) \\
\eta_{rrr} &= v_{r,rr} & & \qquad\qquad (D.79)
\end{aligned}
$$

for the particular displacement field of eq. (D.25) the only non-vanishing terms in the second gradient of displacement are:

$$\eta_{\theta rz} = -\alpha, \qquad \eta_{zr\theta} = -\alpha \qquad (D.80)$$

The constitutive equations are the result of $\sigma_{ij} = \partial w / \partial \varepsilon_{ij}$ and $\tau_{ijk} = \partial w / \partial \eta_{ijk}$ where $\boldsymbol{\sigma}$ is the second order symmetric stress, $\boldsymbol{\tau}$ is the third-order stress and the strain energy w depends upon $\boldsymbol{\varepsilon}$ and $\boldsymbol{\eta}$ in the manner:

$$
\begin{aligned}
w = \tfrac{1}{2}\lambda \varepsilon_{ii}\varepsilon_{jj} + \mu \varepsilon_{ij}\varepsilon_{ij} + a_1 \eta_{ijj}\eta_{ikk} + a_2 \eta_{iik}\eta_{kjj} \\
+ a_3 \eta_{iik}\eta_{jjk} + a_4 \eta_{ijk}\eta_{ijk} + a_5 \eta_{ijk}\eta_{kji} \qquad (D.81)
\end{aligned}
$$

where λ and μ are the standard Lame constants, and the additional a_n are additional stiffness constants of the dimension (stress) $\times$ (length)^2. For the special case of torsion:

$$
\begin{aligned}
\sigma_{rr} &= \lambda(\varepsilon_{rr} + \varepsilon_{\theta\theta} + \varepsilon_{zz}) + 2\mu\varepsilon_{rr} \\
\sigma_{\theta\theta} &= \lambda(\varepsilon_{rr} + \varepsilon_{\theta\theta} + \varepsilon_{zz}) + 2\mu\varepsilon_{\theta\theta} \\
\sigma_{zz} &= \lambda(\varepsilon_{rr} + \varepsilon_{\theta\theta} + \varepsilon_{zz}) + 2\mu\varepsilon_{zz} \\
\sigma_{\theta z} &= \sigma_{z\theta} = 2\mu\varepsilon_{\theta z} \\
\tau_{\theta rz} &= 2a_4\eta_{\theta rz} + 2a_5\eta_{zr\theta} \\
\tau_{zr\theta} &= 2a_4\eta_{zr\theta} + 2a_5\eta_{\theta rz} \qquad (D.82)
\end{aligned}
$$

And replacing eq. (D.76) and eq. (D.80) into eq. (D.82) the constitutive equations produce:

$$\begin{aligned}
\sigma_{rr} &= \sigma_{\theta\theta} = \lambda(2\xi + \epsilon) + 2\mu\xi \\
\sigma_{zz} &= \lambda(2\xi + \epsilon) + 2\mu\epsilon \\
\sigma_{\theta z} &= \sigma_{z\theta} = \mu\alpha r \\
\tau_{\theta rz} &= \tau_{zr\theta} = -2\alpha(a_4 + a_5)
\end{aligned} \tag{D.83}$$

The equilibrium relations in Cartesian coordinates are:

$$f_k + (\sigma_{ik} - \tau_{ijk,j})_{,i} = 0 \tag{D.84}$$

where f_k are the body forces. Fleck & Hutchinson (1997) decompose $\boldsymbol{\tau}$ in a symmetric tensor τ^S_{ijk} defined by

$$\tau^S_{ijk} = \tfrac{1}{3}(\tau_{ijk} + \tau_{jki} + \tau_{kij}) \tag{D.85}$$

and a remainder τ^A_{ijk} such that

$$\tau_{ijk} = \tau^S_{ijk} + \tau^A_{ijk} \tag{D.86}$$

Fleck & Hutchinson (1997) present the following expression for the couple stress m_{jp} in terms of τ^A:

$$m_{jp} = \tfrac{4}{3} e_{ikp} \tau^A_{jik} = \tfrac{4}{3} e_{ikp} \tau_{jik} \tag{D.87}$$

Substitution of eq. (D.83) into eq. (D.85), eq. (D.86) and eq. (D.87) produces

$$\tau^S_{r\theta z} = \tau^S_{\theta zr} = \tau^S_{z\theta r} = \tau^S_{rz\theta} = \tau^S_{\theta rz} = \tau^S_{zr\theta} = -\tfrac{2}{3}\alpha(a_4 + a_5) \tag{D.88}$$

$$\tau^A_{\theta rz} = \tau^A_{zr\theta} = -\tfrac{4}{3}\alpha(a_4 + a_5) \tag{D.89}$$

$$\tau^A_{r\theta z} = \tau^A_{rz\theta} = \tau^A_{\theta zr} = \tau^A_{z\theta r} = \tfrac{2}{3}\alpha(a_4 + a_5) \tag{D.90}$$

$$m_{zz} = -m_{\theta\theta} = -\tfrac{8}{3}\alpha(a_4 + a_5) \tag{D.91}$$

The relation between the torsional moment and the stresses and couple stresses is again, eq. (D.63), using the notation by Fleck & Hutchinson (1997)

$$M_T = \int_A \Big[\sigma_{z\theta} r + m_{zz}\Big) dA = \int_A \Big(\mu\alpha r^2 - \tfrac{8}{3}\alpha(a_4 + a_5)\Big] dA \tag{D.92}$$

which produces

$$M_T = \mu\alpha J - \tfrac{8}{3}\pi\alpha(a_4 + a_5)R^2 \tag{D.93}$$

The solution then has the same form as the one presented for micropolar theories eq. (D.66) and eq. (D.73) where, again, for small values of R the torque is proportional to R^2.

D.3.5 Cosserat theory using equations by Eringen

In symbols by Eringen (1968) the constitutive equations are (Lakes 2001):

$$\sigma_{kl} = \lambda\varepsilon_{rr}\delta_{kl} + (2\mu + \kappa)\varepsilon_{kl} + \kappa e_{klm}(\omega_m - \phi_m) + C_1\phi_{r,r}\delta_{kl} + C_2\phi_{k,l} + C_3\phi_{l,k}$$

$$m_{kl} = \alpha\phi_{p,p}\delta_{kl} + \beta\phi_{k,l} + \gamma\phi_{l,k} + C_1\varepsilon_{pp}\delta_{kl} + (C_2 + C_3)\varepsilon_{kl} + (C_3 - C_2)e_{klm}(\omega_m - \phi_m) \quad \text{(D.94)}$$

where α, β, γ, λ, κ and μ are elastic constants, C_1, C_2 and C_3 are also elastic constants that exist only in case of non-centrosymmetric materials, $\mathbf{m}$ is the tensor of couple stresses, $\mathbf{e}$ is the permutation tensor. The strains are defined according to eq. (D.8) and in cylindrical coordinates according to eq. (D.75) $\boldsymbol{\omega}$ is the vector of macrorotations defined by eq. (D.1), and $\boldsymbol{\phi}$ is the microrotation vector.

The tensorial constants are related to the following technical constants:

1. Young's modulus $E = (2\mu + \kappa)(3\lambda + 2\mu + \kappa)/(2\lambda + 2\mu + \kappa)$,
2. shear modulus $G = (2\mu + \kappa)/2$,
3. Poisson's ratio $\nu = \lambda/(2\lambda + 2\mu + \kappa)$,
4. characteristic length for torsion $l_t = \sqrt{(\beta + \gamma)/(2\mu + \kappa)}$,
5. characteristic length for bending $l_b = \sqrt{\gamma/2(2\mu + \kappa)}$,
6. coupling number $N = \sqrt{\kappa/2(\mu + \kappa)}$, and
7. polar ratio $\Psi = (\beta + \gamma)/(\alpha + \beta + \gamma)$

To avoid confusion with the new elastic constants, the displacement field from eq. (D.25) is now written as:

$$\begin{aligned} v_z &= \epsilon z \\ v_\theta &= b_0 r z \\ v_r &= \xi r \end{aligned} \quad \text{(D.95)}$$

The microrotation field is:

$$\begin{aligned} \phi_z &= b_0 z \\ \phi_\theta &= 0 \\ \phi_r &= g(r) \end{aligned} \quad \text{(D.96)}$$

In cylindrical coordinates the strains are:

$$\begin{aligned}
&\varepsilon_{rr} = \varepsilon_{\theta\theta} = \xi \\
&\varepsilon_{rz} = \varepsilon_{zr} = \varepsilon_{\theta r} = \varepsilon_{r\theta} = 0 \\
&\varepsilon_{\theta z} = \varepsilon_{z\theta} = \tfrac{1}{2} b_0 r \\
&\varepsilon_{zz} = \epsilon
\end{aligned} \tag{D.97}$$

The macrorotations in cylindrical coordinates are:

$$\begin{aligned}
&\omega_r = \tfrac{1}{2r}(v_{z,\theta} - r v_{\theta,z}) \\
&\omega_\theta = \tfrac{1}{2}(v_{r,z} - v_{z,r}) \\
&\omega_z = \tfrac{1}{2r}(v_\theta - v_{r,\theta} + r v_{\theta,r})
\end{aligned} \tag{D.98}$$

replacing eq. (D.95) into eq. (D.98)

$$\begin{aligned}
&\omega_r = -\tfrac{1}{2} b_0 r \\
&\omega_\theta = 0 \\
&\omega_z = b_0 z
\end{aligned} \tag{D.99}$$

Inserting eq. (D.96), eq. (D.97) and eq. (D.99) into eq. (D.94) the following result for constitutive equations is produced:

$$\begin{aligned}
&\sigma_{rr} = b_0 C_1 + g'(r)(C_1 + C_2 + C_3) + \xi(2\mu + 2\lambda + \kappa) + \epsilon\lambda \\
&\sigma_{\theta\theta} = b_0 C_1 + g'(r) C_1 + \xi(2\mu + 2\lambda + \kappa) + \epsilon\lambda \\
&\sigma_{zz} = b_0(C_1 + C_2 + C_3) + g'(r) C_1 + 2\xi\lambda + \epsilon(2\mu + \kappa + \lambda) \\
&\sigma_{\theta z} = b_0 \mu r - \kappa g(r) \\
&\sigma_{z\theta} = b_0 r(\mu + \kappa) + \kappa g(r) \\
&\sigma_{r\theta} = \sigma_{rz} = \sigma_{\theta r} = \sigma_{zr} = 0 \\
&m_{rr} = b_0 \alpha + g'(r)(\alpha + \beta + \gamma) + \xi(2c_1 + C_2 + C_3) + \epsilon C_1 \\
&m_{\theta\theta} = b_0 \alpha + g'(r)\alpha + \xi(2C_1 + C_2 + C_3) + \epsilon C_1 \\
&m_{zz} = b_0(\alpha + \beta + \gamma) + g'(r)\alpha + 2\xi C_1 + \epsilon(C_1 + C_2 + C_3) \\
&m_{\theta z} = b_0 C_2 r - (C_3 - C_2) g(r) \\
&m_{z\theta} = b_0 C_3 r + (C_3 - C_2) g(r) \\
&m_{r\theta} = m_{rz} = m_{\theta r} = m_{zr} = 0
\end{aligned} \tag{D.100}$$

The equilibrium equations eq. (D.27) and eq. (D.28) reduce again to eq. (D.33). Replacing eq. (D.100) into eq. (D.33) the two following differential equations for $g(r)$ are produced:

$$r g''(r) + \frac{C_2 + C_3}{C_1 + C_2 + C_3} g'(r) = 0 \tag{D.101}$$

$$rg''(r) + \frac{\beta+\gamma}{\alpha+\beta+\gamma}g'(r) - \frac{2\kappa r}{\alpha+\beta+\gamma}g(r) - \frac{\kappa b_0 r^2}{\alpha+\beta+\gamma} = 0 \tag{D.102}$$

with the boundary condition $m_{rr} = 0$ for $r = R$, that produces the following boundary condition for $g(r)$:

$$g'(R) = -\frac{\xi(2C_1 + C_2 + C_3) + \epsilon C_1 + b_0\alpha}{\alpha+\beta+\gamma} \tag{D.103}$$

If the material is centrosymmetric it is only necessary to satisfy eq. (D.102).

D.3.6 Theory by Aifantis

The simplest form of the constitutive equations in this gradient elasticity theory reads (Aifantis 1999)

$$\boldsymbol{\sigma} = \lambda(\mathrm{tr}\boldsymbol{\varepsilon})\mathbf{1} + 2\mu\boldsymbol{\varepsilon} - c\nabla^2[\lambda(\mathrm{tr}\boldsymbol{\varepsilon})\mathbf{1} + 2\mu\boldsymbol{\varepsilon}] \tag{D.104}$$

where tr denotes trace, λ and μ are the Lame constants and ∇^2 is the laplacian. For the case of torsion of a cylindrical bar, the gradient dependent shear stress-shear strain relation reads

$$\sigma_{z\theta} = 2\mu(\varepsilon_{z\theta} - c\nabla^2\varepsilon_{z\theta}) \tag{D.105}$$

Using eq. (D.52), defining $\phi_{,z} = \alpha$ as the twist for unit length and $\varepsilon_{z\theta} = \gamma$, it is possible to write

$$\epsilon_{z\theta} = \tfrac{1}{2}r\alpha \tag{D.106}$$

and

$$\sigma_{z\theta} = \mu\alpha(r - c/r) \tag{D.107}$$

The torsional moment is related to the stress by

$$M_T = \int_A \sigma_{z\theta} r dA = \mu\alpha(J - \pi c R^2) \tag{D.108}$$

which again has the same form as obtained in micropolar theory.

If the constitutive equation is written as,

$$\sigma_{z\theta} = 2\mu[\varepsilon_{z\theta} - c_1(\nabla\varepsilon_{z\theta}\nabla\varepsilon_{z\theta})^{1/2} - c_2\nabla^2\varepsilon_{z\theta}] \tag{D.109}$$

then the stress is:

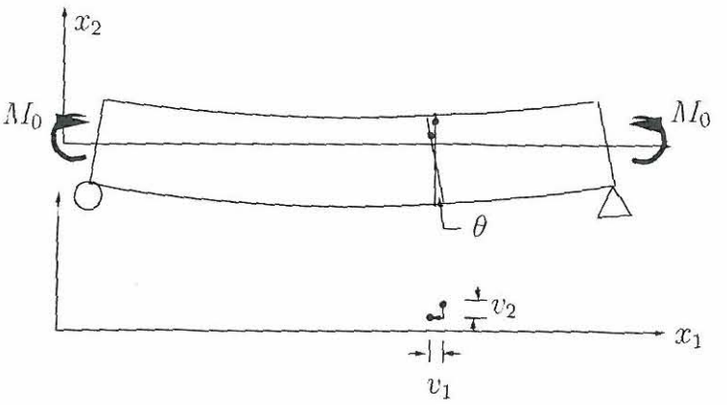

Figure D.5: Deformation by bending in a beam.

$$\sigma_{z\theta} = \mu\alpha(r - c_1 - c_2/r) \tag{D.110}$$

The torsional moment is:

$$M_T = \int_A \sigma_{z\theta} r dA = \mu\alpha(J - \tfrac{2}{3}\pi c_1 R^3 - \pi c_2 R^2) \tag{D.111}$$

In this case a factor R^3 appears in the solution. Aifantis (1999) uses the last form of the solution to approximate experimental results obtained for foam specimens.

D.4 Bending of beams

D.4.1 Classical elasticity

The problem of a beam subjected only to bending will be considered. The deformed beam is shown schematically in figure D.5, cross-sections of the beam remain plane during deformation. It is possible to see that two displacements occur: a vertical displacement v_2 and a longitudinal displacement v_1.

The displacement field is

$$v_1 = -\theta x_2, \qquad v_2 = v_2(x_1), \qquad v_3 = 0 \tag{D.112}$$

The strains are

$$\varepsilon_{11} = -x_2\theta_{,1} \approx -x_2 v_{2,11} \tag{D.113}$$

where

$$\theta \approx v_{2,1} \tag{D.114}$$

The constitutive equations reduce to

$$\sigma_{11} = E\varepsilon_{11} = -Ex_2 v_{2,11} \tag{D.115}$$

where E is Young's modulus of the material. Equilibrium of forces produces

$$\int_A \sigma_{11} dA = -Ev_{2,11} \int_A x_2 dA = 0 \tag{D.116}$$

which means that the neutral axis coincides with the centroid of the section. Equilibrium of moments produces

$$M_3 = -\int_A x_2 \sigma_{11} dA = Ev_{2,11} \int_A x_2^2 dA = Ev_{2,11} I \tag{D.117}$$

where I is the second moment of the area or inertial moment. The final results are

$$v_{2,11} = \frac{M_3}{EI}, \qquad \sigma_{11} = -\frac{M_3 x_2}{I} \tag{D.118}$$

For the simple elastic beam of length L and constant section shown in figure D.5, we obtain

$$v_2 = \frac{M_0}{2EI}(Lx_1 - x_1^2) \tag{D.119}$$

and at the midpoint of the beam

$$v_2(L/2) = \frac{M_0 L^2}{8EI} \tag{D.120}$$

D.4.2 Micropolar theory

In this section it is supposed that the material is centrosymmetric, homogeneous and orthotropic. In this case, the following displacement and microrotation fields are proposed:

$$\begin{aligned} v_1 &= -\omega_3 x_2 \\ v_2 &= v_2(x_1, x_2) \\ v_3 &= 0 \\ \omega_1 &= \omega_2 = 0 \\ \omega_3 &= \omega_3(x_1, x_2) \end{aligned} \tag{D.121}$$

Replacing eq. (D.121) into eq. (D.23) and eq. (D.24) we obtain the the strains and curvatures:

$$
\begin{aligned}
\varepsilon_{11} &= v_{1,1} = -\omega_{3,1} x_2 \\
\varepsilon_{12} &= v_{1,2} + \omega_3 = 0 \\
\varepsilon_{21} &= v_{2,1} - \omega_3 \\
\varepsilon_{22} &= v_{2,2} \\
\kappa_{31} &= \omega_{3,1} \\
\kappa_{32} &= \omega_{3,2}
\end{aligned} \tag{D.122}
$$

The constitutive equations eq. (D.20) and eq. (D.21) in case of an orthotropic centrosymmetric material are written as:

$$
\begin{aligned}
\sigma_{11} &= F_{11}\varepsilon_{11} + F_{12}\varepsilon_{22} = -F_{11} x_2 \omega_{3,1} + F_{1,2} v_{2,2} \\
\sigma_{12} &= 0 \\
\sigma_{21} &= G_{21}\varepsilon_{21} = G_{21}(v_{2,1} - \omega_3) \\
\sigma_{22} &= F_{21}\varepsilon_{11} + F_{22}\varepsilon_{22} = -F_{21} x_2 \omega_{3,1} + F_{22} v_{2,2} \\
\mu_{31} &= H_{31}\kappa_{31} = H_{31}\omega_{3,1} \\
\mu_{32} &= H_{32}\kappa_{32} = H_{32}\omega_{3,2} \\
\mu_{13} &= H_{13}\kappa_{31} = H_{13}\omega_{3,1} \\
\mu_{23} &= H_{23}\kappa_{32} = H_{23}\omega_{3,2}
\end{aligned} \tag{D.123}
$$

The equilibrium equations eq. (D.18) and eq. (D.19) reduce to:

$$
\begin{aligned}
&\sigma_{11,1} + \sigma_{21,2} = 0 \\
&\sigma_{12,1} + \sigma_{22,2} = 0 \\
&\mu_{13,1} + \mu_{23,2} + \sigma_{12} - \sigma_{21} = 0
\end{aligned} \tag{D.124}
$$

Replacing eq. (D.123) into eq. (D.124) produces the following three equations

$$
\begin{aligned}
&- F_{11} x_2 \omega_{3,11} + F_{12} v_{2,21} + G_{21}(v_{2,12} - \omega_{3,2}) = 0 \\
&- F_{21}(\omega_{3,1} + x_2 \omega_{3,12}) + F_{22} v_{2,22} = 0 \\
&H_{13}\omega_{3,11} + H_{23}\omega_{3,22} - G_{21}(v_{2,1} - \omega_3) = 0
\end{aligned} \tag{D.125}
$$

From the last mentioned equation we can obtain $v_{2,1}$ as a function of second derivatives of ω_3 with respect to both directions. In order to solve the problem it is now assumed that ω_3 only depends on x_1

$$
\omega_3 = \omega_3(x_1) \tag{D.126}
$$

This has the following consequences:

$$
\kappa_{32} = \mu_{23} = \mu_{32} = 0 \tag{D.127}
$$

and eq. (D.125) reduces to:

$$-F_{11}x_2\omega_{3,11} + F_{12}v_{2,21} + G_{21}v_{2,12} = 0 \tag{D.128}$$
$$-F_{21}\omega_{3,1} + F_{22}v_{2,22} = 0 \tag{D.129}$$
$$H_{13}\omega_{3,11} - G_{21}(v_{2,1} - \omega_3) = 0 \tag{D.130}$$

From eq. (D.130) is possible to obtain

$$v_{2,1} = H_{13}\omega_{3,11}/G_{21} - \omega_3 \tag{D.131}$$

then $v_{2,12} = 0$. From eq. (D.128) and eq. (D.129) the following is obtained

$$\begin{aligned} v_{2,21} &= \frac{F_{11}}{F_{12}}x_2\omega_{3,11} \\ v_{2,22} &= \frac{F_{21}}{F_{22}}\omega_{3,1} \end{aligned} \tag{D.132}$$

To satisfy eq. (D.132), it is necessary to suppose a linear relation in ω_3 like

$$\omega_3 = \theta x_1 \tag{D.133}$$

where θ is a constant value to be determined. This relation produces

$$\begin{aligned} v_{2,1} &= -\omega_3 = -\theta x_1 \\ v_{2,2} &= \frac{F_{21}}{F_{22}}\theta x_2 \\ v_2 &= \tfrac{1}{2}\theta(\frac{F_{21}}{F_{22}}x_2^2 - x_1^2) \end{aligned} \tag{D.134}$$

The bending moment is

$$M_3 = -\int_A x_2\sigma_{11}dA + \int_A \mu_{13}dA \tag{D.135}$$

$$M_3 = F_{11}\theta I - \frac{F_{12}F_{21}}{F_{22}}\theta I + H_{13}\theta A \tag{D.136}$$

then

$$\theta = \frac{M_3}{(F_{11} - \frac{F_{12}F_{21}}{F_{22}})I + H_{13}A} \tag{D.137}$$

and the deflection can be calculated using eq. (D.134) and eq. (D.137).

$$v_2 = \frac{1}{2}\left(\frac{F_{21}}{F_{22}}x_2^2 - x_1^2\right)\frac{M I_3}{\left(F_{11} - \frac{F_{12}F_{21}}{F_{22}}\right)I + H_{13}A} \tag{D.138}$$

It is possible to write eq. (D.138) as

$$v_2 = \frac{1}{2}\left(\frac{F_{21}}{F_{22}}x_2^2 - x_1^2\right)\frac{M I_3}{E_1 I + H_{13}A} \tag{D.139}$$

where $E_1 = F_{11} - F_{12}F_{21}/F_{22}$ is the elastic modulus of the centrosymmetric material. The deflection of the simple supported beam at the midpoint is

$$v_2(L/2) = \frac{M_0 L^2}{8}\left(\frac{1}{(E_1 I + H_{13}A)}\right) \tag{D.140}$$

It is possible to observe in eq. (D.135), eq. (D.137) and eq. (D.138) that now the curvature only has influence if the cross-section is of small height. This is because the moment depends linearly on the height through the term that includes the cross-sectional area, and with a cube of the height on the terms that depend on the inertia of the cross-section.

D.4.3 Cosserat theory using equations by Eringen

Non-centrosymmetric material

The following displacement field is initially used

$$\begin{aligned} v_1 &= -\phi_3 x_2 \\ v_2 &= v_2(x_1, x_2) \\ v_3 &= 0 \end{aligned} \tag{D.141}$$

The microrotation field is

$$\phi_1 = \phi_2 = 0, \qquad \phi_3 = \phi_3(x_1, x_2) \tag{D.142}$$

The strains are calculated using eq. (D.8), and the results are

$$\begin{aligned} \varepsilon_{11} &= -\phi_{3,1} x_2 \\ \varepsilon_{12} &= \varepsilon_{21} = \tfrac{1}{2}(v_{2,1} - \phi_{3,2} x_2 - \phi_3) \\ \varepsilon_{22} &= v_{2,2} \end{aligned} \tag{D.143}$$

The macrorotations using eq. (D.1) are

$$\omega_1 = \omega_2 = 0, \qquad \omega_3 = \tfrac{1}{2}(v_{2,1} + \phi_{3,2} x_2 + \phi_3) \tag{D.144}$$

Substitution of eq. (D.141, D.142, D.143 and D.144) into eq. (D.94) produces:

$$
\begin{aligned}
\sigma_{11} &= v_{2,2}\lambda - \phi_{3,1}x_2(\lambda + 2\mu + \kappa) \\
\sigma_{12} &= (v_{2,1} - \phi_3)(\mu + \kappa) - \phi_{3,2}x_2\mu \\
\sigma_{21} &= (v_{2,1} - \phi_{3,2}x_2 - \phi_3)(\mu + \kappa) \\
\sigma_{22} &= v_{2,2}(\lambda + 2\mu + \kappa) - \phi_{3,1}x_2\lambda \\
\sigma_{13} &= C_3\phi_{3,1} \\
\sigma_{23} &= C_3\phi_{3,2} \\
\sigma_{31} &= C_2\phi_{3,1} \\
\sigma_{32} &= C_2\phi_{3,2} \\
\sigma_{33} &= 0 \\
m_{11} &= -\phi_{3,1}x_2(c_1 + C_2 + C_3) + C_1v_{2,2} \\
m_{12} &= v_{2,1}(C_2 + C_3) - \phi_{3,2}x_2C_2 - \phi_3C_3 \\
m_{13} &= \gamma\phi_{3,1} \\
m_{21} &= v_{2,1}C_2 - \phi_{3,2}x_2C_3 - \phi_3C_3 \\
m_{22} &= -\phi_{3,1}x_2C_1 + v_{2,2}(C_1 + C_2 + C_3) \\
m_{23} &= \gamma\phi_{3,2} \\
m_{31} &= \beta\phi_{3,1} \\
m_{32} &= \beta\phi_{3,2} \\
m_{33} &= C_1(-\phi_{3,1}x_2 + v_{2,2})
\end{aligned}
\tag{D.145}
$$

The equilibrium equations eq. (D.18) and eq. (D.19) have the following form

$$
\begin{aligned}
& v_{2,21}\lambda + \phi_{3,11}x_2(\lambda + 2\mu + \kappa) = 0 \\
& (v_{2,11} - \phi_{3,1})(\mu + \kappa) - \phi_{3,21}x_2\mu + v_{2,22}(\lambda + 2\mu + \kappa) - \phi_{3,12}x_2\lambda - \phi_{3,1}\lambda = 0 \\
& C_3(\phi_{3,11} + \phi_{3,22}) = 0 \\
& -\phi_{3,11}x_2(C_1 + C_2 + C_3) + v_{2,21}C_1 + v_{2,12}C_2 - \phi_{3,22}x_2C_3 - \phi_{3,2}(C_3 + C_2) = 0 \\
& v_{2,11}(C_2 + C_3) + v_{2,22}(C_1 + C_2 + C_3) - \phi_{3,21}x_2C_2 - \phi_{3,12}x_2C_1 \\
& \qquad\qquad + \phi_{3,1}(C_2 - C_1 - 2C_3) = 0 \\
& \gamma(\phi_{3,11} + \phi_{3,22}) + \phi_{3,2}x_2\kappa = 0
\end{aligned}
\tag{D.146}
$$

From the third equation in (D.146) it is deduced that $\phi_{3,22} = -\phi_{3,11}$ and replacing this result in the last equation in (D.146) it is obtained that $\phi_{3,2} = 0$. Then ϕ_3 is only a function of x_1

$$
\phi_3 = \phi_3(x_1) \tag{D.147}
$$

The equilibrium equations then reduce to:

$$
\begin{aligned}
&v_{2,21}\lambda + \phi_{3,11}x_2(\lambda + 2\mu + \kappa) = 0\\
&(v_{2,11} - \phi_{3,1})(\mu + \kappa) + v_{2,22}(\lambda + 2\mu + \kappa) - \phi_{3,1}\lambda = 0\\
&C_3\phi_{3,11} = 0\\
&-\phi_{3,11}x_2(C_1 + C_2 + C_3) + v_{2,21}C_1 + v_{2,12}C_2 = 0\\
&v_{2,11}(C_2 + C_3) + v_{2,22}(C_1 + C_2 + C_3) + \phi_{3,1}(C_2 - C_1 - 2C_3) = 0
\end{aligned}
\tag{D.148}
$$

From the third equation in (D.148) it is deduced that

$$
\phi_{3,1} = \theta, \qquad \phi_3 = \theta x_1 \tag{D.149}
$$

where θ is a constant to be determined. Replacing eq. (D.149) into eq. (D.148) the equations are

$$
\begin{aligned}
&v_{2,21}\lambda = 0\\
&(v_{2,11} - \theta)(\mu + \kappa) + v_{2,22}(\lambda + 2\mu + \kappa) - \theta\lambda = 0\\
&v_{2,21}C_1 + v_{2,12}C_2 = 0\\
&v_{2,11}(C_2 + C_3) + v_{2,22}(C_1 + C_2 + C_3) + \theta(C_2 - C_1 - 2C_3) = 0
\end{aligned}
\tag{D.150}
$$

From the first equation in (D.150) it is deduced that $v_{2,21} = 0$, and replacing this result into the third equation in (D.150) it is possible to conclude that $v_{2,12} = 0$. It is to be deduced that $v_{2,1}$ is a function of only x_1 and $v_{2,2}$ is a function of only x_2. Expressing these functions as

$$
v_{2,1} = g(x_1), \qquad v_{2,2} = h(x_2) \tag{D.151}
$$

and replacing eq. (D.151) into eq. (D.150) the following equations appear

$$
\begin{aligned}
&g'(x_1)(\mu + \kappa) - h'(x_2)(\lambda + 2\mu + \kappa) - \theta(\lambda + \mu + \kappa) = 0\\
&g'(x_1)(C_2 + C_3) + h'(x_2)(C_1 + C_2 + C_3) + \theta(C_2 - C_1 - 2C_3) = 0
\end{aligned}
\tag{D.152}
$$

where the symbol (') means the derivative of the function. The solution to eq. (D.152) is:

$$
g(x_1) = -\theta x_1 A_1, \quad h(x_2) = -\theta x_2 A_2, \quad \text{and,} \quad v_2 = -\tfrac{1}{2}\theta x_1^2 A_1 - \tfrac{1}{2}\theta x_2^2 A_2 \tag{D.153}
$$

where

$$
\begin{aligned}
A_1 &= \frac{C_1(2\lambda + 3\mu + 2\kappa) + C_2\mu - C_3(3\lambda + 5\mu + 3\kappa)}{C_1(\mu + \kappa) - (C_2 + C_3)(\lambda + \nu)}\\
A_2 &= \frac{-C_1(\mu + \kappa) + C_2(\lambda + 2\mu + 2\kappa) + C_3(\lambda - \mu - \kappa)}{C_1(\mu + \kappa) + (C_2 + C_3)(\lambda + 3\nu + 2\kappa)}
\end{aligned}
\tag{D.154}
$$

The strains and macrorotations are found to be

$$\begin{aligned}
\varepsilon_{11} &= -\theta x_2 \\
\varepsilon_{12} &= \varepsilon_{21} = -\tfrac{1}{2}\theta x_1(1 + A_1) \\
\varepsilon_{22} &= -\theta x_2 A_2 \\
\omega_3 &= -\tfrac{1}{2}\theta x_1(1 - A_1)
\end{aligned} \tag{D.155}$$

and the stresses and couple stresses are:

$$\begin{aligned}
\sigma_{11} &= -\theta x_2[\lambda(1 + A_2) + 2\mu + \kappa] \\
\sigma_{12} &= \sigma_{21} = -\theta x_1(\mu + \kappa)(1 + A_1) \\
\sigma_{22} &= -\theta x_2[\lambda(1 + A_2) + 2\mu A_2 + \kappa A_2] \\
\sigma_{13} &= C_3\theta \\
\sigma_{31} &= C_2\theta \\
\sigma_{23} &= \sigma_{32} = \sigma_{33} = 0\theta \\
m_{11} &= \theta x_2[C_1(A_2 - 1) - C_2 - C_3] \\
m_{12} &= -\theta x_1[C_3(A_1 + 1) + C_2] \\
m_{13} &= \gamma\theta \\
m_{21} &= -\theta x_1(A_1 C_2 + C_3) \\
m_{22} &= -\theta x_2[C_1(A_2 + 1) + C_2 + C_3] \\
m_{31} &= \beta\theta \\
m_{23} &= m_{32} = 0 \\
m_{33} &= -\theta x_2 C_1(A_2 + 1)
\end{aligned} \tag{D.156}$$

The moment is related to the stresses according to eq. (D.135), and the result is

$$M_3 = \theta[\lambda(1 + A_2) + 2\mu + \kappa]I + \gamma\theta A \tag{D.157}$$

The displacement is

$$v_2 = -\tfrac{1}{2}(x_1^2 A_1 + x_2^2 A_2)\frac{M_3}{E_1 I + \gamma A} \tag{D.158}$$

where $E_1 = \lambda(1 + A_2) + 2\mu + \kappa$. For the simply supported beam the vertical displacement at the midpoint is:

$$v_2 = -\frac{M_0 L^2}{8}\left(\frac{A_1}{E_1 I + \gamma A}\right) \tag{D.159}$$

Centrosymmetric material

The same displacement and microrotation fields that were assumed for non-centrosymmetric materials eq. (D.141) and eq. (D.142) will be supposed initially. The macrorotations and strains are the same as in non-centrosymmetric material eq.(D.143) and eq.(D.144). The stresses and couple stresses are

$$\begin{aligned}
\sigma_{11} &= v_{2,2}\lambda - \phi_{3,1}x_2(\lambda + 2\mu + \kappa) \\
\sigma_{12} &= (v_{2,1} - \phi_3)(\mu + \kappa) - \phi_{3,2}x_2\mu \\
\sigma_{21} &= (v_{2,1} - \phi_{3,2}x_2 - \phi_3)(\mu + \kappa) \\
\sigma_{22} &= v_{2,2}(\lambda + 2\mu + \kappa) - \phi_{3,1}x_2\lambda \\
\sigma_{13} &= \sigma_{23} = \sigma_{31} = \sigma_{32} = \sigma_{33} = 0 \\
m_{11} &= m_{12} = m_{21} = m_{22} = m_{33} = 0 \\
m_{13} &= \gamma\phi_{3,1} \\
m_{23} &= \gamma\phi_{3,2} \\
m_{31} &= \beta\phi_{3,1} \\
m_{32} &= \beta\phi_{3,2}
\end{aligned} \tag{D.160}$$

The equilibrium equations reduce to three equations:

$$\begin{aligned}
&v_{2,21}\lambda + \phi_{3,11}x_2(\lambda + 2\mu + \kappa) = 0 \\
&(v_{2,11} - \phi_{3,1})(\mu + \kappa) - \phi_{3,21}x_2\mu + v_{2,22}(\lambda + 2\mu + \kappa) - \phi_{3,12}x_2\lambda - \phi_{3,1}\lambda = 0 \\
&\gamma(\phi_{3,11} + \phi_{3,22}) + \phi_{3,2}x_2\kappa = 0
\end{aligned} \tag{D.161}$$

In order to solve the problem it is now assumed now that ϕ_3 is a function of $x_1$only, $\phi_3 = \phi_3(x_1)$. Equations (D.160) and eq. (D.161) are rewritten as

$$\begin{aligned}
\sigma_{11} &= v_{2,2}\lambda - \phi_{3,1}x_2(\lambda + 2\mu + \kappa) \\
\sigma_{12} &= (v_{2,1} - \phi_3)(\mu + \kappa) \\
\sigma_{21} &= (v_{2,1} - \phi_3)(\mu + \kappa) \\
\sigma_{22} &= v_{2,2}(\lambda + 2\mu + \kappa) - \phi_{3,1}x_2\lambda \\
m_{13} &= \gamma\phi_{3,1} \\
m_{31} &= \beta\phi_{3,1} \\
m_{32} &= m_{23} = 0
\end{aligned} \tag{D.162}$$

and

$$\begin{aligned}
&v_{2,21}\lambda + \phi_{3,11}x_2(\lambda + 2\mu + \kappa) = 0 \\
&(v_{2,11} - \phi_{3,1})(\mu + \kappa) + v_{2,22}(\lambda + 2\mu + \kappa) - \phi_{3,1}\lambda = 0 \\
&\gamma\phi_{3,11} = 0
\end{aligned} \tag{D.163}$$

From the third equation in (D.163) it is deduced that $\phi_3 = \theta x_1$, and replacing this value of ϕ_3 into the other two equations in (D.163) produces:

$$\begin{aligned} &v_{2,21}\lambda = 0 \\ &(v_{2,11} - \theta)(\mu + \kappa) + v_{2,22}(\lambda + 2\mu + \kappa) - \theta\lambda = 0 \end{aligned} \tag{D.164}$$

which means that $v_{2,2}$ is a function of only x_2. It is assumed here that $v_{2,2} = A_3 x_2$ where A_3 is a constant. This supposition produces the following v_2

$$v_2 = \tfrac{1}{2}A_4 x_1^2 + \tfrac{1}{2}A_3 x_2^2 \tag{D.165}$$

where

$$A_4 = \frac{-A_3(\lambda + 2\mu + \kappa) + \theta(\lambda + \mu + \kappa)}{\mu + \kappa} \tag{D.166}$$

The stresses can be obtained replacing eq. (D.166) into eq. (D.162). The moment using eq. (D.135) is:

$$M_3 = [A_3\lambda - \theta(\lambda + 2\mu + \kappa)]I + \gamma\theta A \tag{D.167}$$

Using a solution similar to the one found for non-centrosymmetric materials $A_4 = \theta$ then

$$A_3 = \frac{\theta\lambda}{\lambda + 2\mu + \kappa} \tag{D.168}$$

and

$$\theta = \frac{M_3}{\left((\lambda + 2\mu + \kappa) - \frac{\lambda^2}{\lambda + 2\mu + \kappa}\right)I + \gamma A} \tag{D.169}$$

For the simple beam, the deflection at midpoint is:

$$v_2(L/2, 0) = \frac{M_0 L^2}{8}\left(\frac{1}{E_2 I + \gamma A}\right) \tag{D.170}$$

where E_2 is a modified elastic modulus of the material defined by

$$E_2 = (\lambda + 2\mu + \kappa) - \frac{\lambda^2}{\lambda + 2\mu + \kappa} \tag{D.171}$$

Another possible solution is found when A_3 is adjusted to produce

$$\theta = \frac{MI_3}{EI + \gamma A} \tag{D.172}$$

where E is Young's modulus of the material. In order to obtain eq. (D.172) is necessary that

$$A_3 = \theta\left(\frac{2\lambda^2 + 12\lambda\mu + 6\lambda\kappa + 8\mu^2 + 8\mu\kappa + 2\kappa^2}{\lambda(2\lambda + 2\mu + \kappa)}\right)$$
$$A_4 =) = -\theta\Lambda \tag{D.173}$$

where

$$\Lambda = \frac{\lambda^2(12\mu + 5\kappa) + \lambda(28\mu^2 + 29\mu\kappa + 7\kappa^2) + 16\mu^3 + 24\mu^2\kappa + 12\mu\kappa^2 + 2\kappa^3}{\lambda(2\lambda + 2\mu + \kappa)(\mu + \kappa)} \tag{D.174}$$

The deflection at midpoint is

$$v_2(L/2, 0) = \frac{MI_0L^2}{8}\left(\frac{\Lambda}{EI + \gamma A}\right) \tag{D.175}$$

D.4.4 Theory by Fleck and Hutchinson, 1997

Again, initially the displacement field is considered in a general way as:

$$\begin{aligned} v_1 &= -\omega x_2 \\ v_2 &= v_2(x_1, x_2) \\ v_3 &= 0 \\ \omega &= \omega(x_1) \end{aligned} \tag{D.176}$$

where ω was supposed to be a function of x_1 only, This restriction was established in order to find a solution to the problem. The strains are calculated using eq. (D.8), and the results are:

$$\begin{aligned} \varepsilon_{11} &= -\omega_{,1} x_2 \\ \varepsilon_{12} &= \varepsilon_{21} = \tfrac{1}{2}(v_{2,1} - \omega) \\ \varepsilon_{22} &= v_2, 2 \end{aligned} \tag{D.177}$$

The non-vanishing terms in the tensor corresponding to the second gradient of displacements are

$$\begin{aligned}
\eta_{111} &= -\omega_{,11}x_2, & \eta_{211} &= -\omega_{,1} \\
\eta_{112} &= -\omega_{,1}, & \eta_{121} &= v_{2,11} \\
\eta_{221} &= v_{2,12}, & \eta_{122} &= v_{2,21} \\
\eta_{222} &= v_{2,22}
\end{aligned} \tag{D.178}$$

The results of replacing eq. (D.178) into the constitutive equations found by deriving eq. (D.81) are:

$$\begin{aligned}
\sigma_{11} &= v_{2,2}\lambda - \omega_{,1}x_2(\lambda + 2\mu) \\
\sigma_{12} &= \sigma_{21} = \tfrac{1}{2}\mu(v_{2,1} - \omega) \\
\sigma_{22} &= (v_{22}(\lambda + 2\mu) - \omega_{,1}x_2\lambda \\
\tau_{111} &= -2\omega_{,11}x_2(a_1 + a_2 + a_3 + a_4 + a_5) + v_{2,21}(2a_1 + a_2) + v_{2,12}(a_2 + a_3) \\
\tau_{112} &= -\omega_{,1}(a_2 + 2a_3 + 2a_4 + 2a_5) + v_{2,22}(a_2 + 2a_3) + v_{2,12}a_3 \\
\tau_{211} &= -2\omega_{,1}(a_1 + a_4 + a_5) + v_{2,22}(2a_1 + a_2) \\
\tau_{121} &= 2v_{2,11}(a_4 + a_5) \\
\tau_{122} &= -\omega_{,11}x_2(2a_1 + a_2) + 2v_{2,21}(a_1 + a_4) + 2v_{2,12}a_5 \\
\tau_{221} &= -\omega_{,11}x_2(a_2 + a_3) - \omega_{,1}a_3 + v_{2,21}(a_2 + 2a_5) + 2v_{2,12}(a_3 + a_4) \\
\tau_{222} &= -2\omega_{,1}(a_1 + a_2 + a_3) + 2v_{2,22}(a_1 + a_2 + a_3 + a_4 + a_5)
\end{aligned} \tag{D.179}$$

The equilibrium equations eq. (D.84) are satisfied with the following solution:

$$\begin{aligned}
\omega &= \theta x_1 \\
v_1 &= -\theta x_1 x_2 \\
v_2 &= \tfrac{1}{2}A_5 x_1^2 + \tfrac{1}{2}A_6 x_2^2 \\
v_3 &= 0
\end{aligned} \tag{D.180}$$

The non-vanishing terms in strains and the second gradient of displacements now are

$$\begin{aligned}
\varepsilon_{11} &= -\theta x_2 \\
\varepsilon_{12} &= \varepsilon_{21} = \tfrac{1}{2}x_1(A_5 - \theta) \\
\varepsilon_{22} &= A_6 x_2 \\
\eta_{211} &= \eta_{112} = -\theta \\
\eta_{121} &= A_5 \\
\eta_{222} &= A_6
\end{aligned} \tag{D.181}$$

The stresses and third order stresses are

$$
\begin{aligned}
\sigma_{11} &= A_6 x_2 \lambda - \theta x_2(\lambda + 2\mu) \\
\sigma_{12} &= \sigma_{21} = \tfrac{1}{2}\mu x_1(A_5 - \theta) \\
\sigma_{22} &= A_6 x_2(\lambda + 2\mu) - \theta x_2 \lambda \\
\tau_{112} &= -\theta(a_2 + 2a_3 + 2a_4 + 2a_5) + A_6(a_2 + 2a_3) \\
\tau_{211} &= -2\theta(a_1 + a_4 + a_5) + A_6(2a_1 + a_2) \\
\tau_{121} &= 2A_5(a_4 + a_5) \\
\tau_{221} &= -\theta a_3 \\
\tau_{222} &= -2\theta(a_1 + a_2 + a_3) + 2A_6(a_1 + a_2 + a_3 + a_4 + a_5)
\end{aligned} \tag{D.182}
$$

The equilibrium equations eq. (D.84) reduce to the single one

$$
\tfrac{1}{2}\mu(A_5 - \theta) + A_6(\lambda + 2\mu) = 0 \tag{D.183}
$$

and the non-vanishing couple stresses eq.(D.87) are

$$
\begin{aligned}
m_{13} &= -\tfrac{4}{3}\theta(a_2 + 2a_3 + 2a_4 + 2a_5) + \tfrac{4}{3}A_6(a_2 + 2a_3) - \tfrac{8}{3}A_5(a_4 + a_5) \\
m_{23} &= -\tfrac{4}{3}\theta a_3
\end{aligned} \tag{D.184}
$$

Finally the moment is related to stresses by

$$
M_3 = \int_A (-\sigma_{11} x_2 + m_{13}) dA = [\theta(\lambda + 2\mu) - A_6\lambda]I + m_{13}A \tag{D.185}
$$

In the same way presented in micropolar theory, it is possible to use $A_5 = \theta$ in that case eq. (D.183) indicates that $A_6 = 0$ and

$$
\theta = \frac{M_3}{(\lambda + 2\mu)I + \frac{4}{3}[a_2 + 2a_3 + 4a_4 + 4a_5]A} \tag{D.186}
$$

and the deflection at the midpoint of the beam shown is

$$
v_2 = \frac{M_0 L^2}{8}\left(\frac{1}{(\lambda + 2\mu)I + \frac{4}{3}(a_2 + 2a_3 + 4a_4 + 4a_5)A}\right) \tag{D.187}
$$

Another solution could use $M_3 = \theta EI + m_{13}A)$, so

$$
A_6 = \theta(1 - 2\nu - 2\nu^2)/\nu \tag{D.188}
$$

where ν is the Poisson relation, and

$$
A_5 = \theta\frac{-3 + 10\nu - 8\nu^3}{1 - 2\nu} \tag{D.189}
$$

Replacing eq. (D.188) and eq. (D.189) in eq.D.180 produces for the deflection in the middle point of the beam:

$$v_2 = \frac{M_0 L^2}{8}\left(\frac{A_5}{EI + A_7 A}\right) \tag{D.190}$$

where

$$A_7 = \tfrac{4}{3}(a_2 + 2a_3 + 2a_4 + 2a_5) + \tfrac{4}{3}(1 - 2\nu - 2\nu^2)(a_2 + 2a_3)/\nu + \\ - \tfrac{8}{3}A_5(a_4 + a_5) \tag{D.191}$$

D.5 Conclusions

The solution to the problem of axial force it not affected by the use of micropolar theories when centrosymmetric materials are used. But when non-centrosymmetric materials are considered, the solution can be different from the classical one. The effect of non-centrosymmetry when axial force is considered, consists in torsion appearing as a secondary effect of the axial force. The solution could be of interest in case of rods or cables made, for example with twisting fibers. When the strain gradient theory by Aifantis (1984) is used, it is found that under constant axial force, the strains are not constants and have a maximum value in the middle of the bar. In this theory the variation of the strain field is maximum near the ends of the bar, otherwise it is almost constant.

The problem of torsion of a cylindrical rod in every one of the higher-order theories is affected by scale factors, This is reflected in the fact that the torsional moment not only depends on the polar inertia of the section, as is required by the classical solution, but also depends on the square of the radius of the section. For small values of radius, the dependence on the square of the radius could be of importance, while larger values tend towards the classical solution. It is remarkable that all theories tend to produce results of the same form, this being the solution of the theory by Fleck & Hutchinson (1997) the most easy one to find, since it does not depend on previous results of differential equations. Again it is possible to see that in non-centrosymmetric materials, a dependence between axial force and torsion exists. In the case of only torsion applied over the rod, a longitudinal displacement and axial force can be produced. The theory using the relation (D.1) and the theory by Fleck & Hutchinson (1997) produce, as expected, a symmetric strain tensor. The theory by Aifantis predicts an additional dependence between the torsional moment and R^3.

In the case of bending, the solutions presented for higher order theories are limited by suppositions such as that a linear relation between the curvature and x_1 exist. The effect of considering higher order theories is again reflected in a scale dependence of the phenomenon, this time through the height of the section.

When, in the solution presented for micropolar theories using equations by Eringen, and in the theory by Fleck & Hutchinson (1997), a classical material is considered by setting as zero the appropriate constants, the solution differs from the

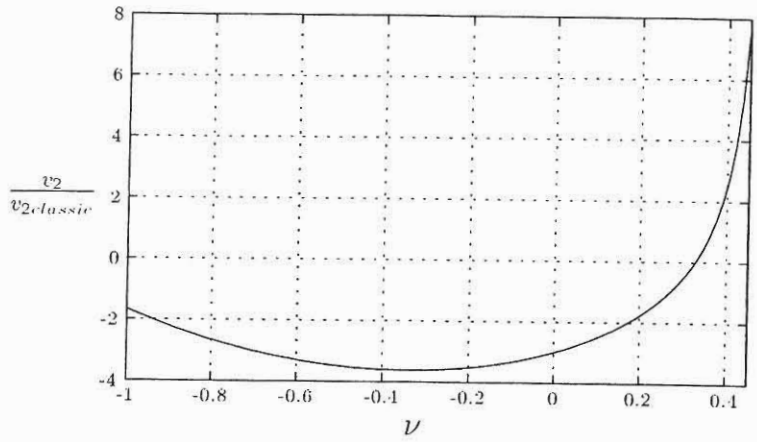

Figure D.6: Variation of the displacements for the theory by Fleck & Hutchinson (1997), compared to the classical solution for different values of Poisson's ratio when A_5 and A_6 are selected to produce $M_3 = \theta EI + m_{13}A$.

classical one. The solution is affected by a factor, even if in the solution the constants are defined to produce $\theta = M_3/(EI)$ as expected for a classical material. In figure (D.6) the displacements of the beam used as example supposing a classical material are compared to the theory by Fleck & Hutchinson (1997) and the classical solution as a function of different values of the Poisson's ratio ν.

Bibliography

Aifantis, E. C. (1984), 'On the microstructural origin of certain inelastic models', *J. Eng. Mater. Technol.* **106**, 326–330.

Aifantis, E. C. (1999), 'Strain gradient interpretation of size effects', *Int. J. of Fracture* **95**, 299 314.

Altan, B. S., Evensen, H. A. & Aifantis, E. C. (1996), 'Longitudinal vibrations of a beam: A gradient elasticity approach', *Mechanics Research Comunications* **23**(1), 35 40.

Byskov, E. (1999), *Elementary Continuum Mechanics for Everyone*, third extended edition edn, Aalborg University, Aalborg, DK.

Chakrabarty, J. (1987), *Theory of plasticity*, Engineering Mechanics Series, Mc.Graw-Hill Book Company, Singapore.

Christoffersen, J. (2000), Material curvature. Unpublished notes on Nonlinear Micropolar Theories.

Cosserat, E. & Cosserat, F. (1909), *Theorie des Corps Deformables*, Hermann et Fils,, Paris.

Cowin, S. C. (1970), 'An incorrect inequality in micropolar elasticity theory', *J. appl. Math. Phys. (ZAMP)* **21**, 494–497.

Eringen, A. C. (1968), *Theory of micropolar elasticity*, Vol. 1, Academic Press.

Eringen, A. C. (1972), 'Linear theory of nonlocal elasticity and dispersion of plane waves', *Int. J. Engng. Sci.* **10**, 425–435.

Fleck, N. A. & Hutchinson, J. W. (1993), 'A phenomenological theory for strain gradient effects in plasticity', *J. Mech. Phys. of Solids* **41**, 1825–1857.

Fleck, N. A. & Hutchinson, J. W. (1997), Strain gradient plasticity, *in* 'Adv. in Applied Mechanics', Vol. 33, Hutchinson, J. W., Wu T.T., pp. 295 361.

Fleck, N. A. & Hutchinson, J. W. (2001), 'A reformulation of strain gradient plasticity', *J. Mech. Phys. of Solids* **49**, 2245 – 2271.

Koiter, W. T. (1964), Couple stresses in the theory of elasticity, I and II, *in* 'Proc. Ned. Acad. Wet. (B)', Vol. 67, pp. 17–44.

Kröner, E. (1967), 'Elasticity theory of materials with long range cohesive forces', *Int. J. Solids and Structures* **3**, 731 742.

Lakes, R. (2001), 'Elastic and viscoelastic behavior of chiral materials', *Int. J. of Mech. Sciences* **43**, 1579–1589.

Mindlin, R. D. (1965*a*), 'Second gradient of strain and surface-tension in linear elasticity', *Int. J. Solids Struct.* **1**, 417–438.

Mindlin, R. D. (1965*b*), 'Stress functions for a cosserat continuum', *Int. J. Solids and Structures* **1**, 265–271.

Pamin, J. K. (1994), Gradient dependent plasticity in numerical simulation of localization phenomena, PhD thesis, Technische Universiteit Delft.

Toupin, R. A. (1962), 'Elastic materials with couple stress', *Arch. Rational Mech. Anal.* **11**, 385–414.

Appendix E

The program 'crack'

Contents

E.1 Introduction

In order to implement and test some of the techniques used to analyze the process of cracking in structural elements, the computer program 'crack' was developed by the author. The program makes use of the finite element method to solve problems where interface elements or elements with embedded discontinuities might be used.

The program, originally conceived to be one single program, was divided into three sub-programs. The first is a preprocessor program called 'crp', the second is a program for processing and solving systems of equations, this is called 'crs'. The third program is made for post-processing and producing graphical output and is called 'crg'.

All three sub-programs work on a common database. The input data required can be generated interactively using the program 'crp' or using a single ASCII file with extension '.dat'. This data file can be generated using alternative programs. All of the database used for the program is in ASCII format, so that it can be easily read and modified by the users.

All of the three sub-programs share some common C−+ classes and functions, some of these can conform a library by themselves, but here the classes are just included in every one of the three sub-programs.

The program includes 22 different kinds of elements; some of these, however, are not completely implemented because they are not being used by the author as part of the research on material instability. Here, references are made only to the elements that are completely implemented.

All of the sub-programs were developed in the computer language C++. The sub-programs are copyrighted under the terms of the GNU general public license. The program was developed using the Kdevelop C/C++ Integrated Development Environment which can be found on http://www.kdevelop.org. Additionally, the program makes use of the libraries QT and the program Qt designer from Trolltech that can be found on http://www.trolltech.com/qt/. The sub-program 'crg' also uses the library dislin from Helmut Michels (Max-Planck-Institut für Sonnensystemforschung) http://www.linmpi.mpg.de/dislin/. All three subprograms make extensive use of the GNU scientific library, which is used for the implementation and manipulation of matrices and vectors. This library can be found on http://sources.redhat.com/gsl/.

The author has modified and created a C class based on the program 'sparse' for solution of sparse matrices created by Kenneth Kundert and Alberto Sangiovanni-Vincentelli from the University of California at Berkeley. The original program 'sparse' can be found on http://www.netlib.org/sparse/index.html.

E.2 The pre-processor 'crp'

The pre-processor program 'crp' allows the interactive creation of the input database required for the crack program. Alternatively, the ASCII file `database_name.dat` is required for the program 'crs'. This file can be created using other programs or a text editor, thus avoiding the need for using this sub-program. To create the file using a text editor, users are required to follow the instructions in section E.3.

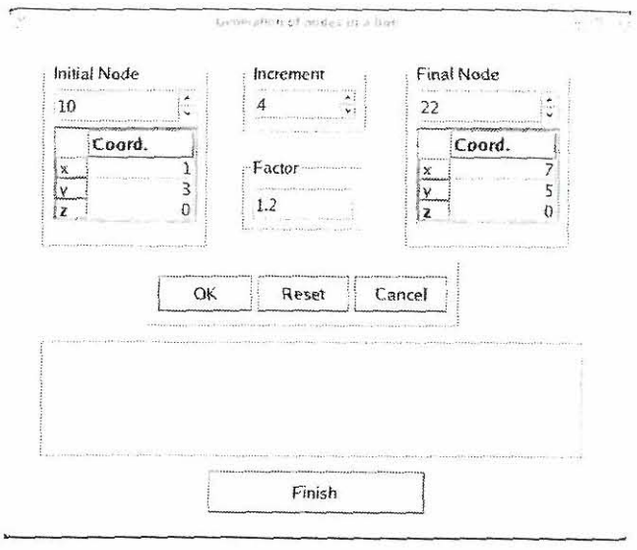

Figure E.1: Formulary used for generation of nodes along a line.

The sub-program 'crp' is interactive and the user can use it in order to create the database (including the `database_name.dat` file).

The first step to create the database consists in giving some general information about the size of the problem, this can be done using the formulary on the menu `<Edit->General information>`. The information required is the number of nodes, elements, nodes with restrictions, number of degrees of freedom in every node, and number of nodes with known forces different from zero). These parameters can be changed during the process of creation of the problem, however, it is recommended that these quantities be defined as accurately as possible.

The user can generate some of the nodes. In particular, to generate nodes along a line, users are required to fill in the formulary shown in figure E.1, this formulary is found on the menu in `Edit->Nodes->Line`.

To generate nodes in an area, it is necessary to specify the four corner nodes, and to fill the formulary shown in figure E.2 which can be found under the menu `Edit->Nodes->Area`.

As a result of the filled-in formularies as in figure E.1 and in figure E.2, the resulting nodes are shown in figure E.3.

If the option `<gen_interfacial>` is used in the formulary shown in figure E.2, the result is shown in figure E.4.

The user can also generate one- or two-dimensional elements with two, three or four nodes automatically.

After the process of creating the nodes, elements, element properties and material properties, it is possible to generate a table of degrees of freedom for the problem. Once this table is created, it can be modified by the user (not recommended).

If the system includes interface elements, where a large slip is going to be considered, then it is necesary to fill a table creating lists of adjacent interface elements, in this form the processor will treat them as a group where the connectivities will be dynamically updated during the analysis.

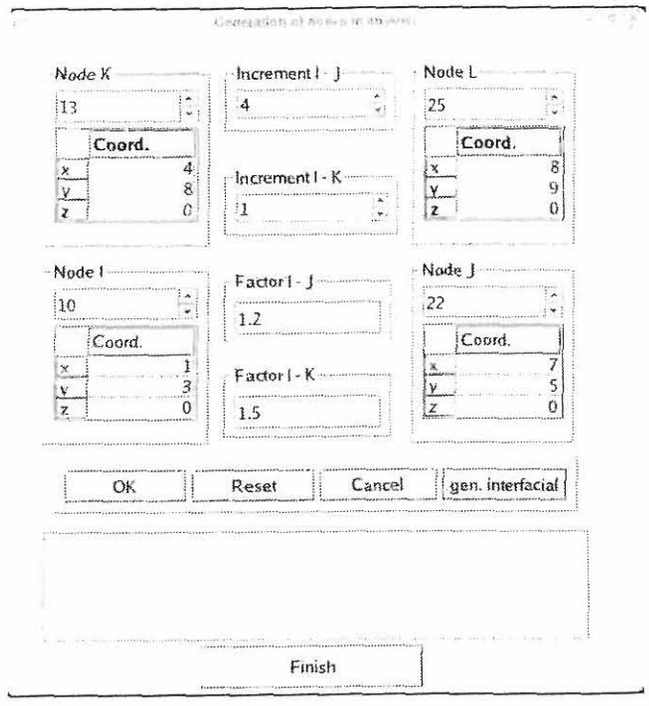

Figure E.2: Formulary used for generation of nodes in an area.

E.3 The '.dat' file

E.3.1 Introduction

The purpose of the program 'crp' is to create a file named `database_name.dat`; this file is an ASCII file with the following characteristics:

1. Commentaries can be placed everywhere starting in the first column of the line, if a commentary is going to be inserted, the first characters must be '/'.

2. The separator between data must be the space character, any number of space characters is allowed, between two data.

3. If, in a line, more information is expected than the information actually supplied, this information will be supposed to be zero.

4. The file is divided into several sections, every section starts with a name in capital letters. The sections to be considered are: GLOBAL, NODES, ELEMENTS, EPROP, MATERIALS, CONSTANTS, RESTRICTIONS, FORCES and LISTS.

E.3.2 The GLOBAL section

A line with the following information is required: number of nodes, number of elements, number of materials, number of groups of properties associated with one type of elements, number of degrees of freedom in every node, number of nodes with restrictions, and number of nodes with nodal forces.

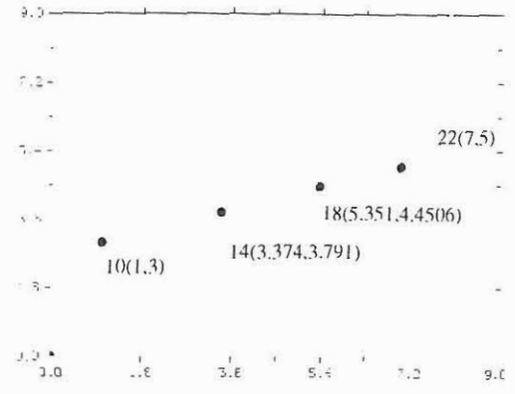

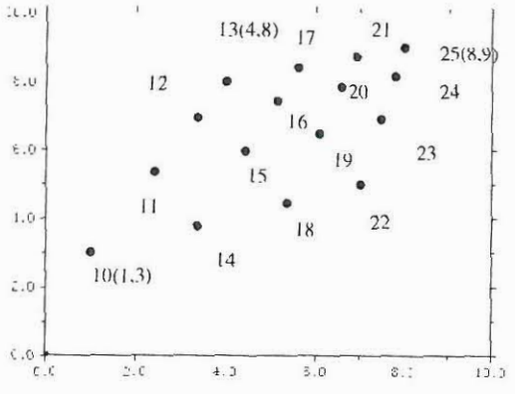

Figure E.3: Nodes generated using the formulary filled as in (a)figure E.1 and (b)figure E.2.

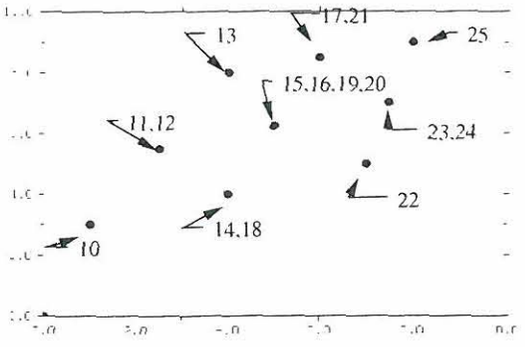

Figure E.4: Nodes generated using the formulary filled as in figure E.2 using the option to generate interface.

Example:

```
/ This is the file :/home/i6gcc/crackwork/twoinc/0g/i0.dat
/
/ Global parameters defined for the problem
/
GLOBAL
/ N.Nds N.Elmts N.Mat N.Cts N.DOF. N.Restrict N.Forces
 10722   7933     5     5     2      213         2
```

E.3.3 The NODES section

In this section, a line is required for every one of the nodes in the system. The line must contain the number of the node and the coordinates x, y and z for the node.

Example:

```
/ Coordinates of nodes
NODES
/ Number Coord.X Coord.Y Coord.Z
   1        0       0       0
   2        0       0.2     0
   3        0       0.2     0
   4        0       0.4     0
   5        0       0.4     0
   6        0       0.6     0
```

E.3.4 The ELEMENTS section

In this section, the input consists in the nodes for every element. One line must be supplied for every element, the line consists in the number of the element, the

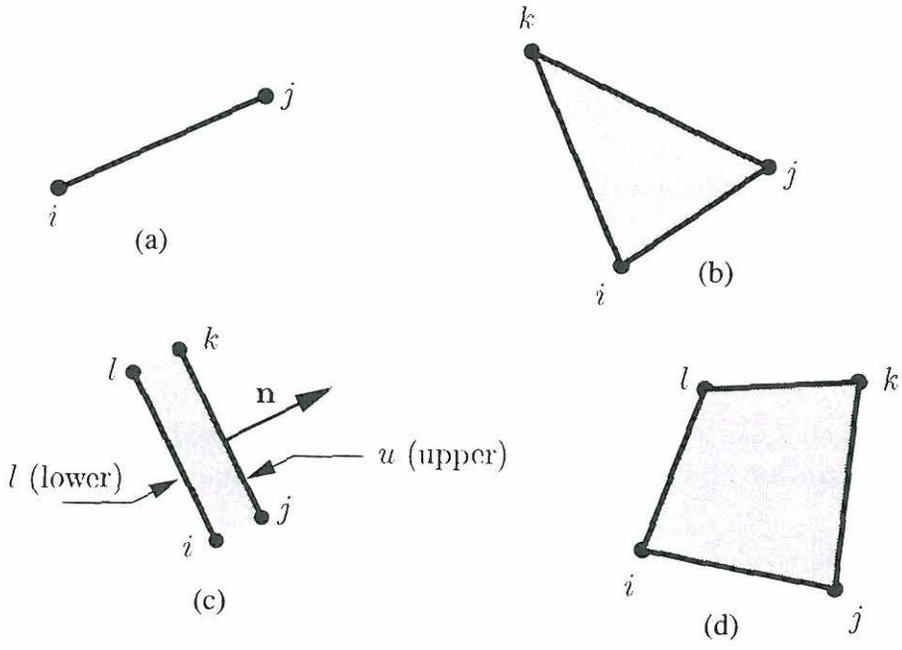

Figure E.5: Nodes for different types of elements. (a)Unidimensional 2-node element, (b)Triangular element, (c)4-node interface element and (d) quadrilateral element.

number of nodes for the element, and, finally, the numbers defining every one of the nodes for the element. The required numeration for different kinds of elements is shown in figure E.5.

Example:

```
10721  11  7.8  0
10722  11  8  0
/ Element description
ELEMENTS
/ Number NumNodes   I     J     K     L
    1        4      5231  5311  5312  5232
    2        4      5233  5313  5314  5234
    3        4      5235  5315  5316  5236
    4        4      5237  5317  5318  5238
    5        4      5239  5319  5320  5240
    6        4      5241  5321  5322  5242
    7        4      5243  5323  5324  5244
    8        4      5245  5325  5326  5246
    9        4      5247  5327  5328  5248
```

E.3.5 The EPROP section

In this section, geometrical and material properties related to each element are defined. One line is required for every element in the system. The line must contain:

the number of the element, the name for this element, the number of material properties to be associated, and the number of geometrical properties associated.

The name of the element must consist of one of the following:

BAR A 2 node bar element for unidimensional problems of elasticity.

BARA A 2 node bar element for one-dimensional problems for elasticity including an embedded crack modeled using the alternative theory presented based on Alfaiate et al. (2003).

BARC A 2 node bar element for unidimensional problems of elasticity including an embedded crack modeled using the extended finite element method.

CRACK1 One node interface element using a simple exponential cohesive model.

CRACK2 Four node interface element, this element can use a cohesive model based on Xu & Needleman (1993) or a frictional model based on Povirk & Needleman (1993).

CRACK2C A 4 node interface element for the analysis of discontinuities using only the Xu-Needleman cohesive model.

CRACKL A 4-node interface element for the analysis of discontinuities including large slip displacements. This element can use the Xu-Needleman cohesive model and the frictional model used by Povirk & Needleman (1993).

TRUSS2D A two node truss element, this element can be used to analyze problems including large displacements.

CST1 A triangular 3-node element for plane stress elasticity.

CST2 A triangular 3-node element for plane strain elasticity.

CSTC1 A triangular 3-node element for plane stress elasticity, including an embedded crack using the extended finite element method. The crack is cohesive according to an exponential function.

CSTC2 A triangular 3-node element for plane strain elasticity, including an embedded crack using the extended finite element method. The crack is cohesive according to an exponential function.

PLANE1 A quadrilateral 4-node isoparametric element for plane stress elasticity.

PLANE2 A quadrilateral 4-node isoparametric element for plane strain elasticity.

PLANE1C A quadrilateral 4-node isoparametric element for plane stress elasticity, including an embedded crack using the extended finite element method. The crack is cohesive according to an exponential function.

PLANE2C A quadrilateral 4-node isoparametric element for plane strain elasticity, including an embedded crack using the extended finite element method. The crack is cohesive according to an exponential cohesive model.

PLANE1X A quadrilateral 4-node isoparametric element for plane stress elasticity, including an embedded crack using the extended finite element method. The crack is modeled using the Xu-Needleman cohesive model.

PLANE2X A quadrilateral 4-node isoparametric element for plane strain elasticity, including an embedded crack using the extended finite element method. The crack is modeled using a Xu-Needleman cohesive model.

PLANE1A A quadrilateral 4-node isoparametric element for plane stress elasticity, including an embedded crack using the alternative method. The crack is cohesive according to an exponential function.

PLANE2A A quadrilateral 4-node isoparametric element for plane strain elasticity, including an embedded crack using the alternative method. The crack is cohesive according to an exponential function.

Example:

```
7932  4  10720  10721  10641  10640
7933  4  10641  10721  10722  10642
/ Element properties
EPROP
/Numberm  Type  Material Constants
    1     CRACKL   1          1
    2     CRACKL   1          1
    3     CRACKL   1          1
    4     CRACKL   1          1
    5     CRACKL   1          1
    6     CRACKL   1          1
    7     CRACKL   1          1
```

E.3.6 The MATERIALS section

In this section the material properties associated with a group are specified. One line is required for every group of material properties.

The line must contain the following information: (a) number of the group of this material, (b) Elastic modulus or C_n if a frictional model is going to be defined. (c) Poisson ratio or C_s if the frictional model is used, (c) σ_u, (d) G_f for the exponential cohesive model or ϕ_n for the Xu-Needleman cohesive model, (e)τ_u for the

Xu-Needleman cohesive model, (f) μ_s static friction coefficient, (g) dynamic friction coefficient, (h) d_c (i) $\dot{q}_1$, (j) $\dot{q}_0$, (k) p, (l) m and (m) θ_0. Where C_n and C_s are the normal and tangential stiffnesses associated with the interface, respectively. σ_u and τ_u are the maximum normal and shear stresses allowed in the cohesive model. G_f or ϕ_n are the work of separation in the exponential or in the Xu-Needleman cohesive model, respectively. d_c is the characteristic slip distance in the frictional model. $\dot{q}_1$ and $\dot{q}_0$ are constant velocities normalizing the frictional model. p and m are constant exponents used in the frictional model and θ_0 is a constant representing an initial value of the internal variable θ in the frictional model.

Example:

```
7931  PLANE2  4  4
7932  CRACK2C  5  5
7933  PLANE2  4  4
/ Materials definition
MATERIALS
/ Nm E/Cn  Nu/Cs S_u  G_f   Tauu mus mud  dc q_1 q_0  p   m  theta0
  1   3000 1000   10  1e-05 1    0.5 0.15 4  10  100  0.5 5  4.6052
  2 175000 0.3     0  0     0    0   0    0  0    0  0   0  0
  3 175000 75000 930  1e-05 500  0   0    0  0    0  0   0  0
  4  30000 0.2     0  0     0    0   0    0  0    0  0   0  0
  5  30000 10000 2.8  0.1   2.8  0   0    0  0    0  0   0  0
```

E.3.7 The CONSTANTS section

In this section, additional geometric characteristics for the system are described. One line is required for every group of geometric characteristics. Every line must contain the following information: (a) number of group of properties; (b) thickness of the element for two-dimensional elements or cross-sectional area for unidimensional elements; (c) hydrostatic initial pressure; (d) a maximum value of coordinate x, defined in such form, that if the displacement of an interface element results in the new (updated) coordinates being greater than this value, then the element will be removed from the analysis. This is used to define an exterior boundary; and (e) a maximum y coordinate, defined in such form, that if the updated coordinates of an interface element are greater than this value, then the element will be removed from the analysis, this is used again to define an exterior boundary.

Example:

```
/ Real constants definition
CONSTANTS
/ Number t/A init.hydrostatic.press.  max.x max.y
    1     1          -5                  0     8
    2     1          -5                  0     0
    3     1          -5                  0     0
    4     1          -5                  0     0
    5     1          -5                  0     0
```

E.3.8 The RESTRICTIONS section

In this section, the restrictions to the system are defined. One line is required for every restricted node. The information in every line consists of: (a) number of the node and (b) a number 1 or 0 for every degree of freedom in the node. A number 1 means that the corresponding degree of freedom is restricted to move, a zero indicates that this degree of freedom is free to move. Maximum 6 degrees of freedom are allowed per node, the three first values correspond to translational degrees of freedom, and the last three to rotational degrees of freedom.

Example:

```
/ Restrictions in nodes
RESTRICTIONS
/ Node ux uy uz rx ry rz
   1    0  1  0  0  0  0
  81    0  1  0  0  0  0
 161    0  1  0  0  0  0
 241    0  1  0  0  0  0
 321    0  1  0  0  0  0
 401    0  1  0  0  0  0
```

E.4 The FORCES section

One line is required for every node with known nodal forces that are different from zero. The information in the line must consist in the number of the node, and the component of the force in the global system of coordinates. Six values can exist, the first three correspond to nodal forces and the last three values correspond to moments

Example:

```
10720  1  0  0  0  0  0
10721  1  0  0  0  0  0
10722  1  0  0  0  0  0
/ Forces in nodes
FORCES
/ Node fx   fy fz mx my mz
  5361  0  150  0  0  0  0
  5442  0  150  0  0  0  0
```

E.4.1 The LISTS section

When a large slip is allowed in interface elements, it is necessary to group the interface elements in lists, indicating the sequence of the elements. Defining the lists of elements allows the program to update the connectivities during the analysis. The lists of 'CRAC2L' elements are defined here, the lists are defined in columns with the numbers corresponding to the elements in the list.

Example:

```
/ List of interface elements
LISTS
/ NumMaxElem      NumLists
/ list1 list2     list3     list4     list5     list6     list7
   25      2
    1     26
    2     27
    3     28
    4     29
    5     30
```

E.5 The finite element analysis using the subprogram 'crs'

E.5.1 Introduction

This sub-program is responsible for processing the information and for producing the results corresponding to displacements and stresses. The sub-program 'crs' gets most of the information required from the file `database_name.dat`.

The information in the file `database-name.dat` is sufficient for a linear elastic static analysis, if this option under the menu `<run>` is activated, the displacements for the linear case are obtained, and if the stresses are required then it is necessary to activate the option `run->stresses`. If changes are done to the database users are required to activate the option `run->reset`.

E.5.2 The times definition

In case of a nonlinear analysis, it is necessary to define the parameters in the formulary on the menu `run->times_definition`, see figure E.6. In this formulary a time curve is defined to be used in case of non-proportional loading. The time curve is constructed by defining a number of points in the curve.

A convergence constant used in the iterative part of the process is required, so are a number of maximum iterations. If the number of maximum iterations is defined as 1, then the program will not iterate during the solution process. Lambda (λ) is defined as the load factor, by default the maximum value of λ is defined as one, but this can be changed in the corresponding option in the formulary.

When iterations are allowed, the step size (the value of Δl) in the arc-length control strategy can change according to the rule

$$\Delta l_{i+1} = \Delta l_i \sqrt{\frac{I_d}{I_i}} \tag{E.1}$$

where I_d is the number of desired iteration, and I_i is the number of iterations required in step i. However, the following criterion is also applied:

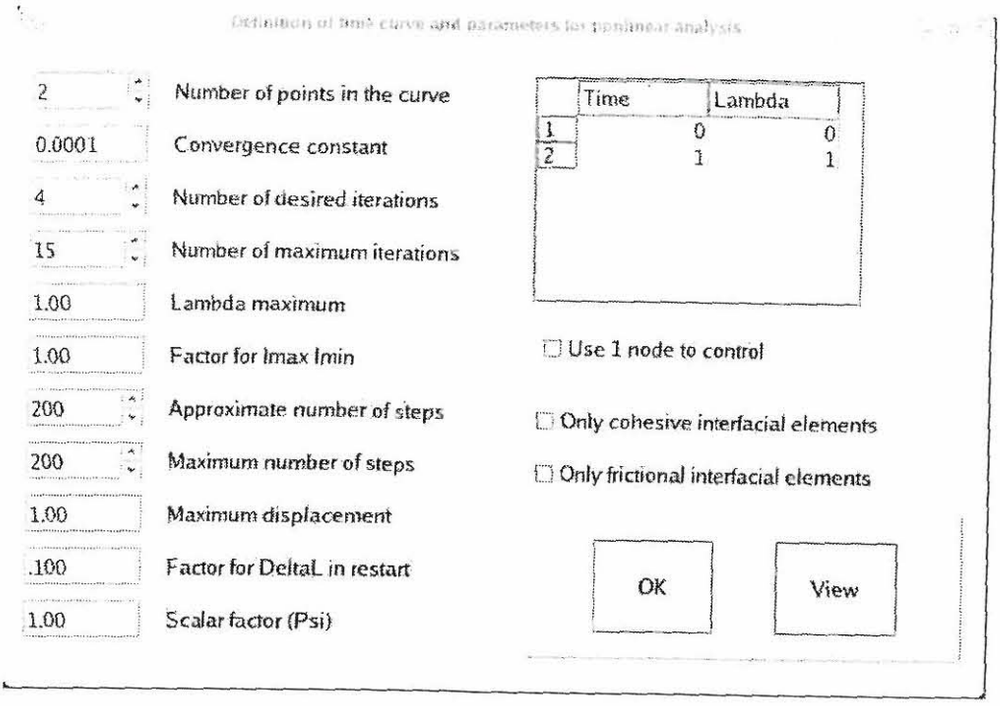

Figure E.6: Formulary used for generation of nodes along a line.

$$\frac{\Delta l_0}{I_{\min}} < \Delta l_{i+1} < \Delta l_0 * I_{\max} \tag{E.2}$$

where $I_{\min} = I_{\max}$ are defined for the user.

The size of Δl in the first step is defined supposing force control (only in the first step). In this force control, the force increment is defined from:

$$\Delta\lambda = \lambda_{\max}/S_d \tag{E.3}$$

where $\lambda_{\max}$ is the maximum value of λ and S_d is the approximate number of steps. Both of the quantities are defined in the formulary.

The program ends when one of the following criteria is fulfilled: a maximum number of steps defined by the user is reached; a maximum displacement is reached; a maximum value of λ is reached.

Sometimes it is necessary to restart an analysis after a number of steps have been done. In this case, it is possible to start with a step size of different value than the original; in this program it is defined after restart in step $i+1$ that:

$$\Delta l_{i+1} = \Delta l_i * I_f \tag{E.4}$$

where I_f is defined for the user in the entry `Factor for DeltaL in restart`. Finally it is necessary to define the value of ψ, where ψ is a constant that takes into account that the displacement and force have different scales. See (Crisfield 1991).

Under normal conditions, the program controls the advancing of the arc-length strategy. This is done by using an energetic criterion which means that the sign of Δl is defined as the one that produces positive external work in the step, i.e.:

$$\Delta W = \mathbf{q}^T \Delta \mathbf{u}_i = \mathbf{q}^T \dot{\mathbf{u}}_i \Delta \lambda_n > 0 \tag{E.5}$$

where W is the external work, $\mathbf{q}$ is the load vector, $\mathbf{u}$ is the displacement vector, and $\dot{\mathbf{u}}$ is the velocity vector.

It is possible to change the advancing criteria in (E.5), and thus control the solution by ensuring the advance of a certain degree of freedom. If the user checks the box corresponding to this in the formulary, then the program asks for the node and degree of freedom to control the advance of the solution.

In case of using interface elements, the user must also indicate if only frictional or only cohesive behavior is desired, otherwise the program will assume both. The transition from cohesive to frictional occurs when:

$$\sqrt{\left(\frac{\Delta u_n}{\delta_n} + 1\right)^2 + \left(\frac{\Delta u_s}{\delta_s}\right)^2} - 1 > 1 \tag{E.6}$$

where Δu_n and Δu_s are the increments in displacement in the normal and tangential directions, respectively, and δ_n and δ_s are the interface characteristic length scales in normal and tangential directions, respectively, according to the Xu-Needleman cohesive model.

E.5.3 Nonlinear run possibilities

After defining the time curve and the other parameters required, the problem can be run. The user can choose between different non-linear possibilities. In all cases, the spherical arc-length control solution is used.

A non-linear analysis of large displacements can be made if truss elements are defined. If this option is used, the solution is performed efficiently, the stiffness matrix is stored in compact form and a modified Cholesky algorithm is used to solve the system of equations. In all other cases of non-linear analysis, the matrix is stored as a sparse matrix and the solution is performed using subroutines developed by Kenneth Kundert from the University of California at Berkeley for the program 'sparse'. The program 'sparse' has been modified here and a C++ class has been built for this program. All the functionality of the original program is conserved, so that the matrices can be expanded; the matrices can be symmetric or asymmetric. The solution uses a modified Gauss solution. In the factorization a relative threshold of 0.001 is chosen (a value of one means complete pivoting, if the value is close to zero, the solution method is Markowitz pivoting without threshold).

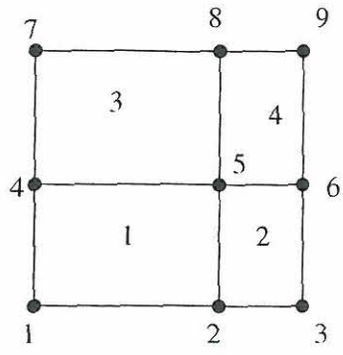

Figure E.7: A simple mesh consisting of four elements, each element has four nodes and a maximum of four elements on the boundary. The total number of nodes is 9.

E.5.4 The output files produced by 'crs'.

Introduction

As a result of running the program 'crs', a database is created. Every file name in the database consists of the database name with different extensions in the form `database-name.ext`. Depending on the options and type of analysis required, some of the files will be generated automatically.

All files are ASCII files, this option is choosen in order to check and debug the program more easily even if this is not the optimal format for the data. In the following part of this section, every output file will be described.

The .con file

This file contains the information about connectivities between elements. This file contains a list of the elements that have a boundary with the element considered. The list is developed for every element in the database.

One line is required for every element. The format is:

first line

$$N_e \quad N_b$$

from the second line:

$$bound_1 \quad bound_2 \quad bound_3 \quad \ldots \quad bound_n$$

where N_e is the number of elements, N_b is the number of elements that can be in the boundary of an element. $_i$ is the element i that shares a boundary with the element corresponding to this line.

For the mesh shown in figure E.7 the file looks like:

```
4  4
2  3  0  0
```

```
1  4  0  0
1  4  0  0
2  3  0  0
```

The .crc.number file

This file contains a list of the cracked elements existent in the step defined by 'number'. The list is shown as a column of values. The format of the file is:

$$\begin{matrix} size \\ element_1 \\ element_2 \\ \vdots \\ element_{size} \end{matrix}$$

where $size$ is the number of elements in the list, $element_i$ is the number identifying the element i on the list.

The .ctp file

This file is a copy of the file `database.cnumber` where `cnumber` is a character 'c' followed by a number indicating the number of the step considered (see the .cnumber file on page 308). This file is created for practical purposes when iterations are required. Normally this file is deleted before the start of the next step.

The .cts file

Contains the geometrical information related to a group of elements. A record is required for every group of geometric information. Every record consists of a line in the following form:

$$value_1 \quad value_2 \quad value_3 \quad \ldots \quad value_{n_{ct}}$$

where n_{ct} is the number of values with geometric information, for one-dimensional elements $value_1 = A$. For two-dimensional elements $value_1 = t$ and $value_2 = \sigma_0$. For interface elements $value_3 = X_{\max}$ and $value_4 = Y_{\max}$ where A is the cross-sectional area, t is the thickness of the element, σ_0 is the value of a hydrostatic pre-stress, $X_{\max}$ is the maximum value of the coordinate x, When the displacement of the element produces an updated coordinate greater than $X_{\max}$, the element is removed form the mesh, and occurs in the same form with $Y_{\max}$.

The .cnumber file

The extension used for this file consists of the character 'c' followed by a number 'number' indicating the step in which the file is created. This file contains the information about the cracked elements in the step. The file consists of one record for every cracked element. Every record consists of one line with the following information:

$$n_e \quad \theta \quad l_{12} \quad A^+ \quad n_v \quad n_n \quad n_\Omega \quad n_\Gamma \quad \kappa_1 \quad \kappa_2 \ldots \quad \kappa_{n_\Gamma} \quad x_1 \quad y_1$$
$$x_2 \quad y_2 \quad \ldots \quad x_{n_v} \quad y_{n_v} \quad nod_1 \quad nod_2 \quad \ldots \quad nod_{n_n} \quad T_{s_1 1} \quad T_{n1} \quad T_{s_2 1} \quad T_{s_1 2}$$
$$T_{n2} \quad T_{s_2 2} \quad \ldots \quad T_{s_1 n_\Gamma} \quad T_{n n_\Gamma} \quad T_{s_2 n_\Gamma} \quad \sigma_{x1} \quad \sigma_{y1} \quad \sigma_{z1} \quad \sigma_{xy1} \quad \sigma_{yz1}$$
$$\sigma_{zx1} \quad \ldots \quad \sigma_{xn_\Omega} \quad \sigma_{yn_\Omega} \quad \sigma_{zn_\Omega} \quad \sigma_{xyn_\Omega} \quad \sigma_{yzn_\Omega} \quad \sigma_{zxn_\Omega}$$
$$v_{0n1} \quad v_{0s1} \quad v_{0n2} \quad v_{0s2} \quad dots \quad v_{0nn_\Gamma} \quad v_{0sn_\Gamma}$$

where n_e is the number identifying this cracked element, θ is the angle between the crack and the x-axis, l_{12} is the length of the crack along this element, A^+ is the area of this element in Ω^+ (see figure E.8) n_v is the number of points required to describe the region Ω^+ in the element, n_n is the total number of nodes describing this element, n_Ω is the number of integration points used for this element, n_Γ is the number of integration points along the line describing the discontinuity, κ_i is the value of the maximum normal jump at the integration point i along the discontinuity, x_i and y_i are the coordinates of the point i describing the region Ω^+, nod_i is a value describing if additional degrees of freedom are required for the node i. A value of 1 means that additional degrees of freedom are required, otherwise a value of 0 is defined, $T_{s_i j}$ is the shear traction along the i direction for the integration point j along the discontinuity, T_{ni} is the normal traction for the integration point i along the discontinuity, σ_{nmi} is the value of the stress nm where n and m are x, y or z for the integration point i, v_{0ni} is the value of initial displacement associated with a pre-stress pressure when the Xu-Needleman model is used. n_v and n_n are defined in figure E.8 for some types of elements.

The .dof file

In this file the degrees of freedom associated with every node are described. One record is required for every node of the system containing:

$$dof_1 \quad dof_2 \quad dof_3 \quad dof_4 \quad dof_5 \quad dof_6$$

where dof_i is the number of the degree of freedom associated with the freedom i on the node, $i \leq 3$ is associated with displacements and $4 \leq i \leq 6$ is associated with rotations.

The .dsp file

This file corresponds to the output for nodal displacements, when a linear static analysis is performed, the displacement for every degree of freedom is presented for every node in the system in this file.

The .elm file

This file contains information related to the nodes describing every element. One record exists for every element on the system containing:

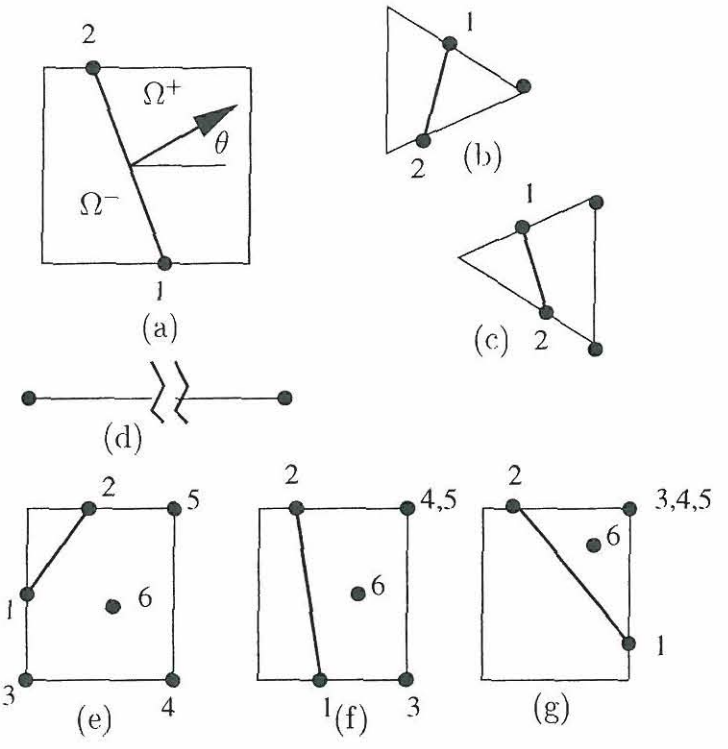

Figure E.8: (a)Definition of θ and Ω^+. (b) $n_v = 3$ $n_n = 3$, (c) $n_v = 4$ $n_n = 3$, (d) $n_v = 2$ $n_n = 2$, (e), (f) and (g) $n_v = 6$ $n_n = 4$.

$$n_n \quad nod_1 \quad nod_2 \quad \ldots \quad nod_{n_n}$$

where n_n is the number of nodes of the element, nod_i is the number assigned to the node i of this element.

The .emp file

This file contains the properties of every element. One register is created for every element containing:

$$Name \quad x_1 \quad y_1 \quad z_1 \quad \ldots \quad x_{n_n} \quad y_{n_n} \quad z_{n_n} \quad mp_1 \quad mp_2 \quad \ldots \quad mp_{n_{mp}} \quad value_1 \quad value_2 \quad \ldots \quad value_{n_v}$$

where *Name* is the name of the element, which must be one of the names described in section E.3.5. x_i, y_i and z_i are the coordinates of the node i describing the element, if the element is two-dimensional the information on z_i is omitted, if the element is one-dimensional, the information of y_i and z_i is omitted. mp_i corresponds to the material properties as defined in the file '.mat' (see page 315), and $value_i$ are the geometric values defined for the element defined in the file '.cts' (see page 308).

The .ept file

Contains the properties for every element. One record is produced for every element containing:

$$Name \quad MatTyp \quad CtsTyp$$

where $Name$ is the name of the element, which must be one of the names described in section E.3.5, $MatTyp$ is the number of the material properties associated with this element and described by a line in the file '.mat' (see page 315) and $CtsTyp$ is the number of geometrical properties associated with this element described for a line in the file '.cts' (see page 308).

The .frc file

This file contains the information associated with nodal forces. A record is required for every node with known nodal forces different from zero. The record consists in a single line containing:

$$N_n \quad f_x \quad f_y \quad f_z \quad m_x \quad m_y \quad m_z$$

where N_n is the number of the node with the forces f_i and moments m_i, where i is the direction of the component of force or moment.

The .fnumber file

The extension used for this file consists of the character 'f' followed by a number 'number' indicating the step in which the file is created. This file contains the information about the friction parameters for every integration point in every interface element, it also has information about parameters used in the Xu-Needleman cohesive model for interface elements.

A register consisting in n_Γ lines is created for every interface element containing the following information:

$$\begin{array}{cccccccccccc}
isChv_1 & \theta_1 & C_{n1} & C_{t1} & u_{n01} & isIn_1 & \dot{q}_1^{slip} & u_{n1} & u_{s1} & g_1 & f_1 & \mu_1 \\
isChv_2 & \theta_2 & C_{n2} & C_{t2} & u_{n02} & isIn_2 & \dot{q}_2^{slip} & u_{n2} & u_{s2} & g_2 & f_2 & \mu_2 \\
 & & & & & \vdots & & & & & & \\
isChv_{n_\Gamma} & \theta_{n_\Gamma} & C_{nn_\Gamma} & C_{tn_\Gamma} & u_{n0n_\Gamma} & isIn_{n_\Gamma} & \dot{q}_{n_\Gamma}^{slip} & u_{nn_\Gamma} & u_{sn_\Gamma} & g_{n_\Gamma} & f_{n_\Gamma} & \mu_{n_\Gamma}
\end{array}$$

where n_Γ is the number of integration points for the element. $isChv_i$ is a flag indicating if this point remains cohesive ($isChv_i = 1$) or if the frictional model must be used. θ_i is the value of the internal parameter θ used in the frictional model. C_{ni} and C_{ti} are the normal and tangential stiffness associated with the interface in the frictional model. u_{n0i} is the value of displacement associated with a pre-stress in the Xu-Needelman cohesive model. $isIn_i$ is a flag indicating if this point must be considered ($isIn_i = 1$) or not($isIn_i = 0$) when the integration is performed. $\dot{q}_i^{slip}$

is the value of the velocity. u_{ni} and u_{si} are the values of the normal and tangential jumps in the interface. In the frictional model used here the friction coefficient is defined as $\mu_i = g_i(\theta) f_i(\theta, \boldsymbol{\sigma})$.

The .gpa file

This file contains information about global parameters used in the analysis of the system. The file consists in a single line containing:

$$n_n \quad n_e \quad n_m \quad n_c \quad n_{dof} \quad n_{rest} \quad n_f$$

where n_n is the number of nodes in the system. n_e is the number of elements in the system. n_m is the number of groups of materials in the system. n_c is the number of groups of geometrical parameters for the element. n_{dof} is the maximum number of nodal degrees of freedom. n_{rest} is the number of nodes with restricted degrees of freedom. n_f is the number of unrestricted nodes with nodal forces different from zero.

The .inc file

This file contains a list of the degrees of freedom for the elements. In this list, the additional degrees of freedom produced when embedded cracks exist are not included.

A register for every element is created containing the following information:

$$dof_{11} \quad dof_{12} \quad \ldots \quad dof_{1n_{dof}} \quad dof_{12} \quad dof_{22} \quad \ldots \quad dof_{n_{ne}n_{dof}}$$

where dof_i is the number of the degree of freedom i for the element. n_{ne} is the number of nodes for the element and n_{dof} is the number of degrees of freedom in a node.

The .itp file

This file contains information about the nodes with additional degrees of freedom. One record exists for every node associated with a cracked element in the current step (this file only exists if new cracked elements appear in the step). The record contains:

$$n_{elem} \quad n_1 \quad n_2 \quad \ldots \quad n_{n_{ne}}$$

where n_{elem} is the number of the new cracked element and n_i is the number of the node i for this element with n_{ne} nodes.

The .inumber file

The extension used for this file corresponds to the character 'i' followed by a number corresponding to the number of the step. The file contains the list of degrees of freedom for every element in the step 'number'. The format is the same as in the file '.inc' (see page E.5.4), but in the elements with nodes with additional degrees of freedom, additional information corresponding to the numeration of these extra degrees of freedom is included.

The .lin file

This file contains information about lists of interface elements, the information is stored as a matrix with the following form:

$$\begin{matrix} n_{el} & n_l & & \\ e_{11} & e_{12} & \cdots & e_{1n_l} \\ e_{21} & e_{22} & \cdots & e_{2n_l} \\ \vdots & \vdots & \ddots & \vdots \\ e_{n_{el}1} & e_{n_{el}2} & \cdots & e_{n_{el}n_l} \end{matrix}$$

where n_{el} is the maximum number of elements in a list, n_l is the number of lists and e_{ij} is the number of the interface element i in the list j.

The .lsnumber file

The extension used for this file corresponds to the characters 'ls' followed by a number indicating the step in which the file was generated. This file contains lists of interface elements. One record is required for every list consisting of a first line including general information about the list, followed by $n_z = n_{ls} \times n_\Gamma$ lines with data related to properties for every integration point along the list, where n_{ls} is the number of elements in the list and n_Γ is the number of integration points for every element in the list.

The first line in the list contains:

$$\begin{matrix} n_l & a & n_z & \Delta s_i & \Delta s_f & Disp & allFrictional & n_{11} & n_{12} & n_{13} & n_{14} & n_{21} & n_{22} \\ & & & & & & & n_{23} & n_{24} & v_{i1} & v_{i2} & v_{e1} & v_{e2} \end{matrix}$$

where n_l is the number of this list, a is the length of the elements in the list, see figure E.9. Δs_i and Δs_f are the tangential displacements at the initial node on the list of elements and at the end point of the list, respectively. $Disp$ is the number of displacements in connectivities that have been required for the list. The variable $allFrictional$ indicates if the behavior of the list is frictional $allFrictional = 1$ or cohesive in some elements $allFrictional = 0$. n_{kl} refers to the degree of freedom associated with the initial and final node on the elements on the list. v_{ij} refers to the values of jump in displacement for the initial point on the list and v_{ej} to the displacement jump at the end of the list.

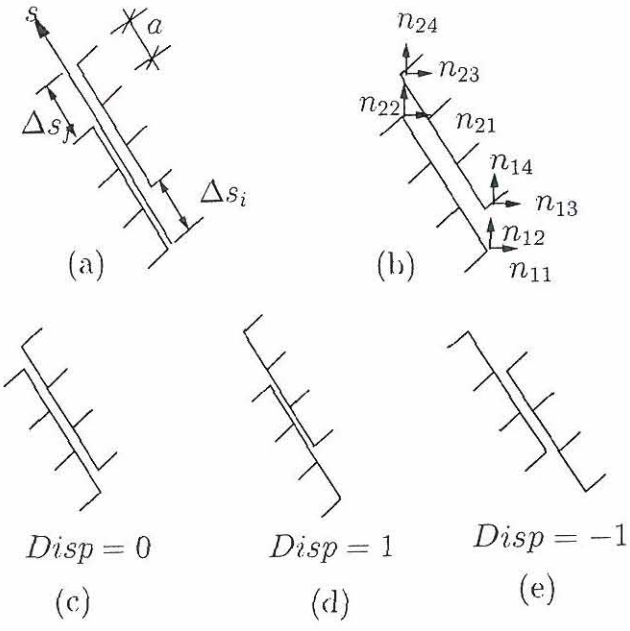

Figure E.9: Interface elements that constitute a list are shown. (a)Definition of geometric parameters, (b) Definition of degrees of freedom for the initial and final nodes. (c) Definition of $Disp = 0$, (b) definition of $Disp = 1$ and (e) definition of $Disp = -1$.

After the first line, n_z lines follow with the following information for every integration point:

$$s_i \quad C_n \quad C_s \quad t_n \quad t_s \quad \theta \quad \Delta u_{n0} \quad Cohesive$$

where s_i is the value of the coordinate s with origin in the first node of the first element in the list as illustrated in figure E.9. C_n and C_s are the normal and tangent stiffness in the Xu-Needleman cohesive model, respectively. t_n and t_s are the tractions at this integration point. θ is the value of the internal parameter in the frictional model. Δu_{n0} is the value of one initial displacement in the curve force-displacement to take into account pre-stresses in the element. $Cohesive$ is a variable indicating if this point remains cohesive ($Cohesive = 1$) or not ($Cohesive = 0$).

After the information for the lists, two additional lines exist at the end of the file. The first corresponds to the number of disconnected elements, i.e. the number of elements that have a face not in contact with the opposite side. The second line is a list of these elements. These two final lines look like:

$$n_d$$
$$e_{d1} \quad e_{d2} \quad \dots \quad e_{dn_d}$$

where n_d is the number of disconnected elements, and e_{di} is the number of the disconnected element i

The .mat file

This file contains the information related to the materials used to model the system. One line is required for every type of material. The line contains:

$$m_1 \quad m_2 \quad \dots \quad m_{n_{mp}}$$

where n_{mp} is the number of material properties required to describe the material and m_i is the value of the property i.

For BAR elements, only $m_1 = E$ is required, where E is the elastic modulus of the material. For plane elasticity, $m_1 = E$ and $m_2 = \nu$, are required where ν is Poisson's ratio.

For plane elements with cracks:

$$m_1 = E, \quad m_2 = \nu, \quad m_3 = \sigma_u, \quad m_4 = G_f \quad m_5 = \tau_u$$

where σ_u is the maximum normal stress, G_f is the work of separation and τ_u is the maximum tangential stress.

For unidimensional interface elements it is required that:

$$m_1 = E, \quad m_2 = 0, \quad m_3 = \sigma_u \quad m_4 = G_f$$

and for two-dimensional interface elements:

$$m_1 = C_n, \quad m_2 = C_t, \quad m_3 = \sigma_u, \quad m_4 = G_f, \quad m_5 = \tau_u, \quad m_6 = \mu_s,$$
$$m_7 = \mu_d, \quad m_8 = d_c, \quad m_9 = \dot{q}_1, \quad m_{10} = \dot{q}_0, \quad m_{11} = p,$$
$$m_{12} = m \quad \text{and } m_{13} = \theta_0$$

where μ_s is the static friction coefficient, μ_d is the dynamic friction coefficient, d_c, $\dot{q}_1$, $\dot{q}_0$, p, m and θ_0 are constant values used for the frictional model.

The .ncr file

This file contains a list of the new cracked elements in the current step. The format for the file is:

$$\begin{matrix} n_{nc} \\ e_1 \\ e_2 \\ \vdots \\ e_{n_{nc}} \end{matrix}$$

where n_{nc} is the number of new cracked elements in the step and e_i is the number of the new cracked element i.

The .nds file

This file contains the coordinates of every node in the system. One record is generated for every node in the system. Every record consists in one line containing:

$$x_i \quad y_i \quad z_i$$

where x_i, y_i and z_i are the Cartesian coordinates of the node i in the global system of coordinates.

The .nls file

This file contains the information about the steps in a non-linear analysis. One record is produced for every step. The record consists in a line containing:

$$n_s \quad \lambda \quad \Delta l \quad n_i \quad s_k \quad \Delta\lambda$$

where n_s is the number of the step, λ is the value of the load factor, Δl is the arc-length used in this step, n_i is the number of iterations performed to equilibrium in this step, s_k is the sign associated with the determinant of the tangent stiffness matrix, and $\Delta\lambda$ is the increment in load factor for this step.

The .nnumber file

The name of this file consists of the character 'n' followed by a number indicating the step in which this file was generated. This file contains a list of the degrees of freedom for every node on the step number. One line is produced for every node containing:

$$c \quad dof_1 \quad dof_2 \quad \ldots \quad dof_{12} \quad o_1 \quad o_2 \quad \ldots \quad o_6$$

where c is a variable indicating if this node is part of a cracked element ($c = 1$) or not ($c = 0$). The first six values of dof_i correspond to the regular degrees of freedom, the last six values correspond to the additional degrees of freedom. The values of o_i are indicators about the position of the node in the element, if $o_i = 1$ it means that the node is in the sub-domain Ω^+, if not $o_i = 0$.

The .onumber file

The name of this file consists of the character 'o' followed by a number indicating the step in which the file is generated. This file contains a list of the elements that are not cracked and are in the sub-domain Ω^+. The file consists of a line indicating the number of elements in the list n_o, followed by the number e_i corresponding to these elements.

$$
\begin{matrix}
n_o \\
e_1 \\
e_2 \\
\vdots \\
e_{n_o}
\end{matrix}
$$

The .pnumber file

The name of this file consists of the character 'p' followed by a number indicating the step in which the file is generated. This file contains a list of the nodal displacements (corresponding to the solution vector) for this step. The file consist of a line indicating the number of values in the list n_{dof} which is equal to the number of degrees of freedom in the system, followed by the corresponding values as:

$$
\begin{matrix}
n_{dof} \\
v_1 \\
v_2 \\
\vdots \\
v_{n_{dof}}
\end{matrix}
$$

where v_i is the value of the displacement, corresponding to the degree of freedom i. The file corresponds to the vector:

$$\mathbf{v}_t = \begin{bmatrix} \mathbf{v} \\ \mathbf{b} \end{bmatrix} \tag{E.7}$$

where $\mathbf{v}_t$ is the vector containing all the displacements for every degree of freedom. $\mathbf{v}$ is the displacement vector for the original degrees of freedom and $\mathbf{b}$ is the vector of displacements for the enhanced degrees of freedom.

The .ptnumber file

The name of this file consist of the characters 'pt' followed by a number indicating the step in which the file is generated. This file contains a list of the nodal displacements (corresponding to the solution vector) for this step. The file consists of a line indicating the number of values in the list n_{dof0} which is equal to the number of initial degrees of freedom in the system, followed by the corresponding values as:

$$
\begin{matrix}
n_{dof0} \\
v_1 \\
v_2 \\
\vdots \\
v_{n_{dof0}}
\end{matrix}
$$

where v_i is the value of the displacement, corresponding to the degrees of freedom i. The displacements are computed as:

$$\mathbf{u} = \mathbf{v} + H_s \mathbf{b} \tag{E.8}$$

where H_s is the heaviside function.

The .ptc file

This file contains information about the patches used in the analysis. One record is generated for every element containing:

$$\begin{matrix} n_e & & & \\ e_{1n_1} & e_{2n_1} & e_{3n_1} & e_{4n_1} \\ e_{1n_2} & e_{2n_2} & e_{3n_2} & e_{4n_2} \\ \vdots & & & \\ e_{1n_{ne}} & e_{2n_{ne}} & e_{3n_{ne}} & e_{4n_{ne}} \end{matrix}$$

where n_e is the number of this element, n_{ne} is the number of nodes in the element. e_{ij} is the number of the element i that is connected to the node j in the element n_e. A maximum of five elements can be considered as connected to a single node.

The .q file

This is a file containing the external forces, the information consist in:

$$\begin{matrix} n_{dof} \\ q_1 \\ q_2 \\ \vdots \\ q_{n_{dof}} \end{matrix}$$

where n_{dof} is the number of degrees of freedom and q_i the external force corresponding to the degree of freedom i.

The .rst file

This file contains the information about nodes with restrictions. One record is produced for every restricted node containing:

$$n_n \quad r_{ux} \quad r_{uy} \quad r_{uz} \quad r_{\theta x} \quad r_{\theta y} \quad r_{\theta z}$$

where n_n is the number of the node with the restrictions r_{ui} and $r_{\theta i}$, where r_{ui} are restrictions in displacement and $r_{\theta i}$ are restrictions to rotation. A value of 0 in r_{ui} or in $r_{\theta i}$ means that the corresponding degree of freedom is free, a value of 1 means that the corresponding degree of freedom is restricted and the value of the displacement in this degree of freedom is known as 0.

The .sol file

This file contains the solution vector for displacements when a linear elastic analysis is performed, the format of the solution is the same as in the file '.ptnumber' described in section E.5.4.

The .snumber file

The name of this file consists of the character 's' followed by a number indicating the step in which the file is generated. This file contains a list of the stresses in all elements. A line is generated for every integration point in every element. If numerical integration is not performed, then a line is generated for the stresses at the midpoint of the element. The line contains:

$$\sigma_{xx} \quad \sigma_{yy} \quad \sigma_{zz} \quad \sigma_{xy} \quad \sigma_{yz} \quad \sigma_{zz}$$

where σ_{ij} is the value of the stress in direction i along the face with a normal in direction j.

In case of interface elements, where the information consists of tractions, the line contains

$$t_s \quad t_n$$

where t_s is the shear traction and t_n is the normal traction in the local system of coordinates.

The .tcr file

This file contains information about the parameters that are going to be used in non-linear analysis. The fist line in the file contains:

$$n_t \quad I_d \quad I_{\max} \quad \epsilon_0 \quad \lambda_{\max} \quad I_f \quad N_{s\max} \quad N_{sdef} \quad u_{\max} \quad onlyCohesive \quad onlyFriction \quad f_{\Delta l} \quad \psi \quad n_c \quad dof_c$$

where n_t is the number of points in the curve time vs λ. I_d is the number of desired iterations. $I_{\max}$ is the number of maximum iteration allowed. ϵ_0 is the convergence constant. $\lambda_{\max}$ is the maximum value of the load factor. I_f is the value of the factor used in equation E.1. $N_{s\max}$ is the maximum number of steps. N_{sdef} is the number of desired steps. $u_{\max}$ is the maximum value of displacement. $onlyCohesive$ and $onlyFriction$ are variables used for controlling the behavior of interface elements with frictional and cohesive behavior, if $onlyCohesive = 1$ and $onlyFriction = 0$ only cohesive behavior is accepted. If $onlyCohesive = 0$ and $onlyFriction = 1$ only the frictional model is used. If both are equal to 1 or 0, the element is supposed as initially cohesive and then frictional. $f_{\Delta l}$ is a factor used to multiply Δl when the restart procedure is initiated. ψ is the value of the scalar factor that takes into

account that the load and displacement use different scales. If $n_c = 1$, it indicates that the sign of $\Delta\lambda$ in the solution algorithm is chosen in order to produce an increment in displacement with the same sign that has the degree of freedom dof_c.

After the first line, the time curve is defined using the values in the file introduced in the following form:

$$\begin{matrix} t_1 & \lambda_1 \\ t_2 & \lambda_2 \\ \vdots & \\ t_{n_l} & \lambda_{n_l} \end{matrix}$$

where t_i is the value of the time at the point i on the curve time vs load factor. λ_i is the value of the load factor corresponding to the time t_i.

E.6 The post-processing program, 'crg'

E.6.1 Introduction

The post-processing sub-program for the program 'crack' is the sub-program 'crg'. This program is able to present the results of all kinds of analyses made by the program 'crs' graphically. The program is completely interactive, the graphical output is produced using the library 'dislin' from Helmut Michels (Max-Planck-Institut für Sonnensystemforschung) http://www.linmpi.mpg.de/dislin/. The default output is the display of the computer, but it can be redefined to a file called `dislinnumber.ext` using the menu `Graphics->Define_output_device`. In case of Cartesian graphics, the output in many cases can be sent to a file with a name defined by the user using the option in the menu `Graphics->Define_output_file`. In that case, the output consists in the file containing, in the first line, the number of lines in the file, and, from the second line to the end, couples of values corresponding to abscissa and ordinate, for every point in the graphic.

The graphics are presented using default values for the window extension and point of view. These values can be modified using the option in the program `Graphics->View_parameters`, where the viewpoint corresponds to the position of an observer looking at the origin of coordinates. A zoom to some part of the system can be done by modifying the values of the minimum and maximum values of X, Y, and Z to display.

Under the menu `<Graphics>`, there are several possibilities that are used to check the system before running the program crs. It is possible to show the nodes, the mesh, constants (referring them to groups of geometrical parameters), materials, it is also possible to check the restrictions and the position of the forces. For the purpose of checking the topology of the system, it is also possible to show the elements in a shrink form, this is the only way to show the interface elements.

When the option to show types of elements is activated, the colors in the output refer to numbers defining the types of elements according to table E.1.

Element name	Number	Element name	Number
TRUSS2D	1	PLANE2C	19
CSTC1	9	BAR	20
CSTC2	10	BARC	21
PLANE1	11	PLANE1X	22
PLANE2	12	PLANE2X	23
CSTC1	14	CRACK2C	24
CSTC2	15	CRACK2L	25
CRACK1	16	BARA	26
CRACK2	17	PLANE1A	27
PLANE1C	18	PLANE2A	28

Table E.1: Numbers assigned to different types of elements.

Under the option `<Graphics>`, it is also possible to see the results in the form of contours of stresses in elements, deformed shapes of the system, and localization of cracks for embedded crack elements.

The program can also produce animations of displacements, stresses and cracks. In order to activate these possibilities,the user must define the parameters associated with the number of steps to show; this is done by using the options existing in the menu `Animate->parameters`. After defining the parameters, the user is required to select the type of output to show (displacements, stresses or cracks), as a result, a graph is created for every step selected and stored as a file. Selecting the option `Animate->play`, the sequence of graphics is shown reproducing the animation. The option `<play>` makes use of the program `dismov` which is part of the program `dislin`. To delete the files corresponding to a particular animation, the user is recommended to use the option `animation->reset`.

Cartesian graphics are shown using the options under the menu `<xy-graphics>`. For the options under `<xy-graphics>`, it is always possible to generate a table of values which is displayed at the screen or saved on the data file defined using the options in the menu `Graphics->define-output-file`.

In the same way as described for a general animation, it is possible to show sequences of Cartesian graphics using the options in the menu entry `<Animate-xy>`.

E.6.2 Files generated by 'crg'

The .mov file

This file includes a list of files used to create animations, all these files have the names displayed in this file. The file looks as follows:

```
movie.tif
movie_1.tif
```

```
movie_2.tif
movie_3.tif
.
.
.
```

The .anp file

This file contains the parameters used for animations, the file consist in a single line containing:

$$s_i \quad s_{inc} \quad s_e$$

where s_i is the initial step to generate the animation, s_e is the final step to generate the animation, and s_{inc} is the step increment such that the animation will show the results in the steps as:

$$s_{n+1} = s_n + s_{inc} < s_e \tag{E.9}$$

The .vwp file

This file contains the information about the graphic parameters to be used in presentations. It consists of three lines containing:

$$\begin{array}{ccc} V_x & V_y & V_z \\ x_{\min} & y_{\min} & z_{\min} \\ x_{\max} & y_{\max} & z_{\max} \end{array}$$

where V_x, V_y and V_z are the coordinates of the viewer. $x_{\min}$, $y_{\min}$ and $z_{\min}$ are the minimum values of x, y and z in the window. $x_{\max}$, $y_{\max}$ and $z_{\max}$ are the maximum values of x, y and z in the window.

E.7 Conclusions

A computer program implementation for analysis of cracks using the finite element method was described.

The program has a library of elements that can be combined in order to get the adequate model for various situations. In particular, the program implements interface elements with cohesive/frictional constitutive laws. The program also includes elements with embedded discontinuities based on the partition of unity, and finite elements with embedded discontinuities based on an alternative approach discussed in chapter 6.

All of the relevant options of the program have been presented, and the database used is described in detail.

Bibliography

Alfaiate, J., Simone, A. & Sluys, L. J. (2003), 'Non-homogeneous displacement jumps in strong embedded discontinuities', *International Journal of Solids and Structures* **40**, 5799–5817.

Crisfield, M. A. (1991), *Non-linear Finite Element analysis of Solids and Structures*, Vol. Volume 1: essentials, John Wiley and Sons, Chichester.

Povirk, G. L. & Needleman, A. (1993), 'Finite elements simulations of fiber pull-out', *Journal of Engineering Materials and Technology* **115**, 286–291.

Xu, X. & Needleman, A. (1993), 'Void nucleation by inclusion debonding in a crystal matrix', *Modelling Simul. Mater. Sci. Eng.* **1**, 111–132.

Structural

ISSN 1395-7953 R0509

Dept. of Building Technology and Structural Engineering
Aalborg University
Sohngaardsholmsvej 57, DK-9000 Aalborg, Denmark
Phone: +45 9635 8080 Fax: +45 9814 8243